Tailor-made molecules for the functionalization of electrodes: from tripodal complexes to thioketal compounds

Inauguraldissertation

zur

Erlangung der Würde eines Doktors der Philosophie

vorgelegt der

Philosophisch-Naturwissenschaftlichen Fakultät

der Universität Basel

von

Alexandrina Stuparu

aus

Slanic-Prahova, Rumänien

Basel 2010

Genehmigt von der Philosophisch-Naturwissenschaftlichen Fakultät der Universität Basel auf Antrag von:

Prof. Dr. Marcel Mayor

Prof. Dr. Edwin Constable

Basel, den 30.03.2010

Prof. Dr. Eberhard Parlow (Dekan)

The work for this thesis has been carried out at the Institute of Nanotechnology, Karlsruhe Institute of Technology (KIT) under the co-supervision of:

Dr. Christophe Stroh

“Facile est inventis addere”

- it is easy to add to things already invented.

Acknowledgements

I am grateful to many people who have been helping me in many ways during my working time in Germany.

First of all, I would like to express my gratitude to my supervisors Prof Dr. Marcel Mayor and Dr. Christophe Stroh for giving me the opportunity to join the group and to do the PhD in an exceptional institute.

I thank Dr. Maya Lukas and PhD student Kerrin Doessel for their fruitful collaboration in performing the STM experiments.

I am grateful to Dr. Olaf Fuhr for measuring X-ray data and Matthias Fischer who determined all elemental analyses.

Furthermore, I thank all my colleagues who tried their best to help me whenever I was in need and to the secretaries who fixed everything related to administration in very fast time.

Apart from the work-related acknowledgements I dearly want to thank all my friends whom I met in Karlsruhe for help and making my stay here an enjoyable experience.

Very special thanks I want to express to my former colleague Mrs. Mira Croitoru who believed in me and always encouraged me to aspire for more. I also want to acknowledge all my former colleagues and my supervisors from Romania who facilitated my way and stimulated me to come here.

Finally and most importantly I would like to thank to my big family from Romania and Germany, for their constant support and never-ending love. It is with deepest gratitude and love which still connects me with Adela, she will be always in my heart.

Alexandrina Stuparu

Karlsruhe 2010

Abstract

The scope of the present PhD work is the synthesis and characterization of new compounds that may exhibit electronic properties for their investigations in nanoscience. Towards the development of new electronically active molecules, we designed and synthesized different classes of compounds according to the desired properties. This thesis is divided into six chapters and contains the results of three years of PhD work at Institute of Nanotechnology KIT, Germany.

» **Chapter 1** contains the introduction with a brief overview about molecular electronics and molecular self-assembly as an important process for fabrication of future nanodevices. Furthermore, several types of metal-complexes on surfaces for electron transport measurements are outlined to explain the motivation of the present work.

» **Chapter 2** focuses on the synthesis and characterization of organic tripodal scaffolds adapted for metal coordination and their subsequent attachment on a metallic surface. Three classes of coordination compounds are involved. The first two structures are based on Schiff-base ligands (*trensal* and *trenpy*) with *O*- or *N*-donor functionality, while the third structure contains the bipyridine motif. The structures are functionalized with sulphur-containing end groups (thiomethyl and thioacetyl groups) or pyridine units as anchoring groups. The variation of the organic structure, anchoring groups, metal ions and counter ions, focused on the targets, is expected to offer comparative properties in the electron transport behaviour. Preliminary studies by STM measurements on Au(111) of two of the series of metal complexes, have been addressed by deposition in "sub-monolayer" concentrations and present the first results of these types of complexes at single molecule level.

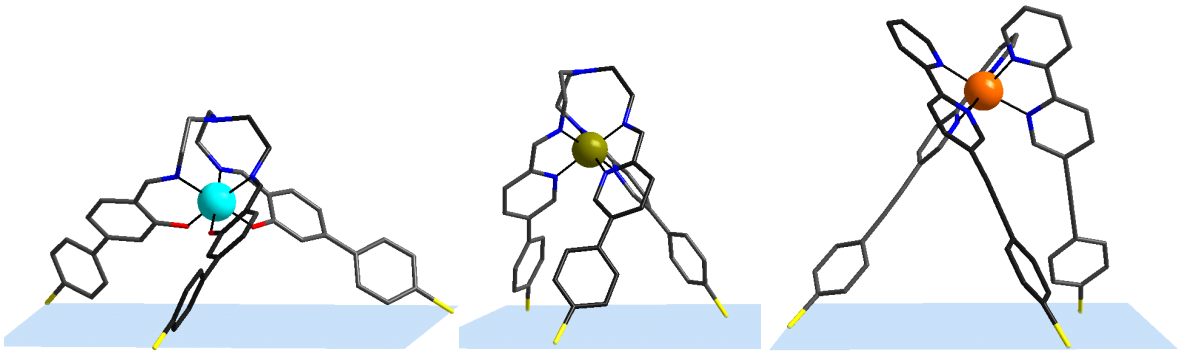

» **Chapter 3** reports about homobimetallic helical complexes considered as molecular metal wires, functionalized with sulphur-containing anchoring groups. The structures investigated so far can be envisioned as a connection of two tripodal structures with anchoring groups on both ends. Metal ion coordination transforms the ligands under application of supramolecular self assembly principles into triple-stranded helical bimetallic coordination compounds. The use of different metal ions offers a

variation of magnetic behaviours which allows for a comparison of properties in the electron transport behaviour.

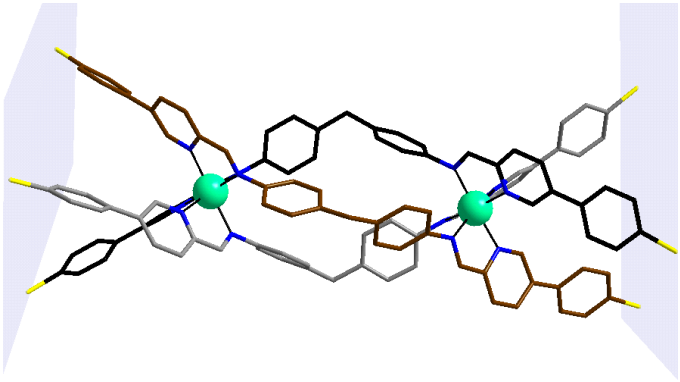

» **Chapter 4** describes a new series of chiral ligands and their Zn(II)-complexes based on the optically active binaphthyl motif as potential chiral materials for optoelectronic devices. Moreover, the novel systems combine the stereochemically defined 1,1'-binaphthyl backbone and a Schiff base coordination environment. The synthetic introduction of different substituents in different positions on the Schiff base phenoxy moiety is designed in order to tune their properties and applications such as electropolymerization and surface attachment for electron transport studies.

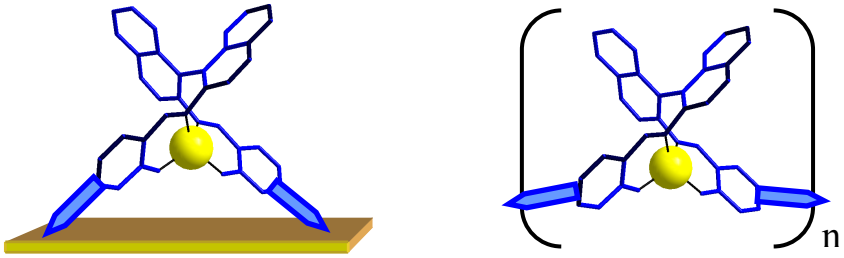

» **Chapter 5** concentrates on the synthesis of molecules containing charged moieties which are equipped with thioketal functional groups. The structural variation of the charged molecules and the synthesis of the corresponding neutral analogues allow for a comparative study on a metallic surface. The thioketal functionality is expected to offer a more stable anchoring facility to the surface by the two sulphur atoms. Thus it is proposed as new anchoring group for gold surface attachment in SAMs for electronic transport investigation.

» **Chapter 6** incorporates the experimental part including the description of the applied materials and instruments required for the present work. In particular, all synthetic pathways and workup procedures are specified together with all the characterization results obtained from the available methods. Special emphasis is put on results received from single crystal X-ray analyses for almost all final compounds.

Abbreviations

Anal.calc.	elemental analysis calculated
anh.	anhydrous
aq.	aqueous
bpy	2,2'-bipyridine
Bu_4NPF_6	tetrabutylammonium hexafluorophosphate
CH_2Cl_2	dichloromethane
dec.	decomposed
DIEA	N,N-diisopropylethylamine
DME	dimethoxyethane
DMF	dimethyl formamide
DMSO	dimethyl sulfoxide
Et_2O	diethylether
ESI-TOF	electrospray ionization time-of-flight
eq.	equivalents
IR	infrared spectroscopy;
	$\tilde{\nu}$ = wavenumber; ν = stretching vibration; δ = deformation vibration;
	comb. = combined; m = medium; s = strong; w = weak
M_r	relative molecular mass
M.p.	melting point
MeOH	methanol
MeONa	sodium methoxide
MeCN	acetonitrile
NMR	nuclear magnetic resonance spectroscopy
	δ = chemical shift; s = singlet; d = doublet; dd = doublet of doublet; t = triplet;
	ddd = doublet of doublet of doublet; J = coupling constants (Hz)
HMQC	heteronuclear multiple quantum coherence
COSY	correlation spectroscopy
Ph	phenyl-
Py	pyridyl-, pyridine
rt	room temperature
STM	scanning tunnelling mycroscopy
SAM	self assembled monolayer
TEA	triethylamine
TGA	thermogravimetric analysis
TMS	trimethylsilyl

TMSA	trimethylsilyl acetylene
trensal	tris (2,2',2"-salicylideneimino)-triethylamine
trenpy	tris (2-((2-pyridyl)-methyl-imino)-ethyl)-amine
UV-vis	ultraviolet/visible spectroscopy

Table of Contents

Table of Compounds

Tripodal metal complexes

No.	Structural formula	Compound name
1.	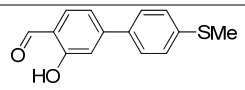	4-(4'-methylthio)-phenyl-salicylaldehyde
2.	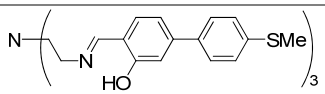	*trensal* ligand, **L**[a]
3. **4.** **5.**	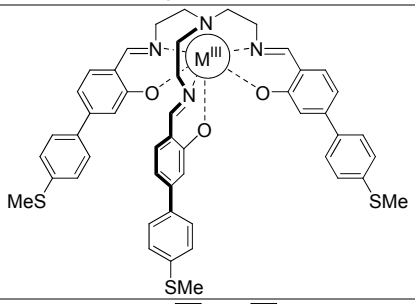	Ga(III)-*trensal* complex Fe(III)-*trensal* complex Mn(III)-*trensal* complex
6.	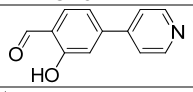	4-(4'-pyridyl)-salicylaldehyde
7.	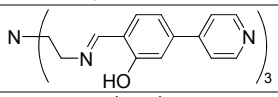	*trensal* ligand, **L**[b]
8.	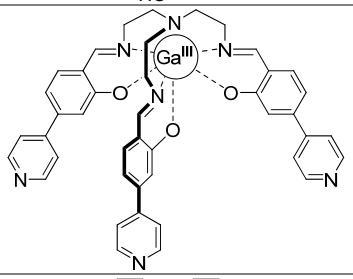	Ga(III)-*trensal* complex
9.	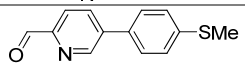	5-(4'-methylthio-phenyl)-pyridine-2-carbaldehyde
10.	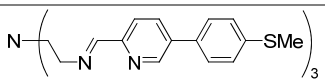	*Trenpy* ligand, **L**[c]
11. **12.** **13.**	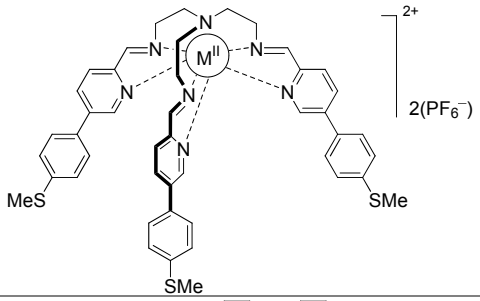	Fe(II)-*trenpy* complex Mn(II)-*trenpy* complex Zn(II)-*trenpy* complex
14.	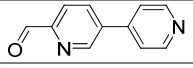	3,4'-bipyridine-6-carbaldehyde
15.	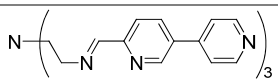	*Trenpy* ligand, **L**[d]

16. **17.** **18.**	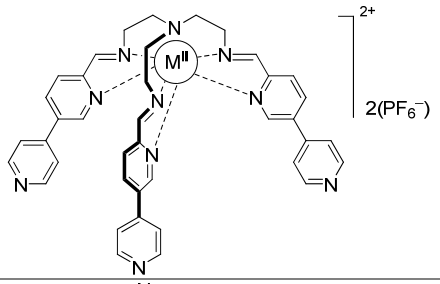	Fe(II) *trenpy* complex Mn(II) *trenpy* complex Zn(II) *trenpy* complex
19[i]. **19[ii].**	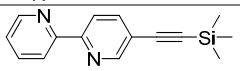 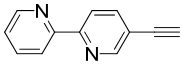	5-(trimethylsilyl-ethynyl)-2,2'-bipyridine 5-ethynyl-2,2'-bipyridine
20.	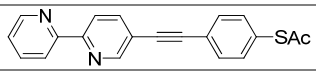	*bpy* ligand, **L[e]**
21[f]. **21[m].**	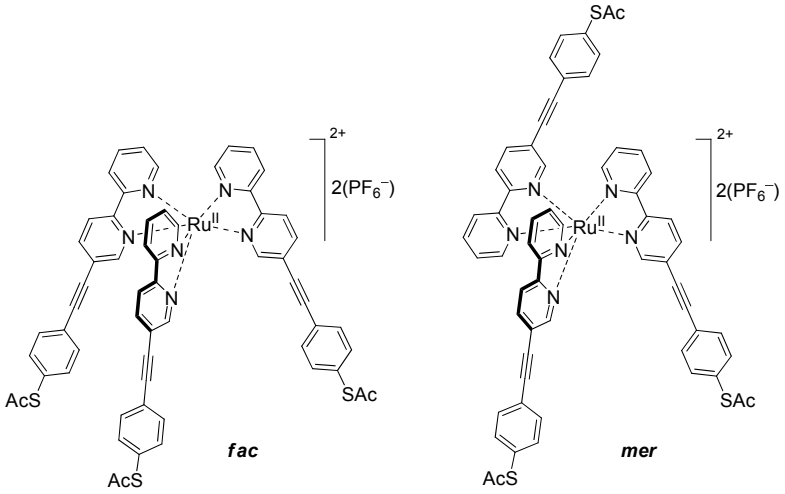	*fac* Ru(II)-complex *mer* Ru(II)-complex

Homodinuclear helicate complexes

No.	Structural formula	Compound name
22.	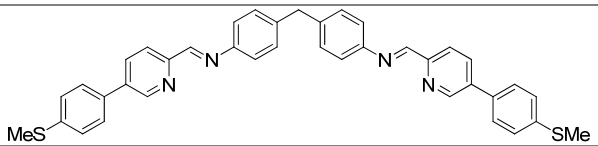	Ligand **L[f]**
23.	$[(L^f)_3Fe_2]^{4+}(PF_6)_4$	Fe_2-helicate complex
24.	$[(L^f)_3Ni_2]^{4+}(PF_6)_4$	Ni_2-helicate complex
25.	$[(L^f)_3Zn_2]^{4+}(ClO_4)_4$	Zn_2-helicate complex

Chiral (R) and (S)-binaphthyl ligands and their Zn(II)- complexes

No.	Formula	Compound name
26$^{(S)}$. **26$^{(R)}$.**	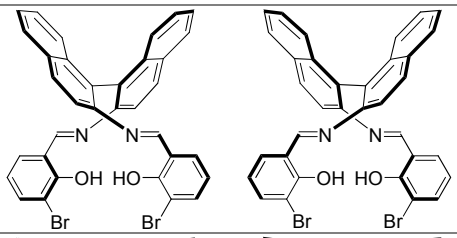	(S)-ligand **L^{g}** (R)-ligand **L^{g}**
27$^{(S)}$. **27$^{(R)}$.**	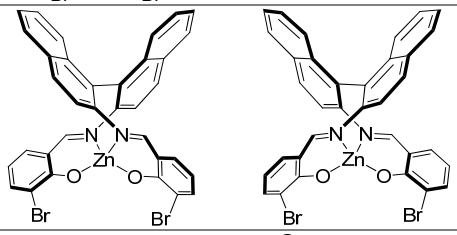	(S)-**ZnL^{g}** complex (R)- **ZnL^{g}** complex
28.	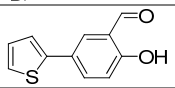	5-(thiophen-2-yl)-salicylaldehyde
29$^{(S)}$. **29$^{(R)}$.**	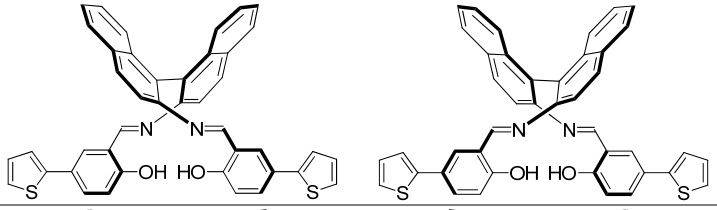	(S)-ligand **L^{h}** (R)-ligand **L^{h}**
30$^{(S)}$. **30$^{(R)}$.**	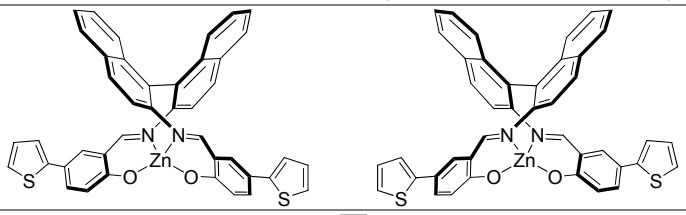	(S)-**ZnL^{h}** complex (R)- **ZnL^{h}** complex
31.	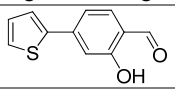	4-(thiophen-2-yl)-salicylaldehyde
***32$^{(S)}$.** **32$^{(R)}$.**	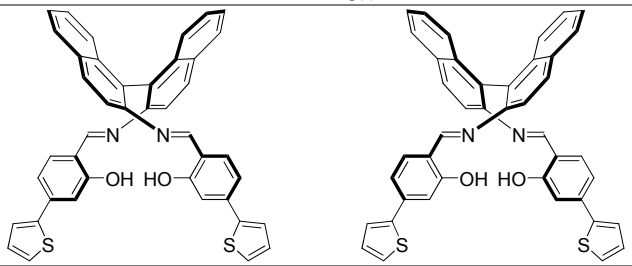	(S)-ligand **L^{i}** (R)-ligand **L^{i}**
***33$^{(S)}$.** **33$^{(R)}$.**	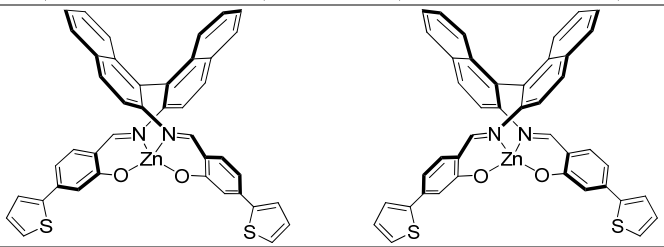	(S)-**ZnL^{i}** complex (R)- **ZnL^{i}** complex

* not isolated pure

Functionalized thioketal compounds for SAM study

No.	Formula
34a. **34b.**	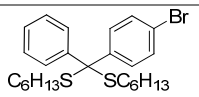 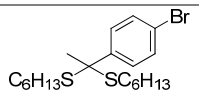
35a. **35b.**	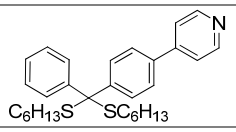 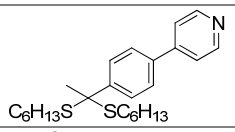
36a	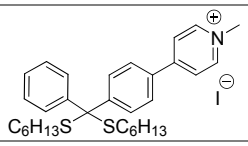
37a	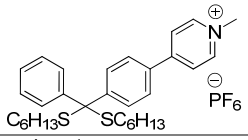
38a. **38b.**	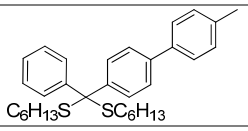 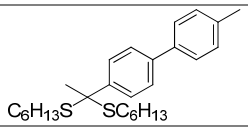

Chapter 1.

Introduction

The work in this thesis is located in the field of organic and coordination chemistry. A special focus is set on synthesis and characterization of functional molecules purposely designed for studies on metal surfaces. The scope of the present work is the combination of certain chemical and structural functionalities in order to generate both, specific properties as well as increased stability of electronically active molecules. As one of the key functions of the molecules is allocated to their possible use in molecular electronics, some general aspects of this topic are introduced. This first chapter compiles an introductory review of the basic concepts and methods which have been reported in the literature. Some exemplary molecular devices, molecular junctions and some methods of analysis are described; in particular scanning tunnelling microscopy is outlined. Furthermore, several types of metal complexes which have been reported to attach on surfaces for electron transport measurements are classified.

1.1. Molecular electronics - general aspects

The miniaturization of electronic devices is a key driving factor in modern computer technology since the formulation of Moore's "law". It relates that the number of transistors that can be fabricated on a silicon integrated circuit is doubling every 18 to 24 months.[1] However, the size of electronic circuits based on conventional silicon semiconductor technology is bound to be reached in time by technological and physical limits. One proposed way of solving this dilemma is the implication of molecular electronics based on organic and organometallic chemistry.

Molecular electronics propose to build electronic devices, i.e. nanometre scaled objects or assemblies based on single or small networks of molecules, incorporating distinct electronic functions. By this an unlimited number of possibilities can introduce a high structural flexibility and tailored purpose determined properties into the new devices production. The electronic response of such arrangements to an exterior trigger is closely related to the molecular structure. One way to analyze the electronic behaviour of a single molecule or a small network of molecules is the determination of its electronic transport properties on metal surfaces.[2 -5]

The main challenge in molecular electronics by using molecules is to realize devices equivalent to transistors, diodes, MOFET (metal–oxide–semiconductor field-effect transistor), or CMOS (complementary metal–oxide–semiconductor) etc., in order to amplify, switch or rectify signals,

interconnect (wires as passive function) or to allow for more complex functions, such as a logic gating or even a full arithmetic and logic unit.[5-7] In all these devices electron transport via tunneling or real charging (electrochemistry) through a specific part or even the entire unit plays a pivotal role, where on molecular basis a lot of theoretical input has been given.[8, 9]

Starting with the works of Kuhn in 1971, and Aviram and Ratner in 1974, in which the first molecular electronic devices have been suggested, a huge development on the frontier of both fields of science, chemistry and physics, paved the way to many functional examples.[10, 11] The first molecular rectifier based on a π–donor and a π–acceptor system, separated by an σ–bonded tunneling bridge which blocks the conjugation has been proposed to simulate the p-n transitions in semiconductors (figure 1a).[11] From this point several molecular diodes have been designed, the first rectification example based on Langmuir–Blodgett (LB) films of amphiphilic molecules (figure 1b) [12] and recently a prototype of single molecule diode have been reported. Single-molecule conductance measurements of a molecular rod (figure 1c) consisting of electron poor and rich subunits being immobilized between two electrodes by sulphur-gold contacts resulted in weak asymmetric diode-like shape of the current-voltage characteristics.[5, 13.]

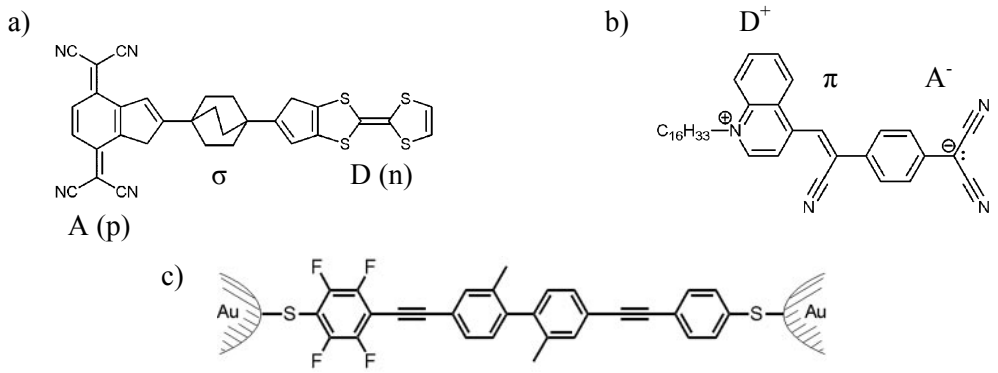

Figure 1. a) First hypothetic molecular rectifier;[11] b) Zwitterionic molecule presenting rectification assembled as Langmuir–Blodgett monolayer between two electrodes;[12] c) Prototype single molecule rectifier.[13]

Performing and understanding the charge transport or more specifically, electron transport through a single molecule is considered the key step in the design of devices as it permits the comprehension of processes occurring in many chemical and biological systems.[14, 15] As a read out tool commonly the current-voltage characteristics (I-V curves) are used, that is the measurement of the current as a function of increased positive or negative voltage. The first derivative of the measured parameters dI/dV allows for exact determination of transport processes, which is a direct method to gain information of chemical and electronic properties of the single molecule.[15] Hence, as a future prospect, chemical and biosensor applications can be derived from the electrical detection of individual binding events. [16]

It is well known that the electrical properties of conductors, semiconductors and insulators are described by their conductivity, defined as: $\sigma = (I/V) \times L/A$, where I is the electric current, V is the applied bias voltage, L is the length and A the cross sectional area of the material. For a single molecule the length and area is difficult to take into consideration, thus in molecular electronics the electronic properties are directly related to conductance G, characterized by Ohm's law with $G = I/V$. For the

measurement of single-molecule conductance, the molecule should be connected in a molecular junction to at least two electrodes through a stable, strong and reproducible contact. However, the conductance depends not only on the properties of the molecule, but also on the electrode material, the molecule-electrode contact and the local environment of the molecule. The measured conductance may be sensitive to temperature, vibration modes of the molecule or surrounding solvent molecules, etc. This makes the production of a single molecule junction a very difficult task, firstly by controlling the measurement details, followed by the evaluation of the real contribution of these effects.[15]

In molecular electronics the investigation of the conductance started with "simple" molecules based on thiol compounds to achieve a good understanding of the electrical conductance of molecular junctions. [4, 17] Later, more complex molecules, focused in principal on conjugated molecules, which due to their extended electron systems exhibit small gaps between their HOMO and LUMO levels, started to be investigated. Additionally, they can become good conductors upon oxidation and reduction.[18] For example, different conjugated oligomers, such as oligo(phenylenevinylene) (OPV) and oligo(phenylene ethynylene) (OPE) were measured and compared.[19, 20]

In the subchapter **1.2.**, more recent reports about metal complexes proposed for electron transport studies will be outlined in more detail.

Currently, scientists try to extend the conceptional two terminal molecular electronic devices such as rectifiers, wires and memory elements to build higher elaborate three terminal devices, e.g. transistors. In this way switching and real logic operations are feasible for quantum computing applications.

1.1.1. Scanning probe microscopy techniques

The most widespread methods for measurement and characterization of molecules contacted by leads are classified as: break junctions (BJ),[21-23] scanning tunneling microscopy (STM),[24] atomic force microscopy (AFM),[25, 26] crossed-wire junctions,[19, 20, 27] self-assembled monolayers (SAMs) [28] and Hg-drop electrodes (Ninni's junction).[29, 30]

Two specific break junction setups which are frequently used to measure single molecular conductance are mechanically controlled break junction (MCBJ) and electromigration technique.[22, 23, 31] However, in BJs the nature of the contact of the molecule to the electrodes is not known. As a consequence, theory is lacking important information to model the contact geometry and thus understanding molecular conductance measurements is a difficult task.[15] It is therefore desirable to fully characterize molecular wires which are binding stable to the electrodes. All of the above mentioned methods have their advantages and disadvantages alike. However, single molecule contacts can be characterized and imaged until now only by STM methods, which can perform a sufficiently resolved scan over the molecular and atomic landscape in the scope of measurement domain.

The development of the STM technique for which invention G. Binnig and H. Rohrer [24] received the Nobel Prize in 1981 has facilitated manipulation of single-molecule electronics which can achieve

nanoscale molecular junctions.[32] STM allows for the characterization of the position and surrounding of single molecules with submolecular resolution.[33] This analytical method is not only capable of imaging structures at surfaces with atomic resolution but can also provide information on the electronic properties of the molecule-contact. This is realized by measuring I-V characteristics in the so called scanning tunneling spectroscopy (STS). It can be also useful for understanding binding sites and reaction processes. [34] In addition, the tip can be used to manipulate atoms and molecules on surfaces and to induce chemical modifications on the surfaces on atomic scale.[35]

A schematic picture of the experimental setup of an STM is shown in figure 2. There, a predefined and almost ideally smooth crystal phase of a single crystalline metal provides a conducting surface, whereupon the molecule of interest is placed in ultrahigh vacuum. A metallic tip consisting of a close to pyramidal shape defines the counter electrode to the substrate surface. As the tip approaches the surface with a remaining separation of about one nanometre a current (pA to nA) can be detected when a small bias (mV to V) is applied between tip and substrate. This small current occurs on basis of the quantum mechanical tunneling effect and depends exponentially on the tip-sample distance. As a tool to establish height profiles and images the occurring tunneling voltage and the determination of the z-position of the piezoscanner can be used.[34]

Ideally the bias voltage results in direct imaging of the shape of individual molecular orbitals.[36] When a sample is biased positively, electrons flow from tip to the surface (figure 2), while negative bias has the revers effect. Depending on the direction of the flow either the highest occupied molecular orbital (HOMO) or the lowest unoccupied molecular orbital (LUMO) of the molecule can be involved in the tunneling.

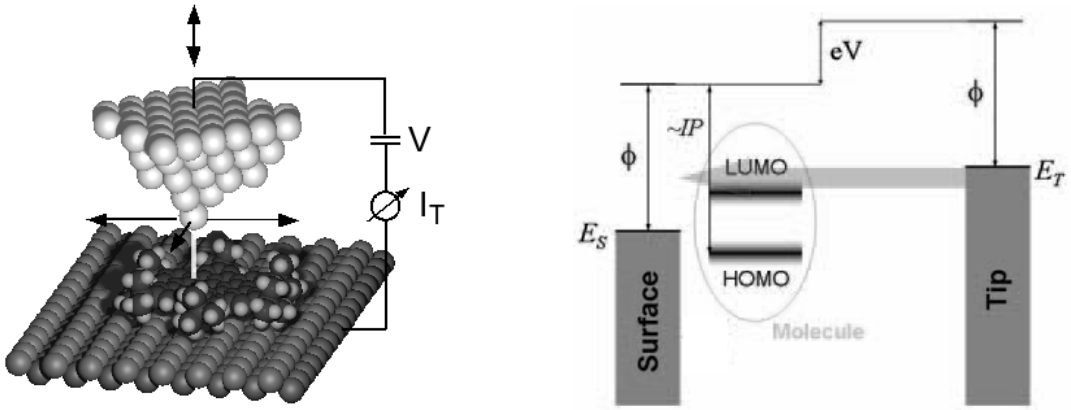

Figure 2. Schematic experimental setup STM tip based molecular junctions and the energy profile for an STM junction after applying a positive bias voltage to the sample; Φ – work functions of the electrode, IP – ionization potential, E_S, E_T – Fermi levels of surface and tip respectively and gap voltage in eV.

1.1.2. Integration of molecules for electronic transport measurements - from self-assembled monolayers to single molecules

Several deposition methods, such as sublimation in ultra-high vacuum (UHV), self assembly in solution, pulse injection deposition etc, are used to deposit single molecules on electrodes or on a surface serving as an electrode. The self-assembled monolayers (SAMs) grown from vapours or solutions, Langmuir and Langmuir-Blodgett (LB) films are the most frequently used techniques to modify a solid surface with a functional molecular film. Such an ultrathin film is formed on a solid surface by immobilizing molecules through anchoring groups or amphiphilic units.[37]

Molecular self-assembly and molecular recognition are considered being important aspects of "bottom-up approach" in nanotechnology, which starts from molecules and builds up nanostructures. Using molecular self-assembly the desired structure is programmed by the shape and functional groups of the molecules. A broad spectrum of processes has been called self-assembly derived from observations made in nature. Depending on the field of science, the concept of self-assembly has received different definitions in biology, chemistry and physics.

In general sense, self-assembly can be defined as a phenomenon in which atoms, molecules, or groups of molecules arrange themselves spontaneously into well-defined ordered structures (supramolecular species) by intermolecular interactions, without external intervention. Self-assembly is based on molecular recognition, pre-organization and complementarity concepts favoured by thermodynamic and kinetic control. J.M. Lehn wrote: "*Self-assembly is the broader term. It can be taken to designate the evolution of few/ many components, resulting in the formation of discrete/ extended entities at either the molecular, covalent or the supramolecular, non-covalent level. […] The formation of supermolecules results from the recognition-directed spontaneous association of a well-defined and limited number of molecular components under the intermolecular control of the non-covalent interactions that hold them together".*[38] "*Self-organization offers to molecular nanotechnology a powerful alternative to both top-down miniaturization and bottom-up nanofabrication approaches. […] Self-organization offers the full range of self processes that determine the internal build up, the functional integration, and the operation of the entity (such as self-selection or self-wiring), as well as its external connection to the environment (self-connection for addressing and sensing). The most complex object we know, the brain, builds up by self-organization and is self-wired and self-integrated, as well as self-connected through our senses*".[39]

Self-assembly of molecules on surfaces from SAMs to layer-by layer (LbL) growth of multilayers, became a technologically promising process to construct two-dimensional and three-dimensional systems on surfaces with emphasis on development of sensors, catalysts and molecular electronics.[40, 41]

SAMs are ordered molecular assemblies that are formed spontaneously by the adsorption interactions of a specific headgroup to a substrate. Figure 3 shows a schematic representation, including the constituents of the organized molecules in SAM (headgroup, chain or backbone, endgroup).[37]

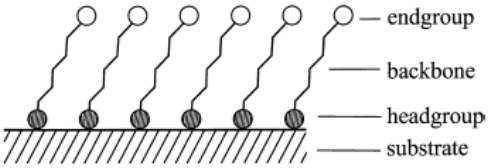

Figure 3. Schematic representation of SAM; the chemisorbing head groups and end groups (circles) can be chosen from a variety of chemical functionalities. [37]

Self-assembly processes at surfaces, after the physicists' classification, are based on chemisorption or physisorption interactions. Physisorption is characterized by a weak interaction between the adsorbing molecules and the substrate. Contributions to the interaction forces in physisorption are the van der Waals forces. Chemisorption is characterized by the formation of a chemical, usually covalent bond between the adsorbate and the surface. Organosilicon on SiO_2 and Al_2O_3, alkanethiols, sulfides and disulfides on Au, thiol-functionalized molecules on Au, Ag, Cu or Pt-substrates, alcohols and amines on Pt, carboxylic acids on Al_2O_3 and Ag are some example of this type of self-assembly.[40, 42]

A widely used method to obtain SAMs is the attachment of molecules terminated with thiol groups to electroactive surfaces such as gold electrodes.[40] The self-assembling mechanism for simple alkanethiol molecules has been proposed (figure 4.). At low surface coverage the molecules are lying flat on the surface and have high mobility. At higher coverage, the molecule assemble ordered in a flat-laying way on the surface, while only in high saturated density the molecules self-assemble in a highly ordered monolayer which stands upright, forming an approximate angle of 30° to the surface.[43]

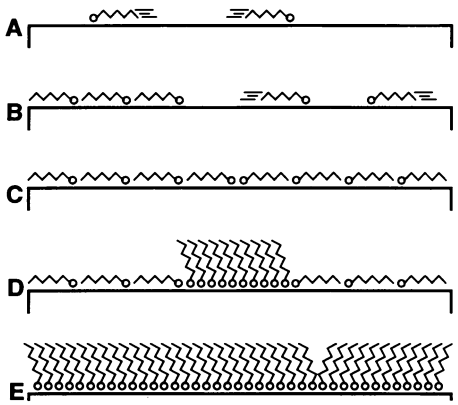

Figure 4. Schematic representation of the self-assembly mechanism for alkanethiols on Au(111); A) highly mobile phase at low coverage; B) and C) laying stripes of molecules at increased coverage; D) stripes of laying molecules and upright standing of organized molecules E) highly ordered monolayer.[43]

The electronic properties of alkane-thiol monolayers on gold surfaces, which are acting as molecular insulators, have been studied in various experiments. In a homologue series, charge is transported by tunneling and current is decreasing exponentially with chain length according to:
$I = I_0 \exp(-\beta_N N)$, where N is the number of methylene groups in the chain and β_N is found to be 1 per methylene group. However, there are disagreements between molecular conductivities measured by different experiments.[44, 45] To measure the conductance through a single molecule in SAM, one way to reduce the problems associated with not a well defined tip-molecule contact, is to insert the molecule of interest into a matrix (SAM) formed by another molecule which is less conducting (figure 5).[15, 46] Yet,

the matrix interacts with the probe molecule and recently has been considered that the influence of surrounding molecules in dense SAMs cannot be singled out.[45, 47] On the other side, introduction of additional functional units can disturb the interactions responsible for high ordering of molecules in SAMs.[41] In high dilution, similar to alkanethiol molecules, most of the molecular "wires" lie down on the surface. [48]

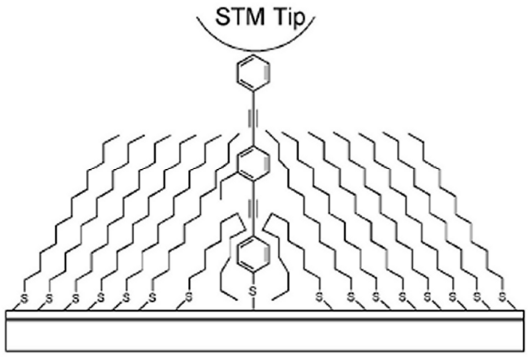

Figure 5. Inserted molecular wire in alkanethiol SAM addressed by STM tip.[46]

1.1.3. Multipod structures for surface attachment

In order to control molecular spacing, molecules with multiple attachment points are considered desirable to keep the molecular orientation rigid on the surface. In this purpose a precursor SAM molecule containing a dendron with multiple anchor sites has been proposed.[41] Examples of rigid tripodal molecules containing –COOH, $–PO_3H$ or –SH binding groups, showed in figure 6, are regarded to provide a stable, three-point attachment to the solid surface.[49 -54]

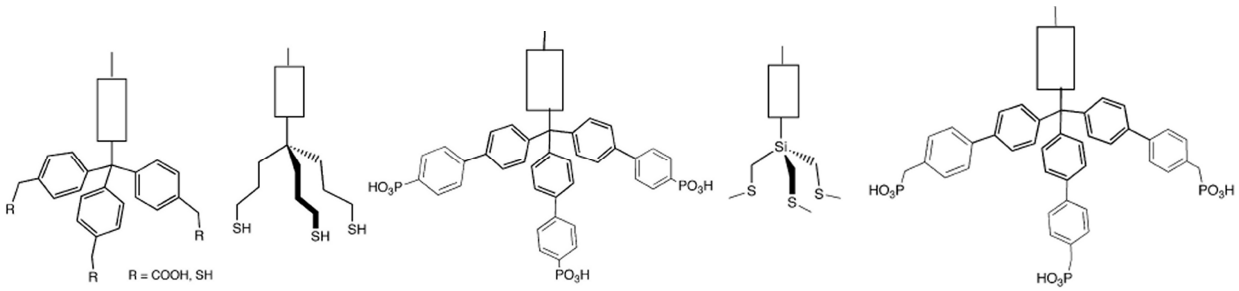

Figure 6. Partial structures of multipod anchoring groups for surface attachment.[41]

Four or more anchoring groups have also been reported.[55] Photoelectrochemical systems with multipod anchoring groups consisting of a sensitizer unit have been reported.[50, 56 -58] It has been suggested that the molecular arrangement at the surface and the sensitizer distance to the metal oxide surface play an important role in the interfacial electron transfer reaction. An example is given in fig. 7.[56]

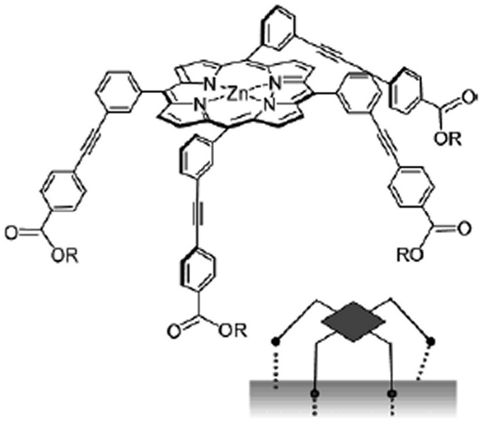

Figure 7. Structure of tetrapod for surface attachment [56]

Trinuclear Ru complexes containing six phosphonate anchor groups for immobilization on an indium-tin oxide (ITO) electrode have been recently reported (figure 8).[59] The "canopied" structure was proved by AFM measurements as molecular dots with almost the same average height of 1.2 nm all over the surface. Further, a rotaxane with a tripodal phosphonate anchoring group on a TiO_2 nanoparticle surface has been reported.[51, 52] In this rotaxane system, the shuttle movement of a crown ether was controlled by the oxidation state of a viologen-based axle moiety. A proposed electric field-driven molecular motor with tripod base sulphur containing for surface binding has been also synthesized. However, this motor has not been reported to be functional.[60]

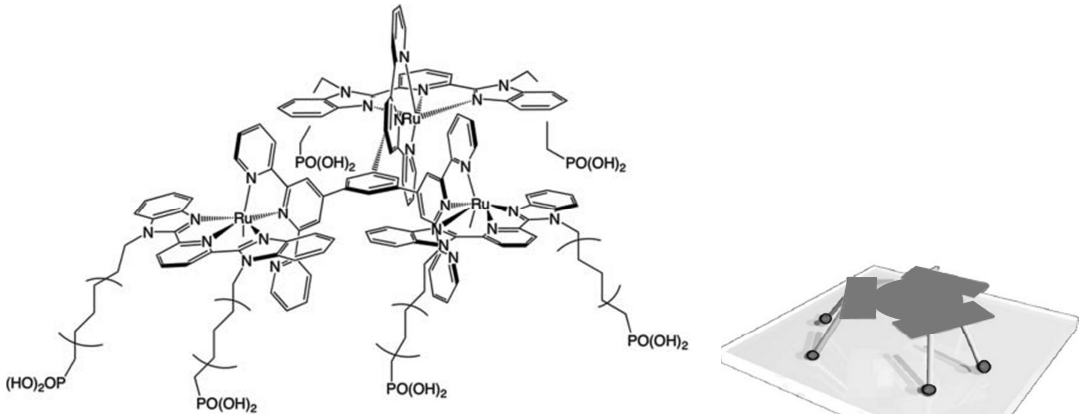

Figure 8. Structure of multipod trinuclear Ru complex with six phosphonate units for surface attachment.[59]

These types of molecules with multiple anchoring ligands were supposed to bind stronger to the solid substrate than molecules with one anchoring group. In general the anchoring structures have been analyzed by electrochemical characterization. However, to our knowledge, STM measurements which exactly image the position of multipod molecules standing and binding to the surface have not been reported so far.

1.2. Electron transport through metal complexes

In the last years the particular use of metal-complexes in electronic transport studies has attracted a special interest because of their exceeding electronic properties in comparison to purely organic materials. Thus the reduction-oxidation window offered by such metal complexes combined with their possibility for immobilization on metallic surfaces promises to yield purpose-tuned properties and unique functions for functional nanodevices like e.g. data storage.

In the numerous reports about metal complexes which were designed for surface studies only few examples specify electron transport on a single molecule level. The following section introduces representative examples of several classes of metal complexes which were studied by STM either in SAMs or as single molecules.

1.2.1. Ferrocene complexes

Ferrocene exhibits fast and reversible one-electron transfer on solid electrodes, whose redox reactions are often used as potential calibration standard in electrochemical measurements. It is therefore considered being a good model for studying electron transport phenomena.[61]

Experiments have shown that ferrocene compounds self-assembled in monolayers exhibit negatively differential resistance (NDR) effect, which further demonstrates rich and interesting electronic properties of the molecule.[62 -65] The phenomenon of NDR is characterized by decreasing current through a junction at increasing voltage (figure 9). NDR is the driving factor in several electronic components, for example resonant tunneling diodes (RTDs) in a two-terminal device.

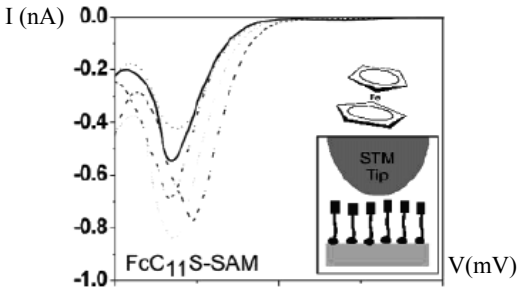

Figure 9. I-V curve exhibiting the NDR behaviour in a Ferrocene tunnel junction system measured by STM [65]

The conductances of wired ferrocene molecules (figure 10) with two thiol linkers between gold electrodes have been determined by using electrochemical STM-based break junction technique. The conductance histograms of many individual molecular junctions show broad peaks which reflect large fluctuations in the conductance of the molecules. By measuring the current through a molecular junction while sweeping the potential, a switching effect of the molecules from the low-conductance reduced state to the high-conductance oxidized state has been proposed.[61]

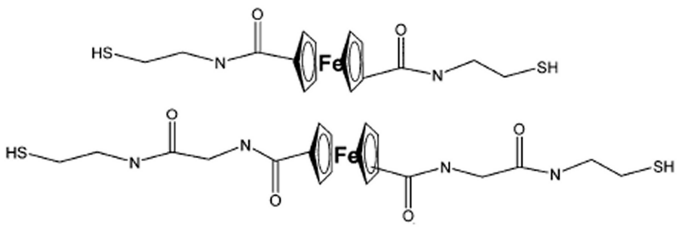

Figure 10. Ferrocene sulphur functionalized molecules wired in electrochemical STM-based break junction [61]

1.2.2. Porphyrin complexes

Electron tunneling studies have been addressed to the insertion influence of metallic ions into the porphyrin scaffold, which consequently changed the redox properties in various metal-porphyrins.[66-68]

A series of porphyrins in which each porphyrin bears S-acetylthiol-derivatized linkers were used for SAM formation on Au electrodes after which electrochemical STM measurements were carried out.[53, 69-71]

The SAM of metal-free porphyrins functionalized with thioacetyl groups deposited on gold substrate blocked the electron transport from the gold electrode to solution. On the contrary, the deposited metal-porphyrin complexes have increased the electron transport ability in comparison to the uncomplexated porphyrins.[72]

Studies for potential memory-devices have been carried out based on In_2O_3 nanowires coated with SAMs of porphyrins and investigated by SEM technique (figure 11a).

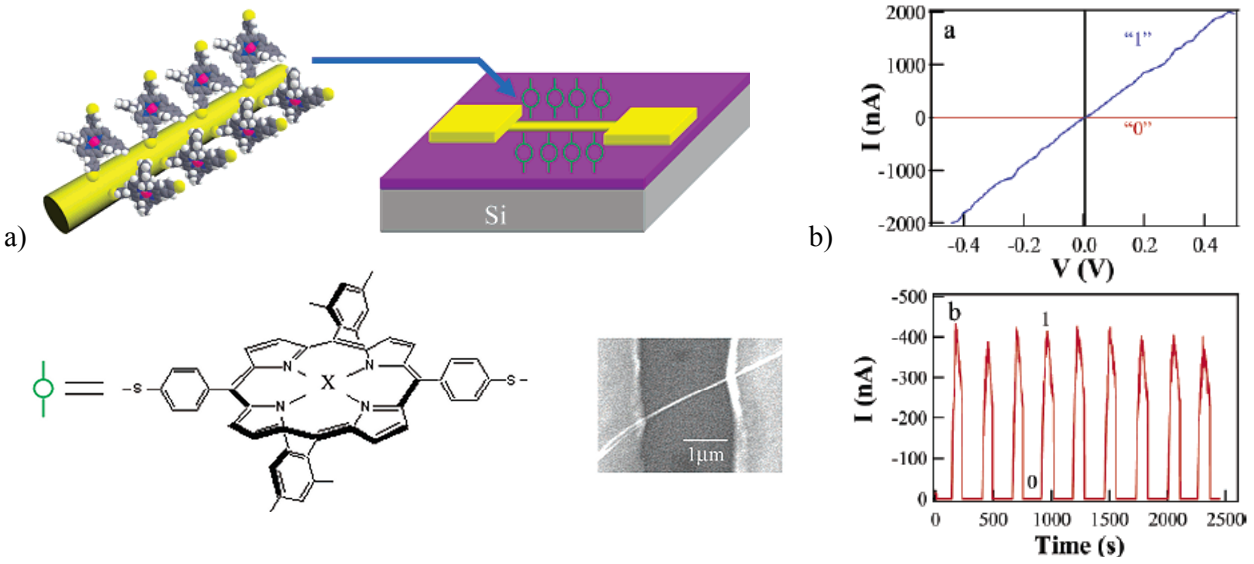

Figure 11. a) Device formed from monolayer of porphyrin molecules on In_2O_3 nanowire transistor SEM image of the porphyrin device; b) I-V curves for one state "1" and one state "0" of the Co(II)-porphyrin device and the recorded current repeatedly written into states "1" and "0".[73]

Devices with redox-active Co(II)-porphyrin complexes exhibited efficient memory operation while analogous uncomplexed porphyrin devices exhibited no memory effects. The Co(II)-porphyrin device with typical n-type field effect transistor behaviour exhibited reliable on/off operations where the

charge stored in the molecules represented the bit and the nanowire conductance was used as the readout (figure 11b). A mostly metal-centered oxidation offered by the $Co^{2+/3+}$ redox couple has been considered being the key factor for achieving the memory effect. The writing operation was performed by applying a negative voltage pulse which led to positive charges injected into the self-assembled molecules, bringing them into oxidized state. Applying a positive bias to the gate returned the porphyrin to its reduced form and brings the nanowire device to a low-conductance state. Information was stored via removing electrons from the porphyrin units by applying a bias voltage between the electrodes above the molecular oxidation potential. It was shown that multiple oxidation states (i.e. neutral, monocation, and dication) of the porphyrins can be reversibly obtained.[69, 73]

1.2.3. Schiff-base complexes

Several SAMs of Schiff-base complexes on graphite, quartz, gold or in Langmuir-Brodgett (LB) films based on Zn(II)-, Ni(II)-, Co(II)-, Cu(II)-bis(salicyliden)-derivate complexes have been reported.[74 - 76] STM characterization applied for this type of deposited complexes showed highly 2D ordered lamellar arrays (figure 12) and the nature of interactions implied in their organization has been discussed. However, the complexes appear to be suitable for nanopatterning of surfaces, to our knowledge electron transport characterization has not been reported. In some cases electron-transfer reactions of these salen-complexes have been addressed electrochemically.[77]

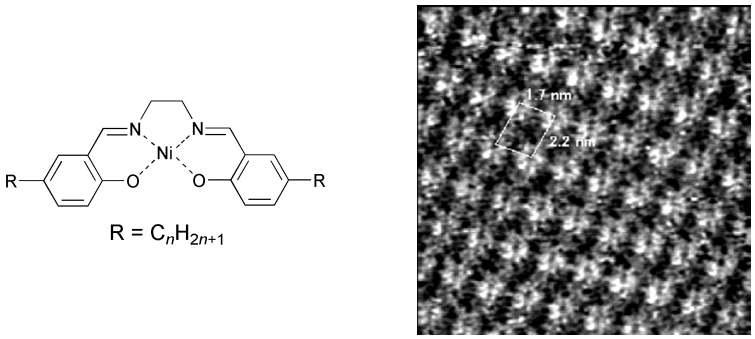

Figure 12. Example of Schiff-base complex structure on HOPG and its STM image of high 2D ordered SAM.[76]

1.2.4. Polypyridine based metal-complexes

Directed electrochemical charge transport at the single-molecule and monolayer levels have been addressed to different redox active metal complexes in solution on electrodes by STM and MCBJ techniques.[78 -81.]

A couple of bis(2,2'-bipyridyl) osmium(II)-complexes has been attached via 4,4'-bipyridyl linkers on single crystal Au(111) or Pt(111) surfaces in an electrochemical STM experiment setup (figure 13). In this way single molecule transistor behaviour was suggested, including the gate electrode acting as

the third terminus. High amplification of on-off ratios have been realized by adjusting the gate voltage in such a way that the electrochemical transition of the Os(II)/Os(III) redox couple is set in between the Fermi levels of the electrodes. Thus, sequential interfacial electron transport implying the population and depopulation of redox levels has been described. The mechanism of the ET has been proposed to occur coherent for a significant number of electrons by thermal activated hopping according to results obtained from two-dimensional electrochemical STM and STS. In order to support the results theoretically, results from monolayer experiments were used to connect single-molecule conductance with electrochemical kinetics. As a conclusion strong electronic coupling is responsible for strong distance dependence of the tunnelling current.[78, 79]

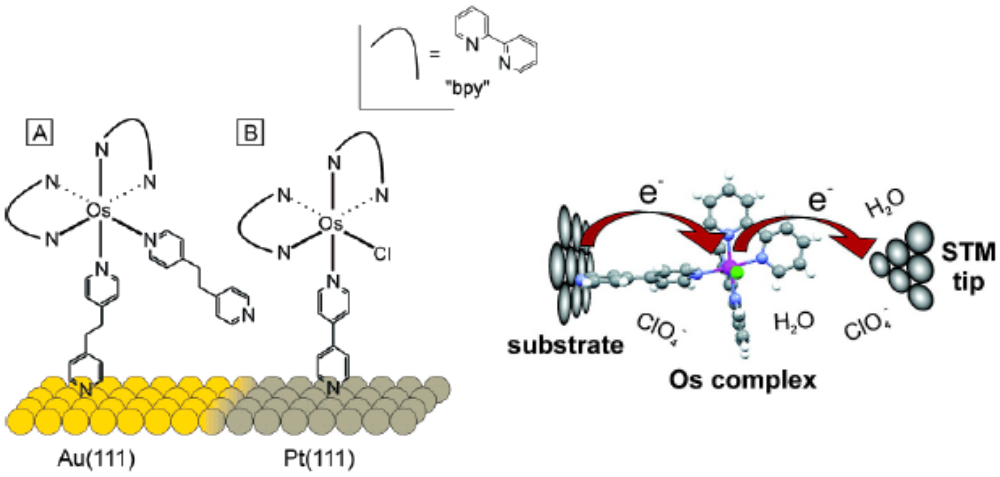

Figure 13. Bis(2,2'-biypyridyl) osmium(II) complexes on surfaces and mechanism of electron transport through individual complexes.[78, 79]

In another electrochemical STM setup experiment, SAMs of terpyridine based complexes of Ru(II) and Os(II) were studied and compared with their electrochemical behaviour. Due to higher repulsive interaction energies of the terpy complexes in comparison to bpy based analogues the surface coverage was found to be lower for the former. Additionally, the formation of hexagonal arrays in the case of terpy complexes was described. From potential sweep scans the peak current dependence from the scan rate was used to determine interaction energies within the monolayer.[80]

Single molecule transistors have been constructed by applying thiol functionalized Co(II)-bis(terpyridine) complexes (figure 14) in a junction setup created by electromigration technique. Depending on the length between the linking sulphur groups normal Coulomb blockade behaviour at low bias voltages (long linker) or Kondo effect features at cryogenic temperatures in presence of a magnetic field (short linker) has been described. The Kondo effect occurs only for the shorter molecule and is observed as a peak in the differential conductance at 0 V. At very low temperatures the unpaired electron of the Co(II) ion is considered to be located on an spatial island which couples strongly to the conduction electrons of the gold electrodes and thus creates two non-degenerate states if an external magnetic field is applied.[82]

Figure 14. Co(II)-bis(terpyridine) complexes proposed as single molecule transistors in a junction setup created by electromigration technique.[82]

Single-molecule charge transport through a Ru(II)-bis(terpyridyl) complex (figure 15) with p-acetyl-mercapto phenylacetylene units for anchoring to Au electrodes, has been investigated in MCBJ in UHV conditions at various temperatures and compared with DFT calculations.

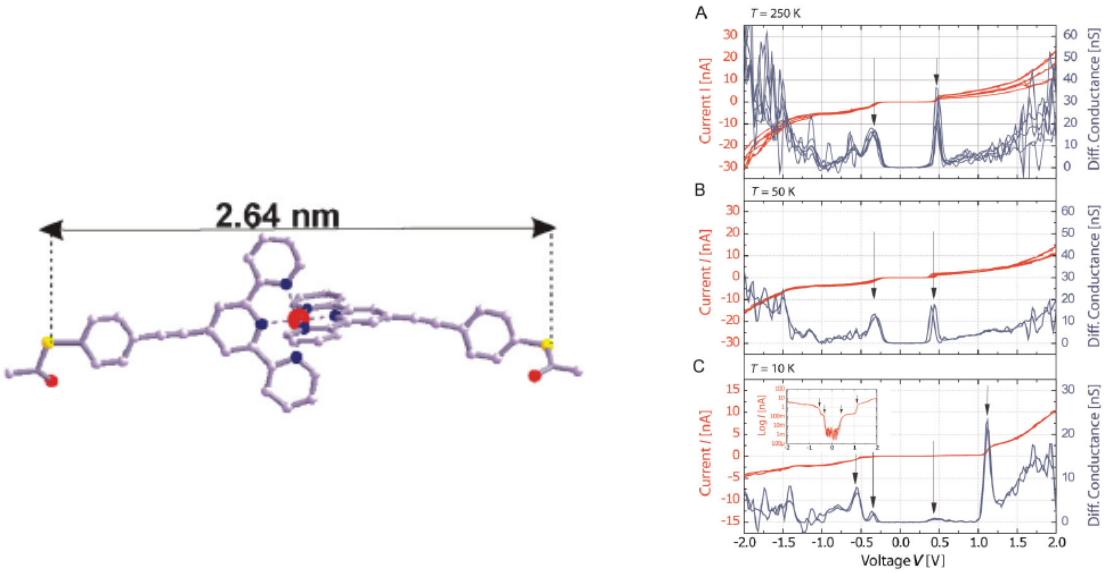

Figure 15. Structure of Ru(II)-bis(terpyridyl)-complex studied in MCBJ and the I-V electronic transport properties at different temperatures of the Cardan-joint-type molecule.[81]

As a result of the opening and closing movement of the break junction electrodes, the I-V characteristics changed considerably in magnitude which was attributed to a cardan-like buckling and straightening of the molecule around the central Ru-coordination subunit (figure 15). Resonant transport through the LUMO was suggested by *ab initio* calculations.[81]

1.2.5. Grid-type supramolecular transition metal assemblies

Grid-type supramolecular metal complexes (figure 16) obtained by self-assembly of transition metal ions and designed ligands are arranged in rigid and highly symmetric structures, exhibiting interesting magnetic[83] and electrochemical properties.[84, 85] STM studies of densely packed monolayers of

$[Co^{II}_4L_4]^{8+}$ grid complexes on graphite (figure 16)[86-88] and transport properties by scanning tunneling spectroscopy (STS) have been reported. Different molecular arrangements of complex molecules were observed after scanning: 1D ordered lines (figure 16a), 2D ordered arrays (figure 16b), and isolated, free standing units (figure 16c) [89] and proposed as a three-terminal device.[90] The observation of high-spin states of Mn^{II}_{12} grid-type complex and Fe^{III}_{12} supramolecular assembly with single-molecule magnet behaviour have been also employed in current transport experiments.[91]

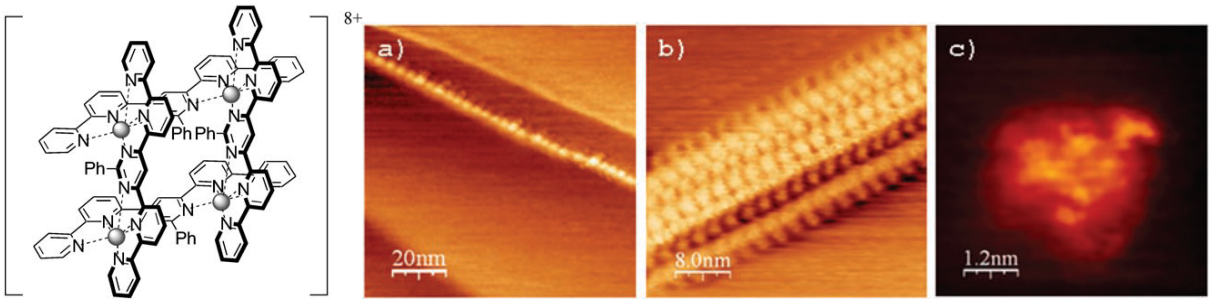

Figure 16. Representation of the $[Co^{II}_4L_4]^{8+}$ complex and STM images grid complex deposited onto a HOPG surface; a) at low concentrations the molecules are aligned along graphite steps into 1D chains; (b) 2D crystal of molecules along a graphite c) an isolated molecule with submolecular resolution.[89]

1.2.6. Metalo-Dendrimers

By varying different parts of the dendrimers their sequential build-up offers the possibility to tune several important properties such as the overall charge state as well as catalytic, redox and photoactive behaviour. Exchangeable parts can be the core structure, terminal functional groups, the ligating structure or different metal ions.[92, 93] As a consequence of their multinuclear structure, the redox-active dendritic molecules started to be investigated as candidates for molecular charge storage.[92] Protonation or coordination of a metal ion to certain ligand units contained in dendrimers can allow switching of the conformation on the surface due to loss of conformational freedom.[93] Dendritic ruthenium-complexes have been reported to possess a stronger, additive MLCT band in the visible light which plays an important role in antenna functions for light harvesting.[92]

Poor possibilities for structural characterization and lack of X-ray crystallographic data of dendrimers makes it a challenging task to image such species with scanning probe techniques.[94] Several STM studies to image the dendrimers concentrated on the self-assembly process on surfaces or other interfaces. In that way even single molecule dendrimers have been determined.[93, 95-97]

An example with 2,2‘-bipyridine Fréchet-type dendrimers organized in SAM on graphite surface under ambient conditions is given in figure 17.[96]

The nonconductive nature of most of the dendrimers especially in high generations makes STM imaging difficult due to a small tunneling probability. Caused by the spherical geometry of these macromolecules consisting of poorly conducting structures high energy barriers for the tunneling are built-up. Considerable effort has been allocated to the inclusion of more conductive functionalities into the structure of the dendrimers (e.g. porphyrins, phenyl rings).[97]

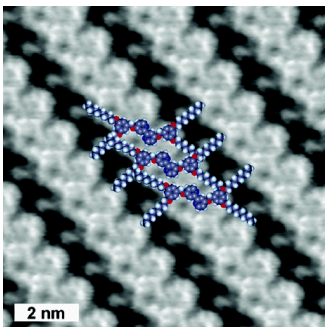

Figure 17. STM image of 2,2'-bipyridine Fréchet-type dendrimers in SAM on graphite.[96]

More recently the introduction of metal ions into the dendritic scaffold lead to significant enhancement of the electron transport efficiency, thus visualization of intramolecular hyperfine features consistent with the location of dendrimer termini (figure 18A) was enabled. Four (G4) or eight (G8) generation of poly(amido-amine) PAMAM-NH_3 dendrimers have been employed in STM and STS studies on Au(111) surface.[97]

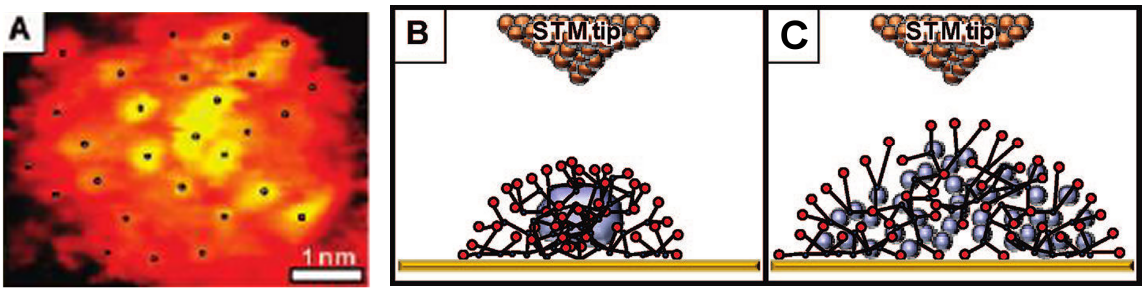

Figure 18. A) STM image which reveal the hyperfine features (indicated by small circles) of the G4 dendrimer treated with Pt(II); B) Pt(0) nanoparticle encapsulated in dendrimer formed by tunneling electron reduction of Pt(II) ions under UHV; C) Pt(II) ions remain coordinated in dendrimer under ambient conditions.[97]

As a result of the coordination of metal ions (Pt^{2+} or Cu^{2+}) by the organic dendrimer, Coulomb blockade (CB) behaviour was observed by STS in UHV, while in ambient conditions Coulomb staircase (CS) behaviour lead to the overall increased tunneling efficiency. The two behaviours are explained schematically in figure 18B and C: under UHV, Pt(0) nanoparticle encapsulated in dendrimer is formed by tunneling electron reduction of Pt(II) ions and under ambient conditions Pt(II) ions remain coordinated in dendrimer.

Other not further classified types of metal complexes on surfaces investigated in SAM or at single molecule level by STM imaging or even STS techniques for transport properties, have been reported and can be found in more specific works. Some selected examples are a) a trans Pt(II)-complex as a single insulating molecule,[98] b) ferric wheels with direct location addressability of the individual metal ions by STS,[99] c) localization of spin centers with STM by magnetic interactions of Co-complexes at metallic surfaces using the Kondo effect. [100]

Chapter 2.

Tripodal metal complexes

This chapter is focused on the synthesis of functionalized molecules to stand on their own on a metallic surface for electron transport investigation at single molecule level without the influence or support of surrounding molecules.

The possibility to lock a principally flexible organic structure by metal coordination into a rigid three-dimensional tripod complex is a primary motivation to us. Additionally, the potential properties of these complexes can be fine tuned by varying the metal ions.

Up to now the majority of surface studies were carried out on planar molecules, e.g. phthalocyanines and porphyrins known to lay flat on surfaces. The motivation for employing tripodal molecules to enforce a vertical orientation of the redox-active molecules at a fixed distance from the surface is proposed in order to provide a more robust anchor to surface but also to control electron-transfer and charge-dissipation characteristics.[53, 54, 101] In this respect an organic tripodal scaffold adapted for metal coordination and subsequent attachment on a metallic support was designed (figure 19). The organic scaffold with three terminal anchoring groups should allow for superior stability characteristics and better control of molecular orientation than the structures with a single site of attachment. The variation of the backbone structure, anchoring groups, metal ions and counter ions is expected to offer comparative properties in the electron transport behaviour.

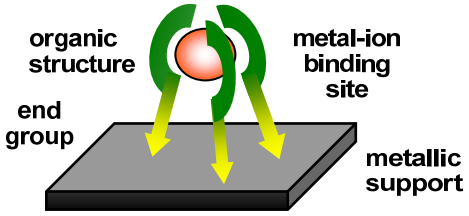

Figure 19. Schematic representation of the designed tripod

Three classes of coordination compounds have been proposed for synthesis of the tripodal scaffold depicted schematically in figure 20.

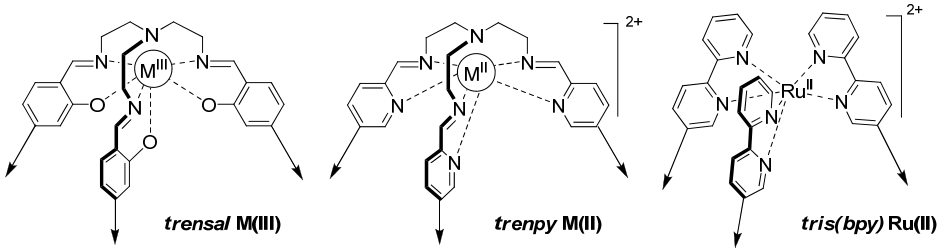

Figure 20. Tripodal functionalized metal complexes for surface decoration based on: Schiff bases ligands (*trensal* and *trenpy*) and *bpy* ligand.

The first two structures are based on Schiff-base ligands *trensal* and *trenpy* with *[N_3O_3]*- or *[N_6]*-donor sets and were used for complexation of different metal ions. The third structure contains the bipyridine ligand motif which was applied for coordination of Ru(II) cation. The M(III)-*trensal* complexes provide a neutral charged structure while the M(II)-*trenpy* and Ru(II)-*trisbpy* complexes form cations with a charge of 2+. The choice of Schiff-base and bipyridine complexes arose from the well-developed and understood coordination chemistry of these types of ligands with a multitude of metal ions. The three types of coordination environment offer the tailored formation of stable metal-complexes combined with an interesting structural variation. As a consequence the magnetic behaviour and dependence of spin state on donor set in systems are influenced by the ligand structure.

For the attachment on the metallic surface three types of anchoring groups are introduced in the tripodal structures in order to establish a different surface dependent behaviour. The structures are terminally functionalized with sulphur-containing end groups (thiomethyl and thioacetyl end groups) or are functionalized with pyridine subunits. The strong interaction of the tripod via sulphur-containing end groups or pyridine nitrogen is expected to provide sufficient stability through self-standing-attachment on the surface.

2.1. Tripodal *trensal* and *trenpy* Schiff base complexes

2.1.1. Introduction

Imines, C=N-R, and their derivatives, constitute a group of compounds known as Schiff bases. Complexes of transitional metal ions with Schiff bases provide a very large and well studied class of compounds of stereochemical and magnetochemical interest. One particular example is represented by the class of *tren*-capped podants such as the *trensal* and *trenpy* ligands and their respective metal complexes. The tripodal ligand structures are obtained by the condensation of tris-(2-aminoethyl)-amine (*tren*) with three equivalents of salicylaldehyde (*trensal*) or with 2-pyridine carboxaldehyde (*trenpy*). Subsequent conversion with metal salts serves as a convenient pathway to afford tripodal metal complexes which have been described for numerous metal ions. The polydentate *trensal* and *trenpy* ligands enclose the metal ion resulting in stable complexes with diamagnetic or paramagnetic properties.

The coordination chemistry of *trensal* compounds includes a large variety of metal ions such as: Cr(III), Mn(III), Fe(III), Co(III), Sc(III), Tc(IV), Rh(III), Cd(III), some metal ions of group 13, Ga(III), In(III), Tl(III) and the lanthanide series.[102 -108] The *trenpy* Schiff base has been used for coordination of: Mn(II), Fe(II), Co(II), Ni(II), Zn(II), Cu(II).[109 -114]

As the various tripodal ligands are equipped with differing donor sets and each type of metal ion is defined by a huge diversity of electronic and spatial parameters, each complex appears different in shape. Thus, geometric control of redox state stability has been applied via tuning both the nature and geometric disposition of the donor set of the ligand.[115] In the particular case of Fe(III)-coordination by

trensal the metal ion appears in high spin (HS), S=5/2 spin state.[102] Moreover, *trenpy* metal complexes offer a coordination environment which can stabilize both high spin and low spin configuration. Thus the magnetic behaviour of the complexes can be tuned. The Fe(II)-*trenpy* complexes are characteristically described as low spin (LS). If the ligand structure is substituted by methyl-groups in the vicinal position to the coordination site the resulting Fe(II)-complex has been found to exhibit spin cross-over behaviour.[113] Perspectively, the study of spin state control via geometry promises access to important applications e.g. optical information technology.[116]

2.1.2. Results

2.1.2.1. M(III)-*trensal* complexes

This section describes the synthesis and characterization of *trensal* tripodal metal complexes functionalized with thiomethyl or pyridine end groups. A series of coordination compounds was synthesized by varying the metal ion, ranging from: Ga(III) and Mn(III) to Fe(III). The neutral complexes present diamagnetic behaviour in case of Ga(III)-complexes, while Fe(III)- and Mn(III)-complexes are paramagnetic. In addition, their molecular structures have been determined by single crystal X-ray diffraction.

Synthesis of M(III)-*trensal* complexes

The *trensal* ligands and their metal-complexes with thiomethyl or pyridine end-groups have been synthesized in three steps shown in schemes 1 and 2. Since the two ligands and their complexes are very similar they will be discussed in parallel. First, the designed legs were prepared through a Suzuki-type cross-coupling reaction between 4-bromo-salicylaldehyde and the appropriate phenyl-boronic acid derivative which gave the corresponding functionalized aldehydes **1** and **6**. An imine-condensation of three equivalents of the functionalized aldehyde with tris-(2-aminoethyl)-amine in ethanol afforded the desired tripodal ligands **2** and **7**. The reactions were performed following reported procedures for similar compounds [102] and afforded the pure ligands. The synthesis of the tripodal Ga(III)-complexes **3** and **8** has been slightly adapted from a method presented in the literature for analogous compounds. Initially, the phenolic groups of the ligand were deprotonated by treatment with a methanolic solution of NaOH (3 eq.) followed by addition of the $Ga(NO_3)_3$ salt.[103] The Mn(III)-complex was prepared following a literature method by reacting the ligand with a $Mn(AcO)_3$ in presence of NaOH.[117] The tripodal Fe(III)-complex was synthesized similarly in presence of NaOH and using $FeCl_3$. Alternatively, the Fe(III)-complex has been obtained by reacting the ligand with $FeSO_4$ and in situ oxidation by air. A similarly reported reaction pathway of in situ oxidization used $Fe(ClO_4)_2$ instead.[117]

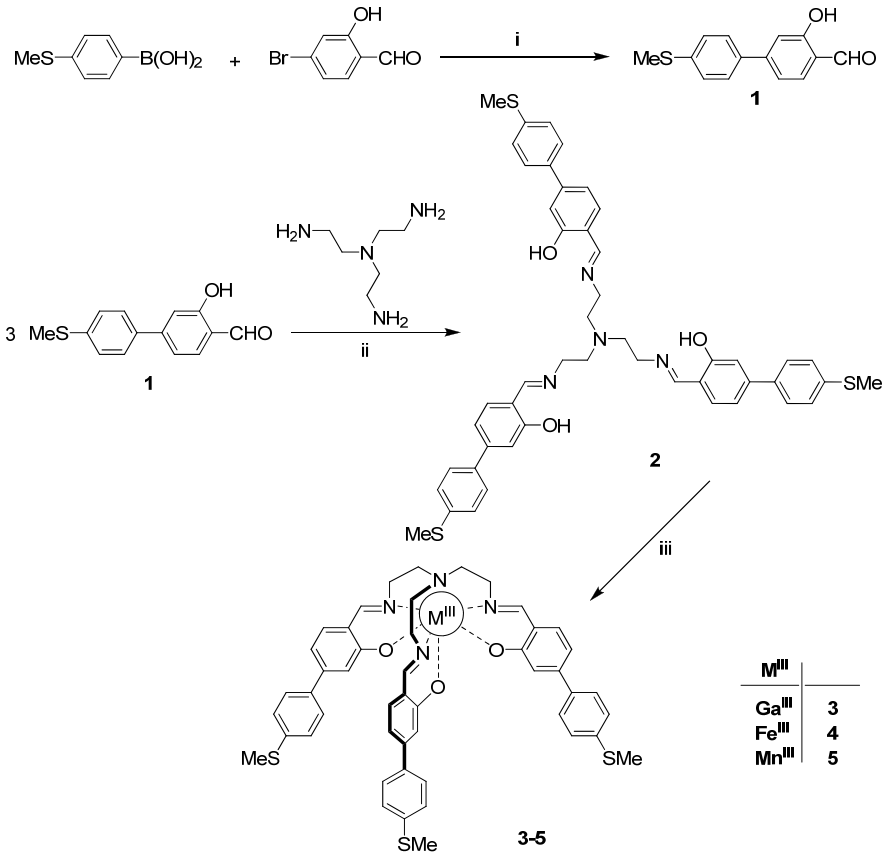

Scheme 1. Synthetic route of *trensal* M(III)-complexes with thiomethyl end groups. Reagents and conditions: (i) $Pd(PPh_3)_4$, Na_2CO_3 aq, toluene/MeOH, N_2, 80°C, 49%; (ii) EtOH, rt, 95%; (iii) (3): $Ga(NO_3)_3$, NaOH, MeOH, reflux, 82%; (4): $FeSO_4$, MeOH, CH_2Cl_2, rt, 61%, or $FeCl_3$, NaOH, MeOH, CH_2Cl_2, rt, 77%; (5): $Mn(AcO)_3$, NaOH, MeOH, CH_2Cl_2, rt, 71%.

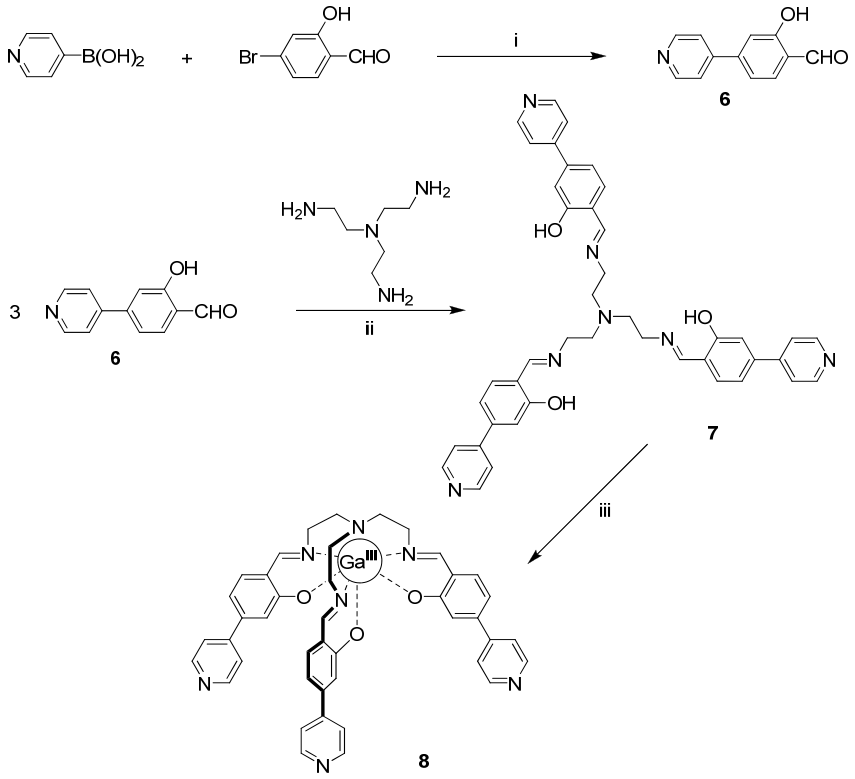

Scheme 2. Synthetic route of *trensal* Ga(III)-complex with pyridine end groups. Reagents and conditions: (i) $Pd(PPh_3)_4$, Na_2CO_3 aq, toluene/MeOH, N_2, 80°C, 64%; (ii) EtOH, rt, 84%; (iii) $Ga(NO_3)_3$, NaOH, MeOH, reflux, 85%.

Characterization of M(III)-*trensal* complexes

NMR Spectroscopic Data

The ^{1}H NMR spectra of the *trensal* ligands **2**, **7** and their Ga(III)-complexes **3**, **8** are consistent with their structures. Since the two *trensal* ligands with thiomethyl or pyridine end groups and their Ga(III)-complexes are structurally analogous, they will be treated in parallel. The spectra are shown in figures 21 and 22. The signal shifts were assigned after reported values for similar compounds combined with the analysis of the coupling constants (table 1).

Table 1. ^{1}H NMR chemical shift (CD_2Cl_2) of the ligands **2**, **7** and their Ga(III)-complexes **3**, **8**.

Proton signals δ (ppm)	Ligand, **2**	Ga-complex, **3**	Ligand, **7**	Ga-complex, **8**
SCH_3	2.51	2.47	-	-
CH_2	2.85 3.58	2.85 3.07 3.32 3.80	2.88 3.72	2.87 3.11 3.34 3.81
Ph^A H-3 H-5 H-6	7.10 6.72 6.43	6.69 6.83 7.16	7.17 6.78 6.58	6.96 6.88 7.24
Ph^B	7.28 7.47	7.24 7.56	-	-
Py	-	-	7.41 8.60	7.50 8.56
CH=N	7.98	8.14	8.06	8.19
OH	13.74	-	13.81	-

Table 2. ^{13}C NMR chemical shift (CD_2Cl_2) of the ligands **2**, **7** and their Ga(III)-complexes **3**, **8**.

Signals δ (ppm)	Ligand, **2**	Ga-complex, **3**	Ligand, **7**	Ga-complex, **8**
SCH_3	15.4	15.4	-	
CH_2	55.6, 57.9	57.0, 61.8	55.5, 57.9	57.0, 61.9
Ph / Py	114.6, 116.9, 117.8, 126.6, 127.4, 132.1, 136.8, 138.9, 143.9	113.1, 116.6, 119.78, 126.4, 127.4, 135.3, 137.0, 138.7, 146.5	115.2, 116.9, 119.1 (q), 121.5, 132.2, 141.5 (q), 147.2 (q), 150.5	113.1, 117.8, 120.6, 121.6, 135.7, 144.3, 147.6, 150.3
C-OH	161.6	169.0	161.7	168.9
CH=N	165.8	170.0	165.6	170.2

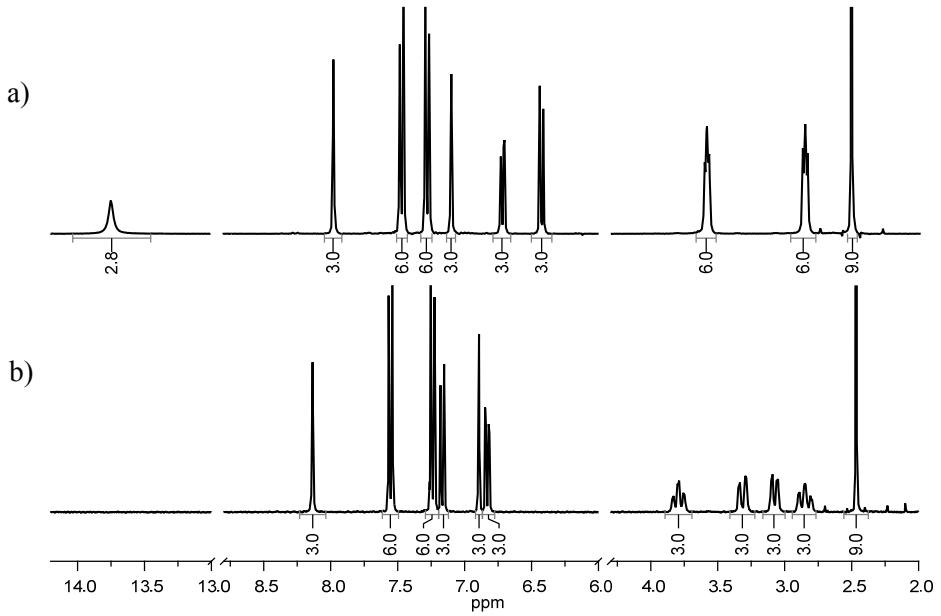

Figure 21. ^{1}H NMR spectra (CD_2Cl_2) of: a) ligand **2**; b) Ga(III)-complex **3** with thiomethyl end groups

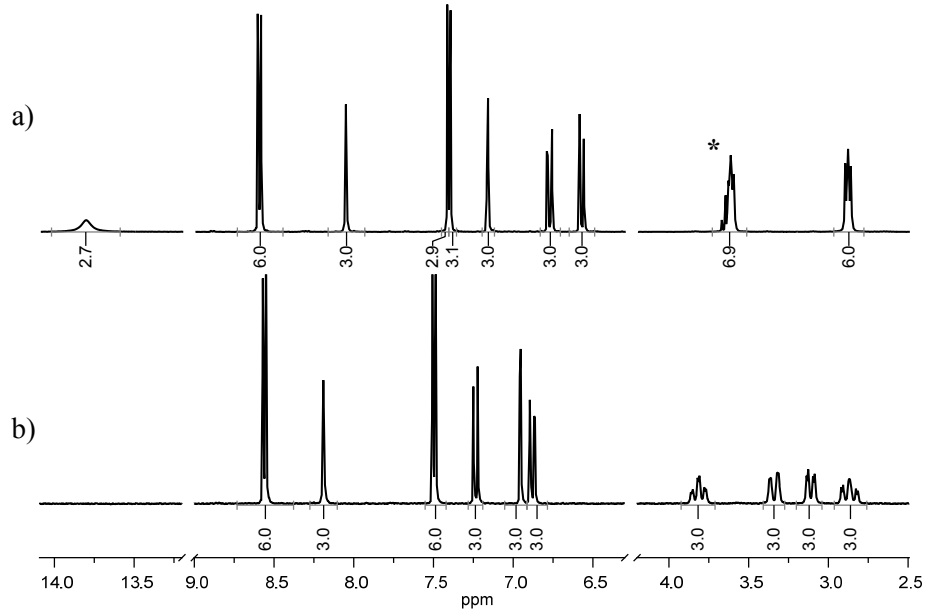

Figure 22. ^{1}H NMR spectra (CD_2Cl_2) of: a) ligand **7**; b) Ga(III)-complex **8** with pyridine end groups; * residual EtOH

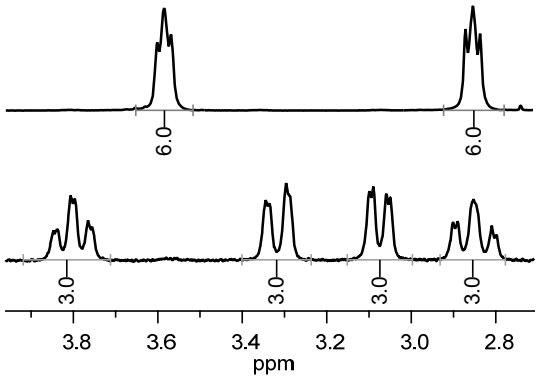

Figure 23. ^{1}H NMR spectra zoom showing the AA'XX' spin system of the ligand **2** and AA'BB' spin system of the Ga(III)-complex **3**

The ^{1}H NMR spectral features of the ligands **2**, **7** include the phenolic proton resonances at about 13.8 ppm (s). This value is higher than the expected chemical shift for phenols, e.g. the hydroxy proton resonance in the starting salicylaldehyde derivates **1** and **6**, is situated at about 11.1 ppm. This significant downfield shift has be explained as a combination of three factors: the formation of hydrogen-bond, the O-H···N group lying coplanar with the aromatic ring, thus deshielded by the induced aromatic ring current and the additional deshielding given by the hydrogen-bonding of the phenolic OH with an unsaturated azomethine.[118] The presence of the imine function is indicated by the proton resonances at about 8 ppm (s). Furthermore, the two methylene groups give an AA'XX' splitting pattern (figure 23) at about 2.85 ppm (t) and 3.6 ppm (t), consistent with similar reported compounds.[103, 118, 119] While for the ligand terminated with pyridine units **7** the characteristic signals for pyridine function are evidenced at 8.6 and 7.4 ppm, the ligand with thiomethyl end groups **2** additionally contains the signal for the thiomethyl groups at 2.5 ppm.

The ^{1}H NMR spectra of the Ga(III)-complexes **3**, **8** present only one set of signals which supports that the three chelating legs of the ligand remain chemically equivalent after coordination. This equivalence demonstrates the C_3 symmetry of their structures in solution. An evident difference between the Ga-complexes and the free ligand is the absence of the phenolic resonance. The complex formation is supported by the small shifts of the imine protons involved in coordination and the shift of the phenyl protons close to the coordination center (downfield of H-5, H-6, upfield of H-3), all in respect to the free ligands. Another significant difference in the spectra of the Ga(III)-complexes (figure 23) compared to the ligands is observed in the signals of the ethylene protons. In the free ligand, the two protons of each methylene group are magnetically equivalent as a result of free rotation. These protons become non-equivalent as a result of the chelation by Ga(III) ion and form an AA'BB' spin system already described for similar systems including more detailed investigation, coupling constants and NMR spectra simulation have been reported previously for similar compounds.[103, 104] This spin system consists of distinct resonances corresponding to each of the four hydrogen atoms. Two protons H1A and H2A appear as two doublets at 3.07 and 3.33 ppm while the two protons H1B and H2B appear as two triplets at 2.85 and 3.79 ppm, respectively. This feature indicates a rigid structure of the metal complexes in solution which is consistent with the conformation found in the single crystal X-ray structure analysis as shown by axial/equatorial Newman representation (figure 24). In the crystallographic studies the close proximity of the H2B ethylene hydrogen atoms and imine groups of the neighbour leg is observed. They strongly interact with the π electron density of the imine bond causing a deshielding of their signal.

The ^{13}C NMR spectra additionally confirm the structures of the ligands and their Ga-complexes and are listed in table 2. Each spectrum for the ligand **2** and Ga(III)-complexes **3** consists of 14 signals, while the ligand **7** and Ga(III)-complex **8** contains 12 signals as expected. The resonance at 15.5 ppm is assigned to the thiomethyl group. The two resonances in the region of 55.5 and 61.9 ppm are assigned to the ethylene carbons. The signals attributed to the imine carbon atoms are slightly shifted upon coordination to 170 ppm in respect to the free ligands (table 2).

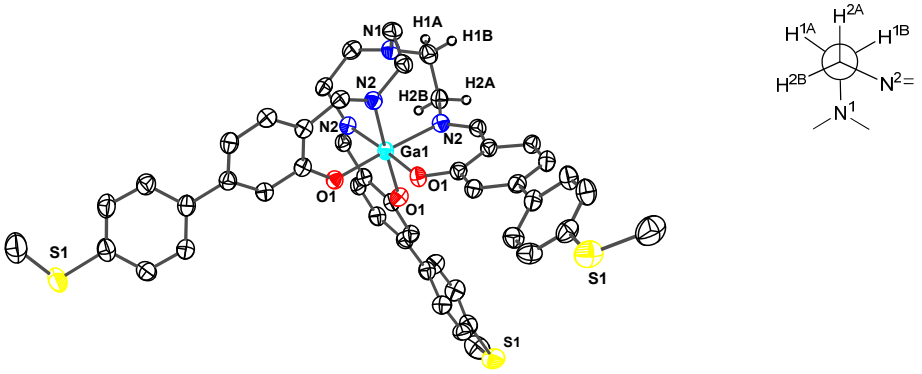

Figure 24. Single crystal X-ray structure *trensal* Ga(III)-complex 3 showing the ethylenic hydrogen atoms of one leg and the Newman projection of the ethylenic hydrogen atoms

Single crystal X-ray structures of M(III)-trensal complexes

The single crystal X-ray structures of the *trensal* complexes **3** and **8** with Ga(III), **4** with Fe(III) and **5** with Mn(III) ions are shown in figure 25. The crystallographic data and selected bond lengths and angles can be found in the Annex**.**

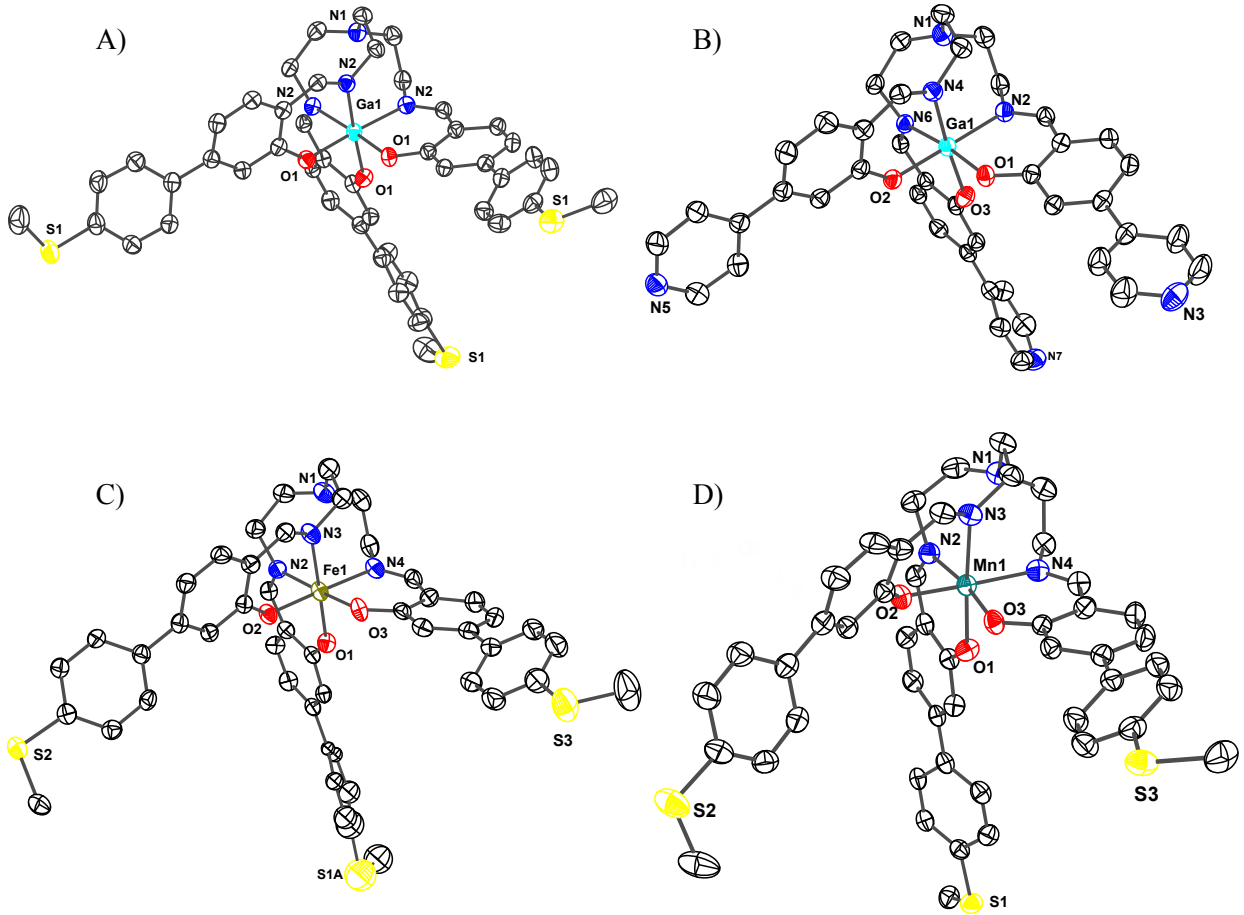

Figure 25. Single crystal X-ray single structures of: A) *trensal* Ga(III)-complex **3**; B) *trensal* Ga(III)-complex **8**; C) *trensal* Fe(III)-complex **4**; D) *trensal* Mn(III)-complex **5**. The hydrogen atoms and solvate molecules were omitted for clarity (ellipsoid plot drawn at 50% probability level).

All four M(III)-complexes present isostructural neutral complexes with triple salicyl-imine functions of the ligand completely encapsulating the M(III) ion. The apical nitrogen N1 is not involved in coordination and has a long distance to the metal in the range 3.31-3.42 Å. The ligand acts as a hexadentate ligand with three N- and three O-atoms which form for all *trensal* complexes a distorted *fac*-octahedral coordination geometry presented already in literature for similar complexes.[102, 103, 117, 120 -123] The M(III) ions lie on a three-fold axis (figure 26). The Ga-complex with thiomethyl groups **3** is highly symmetric with a C_3 space group, while the other M(III)-*trensal* complexes are pseudo-C_3 symmetric. However, the Ga-complex with pyridine-end units **8**, present a high symmetry in solution as showed by ^{1}H NMR. The deviation from symmetry of their crystal structures is probably caused by intermolecular packing in the crystal.

***Trensal* Ga(III)-complexes with thiomethyl end groups 3**

The tripodal Ga(III)-complex with thiomethyl end groups **3**, illustrated in figure 25A and 26, crystallizes in a trigonal R-$\bar{3}$ space group which implies total equality of the ligand legs. As the molecule has C_3 symmetry, the structure is defined by one third of the molecule. The three legs of the ligand form between N3 and O3 equilateral triangles with the ideal angle of 60°. Bond angles between coordinating atoms and the metal are deviated from 90° due to the chelate geometry: N2-Ga-N2'= 93.85°, N2-Ga-O=90.16°, N2-Ga-O'=85.54°, N2-Ga-O''=175.98°, and O-Ga-O'=90.48°. The differences between the Ga-N(2) and Ga-O distances, 2.10 Å respective 1.93Å and the deviation of the perpendiculars formed by N2-Ga-O1 sustain the octahedral distortion of the complex along the C_3 axis. The chelate rings formed by coordinating N and O atoms and the salicylidene-imine moieties are nearly coplanar with a dihedral angle between the chelating plane and the salicylidene-imine ring of 9°. The height of the entire molecule, between the apical N1 and the plane formed by the sulphur atoms is 8.24 Å. The distance N1-S has an average of 12.9 Å and the distances between gallium ion and sulphur atoms have an average of 11.0 Å. The distances between the three sulphur atoms of the ligand legs are identical with 17.2 Å.

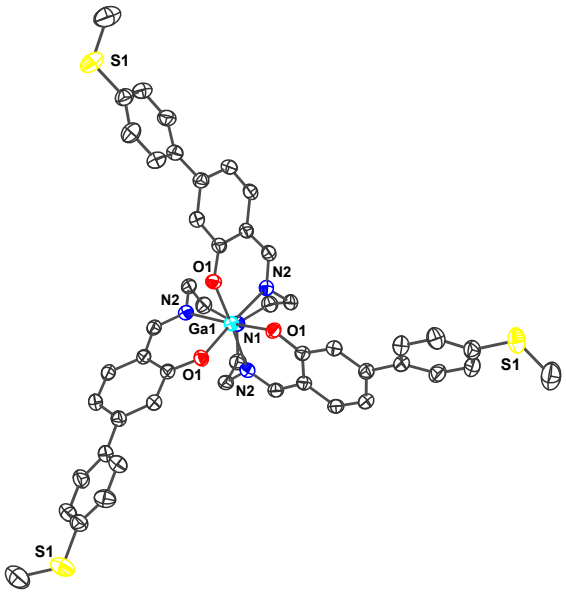

Figure 26. View along C_3 axis of *trensal* Ga(III)-complex **3**; the hydrogen atoms and the CH_2Cl_2 solvate molecule were omitted for clarity (ellipsoid plot drawn at 50% probability level).

The unit cell contains six molecules of Ga(III)-complex with each molecule having a CH_2Cl_2 solvate molecule close to one leg. The crystal packing exhibits two dimensional layers arrangement (figure 27). Each layer is separated by a distinct layer of solvate molecules. The phenolic units of each complex molecule is in weak intermolecular edge-to-face C-H···π interaction (3.35 Å, CH-centroid) with the phenyl rings of neighbouring molecules.

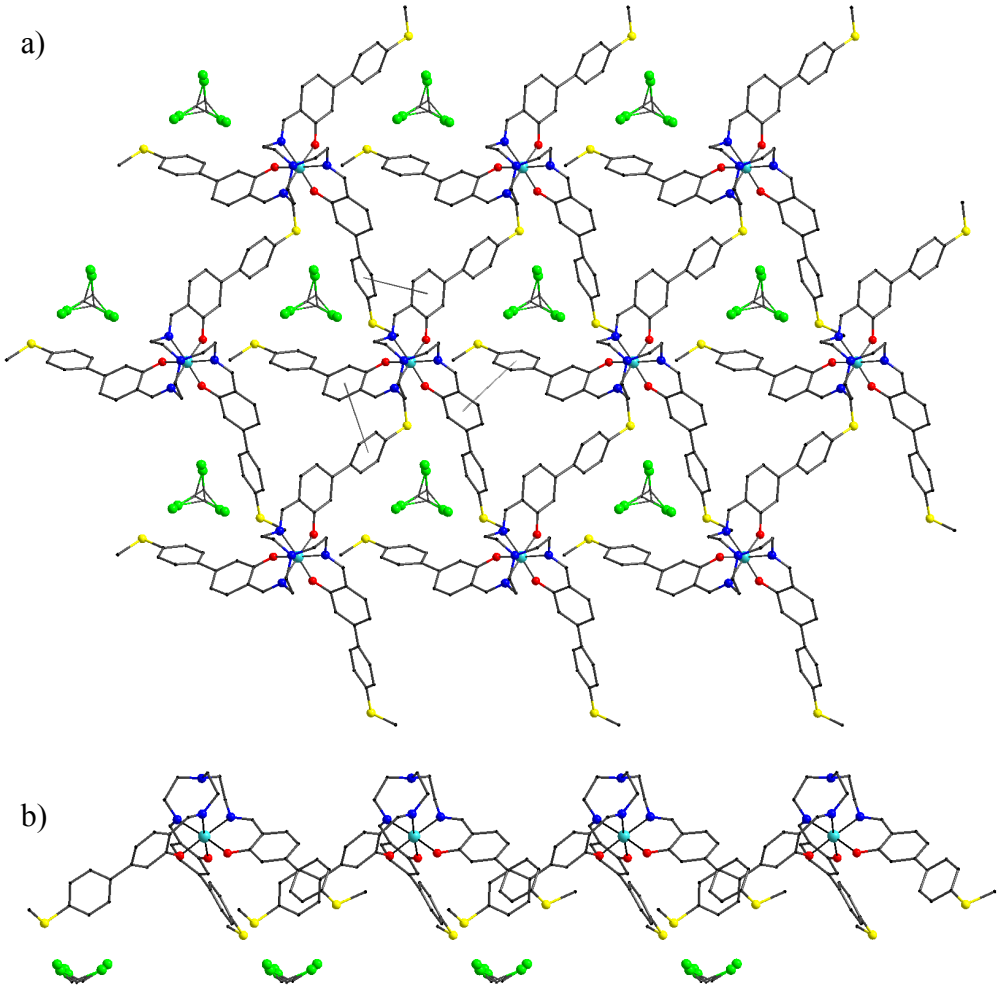

Figure 27. Molecular packing mode of the tripodal *trensal* Ga(III)-complex **3** obtained from single crystal X-ray diffraction; a) view along C_3 axis one of layer packing; the connecting lines between phenyl and phenolic units show the weak edge-to-face C-H···π intermolecular interactions of 3.35 Å. b) view perpendicular to the C_3 axis. The hydrogen atoms were omitted for clarity (sticks drawn).

***Trensal* Ga(III)-complex with pyridine end groups, 8**

Relatively to the highly symmetric Ga-complex **3** presented before, the complex with pyridine end groups **8** comprises a monoclinic space group $P2_1/n$. The unit cell contains four molecules of the Ga-complex. For each complex molecule one CH_2Cl_2 solvate molecule is filled inside the cavity formed by the three legs and has a close position to the phenolic groups (figure 28). The hydrogen atoms of CH_2Cl_2 can be considered to be in very weak interaction with the phenolic oxygen atoms (2.37Å). The crystal packing presents the complex molecules paired up as shown in figure 28. Intermolecular π···π stacking interactions between the phenolic groups of the neighbouring molecules are evidenced (3.74 Å, centroid-centroid).

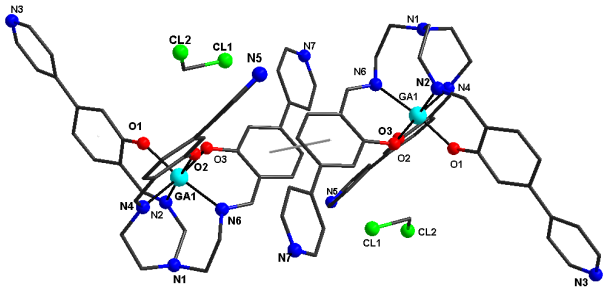

Figure 28. Molecular packing of the tripodal *trensal* Ga(III)-complex **8** obtained by single crystal X-ray structure, showing one of the π···π intermolecular stacking interactions (3.74 Å). The hydrogen atoms were omitted for clarity (sticks drawn).

***Trensal* Fe(III)-complex with thiomethyl end groups**, **4**

The molecular structure of *trensal* Fe(III)-complex presents a similar structure as found for the Ga(III)-complexes. A more distorted octahedral geometry than the Ga(III)-complexes is evidenced with the angles significantly deviated from 90°, ranging between 84.3 – 96.7° (Annex). The bond lengths are close to Ga(III)-complex values and present the same nearly coplanar chelate rings to salicylidene units.

From both methods of synthesis were obtained similar results of single crystal X-ray analysis although a completely different solubility of two compounds was observed. The two crystal structures data of the same *trensal* Fe(III)-complex differ only by the crystal space group and slight differences of lengths and bond angles (Annex). For both structures some of the phenylene thiomethyl end units are found refined in two positions and contribute to the slight deviation from C_3 symmetry. The difference in solubility obtained from the two synthetic methods is probably the effect of small differences in the crystal packing of the two structures. Intermolecular edge to face and π···π stacking interactions have been observed for both cases between the phenolic units of neighbour molecules shown in figure 29 (first synthetic method: 3.61 Å, centroid-centroid and 2.6 Å, CH-centroid; the second method: 3.74 Å, centroid-centroid and 2.5 Å, CH-centroid).

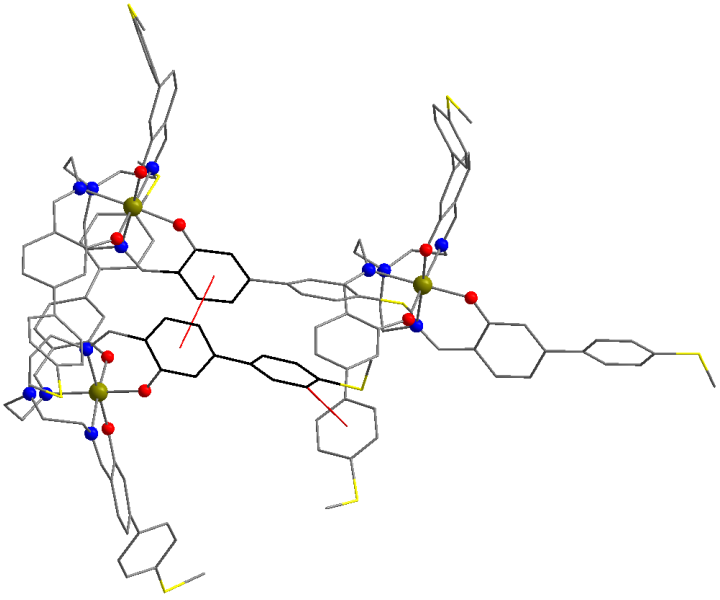

Figure 29. Molecular packing of the tripodal *trensal* Fe(III)-complex **4** showing the intermolecular stacking interactions π···π of 3.72 Å and edge to face of CH···π of 3.72 Å (red lines). The hydrogen atoms were omitted for clarity (sticks drawn).

***Trensal* Mn(III)-complex with thiomethyl end groups, 5**

The Mn(III)-complex crystallizes in monoclinic crystal system with $P2_1$ space group with four complex molecules per unit cell. Within the unit cell two different Mn(III)-complexes can be found which differ slightly in bond angles and bond lengths.

In contrast to the other *trensal* Schiff base complexes the molecular structure of the Mn(III)-complex is distinctly distorted from a regular coordination polyhedron. Results obtained by single crystal X-ray diffraction reveal that the cisoid angles within the hexadentate coordination sphere deviate significantly from the ideal value of 90° which would appear in an ideal octahedron (Annex).

Like in the other complexes the Mn(III) ion is coordinated by three imino-nitrogen atoms and three salicylen-oxygen atoms. These six donor atoms comprise three pairs of one imino group and one salicylate each originating from one of the legs. Within the leg moiety the N,O donor set form a chelate for the Mn(III) ion. Two chelate rings formed by coordinating N and O atoms are nearly coplanar to the salicylidene-imine plane while for the third leg the chelate ring features a dihedral distortion of 18° between the chelating plane and the salicylidene-imine plane. As a consequence of this dihedral distortion, the Mn(III)-complex molecule is considerably deviated from C3 symmetry in contrast to the Ga(III)- and the Fe(III)-complexes (figure 30).

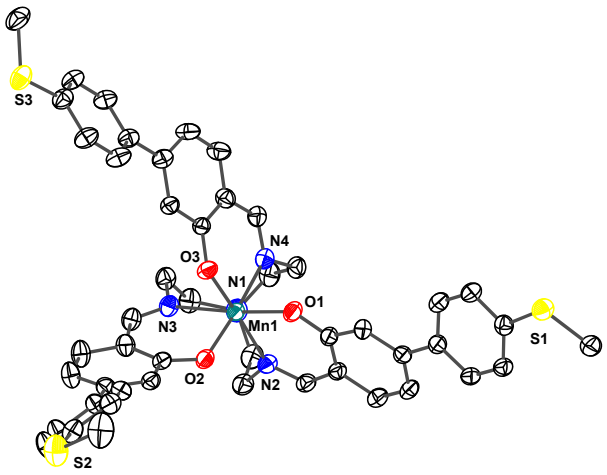

Figure 30. Single crystal X-ray structure of *trensal* Mn(III)-complex **5** showing the deviation from C_3 symmetry. The hydrogen atoms and the CH_2Cl_2 solvate molecule were omitted for clarity (ellipsoid plot drawn at 50% probability level).

As another measure how strong the ligand structure is distorted the bite angles of each of the legs can be taken into account, where O2-Mn-N3 = 85.08°, N2-Mn-O1 = 86.69° and O3-Mn-N4 = 90.09°. From these values can also be derived that two legs are similar to each other while the third leg obviously adapts a different coordination mode. A reason for this unsymmetrical spatial arrangement of the three legs has been allocated probably to a Jahn-Teller distortion of the high spin Mn(III) centre.[120, 124] As a result, strong elongation of bond distances between the metal ion and the donor atoms along a single axis is observed. The elongated bonds are situated in "trans" position to each other in respect to the metal. Thus, the distances of the atoms along the "elongated axis" are Mn-N3 = 2.333 Å and Mn-O1 = 2.085 Å

which is about 10% longer than their analogues along the other octahedron axes (Mn-N2 = 2,071 Å, Mn-N4 = 2.071 Å, Mn-O2 = 1.912 Å, Mn-O3 = 1.886 Å).

From the bond lengths of the Mn(III) ion to the donor atoms of the ligand we conclude that the metal ion is in a high spin d^4 (S=2) state, as has been reported for other *trensal* Schiff base complexes of Mn(III).[120]

Elemental analysis vs. purity. The presence of water of crystallization.

A significant effort was allocated to obtain analytical pure complexes. The elemental analysis of the all *trensal* M(III)-complexes in first instance results values pointing at the presence of water molecules in the solid state structure. The preference for similar Schiff base complexes to contain water of crystallization has been reported based on X-ray data. Moreover, the water of crystallization can form a hydrogen-bonded network with the oxygen of the phenolic units.[102, 117]

For Ga(III)-complex **3** the elemental analysis corresponding to the analytically pure structure was obtained only after high vacuum drying (100°C and 10^{-3} mbar, one week). A comparative ^{1}H NMR study of both, the pure solvent and the complex, for determination of water quantity in complex supports the elemental analysis with one water molecule per complex. This study was repeated after drying corroborating the removing of the water.

The elemental analysis for Ga(III)-complex **8** corresponds to the content of nearly three water molecules per complex in the solid state structure, which has also been confirmed by ^{1}H NMR. Thermogravimetric analysis supports the content of water by losing a total mass of 6%. The water content was reduced to 0.5 per complex molecule after drying under the same conditions as confirmed by ^{1}H NMR and elemental analysis. The representative NMR spectra are shown in the Annex.

While for the Ga(III)-complex **3** a good elemental analysis was obtained after repeated recrystallization and special condition of drying, the attempts to isolate solvent free Fe(III)- and Mn(III)-complexes failed. Again the elemental analysis supports the presence of one water molecule per complex molecule after drying. The presence of solvent or water cannot be evidenced by ^{1}H NMR for the paramagnetic Fe(III)- and Mn(III)-complexes.

Mass spectrometry, IR and UV vis characterization

The MALDI TOF mass spectra of the *trensal* ligands **2** and **7**, show for each compound a base peak of the corresponding mass $[M+H]^+$. The fragmentation of one leg (A) from the central nitrogen atom (fragment A in figure 31) is evidenced for both ligands as $[M-A]^+$. This leg fragmentation is consistent with literature reports.[118] The Ga(III)-complex **3** shows only the base peak of the corresponding mass at 890.4 $[GaL+H]^+$. The Ga(III)-complex **8** additionally to the base peak exhibits the fragmentation of one leg as $[GaL-B]^+$ presented in figure 32. The Fe(III)-complex **4** presents as expected the base peak at 877.7 of the mass $[FeL+H]^+$. Additionally, low intensity peaks of $[FeL+Na]^+$ or $[FeL+K]^+$ masses are present. Both methods of synthesis present similar results. The Mn(III)-complex **5** contains the base peak of $[MnL+H]^+$ and the combination with one MeOH molecule and Na^+ ion as $[MnL+MeOH+Na]^+$. The ESI

TOF mass spectrum confirms these results. Additionally, different aggregations or fragmentation in $[MnL\text{-}A]^+$, $[MnL+x]^+$, $[(MnL)_2+x]^{1+}$ (where x is H, Na or K) are evidenced in small intensities.

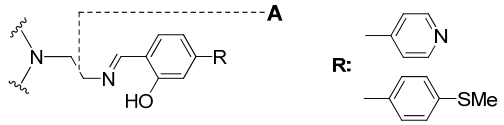

Figure 31. Mass spectrometric fragmentation of the *trensal* ligands **2**,**7**.

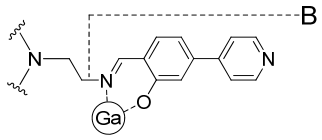

Figure 32. Mass spectrometric fragmentation of the Ga(III)- *trensal* complex **8**

The UV-vis spectra of the compounds **1**-**8** have (table 3) been measured in CH_2Cl_2 solutions. The spectra exhibit the modular composition of the respective chromophores. The spectra of the ligands and their metal complexes are dominated by the $n\rightarrow\pi^*$ and $\pi\rightarrow\pi^*$ transitions of the leg moieties whose appearance is approximately three fold in intensity in comparison to the free legs (226-340 nm). For the ligand **2** a partially allowed transition in low intensity at 416 nm in the blue end of the visible spectrum is responsible for the yellow colour to the *trensal* ligand and is assigned to the imine $\pi\rightarrow\pi^*$ transition.[118] In case of the Ga(III)-complexes, the ligand centered (LC) transitions are slightly red shifted upon coordination to the metal ion. The bands at 386 and 390 nm can probably be assigned to LC or ligand-to-metal-charge-transfer (LMCT) and no other low energy band can be observed. This is different for Fe(III)- and Mn(III)-complexes, where additional bands are observed as low energy shoulders. For the Mn(III)-complex the absorption at 595 nm is of very low intensity and can be assigned to spin-allowed crystal field transitions of the d^4 ion $^5E \rightarrow {}^5T_2$ (octahedral notation in lower symmetry group).[120] In case of the Fe(III)-complex the band at 521 nm can also be assigned to partially allowed crystal field transitions.

The IR spectra of the *trensal* ligands and their complexes, all contain the characteristic strong band in the region 1599-1640 cm^{-1} attributed to the C=N stretching vibration of the imine group. The complexation is confirmed by a slight shift (from 13 to 27 cm^{-1}) to lower energy of the imine band. These results are in agreement with literature findings.[118]

Table 3. Absorption values of the *trensal* ligands **2** and **7** and their M(III)-complexes recorded in CH_2Cl_2;

Compound	Absorption λ [nm] (ε x 10^{-3} [$M^{-1}cm^{-1}$])			
Leg **1**	226 (24.1)	337 (17.6)	-	-
Ligand **2**	226 (74.1)	310 (78.0)	416 (0.625)	-
Ga(III)-complex **3**	240 (73.7)	323 (78.3)	386 (35.3)	-
Fe(III)-complex **4**	235 (76.1)	315 (85.6)	370 sh (38.9)	521 (7.6)
Mn(III)-complex **5**	236 (64.5)	321 (65.8)	407 sh (16.3)	595 (0.750)
Leg **6**	226 (20.1)	279 (31.2)	340 (6.5)	-
Ligand **7**	227 (49.2)	276 (59.5)	331 (18.5)	-
Ga(III)-complex **8**	250 (64.3)	290 (65.7)	390 (21.2)	-

2.1.2.2. M(II)-*trenpy* complexes

This section describes the synthesis and characterization of *trenpy* tripodal metal complexes functionalized with thiomethyl or pyridine end groups. A series of coordination compounds was synthesized by varying the metal ion, ranging from: Fe(II) and Mn(II) to Zn(II). The complexes are charged 2+ and present diamagnetic behaviour in case of Fe(II)- and Zn(II)-complexes, while the Mn(II)-complexes are paramagnetic.

Synthesis of M(II)-*trenpy* complexes

The synthetic pathway of Fe(II)-, Mn(II)- and Zn(II)-complexes **11-13** with three thiomethyl anchoring groups is illustrated in Scheme 3. The Fe(II)-, Mn(II)- and Zn(II)-complexes **16-18** with pyridine end groups, are presented in Scheme 4. Since the two ligands and their complexes are very similar they will be discussed in parallel. A Suzuki-type cross-coupling reaction between 5-bromo-pyridine-2-carboxaldehyde and the respective boronic acid derivate yielded the corresponding functionalized aldehydes **9** and **14**. The following imine condensation between three equivalents of the latter with tris-(aminoethyl)-amine in EtOH afforded the functionalized tripodal *trenpy* ligands **10** and **15**.

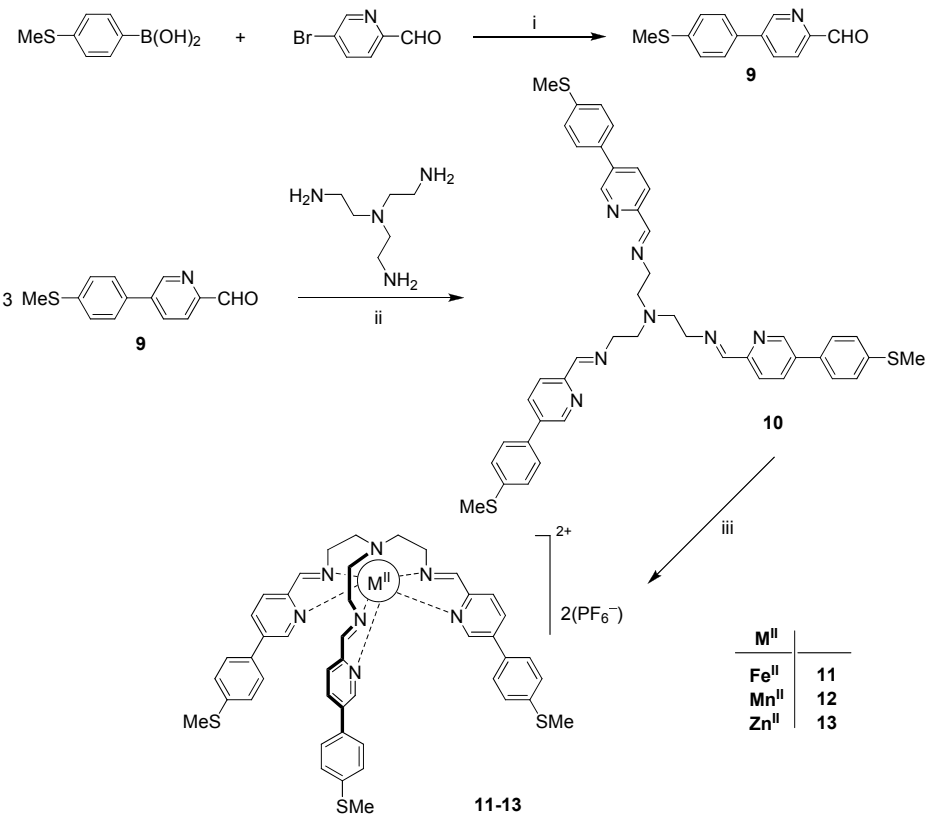

Scheme 3. Synthetic route of *trenpy* M(II)-complexes with thiomethyl end groups. Reagents and conditions: (i) $Pd(PPh_3)_4$, Na_2CO_3 aq., toluene/MeOH, N_2, 80°C, 62%; (ii) EtOH, rt, 86%; (iii) (**11**) $FeCl_2 \bullet 4H_2O$; 5eq. KPF_6, MeOH, rt, 70%; (**12**) $MnCl_2 \bullet 4H_2O$; 5eq. KPF_6, MeOH, rt, 77%; (**13**) $Zn(NO_3)_2 \bullet 6H_2O$; 5eq. KPF_6, MeOH, rt, 75%.

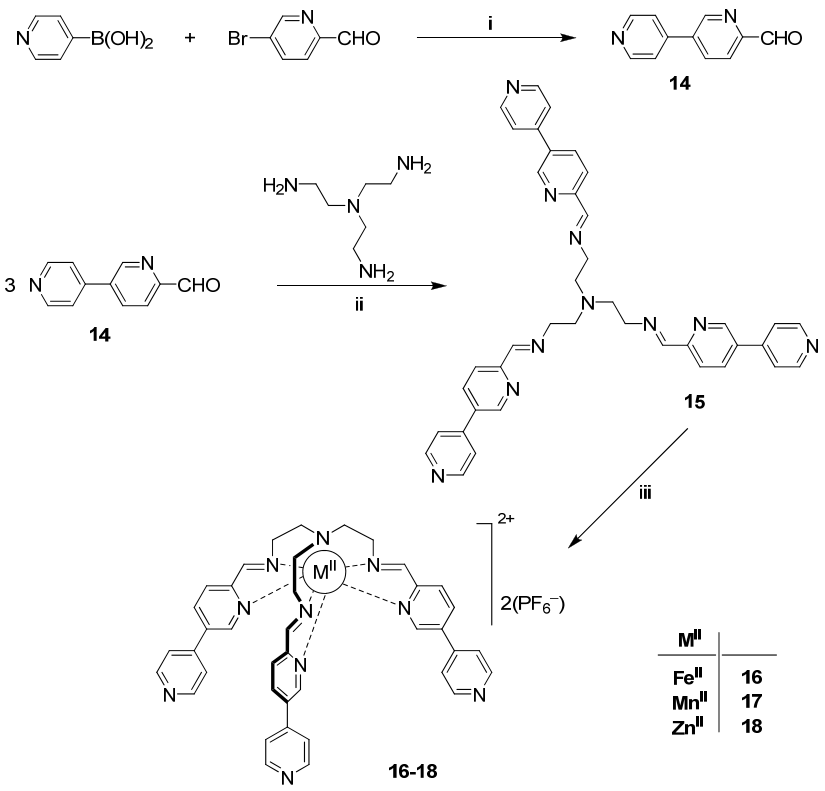

Scheme 4. Synthetic route of *trenpy* M(II)-complexes with pyridine end groups. Reagents and conditions: (i) $Pd(PPh_3)_4$, DME/H_2O, Na_2CO_3, N_2, 80°C, 72%; (ii) EtOH, rt, 56%; (iii) (**16**) $FeCl_2$•$4H_2O$; 5eq. KPF_6, MeOH, rt, 71%; (**17**) $MnCl_2$•$4H_2O$; 5eq. KPF_6, MeOH, rt, 60%; (**18**) $Zn(NO_3)_2$•$6H_2O$; 5eq. KPF_6, MeOH, rt, 72%.

The Fe(II)-complexes have been synthesized after a reported method [125] by mixing a suspension of the corresponding ligand in MeOH with a solution of $FeCl_2 \cdot 4H_2O$. Addition of an excess of KPF_6, induced the precipitation of the desired complex which was isolated by filtration. Recrystallization in acetone/MeOH gave the thiomethyl or pyridine functionalized *trenpy* Fe(II)-complexes. The Mn(II)- and Zn(II)-complexes have been obtained in the same way by mixing the ligand with the corresponding metal salt $MnCl_2 \cdot 4H_2O$ or $Zn(NO_3)_2 \cdot 6H_2O$ in MeOH, followed by addition of an excess of KPF_6.

Characterization of M(II)-*trenpy* complexes

The new *trenpy* ligands, and their M(II)-complexes have been completely characterized by ^1H and ^{13}C NMR, IR, UV-vis spectroscopy, ESI mass spectrometry and elemental analysis. All the characterizations confirm their molecular structure and the purity of the compounds. Additionally, the structures of the Fe(II)-, Zn(II)- and Mn(II)-complexes were determined by single crystal X-ray diffraction. In all metal complexes **11-13** and **16-18** the cations are charged 2+ which is compensated by two PF_6^- anions in each case. The NMR, magnetic measurements and single crystal X-Ray diffraction analysis of the *trenpy* Fe(II)-complexes demonstrate diamagnetic complexes with a low-spin state. While the Fe(II)- and Zn(II)-complexes present diamagnetic behaviour, the Mn(II)-complexes are paramagnetic. Structural data analysis of the later indicates a high spin compound in agreement with published structures.[109, 126] All the complexes are stable in air as well as in solutions. The Fe(II)-complex with

pyridine end groups is highly hygroscopic. Its elemental analysis corresponds to the content of two water molecules per molecule in the solid state structure, which has also been confirmed by ^{1}H NMR. The elemental analyses of all the other complexes prove the absence of water.

NMR Spectroscopic Data

Since the two *trenpy* ligands with thiomethyl or pyridine end groups and their M(II)-complexes are structurally analogous, they will be discussed in parallel. The signal shifts were assigned after reported values for similar compounds combined with the analysis of the coupling constants (table 4).

The ^{1}H NMR spectra of the ligands **10** and **15** shown in figure 33, are consistent with their structural formulae. The signal at 8.32 ppm (s) is assigned to the imine function. The ethylene groups exhibit an AA'XX' splitting pattern at 2.99 (t) and 3.79 (t) ppm as already presented for similar systems.[103, 104] The signal for the thiomethyl groups is found at 2.51 ppm (s) as expected. The ligand structure is also confirmed by ^{13}C NMR. A partial assignment was realized using DEPT135 NMR. The ^{13}C NMR spectrum for *trenpy* ligand with thiomethyl groups **10** consists of 13 signals and the *trenpy* ligand with pyridine end groups **15** of 11 signals. The ethylene carbon atoms are assigned by the two resonances at 55.2 and 59.9 ppm. The imine carbon signals are at δ 162.4 ppm and the thiomethyl groups at 15.3 ppm.

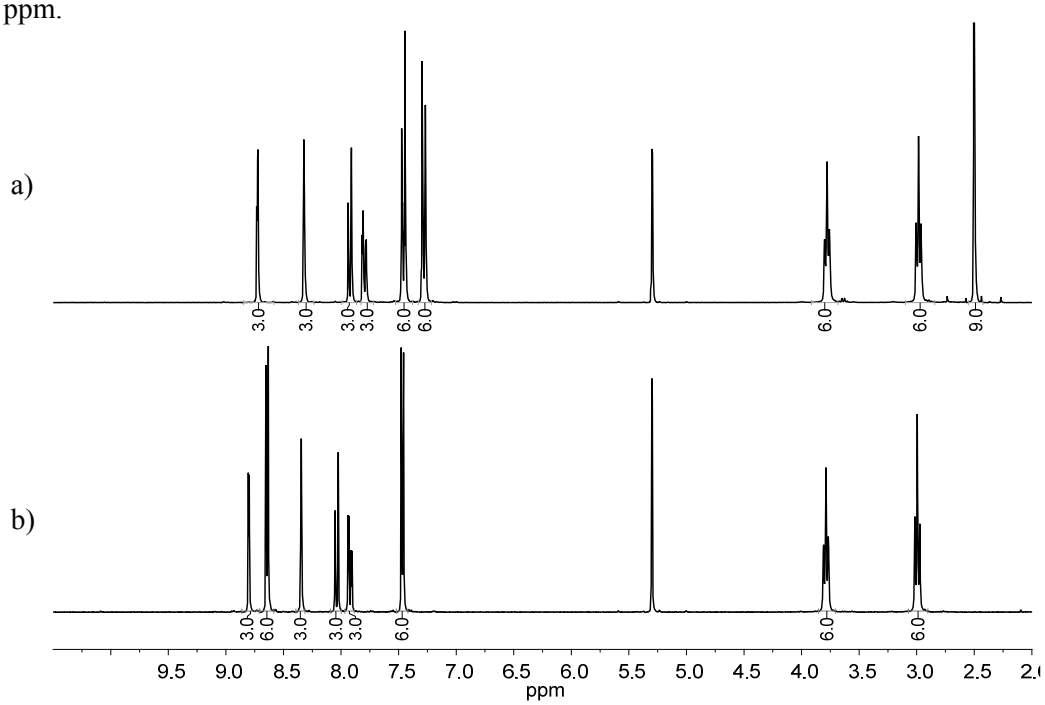

Figure 33. ^{1}H NMR spectra in CD_2Cl_2 of: a) *trenpy* ligand with thiomethyl end groups **10**; b) *trenpy* ligand with pyridine end groups **15**.

The ^{1}H NMR spectra of the Fe(II)-complexes **11**, **16** and Zn(II)-complexes **13**, **18** are shown in figure 34. After complexation the same AA'BB' spin system is observed, which is formed by the non-equivalent ethylene hydrogen atoms as has been presented before for *tren* capped containing complexes. The signals assigned to the imine protons involved in coordination are significantly shifted to low fields,

in particular for Fe-complexes ($\Delta\delta$ = 1.26). While the complexes with pyridine end groups contain the characteristic signals for the pyridine function (figure 34c,d), the complexes with thiomethyl groups present the characteristic signal at 2.47 ppm (figure 34a,b). Additionally, an AX pattern of the phenylic protons has been observed which keeps the chemical shift upon coordination almost constant. While the Zn(II)-complexes show clearly resolved the signals of the ethylenic AA'BB' spin system, for the Fe(II)-complexes the signals are closely assembled and the signals of pyridine protons are overlapped.

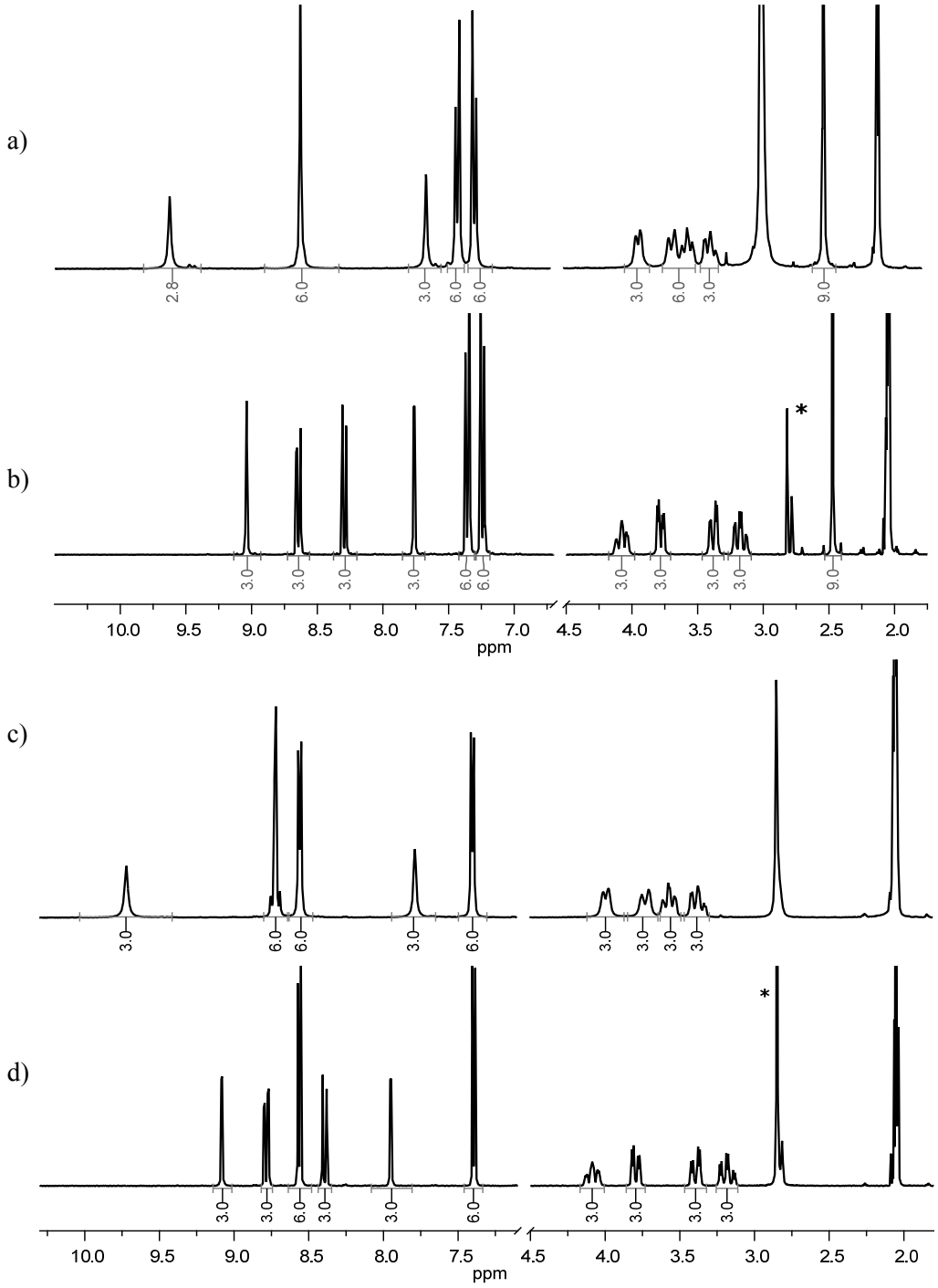

Figure 34. ^{1}H NMR spectra in CD_3COCD_3 (*H_2O, DHO) of the M(II)-complexes: a) Fe(II)-complex with thiomethyl end groups **11**; b) Zn(II)-complex with thiomethyl end groups **13**; c) Fe(II)-complex with pyridine end groups **16**; d) Zn(II)-complex with pyridine end groups **18**.

Table 4. ^{1}H NMR chemical shift of the ligands **10**, **15** (CD_2Cl_2) and their Fe(II)- and Zn(II)-complexes **11**, **13**, **16**, **18** (CD_3COCD_3).

Proton signals δ (ppm)	Ligand, **10**	Fe(II)-complex, **11**	Zn(II)-complex, **13**	Ligand, **15**	Fe(II)-complex, **16**	Zn(II)-complex, **18**
SCH_3	2.51	2.46	2.47	-	-	-
CH_2	2.99 3.78	3.34 3.51 3.63 3.89	3.17 3.38 3.78 4.08	2.99 3.79	3.37 3.57 3.72 3.99	3.18 3.39 3.79 4.09
Py^A	7.80 7.93 8.73	7.61 8.58	7.76 8.29 8.64	7.92 8.04 8.80	7.78 8.78-8.64	7.95 8.39 8.78
Ph	7.27-7.31 7.45-7.48	7.24 7.37	7.24 7.36	-	-	-
Py^B	-	-	-	7.47 8.64	7.40 8.56	7.40 8.56
CH=N	8.32	9.58	9.04	8.35	9.35	9.08

Single crystal X-ray structures of M(II)-trenpy complexes

In general the coordination polyhedra of *trenpy* M(II)-complexes are described as trigonal antiprism (TAP) which itself can be regarded as a very distorted form of a trigonal prism (TP).

The polyhedron model illustrated in figure 35, allows for the structural description and the distortions of coordination geometries found in six-coordinate complexes. The first model presents an octahedral or trigonal antiprismatic geometry and the second a trigonal prism. In case of *trenpy* M(II)-complexes the imine (N_{im}) and pyridine (N_{py}) nitrogen atoms are located at the vertices of the two equilateral triangles showed in the TAP coordination model (figure 35). The metal ion lies between the two triangles. The ratio **a/c** of the triangles lengths is a measure of size difference between the two triangles. The twist angle **Φ** is a projected angle between the two triangles (figure 36). The trigonal antiprismatic conformation has Φ = 60° and trigonal prismatic Φ = 0°. The regular octahedron has Φ = 60° and **a** = **b** = **c**, where **b** is defined as the "bite" chelate angle. The height-to-bite ratio **h/b** in case of an ideal octahedral is 0.816, while it is 1.0 for a trigonal prism.[109]

A summary of the mean values that describe the coordination polyhedron of the *trenpy* M(II)-complexes is given in table 5. There are different kinds of distortions from the D_3 symmetry of an ideal TAP: a) the trigonal distortion toward a TP coordination sphere given by the twist angle **Φ**; b) different sizes of the two triangles defined by the ratio **a/c**; c) the displacement of the metal ion from one triangle towards the other and d) the deviation of the triangles from equilateral arrangement. The Fe(II)-complexes have the most octahedral coordination sphere. The Mn(II)-complexes are the most distorted from an octahedron coordination polyhedron, followed closely by the Zn(II)-complex (figure 37).[109]

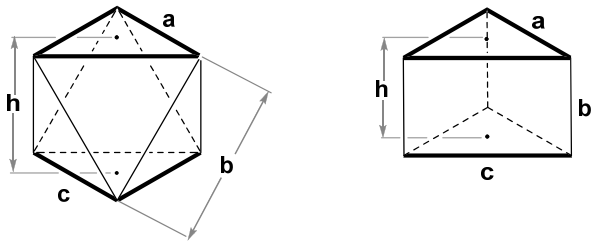

Figure 35. Coordination polyhedron model of TAP and TP. The two triangles have side lengths **a** and **c**. The metal ion lies between the two triangles. The distance between the centres of triangles is the height **h**. The non-bonding distance between chelating imine N_{im} and pyridine N_{py} atoms in the same chelating ring is the bite distance **b**. [109]

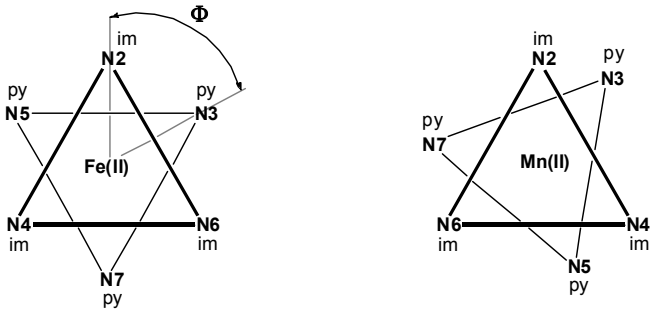

Figure 36. Trigonal antiprism geometry of the Fe(II)- and distorted trigonal antiprism geometry of Zn(II)- and Mn(II)-complexes.

Table 5. Crystallographic summary of the coordination polyhedron values for Fe(II)-, Mn(II)- and Zn(II)-complexes; [a] distances are given in Å, angles are given in degrees; where is the case the parameters are given in mean values;

Parameter [a]	Fe(II)-complex, **11**	Fe(II)-complex, **16**	Zn(II)-complex, **13**	Mn(II)-complex, **12**	Mn(II)-complex, **17**
Φ, twist angle	53.23	54.63	46.64	41.09	41.58
M - N_{ap}	3.47	3.50	2.87	2.54	2.69
M - N_{im}	1.95	1.95	2.11	2.22	2.22
M - N_{py}	1.97	1.98	2.28	2.41	2.38
a	2.91	2.88	3.35	3.64	3.58
c	2.87	2.92	3.11	3.15	3.19
a/c	1.015	0.987	1.077	1.156	1.122
h (height polyhedron)	2.06	2.04	2.25	2.29	2.302
b (“bite distance”)	2.55	2.55	2.69	2.68	2.699
h/b	0.810	0.798	0.834	0.853	0.854
N_{ap} - S plane	11.1	-	11.3	11.7	-
N_{ap} - Py end group plane	-	9.2	-	-	9.9
M - S plane	7.7	-	8.4	9.2	-
M - Py end group plane	-	5.7	-	-	7.3
between S end-groups	9.4 - 10.6	-	8.9 - 9.8	6.2 - 7.1	-
between Py end-groups	-	9.4 - 10.2	-		7.0 - 7.6

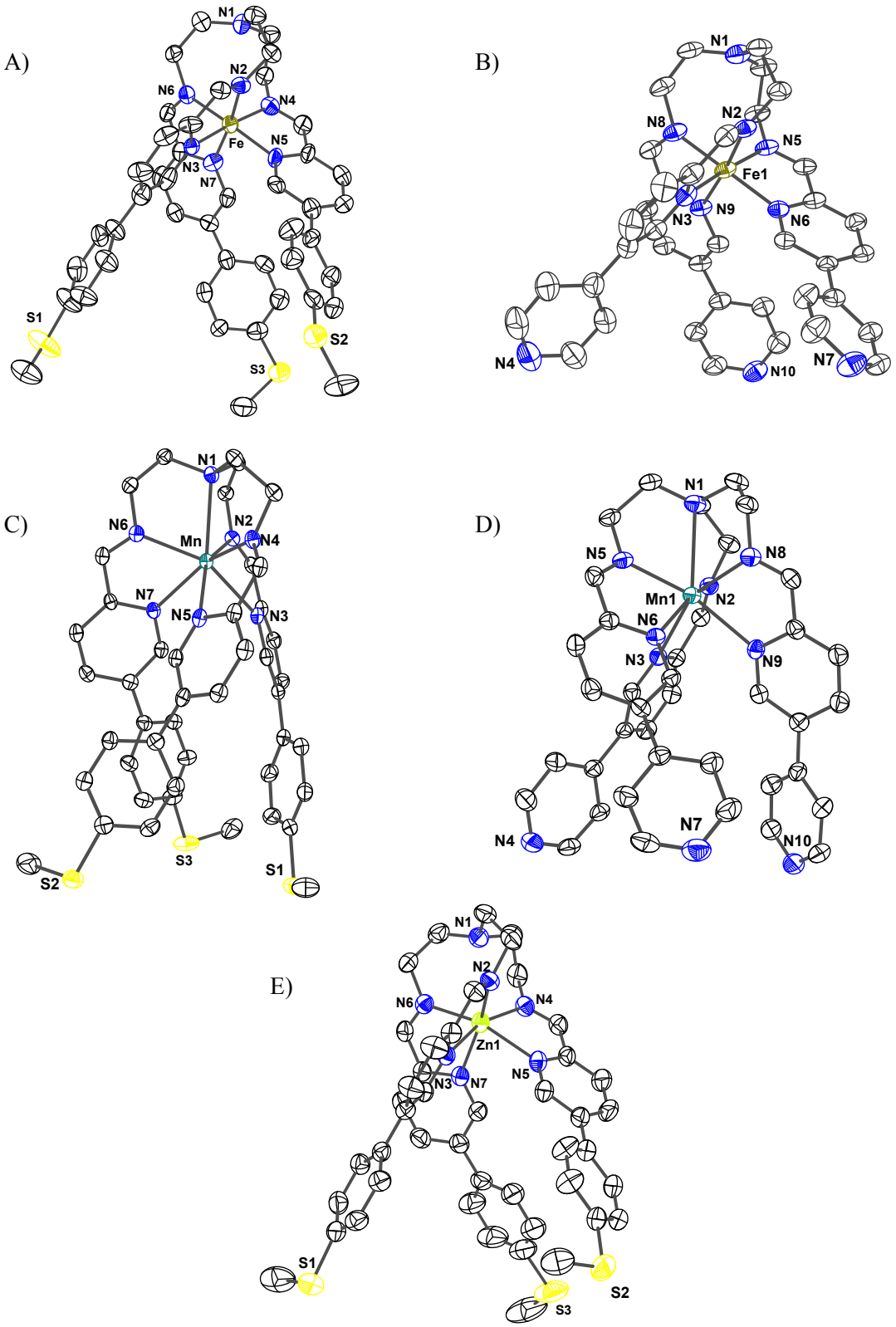

Figure 37. Single crystal X-ray structures of the tripodal M(II)-complexes: A, B) *trenpy* Fe(II)-complexes **11** and **16**; C, D) *trenpy* Mn(II)-complexes **12** and **17**; E) *trenpy* Zn(II)-complex **13**. The hydrogen atoms, PF_6^- counter ions and solvate molecules were omitted for clarity (ellipsoid plot drawn at 50% probability level).

Trenpy **Fe(II)-complexes 11, 16**

The molecular structures of the complex cations **11** and **16** (figure 37A, B) obtained by single crystal X-ray diffraction present a "pseudo" octahedral geometry, characterized by sixfold coordination of

the metal ion. The charge is compensated by two PF_6 anions, in perfect agreement with the mass spectrometric finding of a double charged cation. The potentially heptadentate *trenpy* ligand coordinates to the metal centre through the three pyridine and three imino nitrogen atoms, each set of atoms forming two parallel ideal equilateral triangles. The Fe(II) ion is situated between these two almost coplanar planes.

The two parallel triangles are rotated by 58° (figure 36), thus the geometry is close to the ideal trigonal antiprism. The average values for Fe-N_{py} and Fe-N_{im} bond lengths are 1.94 and 1.97 Å respectively which confirms low spin electronic configuration. Bond angles between coordinating atoms and metal are deviated from 90° (between 80.3 and 97.4°) due to the chelate geometry. The apical nitrogen atom N1 has a long distance of 3.5 Å to the Fe centre for both complexes. This distance is too long to consider any interaction between the atoms and hence it is regarded not to be involved in coordination. The height of the entire molecule, between the apical N1 and the plane defined by the three sulphur atoms is 11.1 Å. The distance between Fe(II) and plane defined by the sulphur atoms is 7.7 Å. The distance N1-S has an average of 12.6 Å and the distances between Fe(II) and sulphur atoms have an average of 9.6 Å. The distances between the three sulphur atoms of the ligand legs range between 9.4 and 10.6 Å.

***Trenpy* Mn(II)-complexes 12, 17**

The molecular structures of Mn(II)-complexes **12**, **17** (figure 37C, D) differ severely from the Fe(II)-complexes. The most apparent difference is that the Mn(II) ion is coordinated by seven nitrogen donor atoms of the *trenpy* ligand contrary to the [N_6] coordination of the Fe(II) complex. The apical nitrogen atom N1 has a distance of about 2.6 Å to the manganese centre, which is much shorter than in Fe(II)-complex (3.47 Å). Thus, a considerable participation to the coordination takes place. The average values for Mn-N_{py} and Mn-N_{im} bonds range between 2.38 and 2.22 Å respectively, which are longer than in Fe(II)-complex (Annex). The Mn(II) atom is located in between two parallel and equilateral triangles which are formed by the three pyridine and three imino N atoms respectively. The planes formed by the two triangles are almost coplanar and their vertices are twisted by an angle of 41°, thus the geometry is distorted from a trigonal prism (figure 36). Similar compounds are reported in literature as a seven-coordinate monocapped distorted trigonal antiprism.[109, 126]

The height of the entire Mn(II)-complex with thiomethyl groups, between the apical N1 and the plane formed by the sulphur atoms is 11.7 Å and the distance between Mn(II) and the sulphur atoms plane is 9.18 Å. The distance N1-S has an average of 12.32 Å and the distances between Mn(II) and sulphur atoms have an average of 9.93 Å. The distances between the three sulphur atoms of the ligand legs are between 6.19 and 7.12 Å.

***Trenpy* Zn(II)-complex with thiomethyl end groups, 13**

The molecular structure of *trenpy* Zn(II)-complex (figure 37E) presents a similar structure as found for the Fe(II)-complexes where the apical nitrogen is not involved in the coordination. A more

distorted "pseudo" octahedral geometry than the Fe(II)-complexes is evidenced by the cisoid N-Zn-N angles which are significantly deviated from 90°, ranging between 74.8 - 106.5° (Annex). The complex contains the same six fold coordination number of the metal ion defined by three imine and three pyridine groups and is charge compensated by two PF_6 anions. The M(II)-N bond lengths assume intermediate values for the Zn(II) complex, laying between Fe(II)- and Mn(II)-complexes. The two triangles consisting of the three imino nitrogen atoms and the three pyridyl nitrogen atoms are twisted with an angle of 46.6° relative to a trigonal prism. This distortion is similar to the Mn(II)-complexes, yet again it has to be emphasized that Zn(II)-complex is only sixfold-coordinated.

Mass spectrometry, IR and UV vis characterization

The ESI mass spectra of the Fe(II)-, Mn(II)-, and Zn(II)-complexes show base peaks for $[ML]^{2+}$ and $[LM(PF_6)]^{1+}$ which confirm their structures. For the Fe(II)- and Mn(II)-complexes the fragmentation or aggregation with PF_6 have been observed in very low intensity as $[LM(F)]^{1+}$, $[(LM)_3(PF_6)_4]^{2+}$, $[(LM)_4(PF_6)_6]^{2+}$. In negative ionization mode only the $(PF_6)^-$ counter ion can be found as expected.

The UV-vis spectral data of the *trenpy* complexes recorded in CH_3CN solutions are presented in table 6. The spectra exhibit a modular composition of the respective chromophores. The spectra are dominated by the $n \rightarrow \pi^*$ and $\pi \rightarrow \pi^*$ transitions of the leg moieties at 246 - 332 nm. However, the peaks appear with threefold intensity in comparison to the free leg **9**. In case of Zn(II)- and Mn(II)-complexes with thiomethyl end groups **12** and **13** the ligand based transitions are slightly red-shifted (349, 351 nm for **12** and 263, 265 nm for **13**), with an absence of further low energy bands. The ligand based bands can be assigned to both ligand centered (LC) and ligand to-metal charge-transfer (LMCT) contributions. This is different for Fe(II)-complex **11** where a strong metal-to-ligand charge-transfer (MLCT) band appears at 576 nm with a blue sided shoulder at 528 nm.[127] Additionally, the band at 364 nm can probably be assigned to a mixture of the LC and LMCT contributions. The M(II)-complexes with pyridine end groups **11-13** exhibit in principal the same transitions as described above for their analogues with thiomethyl end groups **16-18** (table 6).

Table 6. Absorption values and extinction coefficients of the *trensal* ligands **10** and **15**, and their M(II)-complexes in the UV-vis region recorded in CH_3CN

Compound	Absorption λ [nm] (ε x 10^{-3} [$M^{-1}cm^{-1}$])			
Leg **9**	246 (13.1)	332 (22.1)		
Ligand **10**	247 (32.4)	323 (62.2)	-	-
Fe(II)-complex **11**	240 (58.1)	364 (55.6)	528 (8.75)	576 (13.4)
Mn(II)-complex **12**	265 (63.2)	349 (61.9)	-	-
Zn(II)-complex **13**	263 (49.5)	351 (50.1)	-	-
Ligand **15**	265 (61.0)	283 sh (55.3)	-	-
Fe(II)-complex **16**	293 (53.9)	386 (78.3)	530 (8.75)	579 (10.85)
Mn(II)-complex **17**	260 (38.0)	298 (47.5)	-	-
Zn(II)-complex **18**	260 (42.1)	298 (51.5)	344 (1.9)	-

The IR spectra of Mn(II)-complexes and Zn(II)-complexes present the characteristic imine C=N stretch at about 1660 cm^{-1} slightly shifted to higher energy compared to the ligand (figure 38). The two lower energy bands at about 1590 cm^{-1} and 1570 cm^{-1} are assigned to pyridine vibration modes.[109] All the complexes show a very strong band at approx. 840 cm^{-1}, assigned to the stretching vibration of P-F bonds in the PF_6^- anion groups (figure 38a).

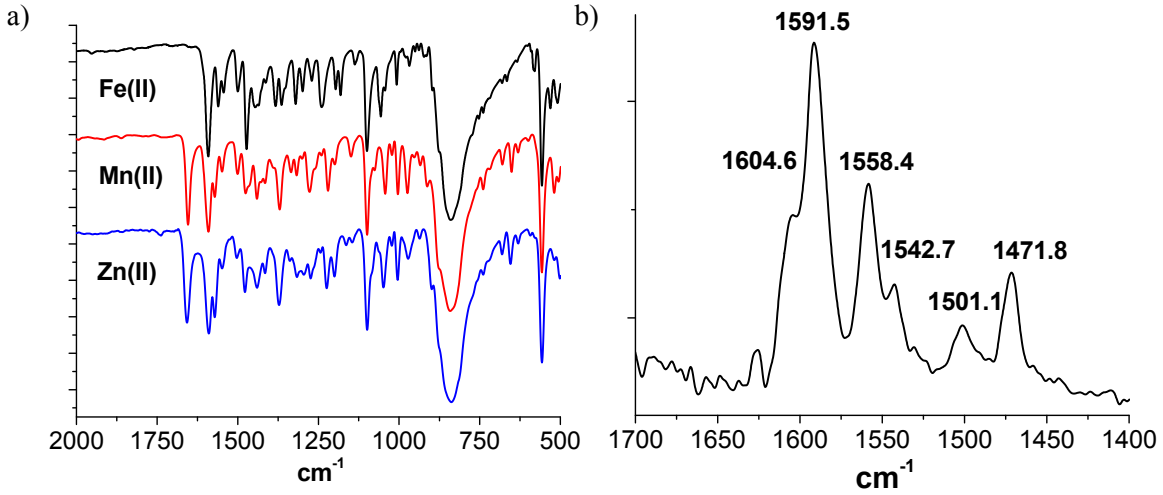

Figure 38. a) IR spectra of the *trenpy* M(II)-complex with thiomethyl end groups **11**, **12** and **13**; b) Raman spectrum of the Fe(II)-complex **11**.

In the case of Fe(II)-complex with thiomethyl end groups **11** the imine C=N stretching vibration mode is not observed. This special behaviour has previously been reported for low-spin analogues and was explained by low energy MLCT transitions that lead only to the resonance Raman enhancement when the exciting frequency approaches that of the MLCT.[109, 128] Raman spectroscopy is a sensitive technique for accurate determination of imine stretching frequencies in low-spin Fe(II)-complexes. The Raman spectrum (figure 38b) reveals the symmetric vibrations at 1605 (medium) assigned to (C=N) and the two pyridine vibrations at 1592 (strong) and 1558 cm^{-1}. The C=N vibration occurs at a smaller value than for other M(II)-complexes, as already described.[109, 128] In the IR and Raman spectra of the Fe(II)-complex with pyridine end groups **16** additionally to the pyridine vibration at 1564 cm^{-1} an intense band at 1603 cm^{-1} is observed, which probably covers contributions from both, imine and pyridine.

Magnetic susceptibility measurement

The magnetic measurement realized for *trenpy* Fe(II)-complex **11** shows that the complex remains low spin up to 350 K as shown in figure 39.

The temperature dependence of the magnetic susceptibility has a value of maximum 0.02 $cm^3K\ mol^{-1}$ with $\mu_{eff} \approx 0.43$ BM. The value of effective magnetic moment (μ_{eff}) in Bohr magnetons has been calculated using the following equation:

$$\mu_{eff}\,(BM) = 2.83[\,\chi_M\,T]^{1/2},$$

where χ_M is the molar susceptibility ($cm^3\ mol^{-1}$) and *T* the absolute temperature (K).[129]

The diamagnetic, low spin character of **11** has been already proved by NMR spectroscopy and X-ray data. Several magnetic studies for this type of compounds are reported.[109] A similar behaviour is assumed for its analogue with pyridine end groups **16** as shown by NMR spectroscopy and X-ray crystallographic study.

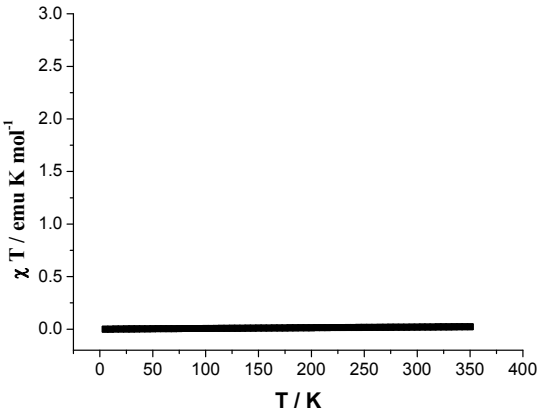

Figure 39. Temperature dependence of the magnetic susceptibility of *trenpy* Fe(II)-complex **11**, exhibiting low spin behaviour from 5-350 K.

Cyclic voltammetry

Cyclic voltammograms for Fe(II)-complex **11** in MeCN anh. electrolyte solution with Bu_4NPF_6 using an non-aqueous reference electrode have been measured. The potential values are calibrated against the ferrocene redox couple as internal standard (Fc^+/Fc at 0.380 V vs. SCE).[130, 131]

The data are consistent with reversible one electron oxidation of Fe(II)/Fe(III) as shown in fig. 40. The Fe(II) $\rightleftharpoons$ Fe(III) half-wave oxidation potential is found at +0.927 V, which is close to the reported oxidation values of similar compounds.[132] The ligand-centered reduction was observed at the potential of -1.117 V in the window (-1.5, 1.5V). As can be seen in figure 40 at higher window potential of (-2, 2.5 V) a total of three reversible reductions at negative potentials are observed. This can be possible attributed to three subsequent single electron reductions at the three different ligand legs.

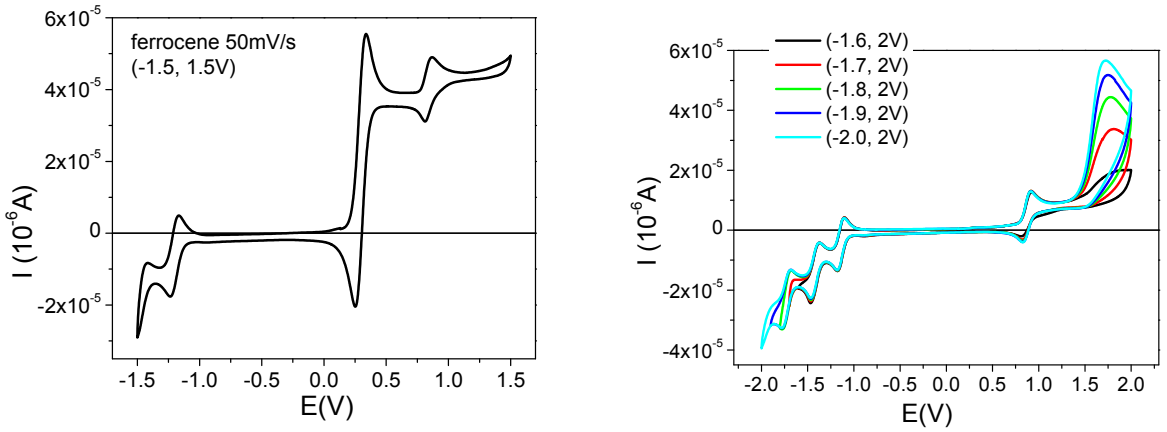

Figure 40. Cyclic voltammograms of Fe(II)-complex **11**; left, in presence of the ferrocene as internal standard (Fc^+/Fc of 0.380 V *vs.* SCE); right, oxidation at +0.927 V and the three reduction potentials.

In summary, we have synthesized and characterized new tripodal Schiff base complexes functionalized with thiomethyl or pyridine end groups for surface investigation. The *trensal* and *trenpy* type of complexes with different metal ions offer structural and electronic variation as well as a dependence of the spin state on the implied donor set in the coordination sphere.

The results of single crystal X-ray diffraction for the tripodal Schiff base complexes clearly show how the free ligands wrap tightly their legs around the metal ions, rendering the α-triimine moiety relatively rigid and co-planar in respect to the three pyridyl or salicyl legs.[109] The coordination of the ligand forces the three legs with thiomethyl or pyridine end groups into a prismatic form rendering the thiomethyl or pyridine end groups into a predestined direction. Thus the metal complexes with thiomethyl end groups could be attached on a suitable flat support such as the Au(111) crystal edge. In case of an ideal tripodal anchoring of the thiomethyl functions, the M(III) or M(II) metal ions take an elevated position toward the surface. As each of those metal ions has a different electronic impact on the coordinated ligand, different tunnelling current characteristics can be expected. Preliminary STM measurements through self-sustained complex molecules have been investigated by deposition in "sub monolayer" on Au(111) from CH_2Cl_2 solutions.

2.2. *Facial* and *meridional* Ru(II)-bipyridine complex

2.2.2. Introduction

In photochemistry, the class of Ru(II)-polypyridine complexes represents important building blocks which have been extensively studied due to their cumulated charge-transfer characteristics, chemical stability, excited state reactivity and lifetime, photophysical and redox properties.[133, 134] These complexes have found extensive application as catalysts in photoinduced electron-transfer processes,[135, 136] photosensitizers for solar energy conversion in artificial photosynthesis [137, 138] and dye-sensitized solar cells.[139, 140] Since the invention of first dye-sensitized solar cell in 1991 by M. Grätzel based on a Ru(II)-tris(2,2'-bpy) complex derivate, the synthesis of a large variety of Ru(II)-complexes received a great interest. Photoactive systems based on polynuclear ruthenium complexes have been developed to enhance photochemical and photophysical properties by antenna-light-harvesting effect.[141, 142] More recently researchers focused not only to increase the efficiency of dye-sensitized solar cells but also to replace the rare ruthenium with other more abundant metal-complexes.[143, 144] Moreover, all these properties and applications attracted the incorporation of this type of metal-complexes in nanotechnology as potential photon-induced switches [145-147] and into molecular machines and devices.[148, 149]

Besides the intensely studied photochemistry, the topology of tris-bidentate complexes of the octahedrally coordinated Ru(II) ion plays an important role. In particular, in case of unsymmetrically functionalized 2,2'-bipyridine ligands, the homoleptic tris-chelate $[RuL_3]^{2+}$ complex adopts two geometrical forms: the facial (*fac*) and meridional (*mer*) stereoisomers. Additionally, these types of metal complexes can adopt two optical isomers Δ and Λ (figure 41). Together these four stereoisomers consist of the same chemical formula but possess different structures which can effect different physical and chemical properties.[150]

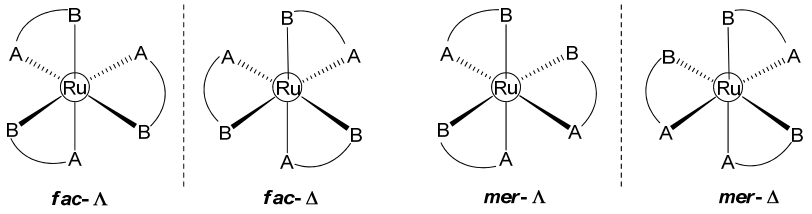

Figure 41. The four stereoisomers (two enantiomeric pairs) of unsymmetrical Ru(II)-*trisbpy* complex

The distinction between the two *fac* and *mer* isomeric species of $[Ru(bpy)_3]^{2+}$ complexes have been realized by ^1H NMR spectroscopy [150, 151] and the full assignment was performed by use of 2D NMR techniques.[151, 152] Evaluations based on NMR spectroscopy of the changes in electron density within ligands occurring upon chelating the Ru(II) ion, were explained in details for the parent $[Ru(bpy)_3]^{2+}$ and compared to theoretical methods. The NMR coordination-induced shifts were described to be affected by

different effects as: σ- and π-electron polarization in coordinated heterocycles, magnetic anisotropy of neighbouring ligands and metal-ligand bonds, van der Waals interactions, and solvent effects.[153]

Here we present the successful synthesis, separation and characterization of a new pair of *fac* and *mer* tripodal Ru(II)-complex for electronic transport studies on metallic surfaces at the single molecule level.

The design, synthesis and isolation of a tripodal metal complex containing three conjugated legs with thioacetyl end groups which geometrically face to one side (*fac* isomer) - suitable for multi-attachment on gold electrodes - turned into our focus. Its analogue, the *mer* isomer is prearranged to connect two legs on one side to metallic surface with the third leg facing free upward for the attachment of a tip e.g. by AFM contact. In this regard we adopted a strategy based on 2,2'-bipyridine motif, capable to contain a conjugated structure with thioacetyl protective end-groups. One major demand on the ligand design is the compatibility with the conditions for complexation and purification.

From previously published works describing the synthesis of unsymmetrical 2,2'-bipyridine Ru(II)-complexes which can adopt the two geometrical configurations *fac* and *mer*, the main problem to synthesize such structures derives from the difficulties in separation of the two isomers. In a statistical approach, in the reaction mixture three parts of *mer*-isomer will be formed to one of the *fac*-isomer, but it can be modified by several parameters. Recent works reported a variety of reaction conditions, solvents and temperatures for improving the formation of one isomer.[150, 154] Strategies for blocking the ligand in a tripodal structure to obtain only the *fac* isomers have been implemented.[155 - 157] Another method applies steric effects by using bulky or electron-withdrawing side groups to preferentially favour one of the isomer.[150, 151, 158] Laborious, expensive and sometimes unsuccessful separation methods are reported, starting with very long 2-3 m cation-exchange chromatography on sephadex columns,[151] preparative silica thick layer chromatography plates[150, 154, 159] or only partial resolution on neutral alumina.[152] Under such difficult conditions very small quantities of isomers can be isolated. Thus only few reports characterize and compare the two geometrical isomers with each other, an important aspect as far as the fabrication of new materials is concerned.[159] Taking all these considerations into account, our strategy required the synthesis of a ligand containing a conjugated longer side which after coordination can be exploited for an easier column chromatography separation. The unsymmetrical *mer* isomer having a longer structure and a smaller diameter compared to the *fac* isomer provides a difference in polarity between the two isomers.

The isolation of each of the two constitutional isomers is of primary importance for the attachment and the geometrical control on the metallic surfaces. However, to our knowledge, single isomer *fac* or *mer* 2,2'-bipyridine based M(II)-complexes have not been reported for metal surfaces studies so far.

2.2.2. Results

Synthesis of *fac* and *mer* Ru(II)-*trisbpy* complexes with thioacetyl end groups

The preparation of the Ru(II)-*trisbpy* complex is depicted in Scheme 5. The ligand synthesis was achieved by Sonogashira coupling reaction of 5-ethynyl-2,2'-bipyridine **19^{ii}**, [160] with 4-(thioacetyl)-iodobenzene.[161] The 5-ethynyl-2,2'-bipyridine was synthesized by Sonogashira reaction with TMSA followed by deprotection of trimethylsilyl group after a slightly modified procedure.[160] The ^{1}H and ^{13}C NMR spectra of these two intermediates are in agreement with the literature.[160]

The complexation reaction was realized by coordination of three eq. of ligand with $Ru(DMSO)_4Cl_2$,[162, 163] in refluxing EtOH under Ar after a modified reported method.[150] The synthesis resulted in both *fac* and *mer* isomers. The *mer* isomer exhibited higher R_f values than the *fac* isomer in the TLC conditions ($MeCN/H_2O/KNO_3$) performed during the reaction and was applied for flash column chromatography on silica gel. The preparative thick layer chromatography silica plates in the same conditions lead in our case only to a partial separation of the two isomers. Column chromatography offers an easier separation of *fac* and *mer* isomers based on a pronounced difference between the polarity and the isomer geometry. The column chromatography separation was realized under Ar gas flow to prevent a possible hydrolysis of the thioacetyl-end groups. After separation, anion metathesis was carried out by application of excess of KPF_6 aq. in MeCN at rt. As an indication of purity of the two isomers after metathesis the TLC (in before mentioned conditions) demonstrated two very distinct spots. The separation of the two isomers is confirmed by ^{1}H NMR and single crystal X-ray diffraction of the *fac* isomer.

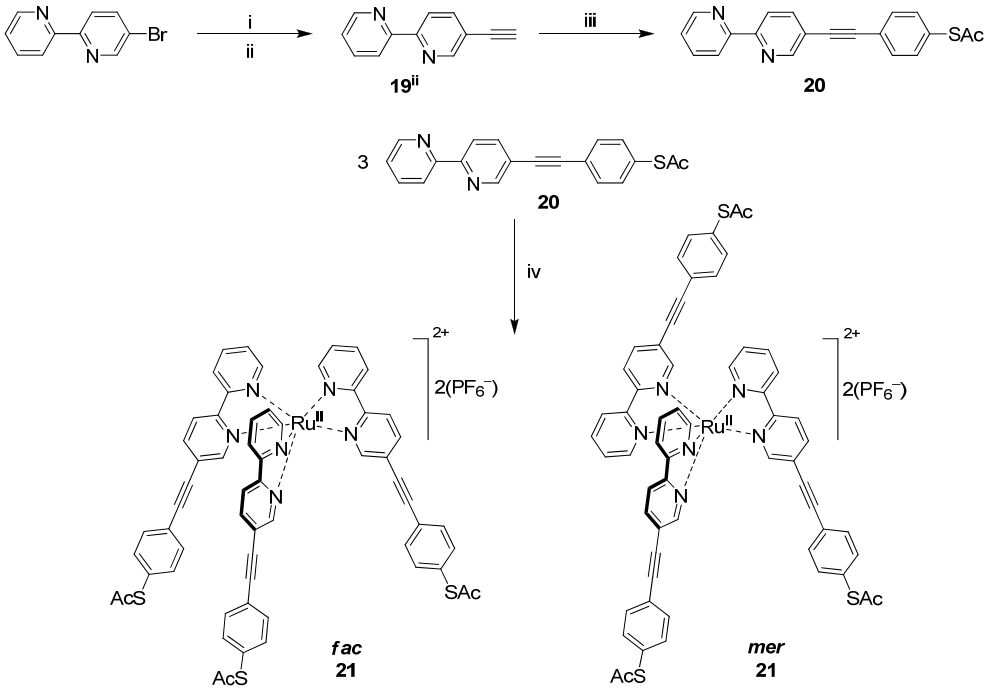

Scheme 5. Synthetic route of the *fac* and *mer* Ru(II)-complex. Reaction conditions: (i) TMSA, $PdCl_2(PPh_3)_2$, CuI, THF/TEA anh., N_2, rt, 91%; (ii) K_2CO_3, CH_2Cl_2/MeOH, rt, 93%; (iii) $PdCl_2(PPh_3)_2$, CuI, THF anh./ DIEA anh., N_2, rt, 50%; (iv) a) $Ru(DMSO)_4Cl_2$, EtOH, Ar, reflux; b) KPF_6 aq., MeCN, rt, 26% *fac*, 10% *mer*.

Characterization of *fac* and *mer* Ru(II)-*trisbpy* complexes with thioacetyl end groups

The ligand **20** and its *fac* and *mer* complexes have been fully characterized by NMR, ESI mass spectrometry, IR, UV-vis spectroscopy, elemental analysis, and confirm their structure and purity. All the characterizations for the Ru(II) *fac* and *mer* complexes are consistent with the formation and separation of both isomers.

NMR Spectroscopic Data

Both, *fac* and *mer* complexes were characterized by NMR spectroscopy. Extensive 1D and 2D NMR spectroscopic techniques - $^{1}H,^{1}H$ correlation spectroscopy ($^{1}H,^{1}H$ COSY90) and $^{1}H,^{13}C$ HMQC - were employed to achieve full assignment of the signals (Annex). From two-dimensional COSY spectrum was determined which protons are spin-spin coupled. Long range coupling can be observed in COSY90 spectra and are characteristically low in energy (Annex). Finally, the two-dimensional $^{1}H,^{13}C$ HMQC spectrum, allowed for the determination of carbon to hydrogen direct connectivity (Annex).

The separation of the two isomers is demonstrated by ^{1}H NMR (figure 42). The *fac* complex exhibits in solution a C_3-symmetry, thus has a clearly resolved NMR spectrum with all three legs chemically equivalent. The *mer* isomer is not symmetric and exhibits a more complex spectrum, where the bipyridine protons appear as multiplets. This makes the interpretation more difficult, nevertheless the integration of these signals is consistent with the structure and keeps the same assignment as in the *fac* isomer.

The first observation which confirms the difference in symmetry of the two isomers is given by the thioacetyl proton signals. The *fac* isomer presents one singlet at 2.39 ppm, while in *mer* isomer are observed two superimposed signals in approximately 2:1 intensity. Compared to the ligand spectrum, the *fac* and *mer* isomers exhibit a significant upfield shift (≈ -1 ppm) of the 6 and 6' protons (α position to the coordinating nitrogen atoms). This strong upfield shift is induced by the interaction of the 6 and 6' hydrogen atoms with the ring current of the pyridine rings of the neighbouring legs. This interaction is caused by the coordination of the ligands and changes the anisotropy of the respective protons. The structural vicinity of these atoms is shown by crystallographic analysis.[152, 153] For the *fac* isomer, these protons appear as two distinct tight doublets keeping the same coupling constants as in the ligand. In the *mer* isomer these protons appear as multiplet, a result of their proximity to different heterocyclic rings. The 3 and 3' protons keep almost the same chemical shift, while 4 and 4' protons present a downfield shift (0.23 ppm) in comparison to the ligand. All these signals are clearly resolved in *fac* isomer, while the *mer* presents multiplets. The phenyl protons are unambiguously identified by keeping the same chemical shift/ coupling constant as in ligand. The 5' proton observed in literature [150, 151] to give a distinct set of signals for the two isomers, is overlapped in our case for the both isomers by the phenyl signal. Our ^{1}H NMR shielding findings given by changes in electron densities after chelation of the ligands, are closely related with the described values.[152, 153]

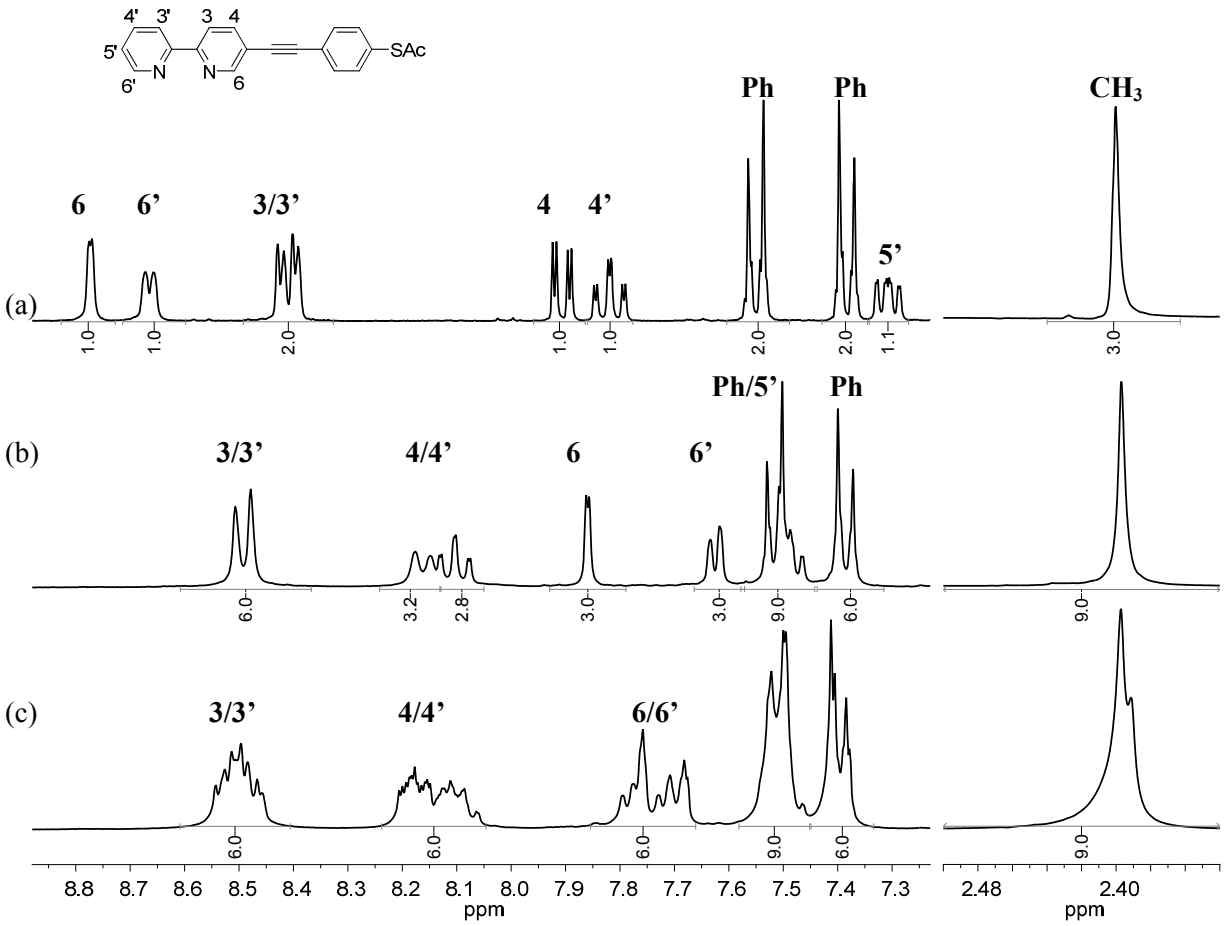

Figure 42. ^{1}H NMR spectra of (a) Ligand **20** in $CDCl_3$ (b) *fac* $[RuL_3](PF_6)_2$ and (c) *mer* $[RuL_3](PF_6)_2$ in CD_2Cl_2; the assignment of the protons are depicted in the structural formula.

The presence of two isomers was also confirmed by the difference of ^{13}C NMR spectra related to the symmetry of the species. ^{13}C NMR characterization can demonstrate the separation of *fac* and *mer* isomers.[153] The *fac* isomer presents 18 signals which support its structure (Annex). An interesting observation of the unsymmetrical *mer* isomer spectra is the presence of three (two in some cases) very close sets of signals (C-6/6', C-3/3') but keeping the same chemical shift/ assignment for all the carbon signals as in the *fac* isomer.

Mass spectrometry, IR and elemental analysis

ESI TOF measurements were applied to the *fac* and *mer* $[RuL_3]^{2+}(PF_6)_2$ salts. Both isomers show the corresponding peak of the $[RuL_3]^{2+}$ molecular ion at m/z = 546.1 and in very small intensity an aggregation as $[(RuL_3)_2(PF_6)_2]^{2+}$ at 1237.2. The counter ion $(PF_6)^-$ is observed at m/z = 144.9 in negative acceleration mode.

The purity of each *fac* and *mer* isomers was confirmed by elemental analysis. The complexes were observed to retain water despite drying in vacuum, as presented in literature for similar Ru-complexes which are supposedly hygroscopic.[154]

The IR spectra of the two *fac* and *mer* $[RuL_3]^{2+}(PF_6)_2$ isomers are essentially the same. Characteristic weak stretching vibration bands (-C≡C-) assigned to acetylene bonds in both isomers are

identified at 2223 cm^{-1} with a shoulder around 2180 cm^{-1}. In the free ligand this vibration appears as a very weak band at 2217 cm^{-1}. For the free ligand the stretching vibration (C=O) corresponding to the thioacetyl functionality is observed at 1696 cm^{-1}, [164] while a slightly shifted frequency is observed for *fac* and *mer* complexes to 1702 and 1705 cm^{-1} respectively. The ring frequencies of the free 2,2'-bipyridine ligand are assigned to 1457 and 1584 cm^{-1} bands. Upon coordination these values are shifted to 1465 and 1598 cm^{-1}.[165, 166] The presence of PF_6 counter ions in each isomer is evidenced by a very intense band at 842 cm^{-1} which refers to the P-F stretching mode.

Absorption and Emission Spectroscopy

In the UV-vis spectrum in MeCN, the ligand exhibits a broad absorption peak at 320 nm (ε = 45870 $M^{-1}cm^{-1}$) with a red-sided shoulder at 336 nm (ε = 35640 $M^{-1}cm^{-1}$). Such transitions are typically n-π^* or π-π^* in character. Excitation into these wavelengths yielded a strong fluorescence signal at 376 nm. The recorded emission-excitation spectrum represents the absorption spectra well and confirms the fluorescence character of the emission.

Table 7. Absorption and emission properties recorded in aerated MeCN at rt; [a] reported values; [b] excited at 471 nm; the emission spectra are uncorrected;

Compound	Absorption λ [nm] (ε x 10^{-3} [$M^{-1}cm^{-1}$])			Emission λ (±1) [nm]
	LC		^{1}MLCT	^{3}MLCT
Ligand	336 (35.64)	320sh (45.87)	-	-
[a]$[Ru(bpy)_3]^{2+}(PF_6)_2$	286 (102.30)	-	452 (16.1)	610
fac-$[RuL_3]^{2+}(PF_6)_2$	325 (102.00)	274sh (48.90)	471 (11.65)	635[b]
mer-$RuL_3]^{2+}(PF_6)_2$	336 (97.05)	274sh (44.32)	471 (11.00)	635[b]

Electronic spectroscopy was carried out on both *fac* and *mer* Ru(II)-complexes. The UV-vis absorption spectra in MeCN of both isomers are very similar (figure 43). There, transitions of the ligand-centered (^{1}LC) and metal-to-ligand-charge-transfer (^{1}MLCT) character dominate the spectrum. The ligand based transitions features are found at 325-335 nm (broad) which is very close to the absorption of the free ligand. The ^{1}MLCT based peak at 471 nm is bathochromic shifted in comparison to the reported values of the $[Ru(bpy)_3]^{2+}(PF_6)_2$ (452 nm ^{1}MLCT, 286 nm ^{1}LC).[167, 168] This can be explained by the extended conjugated π-electron system on the ligand and has been described for other Ru(II)-*trisbpy* complexes.[157, 169].

The emission properties of both complexes have been determined and are very similar. Both resulted in a ^{3}MLCT emission maximum band at 635 (±1) nm after excitation into the ^{1}MLCT absorption band at 471 nm. Emission-excitation of the 635 nm emission signal results in a pronounced peak appearance at 471 nm which confirms the ^{1}MLCT band character of the respective absorption band. The large Stokes shift between the excitation wavelength (471 nm) and the emission wavelength (635 nm) is

typical for $[Ru(bpy)_3]^{2+}(PF_6)_2$ complexes and can be explained by the loss of photonic energy due to internal conversion.

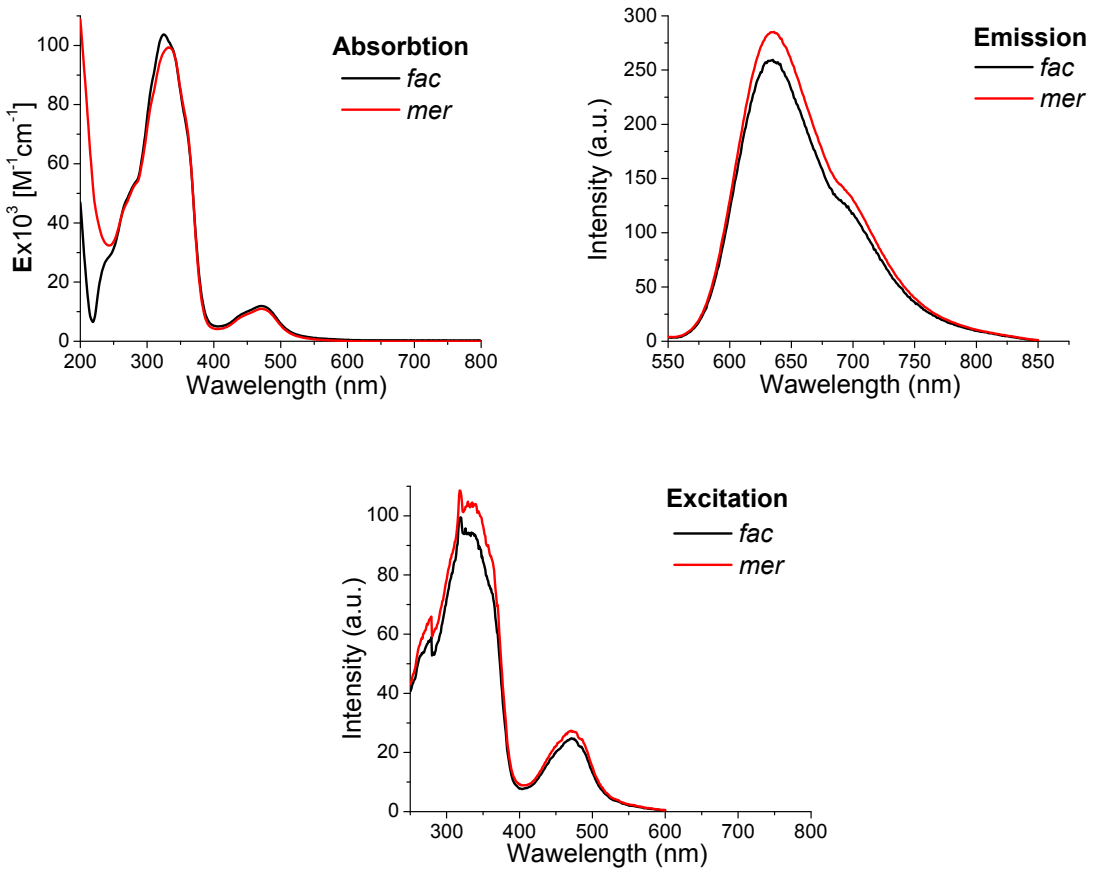

Figure 43. Electronic spectra of *fac* and *mer* $[RuL_3](PF_6)_2$ recorded in aerated CH_3CN at rt under normal atmosphere; (a) absorption spectra (b) emission spectra by excitation at 471 nm; (c) emission-excitation spectra of the 635 nm emission signal.

Single crystal X-ray characterization of fac Ru(II)-trisbpy complex with thioacetyl end groups

Crystals of *fac*-isomer were grown from slow diffusion of Et_2O in MeCN solution of complex, appearing as red needles. The crystals for *mer*-isomer similarly obtained, appeared as branched feathers which proved not being suitable for X-ray diffraction. Details of the crystallographic studies of the structure determination, selected bond lengths and angles are given in Annex.

The X-ray data present for each $[RuL_3]^{2+}$ cation two disordered PF_6 counter ions and contains 1.5 disordered MeCN solvate molecules per complex molecule. Figure 44 illustrates the cation, with the metal coordinated by six nitrogen atoms of the three bidentate bipyridine ligands, in a distorted octahedral arrangement. The three bipyridine ligands are positioned pseudo-symmetric around the central metal (figure 44). One of the terminal thioacetyl groups and two sulphur groups are disordered and thus refined in two positions. The cis-arrangement of each of the three conjugated ligand legs terminated with thioacetyl groups confirms the ^1H NMR studies described before. The mean values of Ru-N bond lengths, of 2.063 Å and N-Ru-N angles of 78.7° and 89.2°, are similar as found in comparable $[Ru(bpy)_3]^{2+}$ structures.[151, 156, 159] The *fac*-complex crystallizes in the triclinic space group $P\bar{1}$, as a racemate. The unit

cell contains the two symmetry related diastereoisomers, one Δ and the other Λ, positioned head to head (figures 45 and 46). The phenyl substituted legs are slightly deviated from planarity to the plane of their bpy groups (between 15 and 26°). The height of the entire molecule from the sulphur plane and 5'-bpy carbon atoms is about 12.64 Å. The three bpy functionalities form together with the sulphur atoms, in respect to the Ru ion, the faces of a triangular prism close to 60°. The distance from Ru ion and the plane formed by the three sulphur atoms is 9.5 Å, while de distances between the sulphur atoms are in average 13 Å.

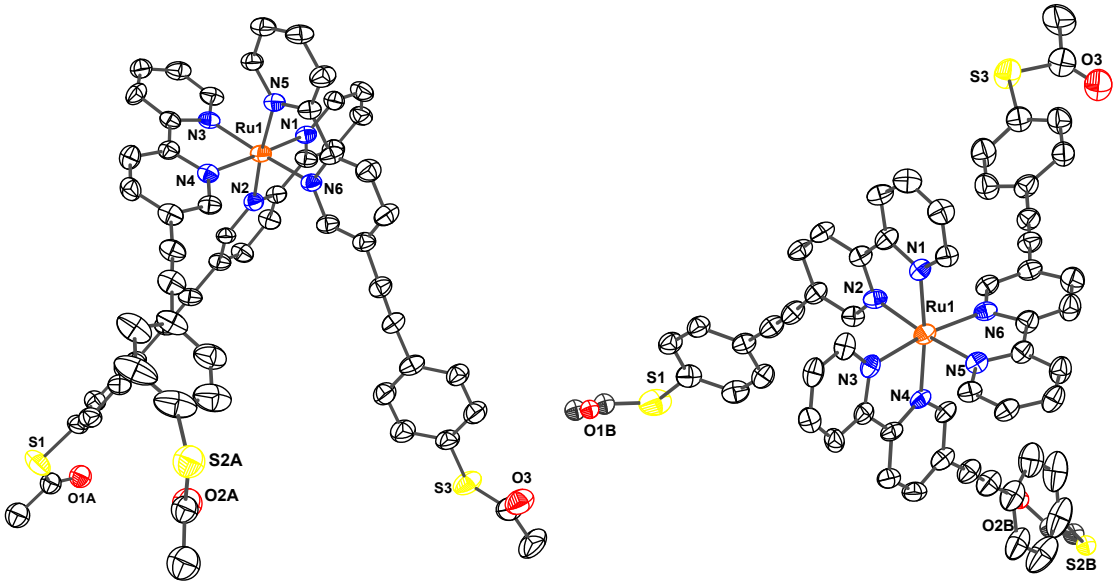

Figure 44. Single crystal X-ray structure of the tripodal *fac*-Ru(II)-complex **21**^{f}. The hydrogen atoms, the two PF_6^- counter ions and the CH_3CN solvate molecules were omitted for clarity (ellipsoid plot drawn at 50% probability level). Left, view perpendicular to the three fold axis; right view along the three fold axis

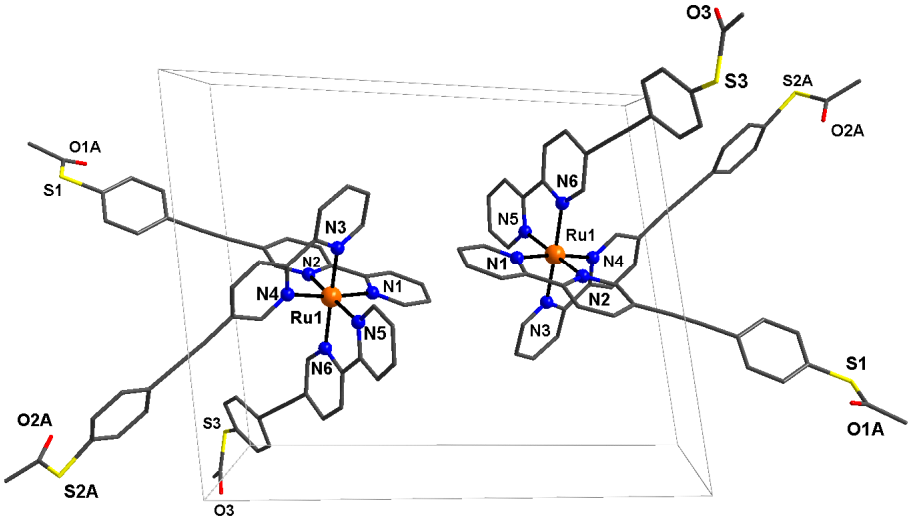

Figure 45. Single X-ray crystal unit cell of the *fac*-Ru(II)-complex **21**^{f} with the two optical isomers Δ and Λ. The hydrogen atoms, PF_6^- counter ions and CH_3CN solvate molecules were omitted for clarity (sticks drawn).

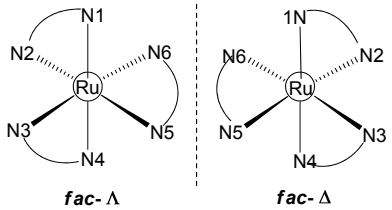

Figure 46. Drawing along the three fold axis of the two optical isomers Δ and Λ present in unit cell.

The crystal packing presents intermolecular π···π stacking interactions (3.86 Å centroid - centroid) between the pyridine and phenyl rings of two very closely positioned neighbour molecules (figure 47). Each cation of Ru(II)-complex is compensated by two PF_6^- counter ions and is accompanied by 1.5 MeCN solvate molecules. One PF_6^- ion is positioned inside the cavity formed by the three legs.

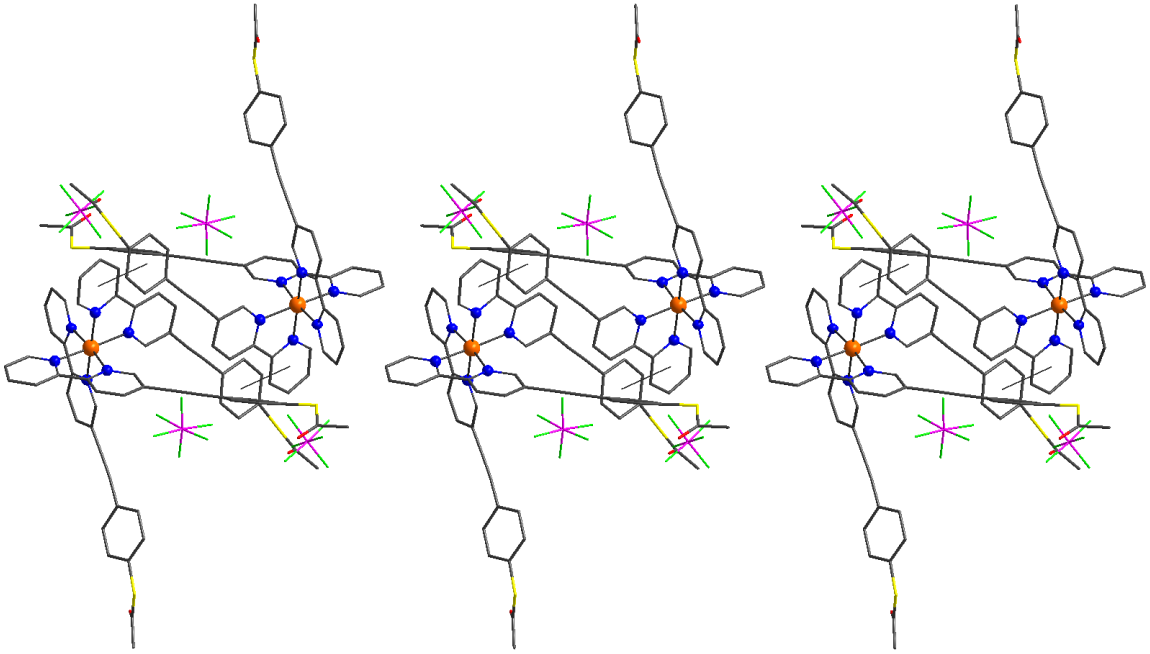

Figure 47. Crystal packing along z axis of the *fac*-Ru(II)-complex **21**$^{\mathbf{f}}$ showing the intermolecular π···π stacking interactions (grey line) between two neighbour molecules (pyridine and phenyl rings, 3.86 Å centroid - centroid) and the position of PF_6 counter ions. The hydrogen atoms and MeCN solvate molecules were omitted from clarity (sticks drawn).

In conclusion the synthetic strategy to functionalize a tripodal metal complex with thiol-protected groups for multi-attachment on metallic surfaces was achieved. We have demonstrated that the separation of the two already functionalized *fac* and *mer* isomers is accessible by an easy and reproducible method. This allows for isolation of reasonable quantities of both isomers required for complete characterization and study on metallic surfaces. The photophysical investigation of both isomers indicates no significant difference between two structural forms as reported for similar structures.[150] The fully conjugated ligands form the two *fac* and *mer* well defined three-dimensional rigid structures which can be viewed as molecular wires which encapsulate the Ru ion. The *fac* isomer is prearranged to connect all three legs on the surface, while the mer isomer is in prospect to connect two legs on the surface which leaves the remaining leg pointing upward. This difference in geometry of the two isomers will be exploited for a comparative study at single molecule level by STM. As the complex conformation is stable, the tripodal structure of *fac* isomer will remain after deposition on metallic surfaces. In particular, the thioacetyl groups are known to deprotect easily in situ on gold surface under formation of covalent sulphur-gold bonds. All these considerations present the two isomers of Ru(II)-*trisbpy* complex as possible candidates for electron transport studies on metallic surfaces.

2.3. STM measurements of tripodal complexes

Experimental set up

The STM experiments were performed by Dr. Maya Lukas and PhD student Kerrin Doessel. The measurements were carried out with a modified Omicron system under UHV conditions with a base pressure of $1 \cdot 10^{-10}$ mbar. The Au(111) crystal was cleaned by several cycles of sputtering and annealing. The crystal was then transferred to the fast-lock of the UHV chamber; the chamber was flooded with nitrogen and opened. A solution of metal-complex (≈ 7µl CH_2Cl_2 anh.) was dropped on the crystal under nitrogen flow to avoid the surface contamination. The chamber was pumped and the crystal was annealed in UHV for 10 minutes at ≈ 40°C to remove the solvent from the surface. Finally the crystal was transferred to the STM and cooled down to temperatures of 30 K. At this temperature the mobility of the molecules on the surface was retained and measurements at single molecule level were possible.

2.3.1. Ga(III)-trensal complex with thiomethyl end groups 3 on Au (111)

Single molecules of Ga(III)-*trensal* complex can be imaged with STM after deposition in sub-monolayer from high diluted solution (≈ 10^{-7} M). Most of the molecules (≈ 60%) stand tilted on two legs on the Au(111) surface (figure 48 and 49). A gap voltage of 2V was used and the feedback current was set to 30 pA.

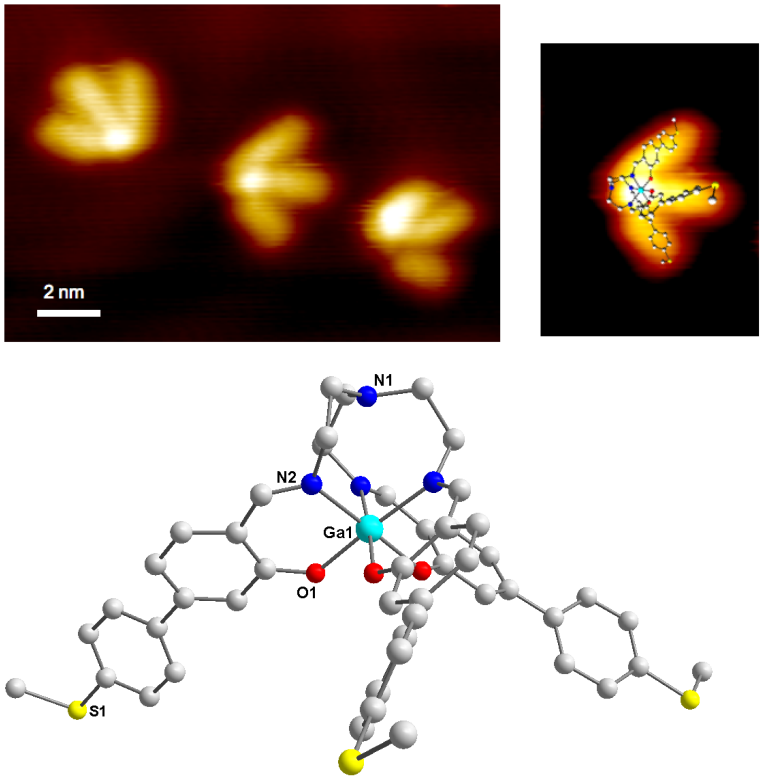

Figure 48. STM images presenting the Ga(III)-complex **3** standing on two legs on Au(111) and its molecular structure obtained by single crystal X-ray diffraction

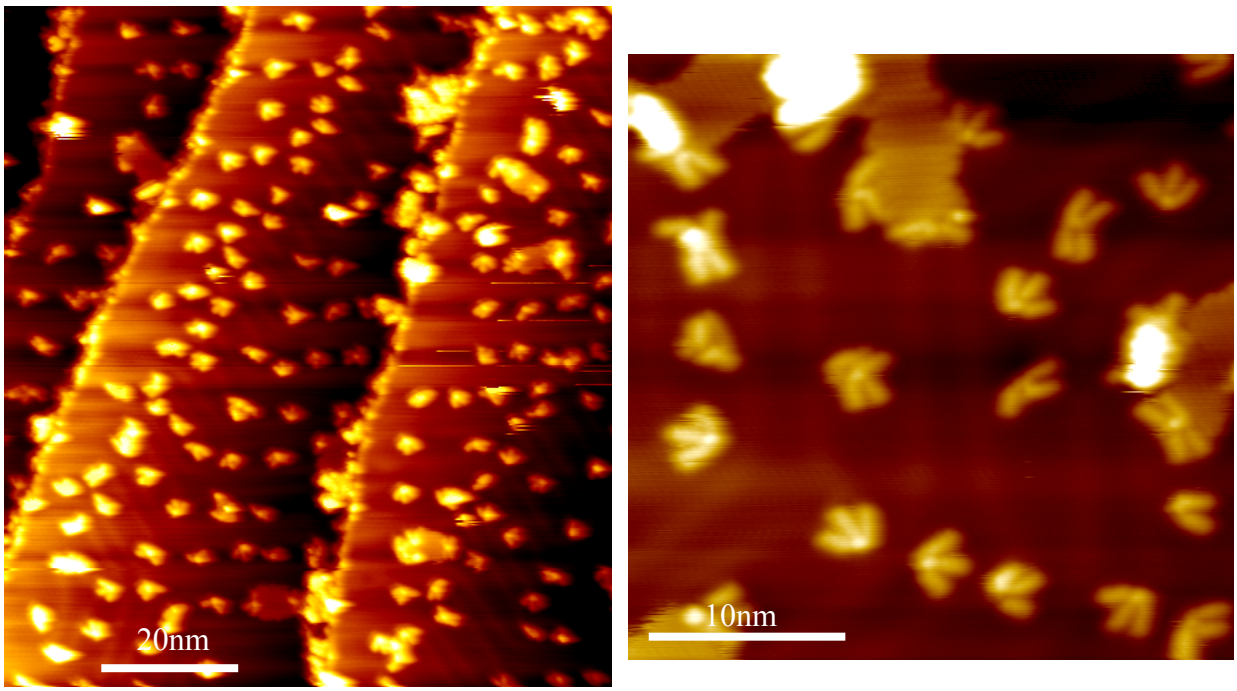

Figure 49. STM images presenting immobilized on Au(111) the Ga(III)-complex **3** in sub-monolayer

Scanning tunnelling spectroscopy could be performed on different sites of the molecule: each of the three legs and the head unit. Preliminary I = f(V) measurements show distinct differences between the gold surface and the molecules.

The measurements were compared to density functional theory calculations of a single free molecule where the surface is not taken into account and the results are in agreement.

At higher concentration the molecules do not tend to cluster on the surface (figure 50).

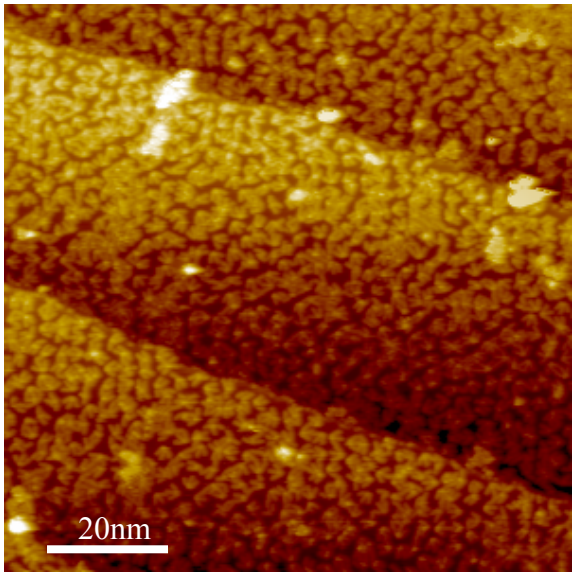

Figure 50. Higher concentration of deposited molecules of Ga(III)-complex **3** on Au(111).

2.3.2. Fe(II)-trenpy complex with thiomethyl end groups 11, on Au (111)

The Fe(II)-*trenpy* complex with thiomethyl end groups **11**, deposited similarly as the Ga-complex forms on Au(111) small clusters of molecules (figure 51). The structural difference, charged two cation closely surrounded by two PF_6 counter ions per each molecule, can explain this behaviour. The tendency to form aggregates with PF_6 counter ions, but in insignificant low intensity is shown before by the ESI mass study.

Study of single molecules lie in the same way on the surface as the Ga(III)-complexes (figure 51). Data from STS or DFT calculations were not yet available at the moment of writing this thesis.

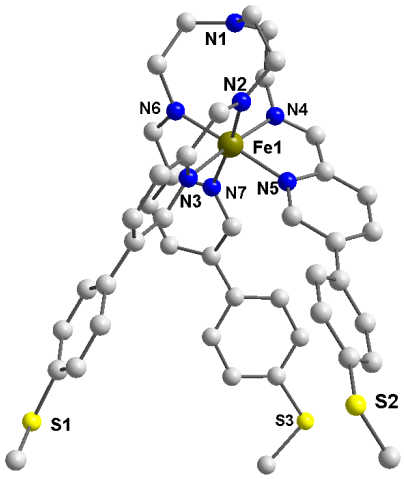

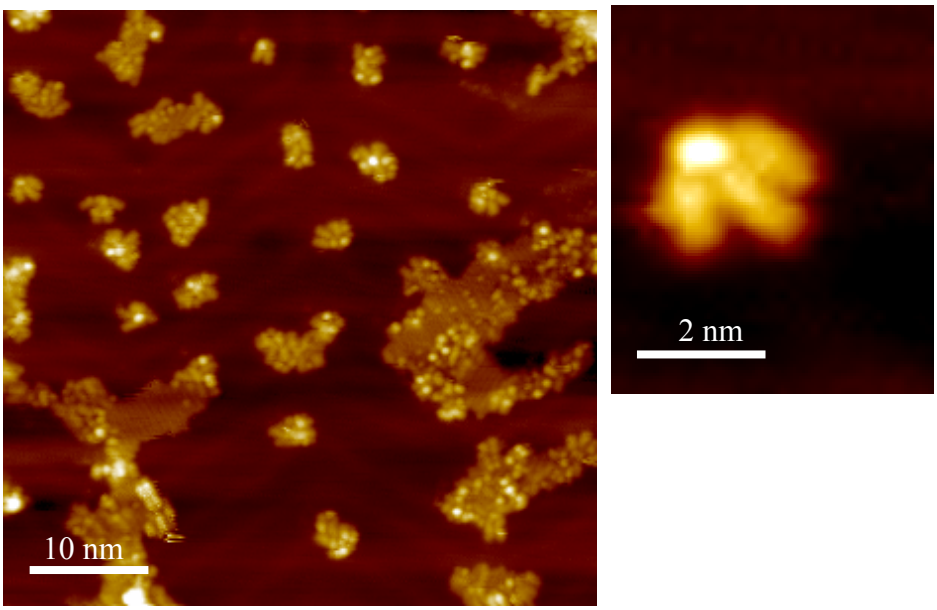

Figure 51. Single crystal X-ray structure of Fe(II)-complex **11** and STM images presenting immobilized the Fe(II)-complex **11** on Au(111).

Chapter 3.

Homodinuclear helicate complexes

3.1. Introduction

This chapter reports about the synthesis and characterization of new bimetallic helicate complexes. The structures are functionalized with anchoring groups on two opposite ends for possible connection between two electrodes as a molecular wire unit. Self-assembly of three organic ligands around two Fe(II)-, Zn(II)- or Ni(II)-cations formed homobinuclear triple stranded architectures. The variation of metal ions leading to diamagnetic or paramagnetic compounds is expected to tune the electronic transport properties. All the metal complexes and their intermediates have been completely characterized by ^{1}H NMR (in case of diamagnetic compounds), ESI, IR, UV-vis techniques and elemental analysis. Additionally, the molecular structures of the Fe(II)- and Ni(II)-helicates have been confirmed by single-crystal X-ray diffraction. The ^{1}H NMR spectra of the Fe(II)-complex exhibit in solution a coalescence effect supported by X-ray crystal structure. In order to discuss this effect some basic theoretical aspects of coalescence phenomena will be introduced.

Aspects of triple-stranded helicates

On molecular level the discovery of helical superstructures in biologically relevant macromolecules, e.g. DNA and RNA, inspired the chemists to synthesize conceptionally derived supramolecular assemblies.

Starting with the pioneering paper of J.-M. Lehn et al on doublestranded helicates containing dinuclear and trinuclear Cu(I)-complexes based on the oligopyridine motif [170] there has been an increased interest in helical architectures. From that point a multitude of double and single stranded helicates up to four-stranded helicates were synthesized.[171] The development of self-assembled helical structures and their properties have been extensively reviewed over recent years.[171, 38, 172 -176]

One way to obtain such synthetic helical systems is to combine basic principles of coordination chemistry with structural models defined by supramolecular chemistry. There, several requirements have to be fulfilled: a) the design of the ligand is adapted to the metal ion which is coordinated; b) complexation of the metal ion results in a stable coordination environment; c) the ligand structure design

consists of separated coordination sites by a bridging or inter-connecting part which allows the helical twist for encapsulation according to the stereochemical demands of the metal ion.[171, 172]

A helix is characterized by a central axis - helical axis - enfolded by a single or multiple strands. The strand distance which forms a complete turn around the axis is called pitch. The arrangement of the strands in a helical high ordered structure can be controlled by different supramolecular interactions, e.g. hydrogen bonds, π-stacking or metal ion coordination.[171] The class of compounds formed by metal-directed self-assembly processes from two or more metal centers and one or more ligand strands, was named helicates.[38] Four important concepts in supramolecular chemistry were introduced for understanding the formation of helical architecture: molecular recognition, self-assembly, self-organization and supramolecular programming.[38, 176]

The helicate complexes introduced a new type of chirality, helicity. The new class of chiral molecules may possess new optical and electronic properties.[177] Every metal center in a helical structure is a center of chirality which will adopt a rotational sense, the right-handed form being P with Δ coordinated metal centers and the left-handed one being M with Λ coordinated metal centers. Generally, there have been described three possible cases to induce chirality between metal centers implying C_2-symmetrical ligands. The particular case of triple helicates is exemplified in figure 52.[176, 178]

a) All centers in a polynuclear system are homochiral. The chirality propagates through the entire molecule where one coordination center induces for the neighbouring coordination center the same chirality. In this case for symmetrical helicates incorporating non-chiral ligand strands, normally a racemic mixture results.

b) One coordination center induces the opposite chirality to the neighbour metal centers. A polynuclear structure with even number of metal centers results in an achiral molecule, a meso structure. With odd number of metal centers a chiral structure is obtained.

c) When no preference for helicity in respect to a neighbour center is present a disordered structure will form.

Different other arrangements may be possible in case that other conformation of metal center than M or P absolute configurations or the bridging domain are displayed, leading to non-helical domains.[176]

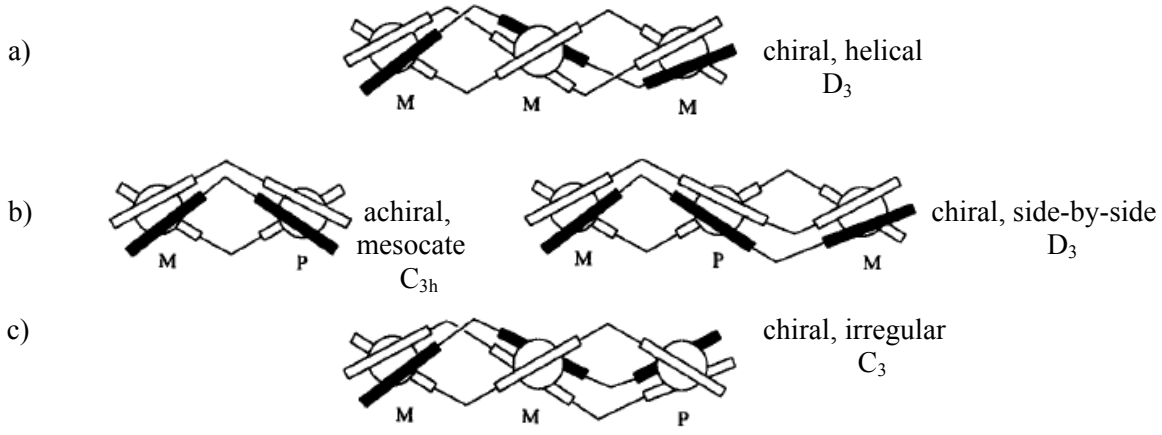

Figure 52. Possible arrangements in triple helical complexes with C_2 symmetrical ligand strands: a) homochiral; b) antichiral, c) disordered. Regular helicates are homotopic while the irregular are heterotopic.[176]

The control of molecular architectures has been demonstrated for several types of ligands. In case of triple helicates based on oligo-bidentate strands, building blocks with octahedral geometries are required.

Williams et al [179, 180] described the first structurally characterized example of triple helicate formed by a Co(II)-complex based on the relatively rigid bis(bisdentate) ligand L^1 (figures 53 and 54).

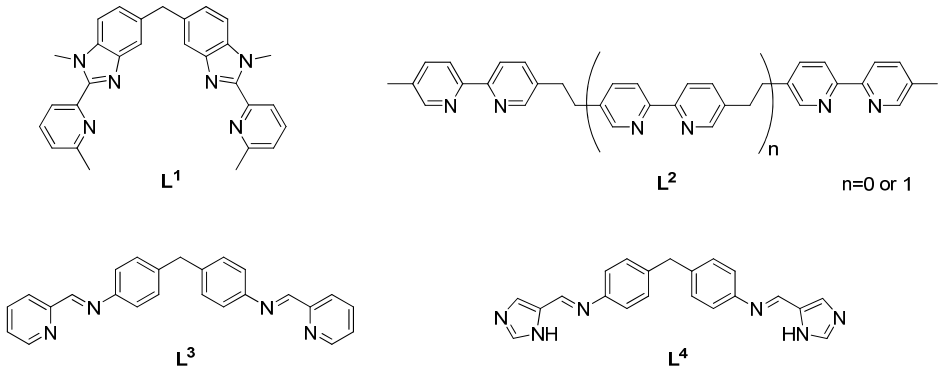

Figure 53. Examples of ligands which form triple-stranded helicates

Metal triple helicates of type M_2L_3 are based on three bis-bidentate ligands interacting with two metal ions which are coordinated in an octahedral ligand field. If a relatively rigid linker between the two coordinating units of the ligand is used which allows a twist between them, then a chiral triple helicate is the most likely structure. In case of less rigid linkers, mesocates and other topologies are possible.[181]

Double stranded helicates can be formed by the bis-bidentated ligand **L[1]** if tetrahedrally coordinating metal ions are applied. Contrary, triple-stranded helicates are obtained if metal ions which prefer octahedral coordination are used (figure 54).[38, 176] In another work the assembly of ligand **L[2]** (figure 53) to double-helicates has been reported with Cu(I) ions which prefer tetrahedral coordination in a $[Cu_3L_2]^{3+}$ arrangement. On the other hand, the utilization of Ni(II) or Fe(II) ions result in the formation of triple-helicates due to octahedral ligand field preference of these ions.[182, 183]

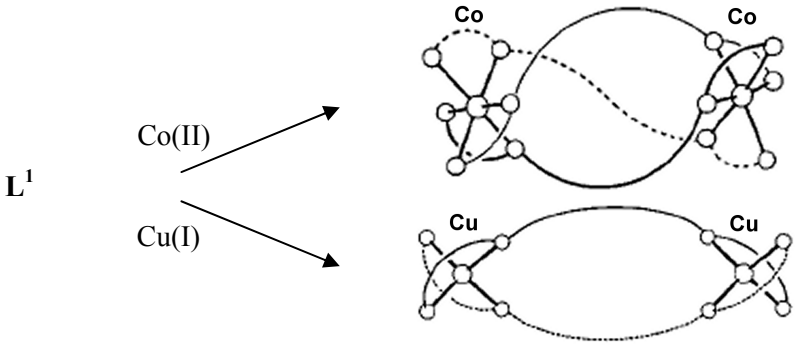

Figure 54. Double and triple stranded helicates formed from L^1 according to tetrahedral Cu(I) or octahedral Co(II) ions

It has been found that ligands based on diphenylmethane bridging motif, L^3 and L^4 or their derivates (figure 53), can form different types of supramolecular structures. If the ligands are coordinated to tetrahedral Cu(I) and Ag(I) the following motifs can be obtained: dinuclear double-stranded helicates,[184, 185] mixtures of double stranded helicates and meso-forms,[186-188] or only molecular boxes as

mesocates.[189, 190] If these types of ligands are coordinated to metals with preferences for octahedral geometries, e.g. Co(II), Fe(II), Zn(II), Ni(II), Ru(II) they exclusively form triple-stranded helicates.[191 -197]

The helical motif offers another approach to design new spin crossover molecules. The possibility to switch the properties of compounds in a controlled way, e.g. switching configurations between high- and low-spin, has attracted the interest for development of new electronic devices.[198] As examples, dinuclear Fe(II)-helical complexes $[L_3Fe_2]^{4+}$ of type L^3 exhibit a diamagnetic behaviour, while L^4 has been described to form spin crossover compounds (figure 53). For the first type of complexes, Fe(II)- ions bind to pyridine units while in L^4 are coordinated to imidazoline units.[198]

Recently has been described how bimetallic triple helicates and double stranded DNA can structurally recognize and bind to each other, forming a three-way junction (figure 55 A, B). This junction is established by the complementarity between the supramolecular structure, with high positively charged cations and the negative charged DNA backbone, combined with the shape of the metal helicate.[199, 200] The nature of the interactions and the type of bindings between the DNA matrix and the helical tetracations has been investigated in a multitude of works.[192, 199, 201, 202] The molecular recognition between DNA and the metal triple helicate has been considered being a new pathway for the development of DNA-interacting therapeutic agents based on metal complexes.[203 -205]

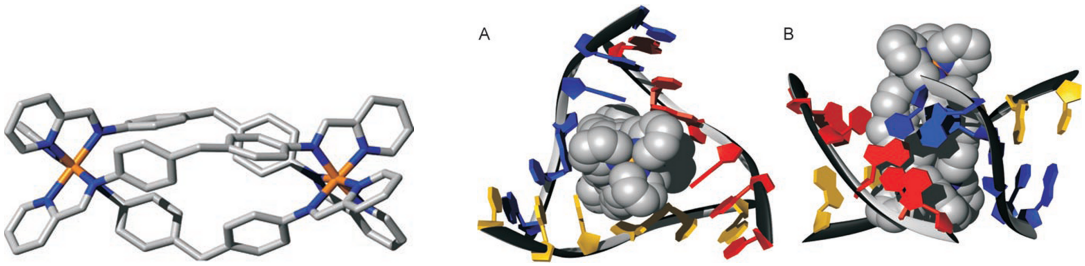

Figure 55. Schematic modelling of Fe_2 triple helicate; A) Top and B) side view of DNA three-way junction containing inside helicate. Gray C, blue N, orange Fe and the bases of the three DNA strands in colour: blue, red, or yellow.[205]

Although, much development for understanding of the helicate formation has been advanced, the mechanism is not completely elucidated. In this direction, the first kinetic studies important for elaborating the self-assembly mechanism and the recognition process implied in formation of helical architecture have been reported.[176, 206, 207]

Polymetallic helical structures have recently attracted attention due to the structural features for contacting two ends to metal electrodes. This makes them good candidates for the fundamental understanding of the effect of metal-metal interactions on electron transfer with potential applications as nanoscale devices. A first step in this direction has been established by producing wire-like metal complexes (figure 56) formed from a helical arrangement of the ligands around the metal ions. Chemisorption of these wire-complexes on Au(111) surfaces has been observed by STM studies. Additionally, pronounced differences in electron transfer were detected upon variation of the metal ions within the helical structures.[208]

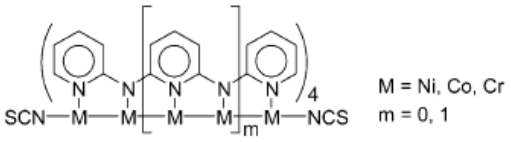

Figure 56. Helical metal string complexes studied on metallic surface.[208]

In another report a series of dinuclear Ru(II)-complexes of type $\{Ru(bpy)_2]_2(L)\}^{4+}$ (figure 57) has been considered to approach a molecular wire behaviour. There, the two metal centers were connected by ligands analogous of L^2. The binuclear complexes exhibited strong metal–metal interactions through the interconnecting ligand L. These interactions can participate in efficient electron-transfer reactions along a sequential redox chain.[209]

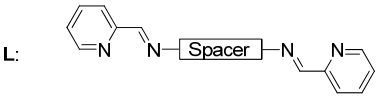

Figure 57. Structure of the ligand L contained in helical $\{Ru(bpy)_2]_2(L)\}^{4+}$, complex.[209]

The possibility to tune the electronic transport properties by varying the ligand structure and metal ions motivated us for further studies of the helical array viewed as molecular metal wires. Whereas the metallic helical motif is one of the most investigated supramolecular architectures [191, 196] and the synthesis of triple-stranded helicates with a multitude of transition metal is well established [174-176, 191] to our knowledge, triple helicates functionalized with anchoring groups for their immobilization on metal surfaces have not been reported so far. One particular point of motivation is the use of an anchoring group which allows for reliable and reproducible surface contact to establish the molecular wire behaviour. The metal-helicates based on the 4,4'-methylene dianiline bridging motif offer an inexpensive and easy synthetic pathway combined with the formation control of triple-helical architecture.[191, 194] In addition, various metals have already been complexed with derivatives of this molecule, and recently an enantiomeric resolution has even been reported with analogous compounds.[210]

Toward the development of new electronically active molecular scaffolds, new bimetallic helical complexes based on a Schiff base ligand formed from the condensation of the 4,4'-methylene dianiline bridging motif and the aldehyde functionalized with thiomethyl anchoring group, were designed and synthesized. This structure can be envisioned as a combination of two tripodal structures which are arranged in a helical architecture with the possibility of contacting both ends to metal electrodes.

Restricted rotation of diaryl systems and aspects of the coalescence phenomena

Diaryl systems with two aryl rings attached to a central unit Z, e.g. CH_2, -CHR, O, CHOH, PCH_3 etc., are the simplest representatives of polyaryl compounds which can display restricted rotation of the aryl groups (figure 58).[211] Such systems have been the subject of several studies which concluded that these molecules can undergo correlated rotation of one ring thus causing rotation of the other. These types of molecules may assume one of two stable conformations according to the so-called "cogwheel

mechanism". There either both aryl groups are arranged in helical conformation or the rings can adopt the perpendicular conformation (figure 58).[211] In this case the rotation of the phenyl groups is fast on the NMR time scale but the rotation speed is considerably reduced if sterically demanding substituents are involved.[212]

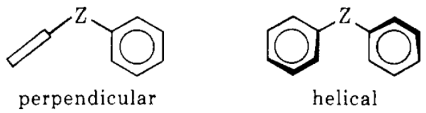

Figure 58. Perpendicular and helical conformations of diaryl systems [211]

The rotational mechanism has been studied by Dynamic NMR spectroscopy (DNMR) after introduction of additional chirality elements which give rise to diastereoisomers. Complexation of diarylmethanes or ortho-substitution of the rings may result in the formation of several different isomers. This leads to a slow rotation of the phenyl rings due to the restricted configuration which makes the hydrogen atoms on phenyl rings inequivalent.[213, 214]

Dynamic processes with an energy barrier between 20 and 100 KJ/mol are usually studied by analysis of temperature-dependent NMR spectra of interconverting species. The interconversion of stereoisomers exhibiting diastereotopic nuclei can be monitored by DNMR when the conversion is slow on the NMR scale. This analysis is based on the fact that the shape of signals of two groups in exchange is temperature-dependent.[215] Several methods can be used in DNMR which use: bandwidths, peak separation, approximate methods for evaluation of rate constants or the complete line shape analysis, etc.[216]

In the simplest case of an exchange process $\boldsymbol{a} \leftrightarrow \boldsymbol{b}$ between two "equally populated sites", for an uncoupled dynamic process, the line shapes represented in figure 59 are observed in variable-temperature NMR spectra. The NMR spectrum is a function of the rate of exchange k and of the difference in their resonance frequencies: $\Delta\nu = \nu_a - \nu_b$. [216]

At low temperature, the exchange is slow, $k \ll \Delta\nu$, and the spectrum consists of two sharp signals, while at high temperature, at fast exchange, $k \gg \Delta\nu$, a single peak is observed. At the coalescence temperature the appearance of the spectrum changes from two separate peaks to a single, flat topped signal. [216]

At the temperature T_c where the two peaks coalesce, the rate constant k_c of the exchange is given by eq. (1), where $\Delta\nu$ is the separation in Hz between the two signals in the absence of exchange: [216-218]

$$k_c = (2^{-0.5})\,\pi\,\Delta\nu \qquad (1)$$

For an exchange process between two nuclei $\boldsymbol{a}$ and $\boldsymbol{b}$ with a coupling J_{ab}, the coupling constant is introduced in equation (1) resulting equation (2). The rate constant k_c at the coalescence temperature is estimated by: [217]

$$k_c = (2^{-0.5})\,\pi\,(\Delta\nu^2 + 6J_{ab}^2)^{0.5} \qquad (2)$$

From the rate constant, the free energy of activation $\Delta G^{\ddagger}$ at the coalescence temperature T_c can be determined by the Eyring equation:

$$k = (k_B \cdot T)/h \exp(-\Delta G^{\ddagger}/RT) \quad (3)$$

where k is the rate constant in s^{-1}, k_B is the Boltzmann's constant, $1.3805 \cdot 10^{-23}$ J/K, h is the Planck's constant, $6.6256 \cdot 10^{-34}$ J·s, R is the gas constant, 1.9872 cal/(mol·K), and T is the temperature in Kelvin.[217]

$\Delta H^{\ddagger}$ and $\Delta S^{\ddagger}$ can be determined from: $\Delta G^{\ddagger} = \Delta H^{\ddagger} - T\Delta S^{\ddagger}$. (4)

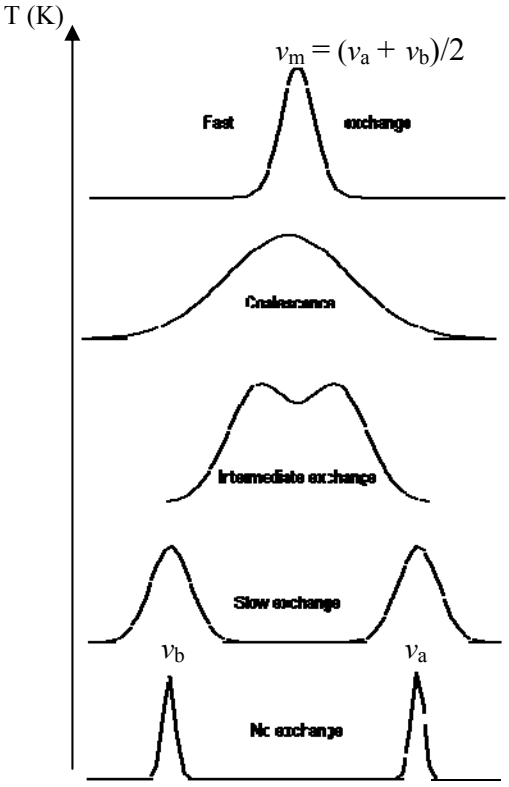

Figure 59. Example of variable-temperature dependent NMR spectra of an uncoupled dynamic system

The simple method to calculate the coalescence is not applicable for processes with complicated NMR spectra, multiple coupling patterns or species with different thermodynamic stability. The coalescence methods and the approximate methods provide less accurate results than the complete line shape analysis, nevertheless are often sufficient quick estimates. In case of more complicated systems, the errors are high and computer programs to simulate the NMR line shapes are required.[217] Typical sources of errors by applying the above described coalescence-method are: the accuracy of determining T_C and determination of $\Delta\nu$ (Hz), the maximum peak separation in the slow-exchange, etc.[217]

3.2. Results

Synthesis of binuclear helicate complexes

Triple helicates are synthesized by the self-assembly of three organic ligands $\mathbf{L^f}$ around two iron(II), zinc(II) or nickel(II) cations (Scheme 6).

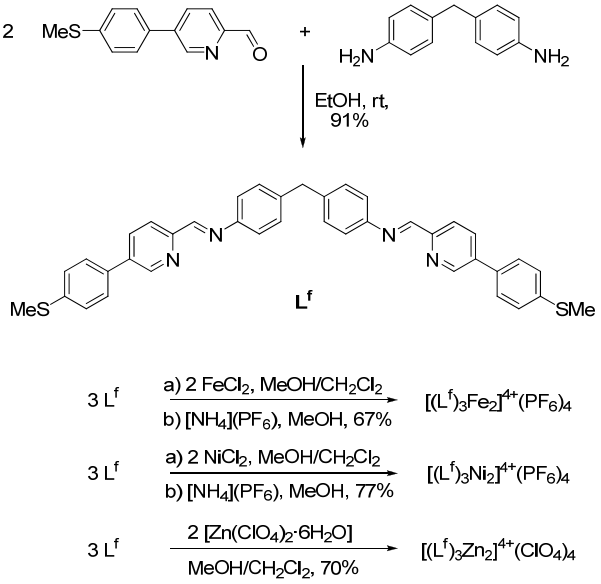

Scheme 6. Synthesis of the functionalized ligand $\mathbf{L^f}$, and the homobinuclear helicate metal complexes

The ligand $\mathbf{L^f}$ has been synthesized from thiomethyl-functionalized aldehyde **9** described in Chapter 2. Twofold imine-condensation of the aldehyde **9** with 4,4'-methylene dianiline in EtOH afforded the desired ligand. The complexes have been prepared by mixing a diluted CH_2Cl_2/MeOH (5/1) solution of the ligand $\mathbf{L^f}$ with a MeOH solution of the corresponding metal salt. While the perchlorate salt of the L_3Zn_2 complex precipitated in the course of the reaction, the hexafluorophosphate salts of L_3Fe_2 and L_3Ni_2 were precipitated by addition of a methanolic NH_4PF_6 solution.[191]

Characterization of binuclear helicate complexes

All resulted metal complexes have been fully characterized and the formation of homobinuclear helicates has been confirmed. The diamagnetic homobinuclear Fe(II)- and Zn(II)-complexes have been completely characterized by ^{1}H NMR, ESI, IR, UV-vis techniques and elemental analysis. Additionally, the Fe(II)- helical structure has been confirmed by single crystal X-ray diffraction. The paramagnetic Ni(II)-complex exhibits a typical ^{1}H NMR spectrum of a paramagnetic compound with signals strongly shifted towards low magnetic field (60 ppm). Its identity has been proved by ESI, IR, UV-vis spectroscopy, elemental analysis and single crystal X-ray diffraction.

^{1}H NMR characterization and coalescence estimation

The helical Fe(II)- and Zn(II)-complexes present simple ^{1}H NMR spectra (figure 60) with one set of signals which demonstrate that their triple helicate structures are maintained in solution.

Single crystal X-ray diffraction refines the results obtained by NMR, especially the exclusive appearance of chiral ΛΛ and ΔΔ isomers. The configuration of the chiral helicates can be clearly supported by the pattern observed for the CH_2 protons in the ^{1}H NMR spectra. Both Fe(II) and Zn(II) complexes (figure 60) display a singlet at 4.0 ppm for the equivalent central methylene groups (non-diastereotopic) compatible with the highly symmetrical D_3 point group. For an achiral meso-form ΛΔ, the diastereotopic CH_2 would form two doublets, which is not the case here.[176]

The signals of thiomethyl group resonate at 2.52 ppm for both complexes. The Ph^B phenyl groups keep the same chemical shift and pattern as found in the aldehyde **9** and ligand $\mathbf{L^f}$ respectively (Annex). A difference between the two complexes consists of the chemical shift of the imine group found at 8.61 ppm in case of Zn(II)-, while for Fe(II)-complex it is sifted to a lower magnetic field at 9.07 ppm. Differences were also evidenced for the pyridine unit pattern positioned in vicinity to the coordination site (figure 60, 61). A contrary behaviour was observed for the central phenyl groups Ph^A, where strong differences in comparison to the free ligand have been observed. While the Zn(II)-helix shows a clearly resolved ^{1}H NMR spectrum with two doublets at 6.32 and 7.02 ppm, the Fe(II)-helix shows two broad bands at 5.68 and 7.00 ppm. This behaviour, attributed to the hindered phenyl ring rotation between the two metals, has already been observed in a similar Fe(II) triple helix.[188, 191] One pair of the phenylene (Ph^A) rings signal is shifted to lower chemical shift even more evident for the Fe(II)-complex. This shift and the signal broadening of the phenylene protons which indicates slow rotation, are consistent with the presence of CH···π interaction between the central phenylene rings [188] observed also in the single crystal X-ray structure analysis. The assignments were based on similar published compounds [188, 203] as well as from the spectra of precursor complexes.

A study of the Fe(II)-complex coalescence effect, realized by variable – temperature dependent NMR measurements over the temperature range of -20°C to 40 C supports this conclusion (figure 61). Two doublets at 40°C of the phenyl Ph^A protons, with H^a at 5.72 and $H^{a'}$ at 7.07 ppm, indicate that the phenyl rings freely rotate within the NMR time scale. At low temperature (-20°C) the two broad bands of the phenyl protons split into four resonances (figure 61). The signal of the H_a protons split into two doublets at 5.12 and 5.76 ppm, while the other $H_{a'}$ signal split into one doublet at 6.42 ppm and a second signal overlapped by the aromatic protons of the Ph^B rings. As the temperature is decreased the rate of rotation decreases and phenyl protons become chemically inequivalent due to the hindered rotation of the twisted phenyl rings.

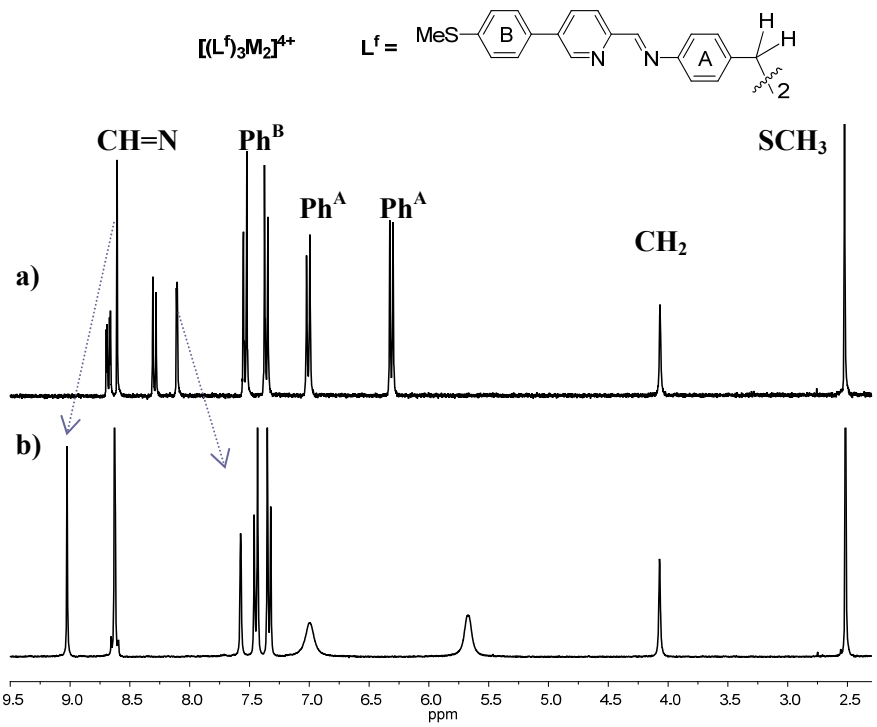

Figure 60. ^{1}H NMR spectra (CD_3CN, 25°C) of: a) the Zn_2(II)-helix; b) the Fe_2(II)-helix

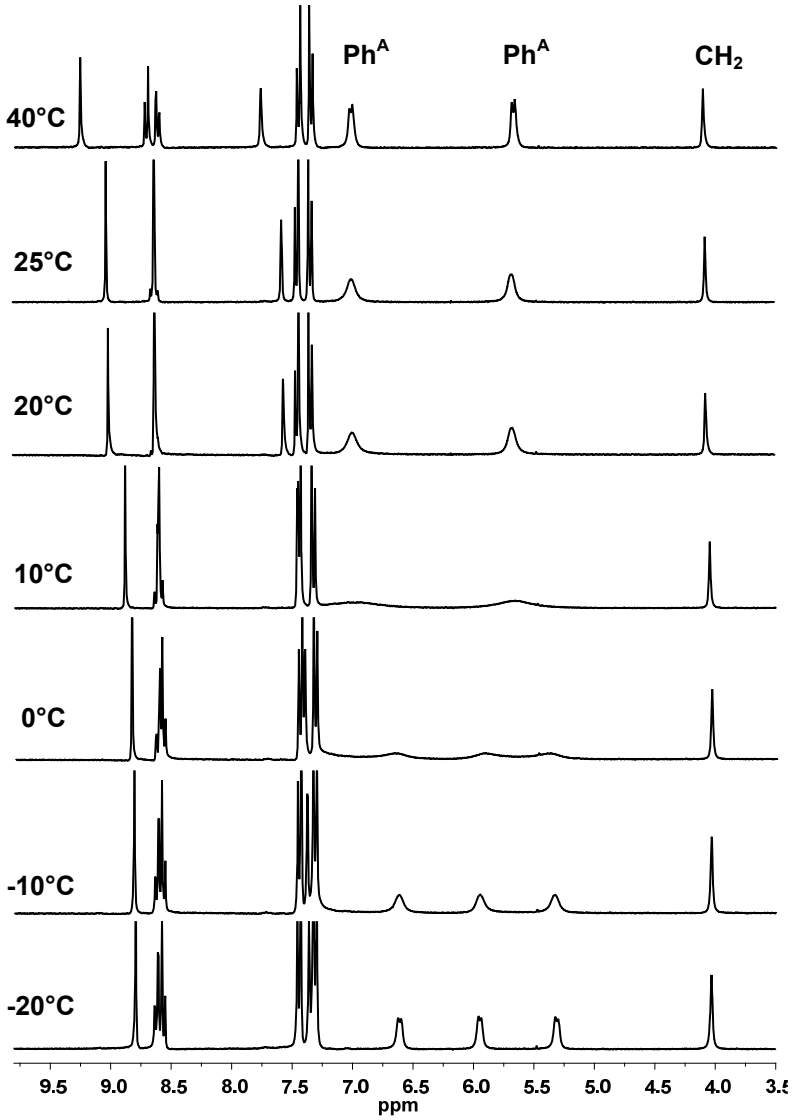

Figure 61. Variable – temperature ^{1}H NMR spectra (CD_3CN) of the Fe_2(II)-helix

The coalescence temperature (T_C) was found at 10°C for both H_a and $H_{a'}$ phenyl protons. The rate constant (k_C) was estimated to 426 s^{-1} for the H_a protons. A simple calculation has been carried out considering a first-order kinetic process and neglecting the coupling of the phenyl protons which does not have a significant contribution. The free energy of activation at the coalescence temperature T_C = 283 K, estimated from the Eyring equation (3) is $\Delta G^{\ddagger}_{283} \approx 13$ kcal/mol. Simplified simulated spectra (figure 62) for H_a and $H_{a'}$ phenylic protons, coalescing with the same rate constant, were realized using WINDNMR-Pro program together with calculated approximate methods for evaluation of rate constants.[216] It is mentionable that the analysis of errors has not been executed, thus the quality of the estimated rate constant and $\Delta G^{\ddagger}_{283}$ was not determined. The complete line-shape analysis, which gives the most accurate results, would be possible by using advanced computing programs due to the overlapped signal in frozen-out configuration and the phenyl proton couplings. The simplified method used in determination of parameters and lack of reports about coalescence effect in similar helical metal complexes with diphenylmethane linkers makes the comparison of rotational barrier energy with other reported diphenylmethane derivates not possible here. However, this preliminary result serves as a reasonable basis of discussion.

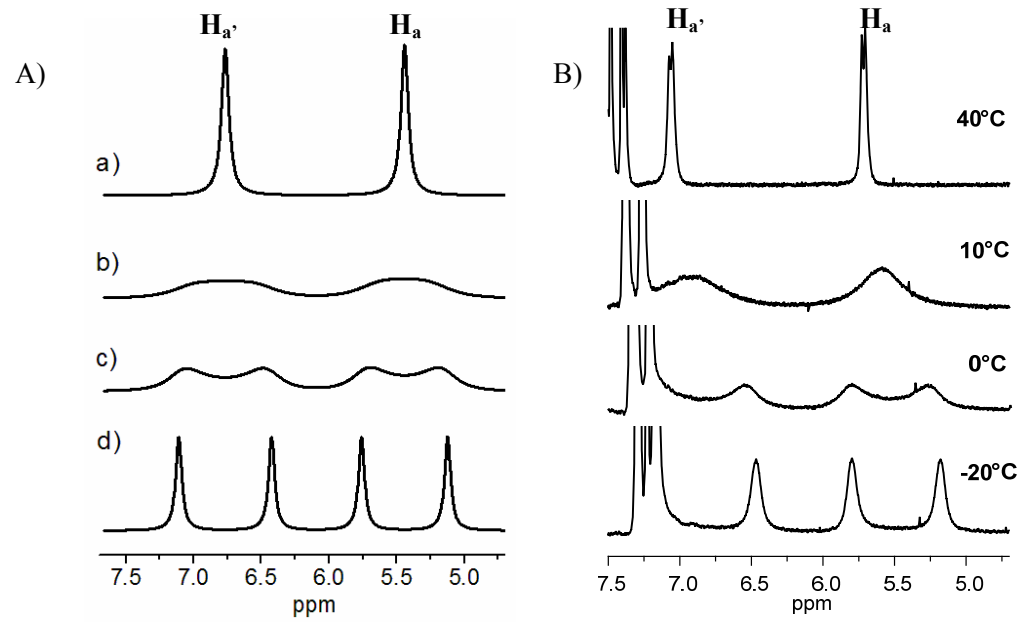

Figure 62. ^{1}H NMR spectra of the Fe_2(II)-helix showing the H_a and $H_{a'}$ protons involved in the coalescence process; A) simulated dynamic spectra; B) experimental spectra (CD_3CN).

Mass spectrometry, IR and elemental analysis characterization

ESI mass spectra of the all three M(II)-dinuclear complexes are consistent with their proposed structure showing the base peak of $[L_3M_2]^{4+}$. While for Zn(II)-perchlorate salt only the base peak is observed, the hexafluorophosphate salts additionally display peaks in low intensity which can be attributed to the aggregation of several helical complexes with the counter ion of forms: $[L_3M_2(PF_6)]^{3+}$, $[L_3M_2(PF_6)_2]^{2+}$, $[L_3M_2(PF_6)_3]^{+}$, etc. The cation/ligand ratio is always in agreement with a triple helical bimetallic structure, supporting its selective formation.

The elemental analyses of the complexes resulted initially that the molecular structure contains two water molecules. Elemental analyses data of similar complexes containing water have been reported in literature.[188, 210] For the Fe(II)-complex, elemental analysis correspond to the analytically pure structure which was achieved after drying at high temperature under reduced pressure (10^{-3} mbar, 100°C, one week). For the Ni(II) complex the removal of only one water molecule was possible after by applying similar conditions.

Single-crystal X-ray diffraction

The single crystal structural analysis obtained for Ni(II)- and Fe(II)-complexes (figure 63) confirm the formation of homodinuclear triple helical structures. Both complexes crystallize in the monoclinic crystal system. In case of the Ni(II)-complex both enantiomers ΛΛ (M) and ΔΔ (P) are present in the helical structure, while for Fe(II)-complex only one isomer is observed in the single crystal (figures 65 and 66). The Ni(II)-complex has been crystallized in the C2/c space group, where the presence of an inversion center and mirror planes allow for the arrangement of a racemate within the crystal packing. The Ni(II)- helical structure of one isomer from the two cation enantiomer, is shown in figure 65. In case of Fe-complex the C2 space group has no symmetry elements showing the presence of only one type of isomer. The FLACK parameter of 0.44(4) indicates that the measured crystal was a racemic twin.

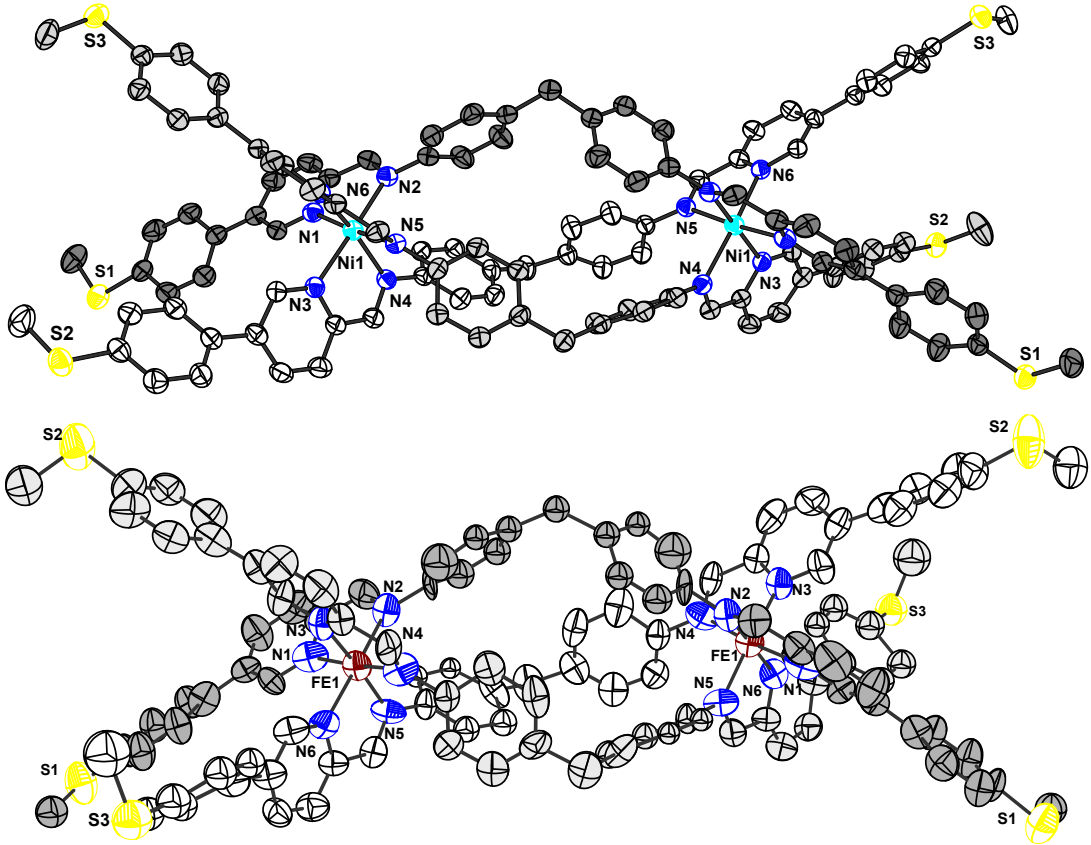

Figure 63. Single crystal X-ray structures of binuclear Ni(II)- and Fe(II)-complexes showing the triple-helical conformation (ellipsoid plot drawn at 50% probability level). A single ΔΔ enantiomer is shown although for Ni(II)-complex both enantiomers are present in the single crystal packing. The hydrogen atoms, solvate molecules and hexafluorophosphate anions are omitted for clarity.

The complexes are isostructural and each consists of two M(II) six-coordinated cations bridged by three ligand moieties. Each M(II) center is coordinated by three pyridine-imine chelating groups which realizes a distorted *fac*-octahedral geometry. Bond lengths and angles are in common range with published values.[188] Details of the crystallographic studies, structures determination, selected bond lengths and angles are given in Annex. For each complex the two metal centers are crystallographically equivalent. In case of the Fe(II) complex the Fe-N bond lengths range between 1.93 - 2.01 Å, indicating that the equivalent metal centers are low spin as already shown by the diamagnetic behaviour in ^{1}H NMR spectra. For Ni(II)-complex the bond lengths Ni-N have been found between 2.09 and 2.13 Å.

Coordination to the metal center forces the twist of bridging phenylene rings and a twist between phenyl units and chelate rings of each ligand, considered responsible for the formation of triple-helical structure.[191] The twist in the center between the phenylene rings planes is almost 78° for Ni(II)-complex and 88° for Fe(II)-complex. This twist arranges the two phenylene rings in intramolecular edge-to-face stacking interactions as already reported,[188, 198] between 2.7 and 3.3 Å for both complexes (figure 64). The CH···π interactions are retained in solutions as evidenced in the NMR spectra by the upfield shield shift of two phenylene protons.[188] For the Fe(II)-complex the intramolecular phenylene stacking interactions are probably stronger than in Zn(II)-complex and leads to broadening of the signals indicating slow rotation. The Zn(II)-complex is expected to have longer distances from the metal ion to the coordination sites,[193, 194] thus a slightly modified structure results.

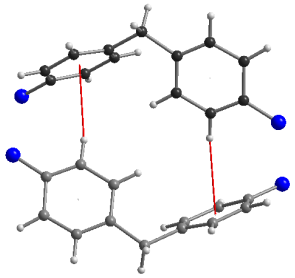

Figure 64. Zoom into the diphenylmethane part of the Fe(II)-complex showing intramolecular edge to face interactions CH···π (C-H, centroid) between central helical strands.

The quality of the Fe complex crystals was poor with diffuse diffraction and the MeCN solvent molecules were difficult to localise because of disorder phenomena. Some phenyl rings and the $[PF_6]^-$ counterions could only be refined as disordered subunits.

Both helical complexes present intermolecular π···π stacking interactions between the phenyl end-groups of 3.9Å (centroid-centroid) showed in figures 65 and 66. The spaces between the layers of molecules are occupied by PF_6 and solvents molecules. The crystal packing of Ni(II)-complex arranges the helical molecules in alternating chains as ΔΔ and ΛΛ enantiomers (figure 65).

As expected, the six sulphur atoms are located on both sides of the helical structures. The intermetallic distances in both complexes are very similar with 1.187 nm for Ni(II) complex and 1.144 nm for Fe(II) complex. The length of the entire molecule is about 2.6 nm. The two planes (figure 67) containing the three exterior sulphur atoms respectively comprise nearly coplanar (9°) arrangement rendering them being almost ideal candidates for the contact between metal electrodes.

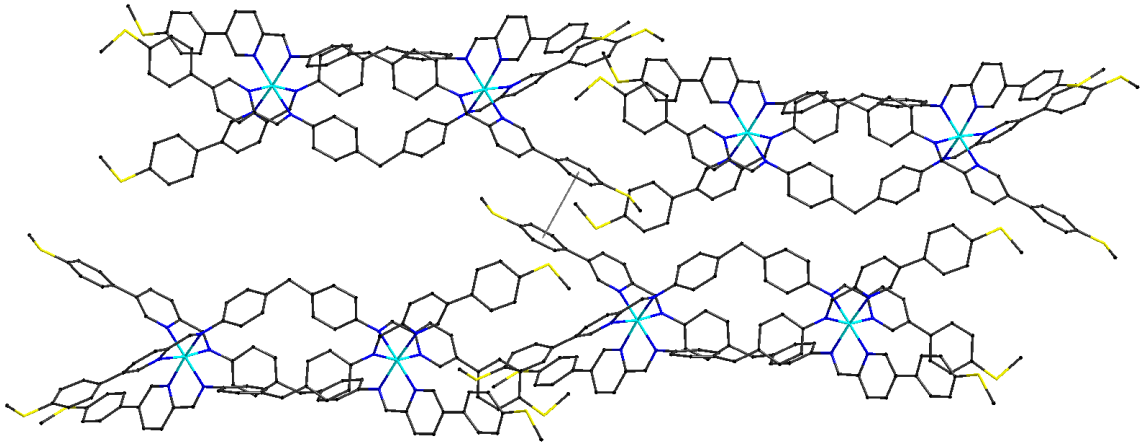

Figure 65. Crystal packing in chains of Ni(II)-complex showing the intermolecular π···π stacking interactions between the phenyl groups of 3.9Å (centroid-centroid) and chains of ΔΔ (up) and ΛΛ (down) helical molecules.

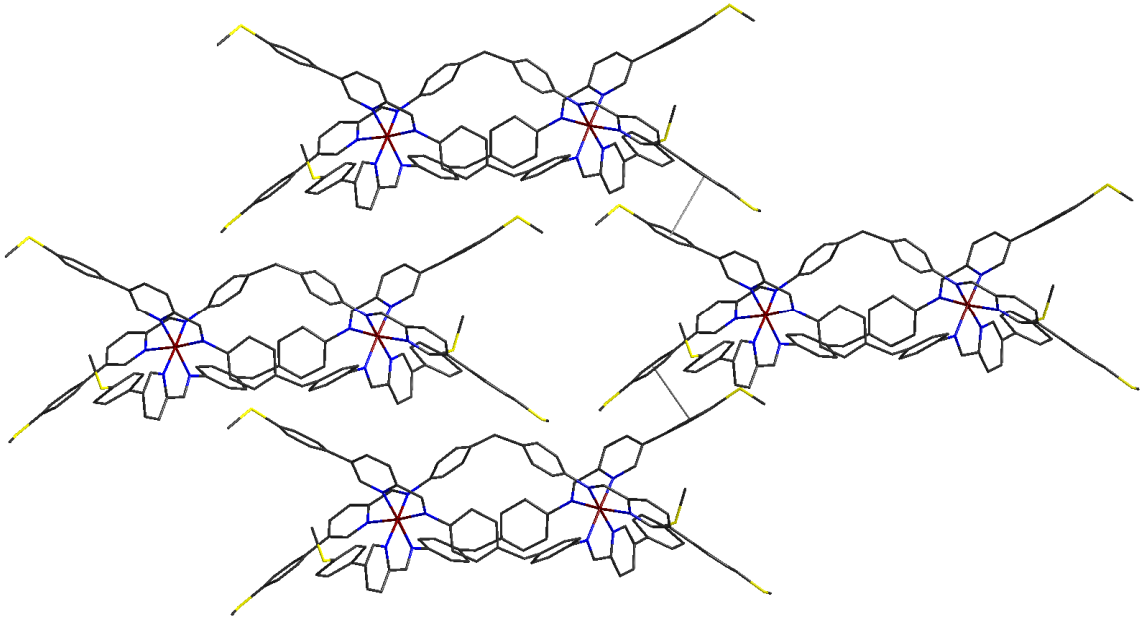

Figure 66. Crystal packing containing single helical isomer of Fe(II)-complex showing the intermolecular π···π stacking interactions between the phenyl end-groups of 3.9Å (centroid-centroid).

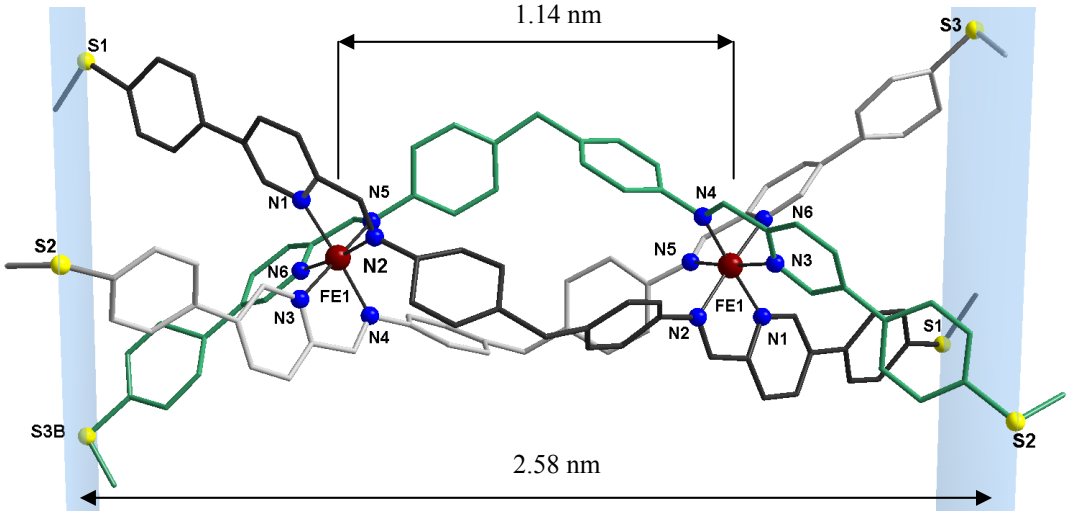

Figure 67. Single crystal X-ray structure of binuclear Fe(II)-complex (sticks drawing). The three ligand strands showing the triple-helical conformation are coloured in green, grey and black. The hydrogen atoms, solvate molecules and hexafluorophosphate anions have been omitted for clarity.

In conclusion, a series of designed dinuclear triple helicates functionalized with thiomethyl anchoring groups for metal surface studies have been synthesized and characterized. The variation of the metal ions by Fe(II), Ni(II) and Zn(II), which introduces different magnetic behaviour is expected to offer a comparative study for electronic transport on the surface. The spectroscopic and crystallographic data support the exclusive formation of chiral helical structures. The $[M_2L_3]^{4+}$ complexes organize the six sulphur atoms located on both sides of the helical structure to offer the possibility for contacting them between electrodes.

Chapter 4.

Chiral (S)- and (R)-binaphthyl ligands and their Zn(II)-complexes

4.1. Introduction

In this chapter new chiral ligands and their Zn(II)-complexes based on the optically active binaphthyl motif have been synthesized and characterized. We describe new systems that combine the stereochemically defined 1,1'-binaphthyl backbone and a Schiff base coordination environment. The reaction of enantiomerically pure 1,1'-binaphthyl-diamine with salicylaldehyde derivates can offer a variety of functionalized chiral binaphthyl Schiff base ligands. Upon coordination with Zn(II) salt, the chiral information of (S)- or (R)-binaphthyl is maintained, leading to the formation of chiral complexes.[219] The structure has been functionalized by introduction of different substituents as bromo and thiophene units or by placing the thiophene in different positions. The structure variation is designed in order to tune their properties and applications. The peripheral thiophene substituent is prone to be used in electropolymerization reactions and surface attachment for electron transport studies. Thus the chirality combined with optical properties makes them possible candidates for the development of new chiro-optical materials.

The (S)- and (R)-ligands and their complexes have been characterized by ^{1}H and ^{13}C NMR, IR, UV-vis, MALDI-TOF techniques. The molecular structure and absolute configuration of the Zn(II)-binaphthyl complexes have been determined by single-crystal X-ray diffraction.

Chiral surfaces with the property to exist in two mirror forms that cannot be superimposed started to attract the interest for technological applications in non-linear optical materials, heterogeneous enantioselective catalysis and sensor devices.[220, 221] The surface chirality has been introduced in two ways: by absorbing chiral molecules on surface or utilizing prochiral compounds where chirality is spontaneously created as a direct result of adsorption. In the last case the chiral organization arises from adsorption-induced asymmetrization.[220] Chiral structures obtained by the adsorption of chiral molecules on the surfaces, maintaining the arrangement and properties of the adsorbed chiral molecules have been less studied.[220] Examples of using the transfer of chirality range from reports of chiral discrimination in Langmuir and LB films of chiral amphiphilic molecules based on binaphthyl derivates [222] to chiral

sensing electrodes by stereoselective binding of binaphthol units.[223] Chiral recognition at single molecule level by STM on di-D and L-phenylalanine on Cu(110) has been addressed recently.[224]

The electrical properties of the first optical active molecular wire containing conjugated molecules based on (S)- or (R)-binaphthyl unit (figure 68) incorporated in a nanowell device by self-assembly on gold have been communicated.[225] For both pure enantiomers similar I-V curves were observed, while for mixtures of isomers the currents are significantly smaller. A possible reason has been attributed to different packing structures between homochiral and heterochiral molecules which emphasizes the investigation of chirality influence on the electrical transport properties.

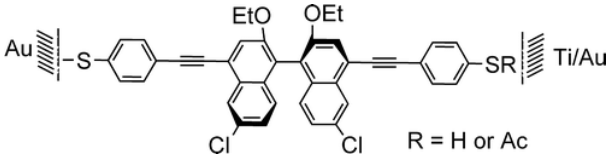

Figure 68. Chiral molecular wire in the nanowell 225

Starting with Noyori, Knowles and Sharpless [219, 226, 227] which invented techniques for catalytic asymmetric synthesis using chiral binaphthyl ligands such as BINAP and binaphthol, there has been an increasing interest to use chiral catalysts for the production of single-enantiomer compounds. Basis for the behaviour to transcribe the asymmetric information upon the activated substrate is the conformation stability of the axially dissymmetric atropisomers. The atropisomers are stereoisomers characterized by axial chirality resulting from hindered rotation about single bonds where the steric strain barrier to rotation is high enough to allow for the isolation of the conformers. The binaphthyl motif is an example of atropisomery given by the restricted rotation around the single bond between the two naphthalene rings. The chiral information can be maintained if the binaphthyl moiety is implied in metal complexes.[219] Thus, the binaphthyl motif was intensively studied to improve the activity and enantioselectivity in catalytic asymmetric synthesis. Derived from 1,1'-binaphthyl-2,2'-diamine their chiral Schiff base complexes can catalyze a multitude of reactions to form chiral products of high enantiometric purity like: asymmetric epoxidation of alkenes, aldol addition reactions, asymmetric hydrogenation of functionalized olefins, etc.[219, 226 -230]

Moreover, the coordination chemistry of synthesized Schiff base metal complexes containing the chiral binaphthyl motif cover a diversity of metal ions: Cr(III), Mn(II), Mn(III), Fe(II), Fe(III), Ru(II), Co(II), Co(III), Ni(II), Pd(II), Cu(II), Al(III), Y(III), Zr(IV).[230] In particular, the number of Zn(II)-metal complexes is limited to few compounds presented in figure 69. [231 -233] X-ray crystal diffraction for this type of Zn-complexes was realized until now only for the structure IV (figure 69). This is probably due to the synthetic difficulty which requires very dry reaction conditions such as glove box apparatus.[231, 233] However, one striking argument to use zinc complexes of Schiff bases is that they have become attractive for their special photo and electroluminescence properties with possible application in optoelectronic devices.[234]

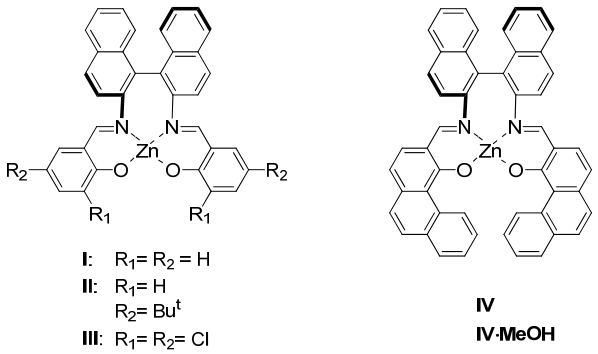

Figure 69. Chiral Zn(II)- binaphthyl Schiff base complexes reported in literature

In the field of enantioselective heterogeneous catalysis another approach for the introduction of chirality in achiral precursor molecules is achieved by using immobilized chiral catalysts. One particular method of immobilization is the polymerization of the modified ligand which in our case is targeted by the distinct use of thiophene in the periphery of the complex structure. One generally interesting feature of polythiophene is its use as a conducting polymer which can be fine tuned by the position of the metal complex moiety in respect to the polymer backbone (figure 70).[235] From the first synthesis as electrically conductive polymers, polythiophene derivatives have been proposed for potential applications in molecular electronics, in organic field effect transistors and optical devices.[236 -239] The use of n-type thiophene has been described in semiconducting films in the construction and operation of organic light-emitting diodes (OLED), in thin film transistors (TFT), field effect transistors (FET) and related devices.[236, 240]

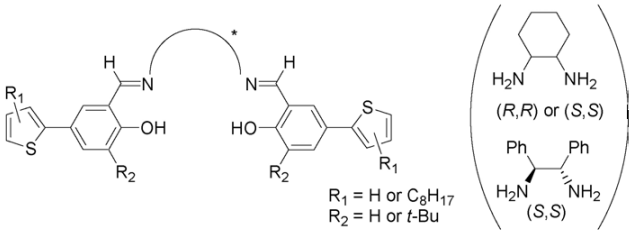

Figure 70. Chiral thiophene salen ligands proposed for metal containing conducting polymers.[235]

In the course of development of new materials we have developed new chiral ligands and their metal complexes based on the optically active binaphthyl motif. The structures are designed to study the behaviour of chiral molecules adsorbed on surfaces and electrochemical polymerization (figure 71).

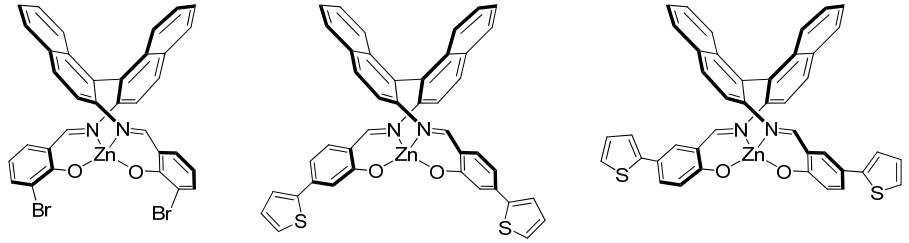

Figure 71. Chiral target molecules proposed for surface studies or electrochemical polymerization

4.2. Results

Synthesis of chiral (S)- and (R)-binaphthyl ligands and their Zn(II)-complexes

In the Schemes 7 and 8, the synthetic pathways and reaction conditions for the formation of three different pairs of (S)- and (R)-Zn(II)- complexes are depicted. Since all (S)- and (R)- binaphthyl ligands and their complexes are very similar they will be discussed in parallel.

First, the designed thiophenyl-aldehydes were prepared through a Suzuki-type cross-coupling reaction between 4- or 5-bromo-salicylaldehyde and the 2-thiophene-boronic acid which gave the corresponding functionalized aldehydes **28** and **31** (scheme 7).

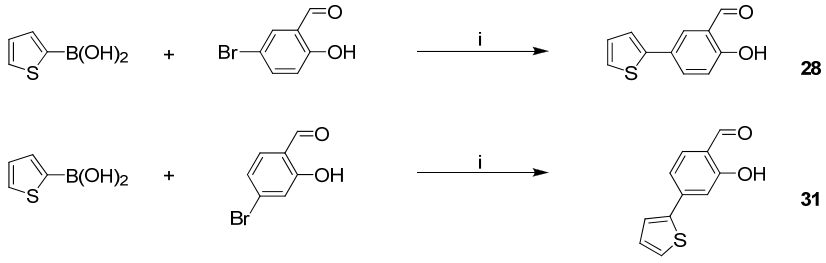

Scheme 7. Synthesis of thiophene functionalized aldehydes **28**, **31**. Reagents and conditions: (i) $Pd(PPh_3)_4$, Na_2CO_3 aq., toluene/MeOH, or DME, 80°C, N_2;

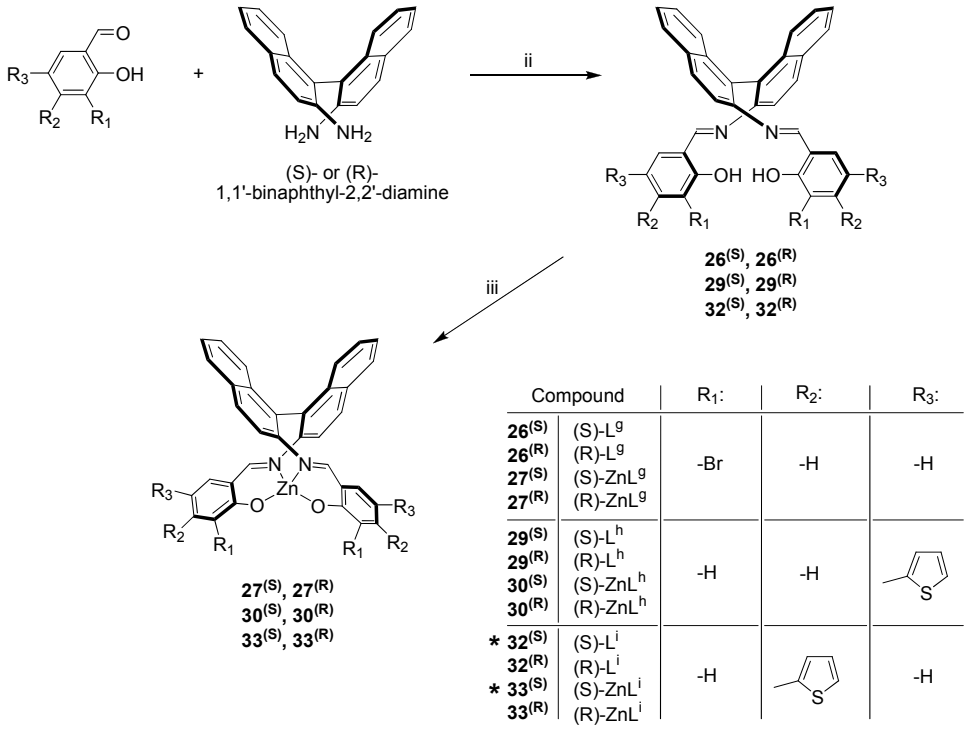

Compound		R_1:	R_2:	R_3:
26$^{(S)}$	(S)-L^g	-Br	-H	-H
26$^{(R)}$	(R)-L^g			
27$^{(S)}$	(S)-ZnL^g			
27$^{(R)}$	(R)-ZnL^g			
29$^{(S)}$	(S)-L^h	-H	-H	
29$^{(R)}$	(R)-L^h			
30$^{(S)}$	(S)-ZnL^h			
30$^{(R)}$	(R)-ZnL^h			
* **32$^{(S)}$**	(S)-L^i	-H		-H
32$^{(R)}$	(R)-L^i			
* **33$^{(S)}$**	(S)-ZnL^i			
33$^{(R)}$	(R)-ZnL^i			

Scheme 8. Synthetic route of Zn(II)-binaphthyl complexes. Reagents and conditions: (ii) EtOH, **L^g**: reflux, **L^h**, **L^i**: 50°C; (iii) MeONa, $Zn(OAc)_2$ anh., MeOH/THF anh., Ar, **ZnL^g**: 65°C, **ZnL^h**, **ZnL^i**: 50°C; *compounds not isolated pure (indicated by the elemental analysis for **32$^{(S)}$** and ^{1}H NMR spectra for **33$^{(S)}$**)

(S)- and (R)-binaphthyl ligands (Scheme 8) were synthesized in good yields using a standard method.[230, 232, 233] A condensation reaction of the enantiopure (S)-(−)-2,2'-diamino-1,1'-binaphthyl with

two equivalents of 3-bromo salicylaldehyde or thiophene functionalized aldehyde **28** and **31** by heating in EtOH gave the pure (S)-ligands. The (R)-isomers were obtained in the same way starting with (R)-(+)-2,2'-diamino-1,1'-binaphthyl. In the next step the ligands were metalated with anhydrous $Zn(OAc)_2$ after an adapted literature method.[231-233]

The complexation required in addition MeONa as a base to deprotonate the phenolic hydrogens. A THF/EtOH anh. solvent mixture was used to dissolve both the ligand and its sodium salt, formed in situ. The resulting yellow fluorescent solutions were heated under Ar to prevent a possible decomposition. The thiophene functionalized Zn(II)-complexes are highly sensitive to wet solvents or air moisture. After removing the solvent to dryness, the yellow precipitate was dissolved in CH_2Cl_2 anh. and the AcONa formed during the complexation reaction was removed by filtration. It is crucial to work in dry conditions. The complexes were recrystallized from CH_2Cl_2/EtOH or MeOH anh. in order to remove the remaining AcONa identified as impurity in ^{1}H NMR.

Characterization of chiral (S)- and (R)-binaphthyl ligands and their Zn(II)-complexes

The (S)- and (R)-ligands and their complexes have been characterized by ^{1}H NMR and ^{13}C NMR, IR, UV-vis, MALDI-TOF spectrometry. The (S)- and (R)-isomers exhibit identical spectral properties. Additionally, the structures of the Zn(II)-complexes **27$^{(S)}$**, **27$^{(R)}$** and **30$^{(S)}$** have been established by single crystal X-ray diffraction.

The ^{1}H and ^{13}C NMR spectra of the ligands and the complexes corroborate their structures. In each case, the spectra are consistent with a single C_2 symmetric compound in solution.[233] As expected the two (S)- and (R)-isomers exhibit identical spectra. Therefore, only the ^{1}H NMR of the (S) isomers of the ligands and their Zn(II)-complexes are shown.

The ^{1}H NMR spectral features of the bromo substituted binaphthyl ligands **26$^{(S)}$**, **26$^{(R)}$** (figure 72a) include the imine proton resonances at 8.66 ppm (s) and the phenolic proton resonances at 12.95 ppm (s). This phenolic value is higher than a usual chemical shift for phenols due to the intramolecular hydrogen bond between the O-H···N atoms.[233] The functionalized (S)- and (R)-thiophene ligands **29$^{(S)}$**, **29$^{(R)}$**, **32$^{(R)}$**, **32$^{(R)}$** contain the same characteristics with the imine resonances assigned at 8.7 ppm and the phenolic proton signals at about 12.3 ppm (figure 73a and Annex). Additionally, the ^{13}C NMR spectra confirm the structures of the ligands. The **26$^{(S)}$**, **26$^{(R)}$** ligands consist of a set of 17 signals each and the thiophene functionalized ligands in 21 signals as expected. The imine carbon resonances are situated at about 162 ppm and C-O (C2) between 157.9 - 161.2 ppm.

In the well resolved ^{1}H NMR spectra of the chiral Zn(II)-complexes a notable difference compared to the free ligands is the absence of the phenolic resonances (figures 72b and 73b). When the ligand is metalated by Zn(II) ion the signals of the protons close to the coordination site are shifted to higher magnetic field.[231] In case of **27$^{(S)}$**, **27$^{(R)}$** complexes, the imine signal shift is $\Delta\delta$ = -0.29 and of H-5 protons $\Delta\delta$ = -0.33 ppm. For the thiophene 4 and 5-functionalized complexes the imine signal shift is $\Delta\delta$=

-0.31 and -0.38 ppm respectively. The carbon atoms which are most affected upon zinc coordination are the imine carbons, shifted with Δδ between 8.5 - 10.4 ppm, and the C-O (C-2) with the shift about Δδ = 9 ppm. All these features support the complexation of Zn(II)-cation by the imino nitrogen and phenolate oxygen atoms and are consistent with similar reported compounds.[231, 232]

The high density of signals in the aromatic region makes additional assignments of the aromatic protons and carbon atoms difficult. For a complete assignment long term measurements and highly elaborated NMR techniques such NOE, 2D long range couplings, etc., would be required. However, the limited stability due to hydrolyzation of the Zn-complexes samples does not allow for such detailed NMR investigations. Nevertheless, the structures were elucidated by single crystal X-ray diffraction.

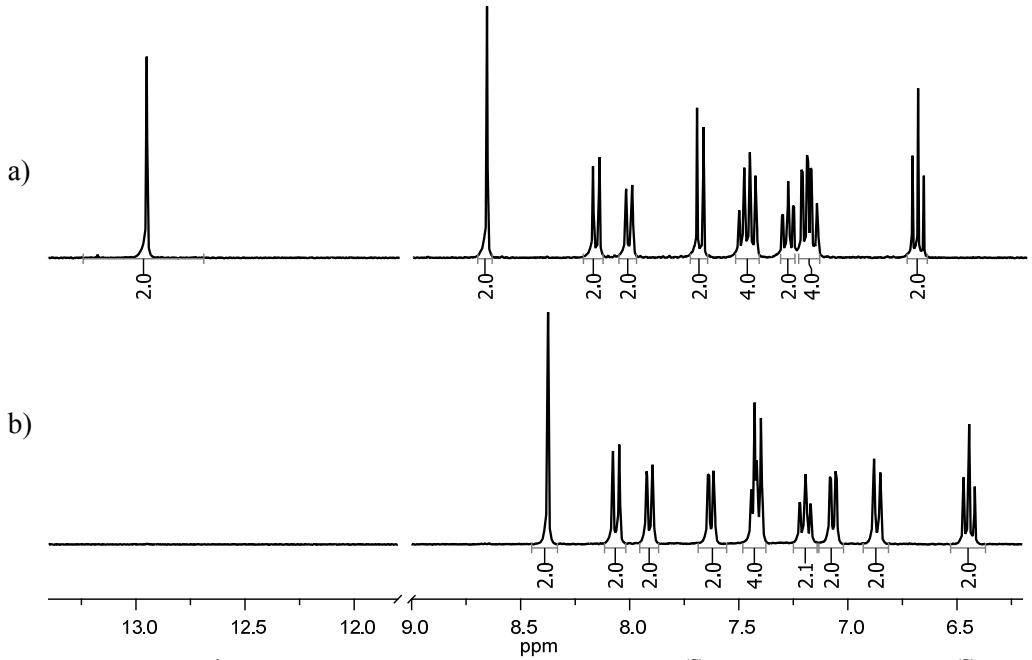

Figure 72. ^{1}H NMR spectra in CD_2Cl_2 of: (a) ligand **26**$^{(S)}$, (b) Zn(II)-complex **27**$^{(S)}$.

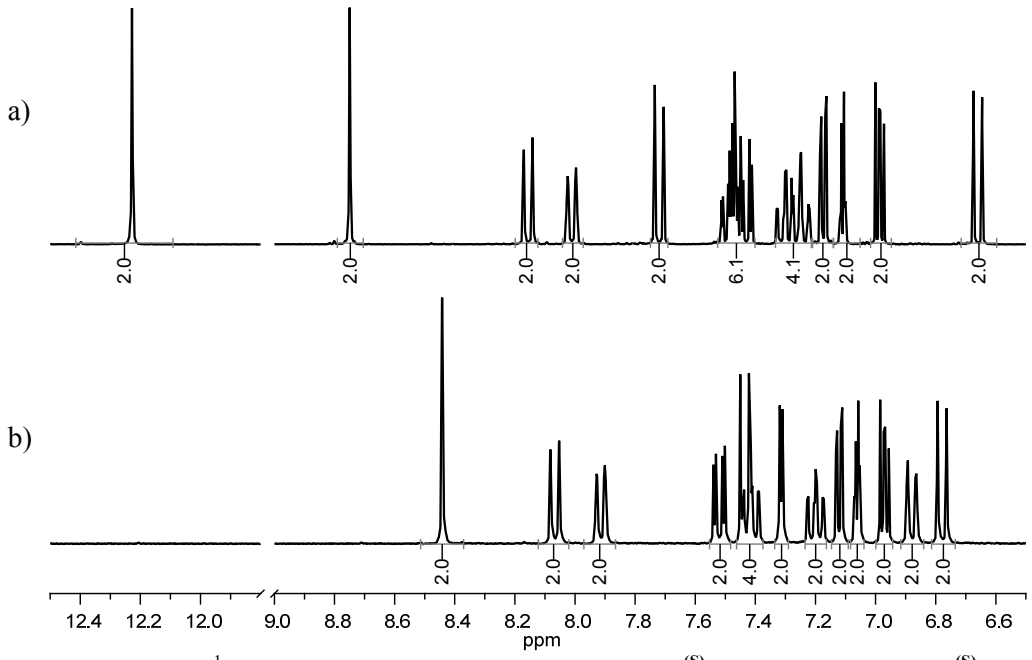

Figure 73. ^{1}H NMR spectra in CD_2Cl_2 of: (a) ligand **30**$^{(S)}$, (b) Zn(II)-complex **30**$^{(S)}$.

The purity of the functionalized aldehydes as well as the resulting (S)- and (R)-ligands was confirmed by elemental analysis. The Zn(II)-complexes were observed to retain solvents despite drying in vacuum. The elemental analyses of the Zn(II)-complexes together with ^{1}H NMR spectra studies confirm the content of solvents and additional water molecules. The complex **27$^{(S)}$** contains 1.25 CH_2Cl_2 and 0.25 MeOH molecules as solvents of crystallization (Annex) while the complex **27$^{(R)}$** has 1.30 CH_2Cl_2 and 0.15 MeOH molecules in the range of experimental error (Annex). The complex **30$^{(S)}$** contains 0.25 CH_2Cl_2, 0.71 MeOH and 1.65 H_2O while the complex **30$^{(R)}$** has 0.25 MeOH, 1.63 H_2O in the range of experimental error. The elemental analyses are in agreement with the ^{1}H NMR spectra findings.

The (S)- and (R)-complexes **27$^{(S)}$**, **27$^{(R)}$** are more stable both as solids and in solution than the complexes functionalized with thiophene, as revealed by ^{1}H NMR spectrometry. The Zn(II)-complexes functionalized with thiophene units are highly sensitive to water and air moisture as reported for similar binaphthyl derivates.[233] The complexes hydrolyzed fast to the corresponding ligands in wet solvents and with the water contained in deuterated solvents, as observed by ^{1}H NMR spectroscopy. Thus, the reaction conditions and the workup required dry solvents which prior to use were further dried over activated molecular sieves. Yet, a complete removal of water from solvents is not possible. We were not able to isolate the 4-thiophene functionalized Zn(II)-complex **33$^{(S)}$** as pure compound in spite of several attempts to purify by recrystallization. The ^{1}H NMR characterization showed that the complex contains 8% of uncoordinated ligand.

The MALDI-TOF spectra of the (S)- and (R)- ligands **26$^{(S)}$**, **26$^{(R)}$** show an intense peak corresponding to the ligand isotopic pattern with molecular mass $[M+H]^+$=650.8 (Annex). The fragmentation of the one branch $[M-A]^+$ as shown in figure 74, is observed as weak signal only when the intensity of the laser is increased.

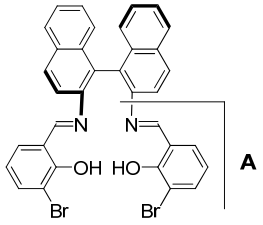

Figure 74. Mass spectrometric fragmentation of the (S)- and (R)-ligands **26$^{(S)}$**, **26$^{(R)}$**

In the chiral Zn(II)-complexes **27$^{(S)}$**, **27$^{(R)}$** the mass spectra present an intense peak corresponding to the molecular mass $[M+H]^+$ at 714.8. The isotopic patterns clearly show the ligand combination with two bromine atoms and a zinc cation (Annex). Additional peaks in low intensity appear as $[M+Na]^+$ at 734.8 and $[M-Zn]^+$ at 650.7. The loss of the Zn atom is probably due to the fragmentation or decomposition with the matrix.

The MALDI-TOF spectra of the (S)- and (R)-thiophene functionalized ligands **29$^{(S)}$**, **29$^{(R)}$**, **32$^{(R)}$**, **32$^{(R)}$** show only the intense peak corresponding to the ligand isotopic pattern with molecular mass $[M+H]^+$ at 657.0 (Annex). Their Zn(II)-complexes present an intense peak corresponding to their molecular masses $[M+H]^+$ at 718.8. For these complexes the loss of the Zn atom with the peak $[M-Zn]^+$ at 650.7 is evidenced in significant intensity.

The IR spectra of (R)- and (S)-ligands and their Zn complexes exhibit peaks corresponding to aromatic stretches in addition to the characteristic imine stretches ν(C=N) around 1600 cm^{-1}.

The UV-vis spectra of the (S)- and (R)-**26**$^{(S)}$ and **26**$^{(R)}$ ligands exhibit characteristic absorption bands from two major chromophores: the salicylaldimine and the binaphthyl backbone. The strong signal at 231 nm can be assigned to a $\pi \rightarrow \pi^*$ transition of the binaphthyl backbone. The broad bands found at lower energy at 324 and 354-369 nm with a shoulder at about 390 nm, are assigned to the imine $\pi \rightarrow \pi^*$ transitions.[233] The metalation reaction leads to a strong decrease in the ε value of the 329 nm absorption band and the disappearance of the broad 354-369 nm band. Upon complexation with the metal, the band at 390 nm in low energy assigned to the imine $\pi \rightarrow \pi^*$ transitions is significantly enhanced.

The UV-vis spectra of the thiophene functionalized (S)- and (R)- ligands **29**$^{(S)}$, **29**$^{(R)}$, exhibit the same bands with the 227 nm signal traced to binaphthyl moiety and the broad band at 371 nm with lower energy assigned to the imine $\pi \rightarrow \pi^*$ transitions. After metalation the 230 and 282 nm bands keep the positions and intensities from the free ligand. A strong red-shift of the imine $\pi \rightarrow \pi^*$ transition band to 419 nm with a lower energy was observed which supports the complexation of the metal ion.[231, 233]

Single crystal X-ray structures of (S)- and (R)-ZnL^g

Single crystal X-ray diffraction studies were realized for both (S)- and (R)- ZnL^g isomers **27**$^{(S)}$, **27**$^{(R)}$. The absolute configurations of both complexes were found as expected to be (S)- or (R)- as shown in figure 75. The crystallographic data, selected bond lengths and bond angles are given in Annex are summarized. Both (S)- and (R)-isomers crystallize in the trigonal crystal system R3. There are nine identical molecules per unit cell. Each molecule of the (S)-complex has in vicinity one CH_2Cl_2 solvate molecule, while each molecule of the (R)-isomer is surrounded by 2.33 MeOH solvate molecules. The coordination environment of the Zn(II) cations for both isomers is identical as expected. The binaphthyl Schiff base acts as a tetradentate ligand, with two nitrogen atoms and two oxygen atoms of the deprotonated phenolic groups, all coordinate to the metal center to form a neutral metal complex. The Zn-N bonds are longer that the Zn-O bonds. The two Zn-N bonds are identical with 2.01 Å for (S)-isomer and 2.02 Å for (R)-isomer. The lengths of the two Zn-O(1) and Zn-O(2) bonds are 1.91 respective 1.93 Å. The rigidity of binaphthyl unit in the ligand structure determines the shape of the complex. Thus two legs of salicylaldimine substructure fold around the metal ion. The legs are very similar to each other which can be seen in comparing O(1)-Zn(1)-N(1), O(2)-Zn(1)-N(2) angles of 95° and 94° respectively. Driven by the structure of the ligand the O(1)-Zn(1)-O(2) angle of 108° is wider than the N(1)-Zn(1)-N(2) angle with 97° respectively. Due to these angles the tetrahedral coordination sphere around the Zn(II)-cation is distorted. The asymmetric binaphthyl group forms an angle between the two planes of the naphthylene rings of 73.8° for the (S)-isomer and 75.5° for the (R)-isomer respectively. Bond lengths and angles to the metal center as well as the dihedral angles between the naphthylene rings are within the range of reported values.[230, 233]

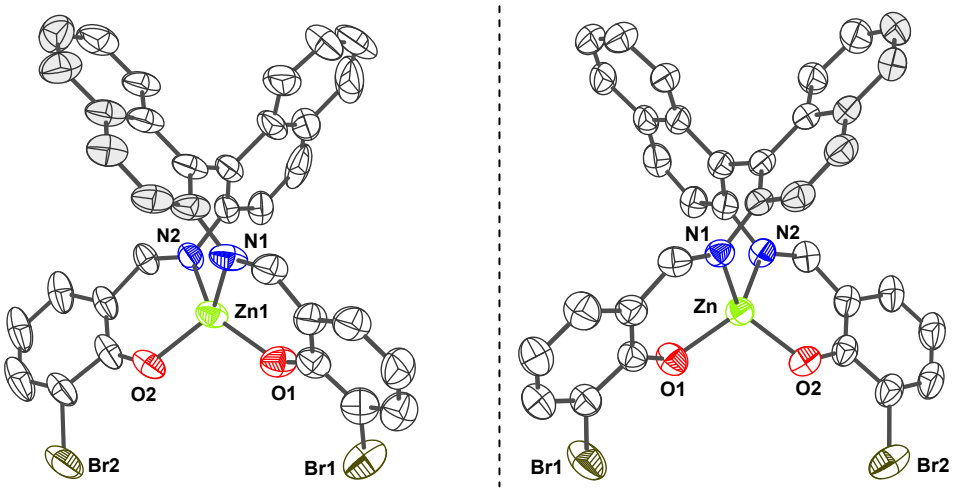

Figure 75. Single crystal X-ray structures of binaphthyl Schiff-base complexes **27$^{(S)}$**, **27$^{(R)}$**, **(S)-ZnL^{g}** (left) and **(R)-ZnL^{g}** (right). The hydrogen atoms, CH_2Cl_2 or MeOH solvate molecules were omitted for clarity (drawing with ellipsoid plot at 50% probability level). The (R)- or (S)- absolute configuration is evidenced by grey colour of the projected binaphthyl carbon atoms.

The chelating moieties formed by the imine and phenoxy functionalities are nearly coplanar to the bromo-phenyl units of the side legs. The dihedral angle between the planes formed by the two chelating moieties N_2O_2 has an angle of 65.32° for (S)- and 63.7° for (R)-isomer respectively. The preference of such complexes for a non planar N_2O_2 arrangement given by the binaphthyl unit has already been reported and compared to the planar N_2O_2 coordination of salen type complexes.[230] The small differences in bond lengths and angles between both isomers (Annex) are probably due to the crystal packing with different solvate molecules. The crystal packing of both (S)- and (R)-isomers (Annex) present edge to face CH···π stacking interactions between binaphthyl and the phenolate units with 3.40 Å, H-centroid for (S)- and 3.17 Å, H-centroid for (R)-isomer.

In case of (S)-complex crystal packing one CH_2Cl_2 solvate molecule has a weak contact to one phenolate oxygen (H···O, 2.65 Å). Attempts to remove the solvent entirely failed at a vacuum of 10^{-3} mbar.

Single crystal X-ray structure of (S)-ZnL^{h}

The absolute configuration of the (S)- ZnL^{h} complex **30$^{(S)}$** is confirmed by single crystal X-ray structure (figure 76). The crystallographic data, selected bond lengths and angles are given in Annex. The complex crystallizes in the trigonal crystal system P 3(1). One of the terminal thiophene groups is disordered and thus refined in two positions.

The coordination geometry of (S)-thiophene complex **30$^{(S)}$** is completely different than the above presented complexes **27$^{(S)}$**, **27$^{(R)}$**. Additionally to the N_2O_2 chelating moieties, the Zn(II)-ion coordinates the oxygen atom of a MeOH molecule with the distance metal - oxygen of almost 2.2 Å. This produces a five coordinate metal center with distorted trigonal bipyramidal geometry. The Zn atom shares a plane with O1, N2 and O7 forming slightly deviated 120° angles to each other. The N1 and O2 are situated

above and below the plane as shown in figure 77 with an angle N1-Zn1-O2 of 170°. There are small differences in the Zn-O and Zn-N distances with 1.95 and 2.18 Å respectively (Annex).

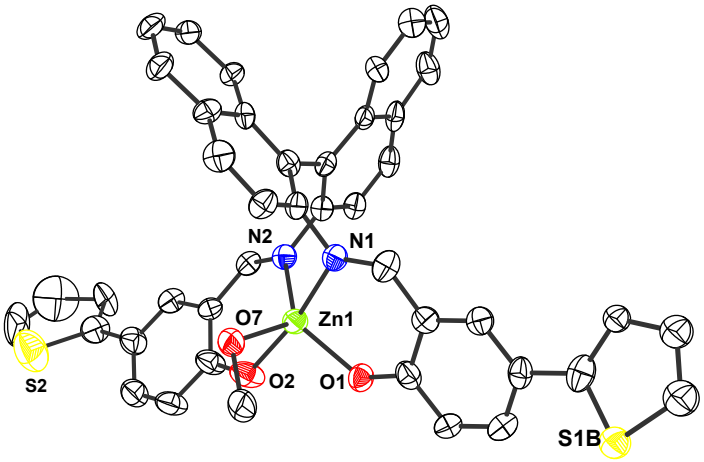

Figure 76. Single crystal X-ray structures of (S)-thiophene binaphthyl complex **30**$^{(S)}$. The hydrogen atoms, CH_2Cl_2 and MeOH solvate molecules were omitted for clarity (drawing with ellipsoid plot drawn at 50% probability level).

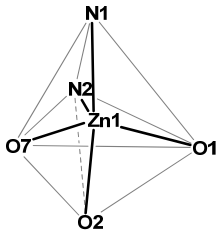

Figure 77. Trigonal bipyramidal geometry of (S)-thiophene binaphthyl complex **30**$^{(S)}$.

The unit cell contains nine molecules of (S)-Zn(II)-complex. There are three distinct molecules of (S)-complex in the asymmetric unit cell (Zn1, Zn2 and Zn3) differing by small conformational changes probably due to the crystal packing (figure 78). Each of these three molecules presents the same distorted bipyramidal geometry with one MeOH molecule coordinated to the metal center. However, the bond lengths and angles of the three molecules are slightly different (Annex). In addition, a change of the dihedral angles between the binaphthyl units of three molecules with Zn1: 66.5°, Zn2: 70.1°, Zn3: 70.2°) are observed. These angles are smaller than for the corresponding analogues **27**$^{(S)}$, **27**$^{(R)}$, but still in the range where the steric repulsions given by binaphthyl moiety are relatively low.[233] The molecules are organized in the crystal by diverse intermolecular π stacking interactions and hydrogen bonding. The hydrogen bond is realized between the hydrogen atom of the coordinated MeOH to the Zn1 molecule and the phenolate oxygen atom of the neighbour Zn2 complex molecule (O-H···O, 2.75 Å, H···O, 1.9 Å, red line). The π···π interaction between the phenolate units (centroid-centroid, 3.6 Å, grey line) of Zn2 and Zn1 molecules and edge-to-face C-H···π interaction between thiophene ring of Zn2 molecule and one ring of the binaphthyl unit from Zn3 molecule (H-centroid, 3.1 Å) are observed. For the three complex molecules, two CH_2Cl_2 solvate molecules are included in the crystal structure. One CH_2Cl_2 molecule has a weak contact to one phenolate oxygen atom (H···O, 2.1 Å). Thus, the failure of all attempts to completely remove the solvent molecules in vacuum is not surprising.

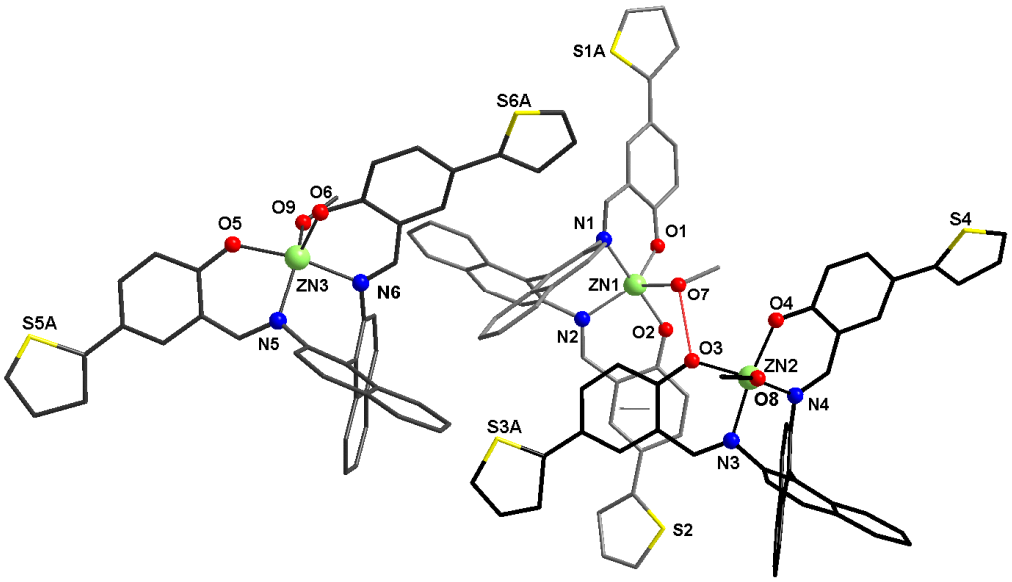

Figure 78. Crystal packing of thiophene binaphthyl complex **(S)-ZnL^{h}**, **30$^{(S)}$** showing the three distinct complex molecules in the asymmetric unit (different grey nuances). The hydrogen atoms and CH_2Cl_2 solvate molecules were omitted for clarity (sticks drawing). The H-bonding (red line) and π stacking interaction are evidenced (grey line).

In conclusion new optically active zinc complexes based on a *salicylidenaldimine* Schiff base and decorated with a chiral binaphthyl unit were synthesized and characterized. The Schiff base component was structurally built up from the enantiopure 1,1'-binaphthyl-diamine and salicylaldehyde derivates and was used for metal coordination. Upon complexation with Zn(II) salt, the chiral information of (S)- or (R)-binaphthyl was maintained. Single crystal X-ray diffraction confirmed the Zn(II)-complex structures and their absolute configuration. Differently substituted salicylaldehydes were used in the synthesis to tune diverse properties and applications. Thus the Zn(II)-complexes are proposed for surface studies and electrochemical polymerization. Photopysical properties such as light emission as well as circular dichroism of the chiral Zn(II)-complexes are currently under investigation.

Chapter 5.

Functionalized thioketal compounds for SAMs study

5.1. Introduction

In this chapter the thioketal functionality as new anchoring group for electronic transport investigations on gold surface is proposed. In order to study the influence of the molecular topology upon the conductivity, functionalized dithioketal compounds received our attention. After developing a compatible synthetic route to introduce the desired functionalities, we obtained a series of different substituted thioketal molecules. The resulted structures comprise a pyridyl unit, its corresponding methylpyridinium iodide or hexafluorophosphate salt as well as the uncharged 4-tolyl analogue.

An introductory overview outlines reported reaction conditions for the synthesis of the target molecules.

The fundamental understanding of charge transport through single molecules is a key issue in molecular electronics.[15, 45] However, chemical functionality and structural requirements have to be adapted to the applied method. In particular, the complexity of the studied system often states a limit. The emphasis of reducing the complexity of molecular structures to a lower level is driven by the necessity of better understanding of the molecule-surface interaction. The field of SAMs on surfaces has been introduced by the use of thiol containing organic compounds such as: alkyl thiols on gold, silver, and copper as well as dialkyl sulfides or disulfides on gold.[241] Higher elaborate systems are to be developed if certain properties, for example special magnetic, electronic and electro-chemical properties shall be gained by the molecules of interest.

Numerous examples in literature report on double quaternized salts of bipyridine known as viologens, with the well understood electrochemistry of redox-active bipyridine center.[242] Electronic properties of alkyl-thiol linkers connected to a 4,4-bipyridinium unit (figure 79a) have been addressed experimentally from macroscale self-assembled monolayers, low coverage phase on gold surface to single-molecular junctions.[243 - 245] A theoretical model for the electron transport mechanism of such systems has also been established.[8] The electrical property of a dipyridinium dithioacetate derivate

(figure 79b) immobilized on Au(111) surface in SAMs was investigated by STM and the NDR properties were observed by STS method.[246]

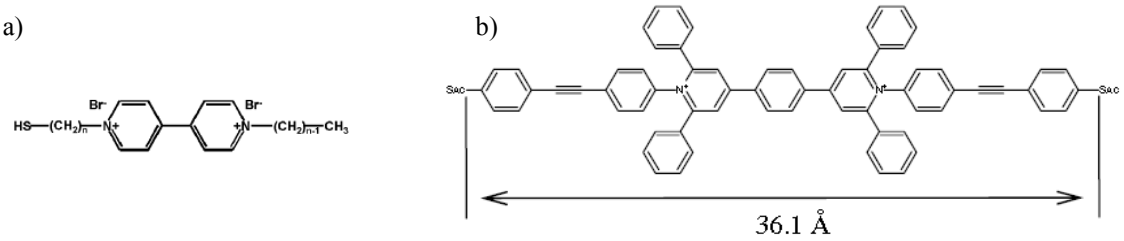

Figure 79. Examples of viologen structures investigated in SAMs on gold surface

This project is focused on the synthesis of molecules containing functionalized thioketal compounds for anchoring on metal surface by self assembly method. In this purpose new thioketal compounds (figure 80) were chosen as target molecules and a plausible synthetic approach was designed. These structures comprise: a) a pyridinium salt, c) a pyridine unit and b, d) their correspondents without charge. The targeted structural analogous charged molecules - one containing phenyl substituent and the second a methyl group connected to the thioketal carbon and their analogues without charge - allow for a differentiated study on the surface. However, to our knowledge, simple pyridinium functionalized molecules containing thioketal groups for metal surface assembly have not been reported so far.

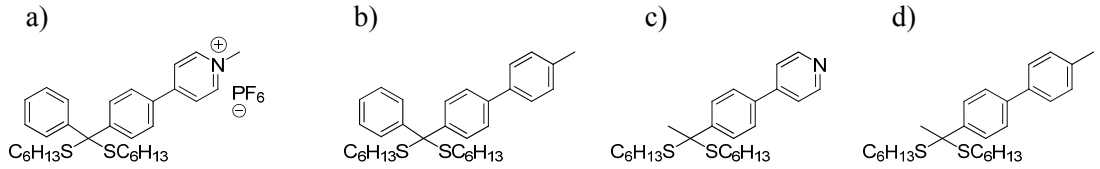

Figure 80. Target thioketal molecules for surface investigation

Organic molecules carrying one or more electrostatically charged groups are called amphiphilic and are used as detergents, surfactants, etc. There especially the formation of charge-separated states and the localization of the charge are of major importance. Charge carrying groups are quarternated amines, imines (positively charged), or deprotonated acidic groups such as sulfonates, phosphonates or carboxylates (negatively charged).[247] Pyridinium salts possess antibacterial properties, ionic liquid behaviour and in particular a high capacity to be absorbed on negatively charged surfaces. [248]

The electron attraction and repulsion forces can be analyzed by measuring the redox properties on the metallic surfaces. Upon reduction the pyridinium unit is transformed into radical state as: $Py^{+} \rightarrow Py^{\bullet}$, thus this radical would also enable the system to be analyzed regarding magnetic properties.

The role of dithioacetals/dithioketals in organic synthesis is well known as protective groups.[249] The study of varied thio-functionalized protective groups is of great importance for surface attachment. The two thio-alkyl groups constitute anchoring points to the gold surface. The dithioketal acts as bidentate surface coordination unit thus a more stable anchoring group to the surface can be expected. Hereby, the two fields of science of amphiphilics and of thiol coordination are combined.

The lack of reports concerning the synthesis of structurally related pyridinium thioketal compounds requires a very careful synthetic approach and documentation of thioketalization conditions.

In general thioacetals and thioketals are prepared by protic or Lewis acid catalyzed condensation of carbonyl compounds with thiols or dithiols. In literature several reported methods for the preparation of thioacetals and thioketals from carbonyl compounds are described [249] employing catalysts as: HCl,[250, 251] $BF_3 \cdot Et_2O$,[252, 253] TMSSMe,[254] TMSCl,[255, 256] Bu_3P,[257] p-TsOH,[258, 259] $(COOH)_2$,[260] $TiCl_4$, [261, 262] $AlCl_3$,[263] CuBr, [264] $NaHSO_4$ - SiO_2,[265] $MoCl_5$ or MoO_2Cl_2,[266] $SOCl_2$ - SiO_2,[267] etc. The thioacetalization/ thioketalization reaction has been studied intensively as a very useful reaction of protecting the carbonyl functionality. Even though a large number of methods have been developed, general methods cannot be applicable for all the carbonyl compounds. As a drawback, some of these methods require strong acidic conditions or expensive reagents, long reaction times or give low yields of the products. The reaction is reversible and thus an excess of thiol together with continuous removal of water are required. The reactions of aromatic ketones are known to occur considerably more slowly compared with aldehydes and do not lead to completion.[267] Applied on ketones, some of the published methods fail completely.[265, 264] Heterocyclic aromatic aldehydes are also thioacetalized with difficulty.[264, 267] The majority types of catalysts are not compatible with the pyridine function. Catalyst such as HCl, BF_3-Et_2O, $AlCl_3$, p-TsOH, fail to produce heterocyclic thioacetals.[266] Although few thioacetalization reactions of aldehyde with pyridine containing units in presence of acids, p-TsOH or $BF_3 \cdot Et_2O$ have been reported before,[264, 267 -271] it is likely that the presence of the pyridine functionality leads to the formation of other products due to protonation, the formation of pyridinium p-toluenesulfonate compounds,[272] or adducts of pyridine-boron trifluoride complexes.[273, 274]

To investigate the reactivity of different ketone structures with several reported procedures applicable for thioacetalization/ thioketalization is a difficult task. Apparently, there is still a need to develop efficient pathways for the synthesis of thioketals containing higher substituted structures. Alternative methods reported in literature to introduce pyridine units in thioacetals or thioketals are the reaction between dithiane lithium salts and pyridine,[275] or treatment of 2-picoline with NDA or KDA (mixtures of ^{t}BuONa or ^{t}BuOK, n BuLi, D^{i}PrA),[276] but these methods cannot be applied to synthesize structures as the target compounds. A more accessible synthetic route is first to introduce the thioketal group in simple ketone structures (scheme 9) and then other functionalities which in the first instance are not compatible with the thioacetalization reaction conditions. For example the pyridine group can be introduced in good yield by standard cross coupling reactions. The thioacetal/ thioketal groups turned out to be compatible with Suzuki and Sonogashira cross coupling conditions [277] and with Menschutkin quaternization in mild conditions, giving good yields. However, the metal salts and MeI are reagents to cleave the dithio acetal and ketal groups in other reaction conditions.[249]

5.2. Results

Synthesis of functionalized thioketal molecules

In the Scheme 9 the synthetic pathway for the formation of functionalized thioketal compounds is depicted. Since they are structural analogues they will be discussed in parallel in a general reaction scheme.

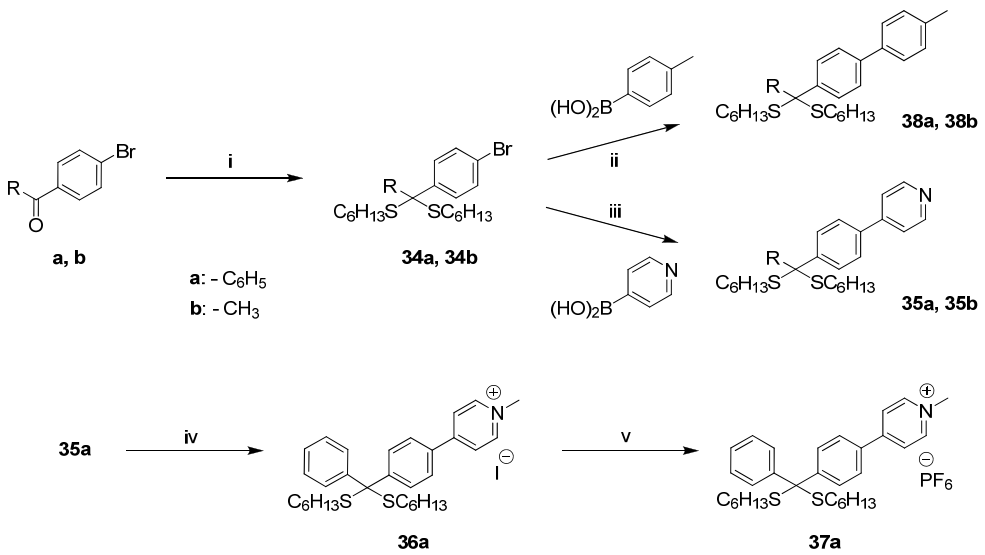

Scheme 9. Synthetic route of pyridinium salts with thioketal groups. Reagents and conditions: (i) $C_6H_{13}SH$, TMSCl, $CHCl_3$, molecular sieves, 60°C, (ii)(iii) $Pd(PPh_3)_3$, DME, Na_2CO_3 aq., N_2, 80°C; (iv) MeI, MeCN, rt, (v) KPF_6, acetone/H_2O, rt.

In the first step the dithioacetal group was introduced and resulted in formation of compounds **34a**, **34b**. The reaction was performed after a published method to convert the carbonyl compound efficiently into thioketal, with excess of thiol in presence of trimethylchlorosilane which activates the ketone function.[255] Then, Suzuki cross-coupling reactions [277] introduced the pyridyl or tolyl units to form the compounds **35a**, **35b**, **38a**, **38b**. The next step, a Menschutkin quaternization by N-alkylation with excess of methyl iodide in MeCN at rt, formed the methyl pyridinium iodide **36a**. The pyridinium hexafluorophosphate salt **37a** was prepared by anion metathesis in acetone/ water and was purified by column chromatography to remove possibly unreacted pyridinium iodide salt.

Characterization of functionalized thioketal molecules

The identity and purity of all new compounds **34a,b - 38a,b** was proved by the complete characterization with the ^1H and ^{13}C NMR, IR spectroscopy, ESI-TOF, MALDI-TOF, UV-vis methods and elemental analyses.

The ^1H NMR spectral data for all compounds are given in table 8 and the spectra of the thioketal compounds **34a-37a** are shown in figure 81.

Since the compounds are structural analogues they will be discussed in parallel. The significant resonances for the thioketal compounds are the proton signal corresponding to the alkyl chains of the thioketal group which retain almost the same chemical shift, coupling constant and peak patterns for all isolated compounds. The introduction of the pyridine or tolyl functionality by Suzuki reaction was confirmed by the presence of the characteristic signal pattern of pyridine respectively of tolyl units (compounds **35a**,**b** and **38a**,**b**). Additionally, a small shift of the aromatic protons after introduction of pyridine functionality appeared in the case of compounds **35a**,**b**. After Menschutkin quaternization (compound **36a**), as a result of N-alkylation, the signals for the pyridinium iodide protons were significantly shifted about 0.47-0.69 ppm to lower magnetic field and the characteristic signal for N-methyl group appeared at 4.58 ppm. In the ^{1}H NMR spectra of the two pyridinium salts **36a** and **37a**, the chemical shifts of the protons are anion dependent,[278] which is indicated by the differences in the proton chemical shift of the methyl and pyridinium groups close to the counterion, as listed in table 8.

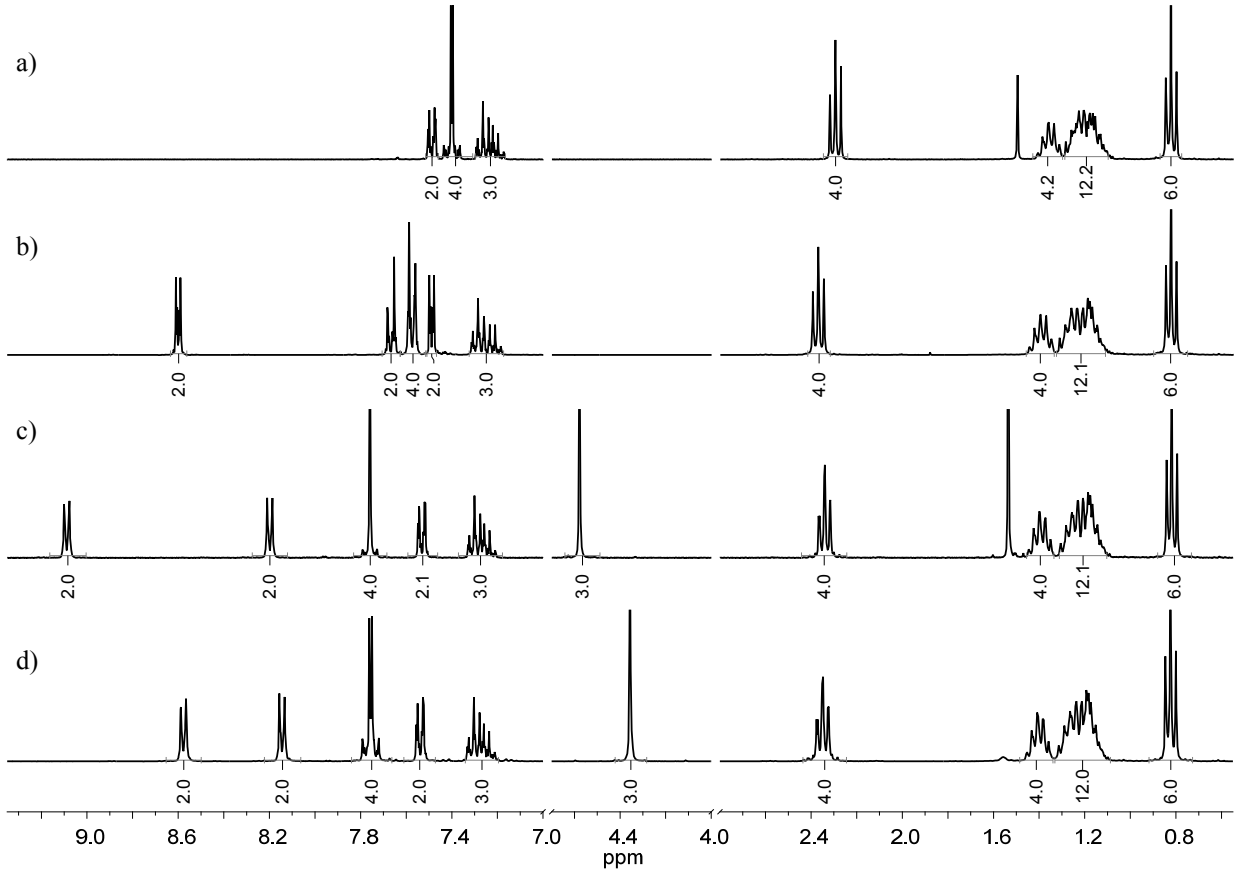

Figure 81. ^{1}H NMR spectra in CD_2Cl_2 of: (a) thioketal **34a**, (b) pyridine thioketal **35a**, (c) pyridinium iodide **36a**, (d) pyridinium hexafluorophosphate salt **37a**.

Additionally, the ^{13}C NMR spectra of all the compounds confirm their structures. Each compound contains the characteristic signals of the alkyl chains in the region between 13.8-31.6 ppm for CH_3, and CH_2 groups. The quaternary carbon atom of the thioketal group exhibits the specific signal in the region of 59.9-68.9 ppm, present for all compounds. The spectra of both pyridinium salts **36a**, **37a** are identical with no significant differences in the chemical shift.

Table 8. ^{1}H NMR chemical shifts of the thioketal compounds and their pyridinium salts in CD_2Cl_2

Compound δ (ppm)	CH_3 thioketal	CH_2 thioketal	CH_3	CH_3 tolyl	SCH_2	N^+CH_3	Ph	Py
Thioketal **34a**	0.83 (6H)	1.11-1.29 (12H) 1.32-1.42 (4H)	-	-	2.30 (4H)	-	7.18-7.30 (3H) 7.37-7.44 (4H) 7.48-7.51 (2H)	-
Thioketal **34b**	0.87 (6H)	1.19-1.37 (12H) 1.44-1.56 (4H)	1.96 (3H)	-	2.48 (4H)	-	7.43 (2H) 7.58 (2H)	-
Pyridine thioketal **35a**	0.85 (6H)	1.16-1.33 (12H) 1.37-1.48 (4H)	-	-	2.39 (4H)	-	7.28-7.34 (3H) 7.57-7.61 (4H) 7.67-7.70 (2H)	7.51 (2H) 8.62 (2H)
Pyridine thioketal **35b**	0.84 (6H)	1.16-1.37 (12H) 1.44-1.54 (4H)	2.02 (3H)	-	2.51 (4H)	-	7.60-7.65 (2H) 7.79-7.84 (2H)	7.51 (2H) 8.61 (2H)
Pyridinium iodide thioketal **36a**	0.82 (6H)	1.13-1.31 (12H) 1.35-1.43 (4H)			2.32 (4H)	4.58 (3H)	7.24-7.33 (3H) 7.52-7.55 (2H) 7.73-7.80 (4H)	8.20 (2H) 9.09 (2H)
Pyridinium PF_6 thioketal **37a**	0.82 (6H)	1.13-1.31 (12H) 1.36-1.45 (4H)			2.35 (4H)	4.37 (3H)	7.26-7.33 (3H) 7.51-7.56 (2H) 7.72-7.79 (4H)	8.15 (2H) 8.58 (2H)
Tolyl thioketal **38a**	0.91 (6H)	1.18-1.54 (16H)		2.42-2.49 (7H)		-	7.26-7.38 (5H) 7.55-7.60 (4H) 7.67-7.70 (4H)	-
Tolyl thioketal **38b**	0.86 (6H)	1.19-1.38 (12H) 1.45-1.33 (4H)	2.02 (3H)	2.37 (3H)	2.52 (4H)	-	7.24 (2H) 7.48-7.57 (4H) 7.73-7.77 (2H)	

The presence of PF_6 counter ion in the pyridinium salt **37a** was confirmed by ^{31}P NMR spectrum which exhibits a septet consistent with six equivalent ^{19}F nuclei (J=1/2) attached to the central ^{31}P. The large J_{PF} of 712 Hz is typical for ^{31}P-^{19}F coupling constant. [279]

After recording NMR the decomposition of the pyridinium salts was observed (three days in solution, CD_2Cl_2 at rt). While for pyridinium iodide salt **36a** the decomposition in ^{1}H NMR spectrum appeared in relatively 4%, for the pyridinium PF_6 salt **37a** the complete removing of the thioketal unit occurred.

The IR spectra of all thioketal compounds contain characteristic multiple bands in the region 2956-2852 cm^{-1} attributed to the stretching vibration ν(C-H) of the CH_2 and CH_3 thioalkyl groups and ν(S)-CH_2 vibrations. The bands between 1491-1439 and 1394 cm^{-1} are assigned to the deformation vibrations δ(CH_2) and δ(CH_3).[280] The pyridine functionality is evidenced by its characteristic pattern with a strong stretching vibration at 1594 cm^{-1}. This band is shifted to 1638 cm^{-1} in the pyridinium salt as an effect of increasing the number of vibrational modes by quaternization.[281] The anion metathesis is proved by very sharp and broad band at 865-830 cm^{-1} of PF_6 counter ion. All these considerations are in agreement with similar thioketals,[282] pyridine or protonated pyridinium compounds respectively.[281] The MALDI-TOF spectra for the pyridine thioketal compounds **35a**, **35b** present the expected base peaks of their corresponding masses $[M+H]^+$ and the fragmentation in low intensity of one S-alkyl group of the thioketal group as $[M-SC_6H_{13}]^+$. In case of the other thioketal compounds **34a**, **34b**, **38a**, **38b**, no product mass signal could be detected due to the fragmentation of thioketal groups in $[M-SC_6H_{13}]^+$.[277]

The pyridinium salts were characterized by ESI mass spectra in MeCN solutions ($6{,}3\cdot10^{-5}$M of **37a** and $6{,}5\cdot10^{-5}$M of **36a**). The mass spectra of both pyridinium salts show in positive mode the expected

molecular peak of the cation at 492.3 and the fragmentation in low intensity of one branch of the thioketal group at 373.3. The pyridinium hexafluorophosphate salt **37a** shows in negative mode only the base peak of the PF_6^- anion at 144.9 as expected. The pyridinium iodide salt **36a** presents only the peak of I^- anion at 126.9. To confirm the elemental analysis of the pyridinium hexafluorophosphate salt ESI mass spectra were performed on a mixture of pyridinium hexafluorophosphate salt **37a** and pyridinium iodide salt **36a** (9:1 v/v in MeCN).

While in the test mixture both peaks, one of the PF_6^- anion at 144.9 and the peak of I^- anion at 126.9 were present, the experiment for pure pyridinium hexafluorophosphate salt **37a** showed no trace of the I^- anion. Hence the purity oft he hexafluorophosphate can be confirmed (figure 82).

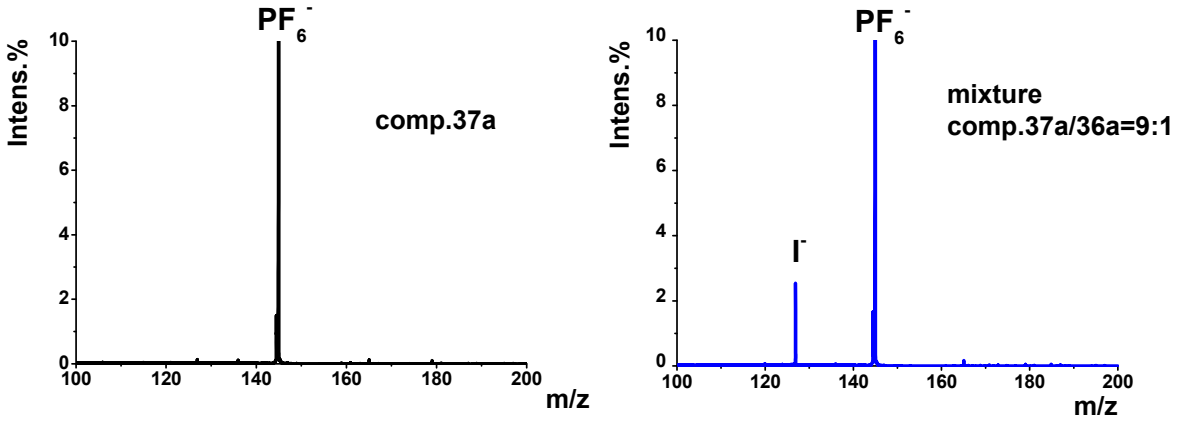

Figure 82. Zoom of ESI mass spectra (10% from 100%), in negative mode, showing the purity test of the pyridinium salt. The left graph presents the pyridinium hexafluorophosphate salt **37a** spectra and the right presents the mixture of pyridinium hexafluorophosphate salt **37a**/ pyridinium iodide salt **36a** (9:1 v/v).

In conclusion a compatible synthetic route of new pyridinium functionalized thioketal target molecules has been realized. The characterization of all new compounds **34a,b-38a,b** support their structures and purity. The purification of the final product, pyridinium hexafluorophosphate salt **37a**, was achieved by using column chromatography and demonstrated by complete characterization.

Chapter 6.

Experimental Section

6.1. Materials and Instruments

The chemicals for synthesis were purchased from Aldrich, ABCR, and Alfa Aesar, with the highest available grade. All the chemicals were used without further purification. All solvents were reagent grade and unless it is specified in the experimental protocol were used without further drying.

Trimethylchlorosilane, $CHCl_3$, CH_2Cl_2, THF, TEA, DIEA, were dried by standard literature procedures and freshly distilled under nitrogen prior to use. THF was dried over Na/ benzophenone and all the other solvents were dried over CaH_2.[283, 284] MeOH, EtOH and CH_2Cl_2 were further dried over activated molecular sieves (3 or 4Å). CD_2Cl_2 and CD_3CN used for the NMR measurements of the compounds from Chapter 5, were dried over activated molecular sieves (4Å).

$Ru(DMSO)_4Cl_2$ has been prepared following standard reported procedure.[162]

5-bromo-2,2'-bipyridine [285] was received from Dr. Frank Schramm (INT) and was further purified by column chromatography. 4-(thioacetyl)-iodobenzene,[161] 5-bromo-pyridine-2-carboxaldehyde,[286] and 5-bromo-salicyl aldehyde [287] were received from my colleague Mr. Matthias Fischer. These compounds have been prepared by my colleagues following standard reported procedures.

Characterizations were performed with the following instruments.

NMR spectra were recorded with a Bruker Ultra Shield DPX300 (^1H at 300 MHz and ^{13}C NMR at 75 MHz). The assignment of ^1H and ^{13}C signals was accomplished with the help of DEPT 135 experiments or, when needed by two-dimensional correlation experiments (COSY, HMQC). The chemical shifts, δ are given in ppm. ^1H and ^{13}C NMR spectra are calibrated to the signals of the deuterated solvents reported in literature. [288]

Melting points were measured with a Büchi Melting Point B-540 apparatus and are uncorrected.

Thin Layer Chromatography (TLC) was carried out on Merck silica gel 60 F_{254} plates or aluminium oxide F_{254}. Column chromatography was realized using Merck silica gel 60 (0.040–0.063 mm) or Merck aluminium oxide 90 active neutral (0.063-0.200 mm).

Elemental analyses were performed by Mr. Matthias Fischer, using the Vario Micro Cube CHNS Analyzer. The data are indicated in mass percent.

Mass spectra were obtained with a MALDI-TOF-MS of PerSeptive Biosystems Voyager–DE PRO (matrix-assisted laser desorption time-of-flight) mass spectrometer. Electrospray ionization (ESI)

spectra were measured on a Bruker microTOF-Mass spectrometer QII from solutions with 10^{-5}-10^{-6} M concentrations. The signals are given in mass-to-charge ratios (*m*/*z*). The relative intensities are given in brackets.

Raman spectra were measured by Dr. Frank Hennrich from INT. The spectra were recorded at 785 nm excitation obtained with a Kaiser Optical Holospec spectrograph which comprises a fiber optic probe head incorporating both excitation laser aperture and collection optics. Spectra were processed via the Kaiser Holoreact program package for Matlab (The Mathworks, Inc.). The sample was run as powder in capillary tube.

Infrared spectra were recorded on Perkin Elmer FT-IR spectrophotometer. The spectra were measured as potassium bromide discs. The absorption bands are given in wave numbers $\tilde{\nu}$ (cm^{-1}).

UV-vis spectra were recorded on VARIAN UV-VIS-NIR spectrophotometer. Emission spectra were measured on a Varian Fluorescencespectrometer Cary Eclipse apparatus using a (1 cm x 1 cm) quartz cell in aerated solutions.

Single crystal X-ray diffractometry was performed by Dr. Olaf Fuhr at INT. The data were collected on a STOE IPDS II diffractometer with graphite monochromated Mo-Kα radiation (l = 0.71073 Å). The structures were solved by direct methods and refined by full-matrix least-squares analysis. The summaries of crystallographic data are presented in supplementary material.

Temperature dependent static susceptibilities of the Fe(II)-*trenpy* complex **11**, were recorded by Dr. Ajay Kumar Mishra, INT. Two continuous cooling and heating cycles (5 K/min) using a MPMS-XL (Quantum Design) SQUID magnetometer over a temperature range of 5↔350 K were applied. The sample was cooled first at zero field with the cooling rate from 300 K to 150 K at 10 K/min, kept 10 min at 150 K than cooling to 5 K with 5 K/min. The system was maintained for equilibrium 5 min then an external field of 1000 Oe was applied. Gelatine capsules were used as sample containers for measurement. The very small diamagnetic contribution of the gelatine capsule had a negligible contribution to the overall magnetization, which was dominated by the sample.

Electrochemistry was performed with help from PhD student Maxim Smetanin. An analytical potentiostat and a conventional single compartment three-electrode cell (5 mL) were used. The working electrode was a Pt wire (1 mm), the counter electrode was a micro Pt electrode and the reference electrode a nonaqueous quasi-reference Ag/Ag^+ wire electrode. Bu_4NPF_6 was previously recrystallized from EtOH and dried under vacuum. The supporting electrolyte Bu_4NPF_6 (0.1 M) in MeCN anh. was degassed with Ar before each measurement. The reference potential was standardized with ferrocene, considering the redox potential of Fc^+/Fc at 380 mV *vs.* SCE.[130] The scan rates were between 20 and 100 mV/s.

6.2. Tripodal metal complexes

6.2.1. Tripodal trensal and trenpy Schiff base complexes

6.2.1.1. M(III)-*trensal* complexes

M(III)-*trensal* complexes with thiomethyl end groups

Compound 1. *Synthesis of 4-(4'-methylthio)-phenyl-salicylaldehyde*

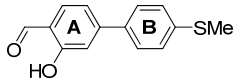

A solution of 4-bromo-salicylaldehyde (513 mg, 2.55 mmol) and 4-(methylthio)-phenyl-boronic acid (643 mg, 3.83 mmol) in toluene/MeOH (40 mL, 3/1) was degassed with N_2 for 30 min. $Pd(PPh_3)_4$ (147 mg, 0.127 mmol) and degassed Na_2CO_3 aq., 2M (811 mg, 7.65 mmol) were added and the mixture was stirred at 70°C under N_2 for 2 days. After evaporation of the solvent, the reaction mixture was diluted with CH_2Cl_2 (200 mL), poured into H_2O (100 mL) and extracted with CH_2Cl_2 (3x150 mL). The combined organic layers were dried over $MgSO_4$ and evaporated under vacuum. The residue was purified by column chromatography (SiO_2, hexane/CH_2Cl_2, 2/1 to 1/1). Recrystallization in CH_2Cl_2/hexane gave the pure compound **1** (308 mg, 49%).

The single crystal X-ray structure of the functionalized aldehyde **1** confirmed in the first instance the correct structure of the tailored scaffold. The structure was determined on single crystal obtained by slow evaporation of hexane/CH_2Cl_2 (figure 83).

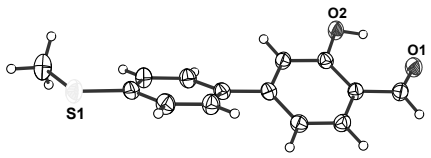

Figure 83. X-ray crystal structure of the compound **1** (ellipsoid plot drawing at 50% probability level).

R_f (SiO_2, CH_2Cl_2/hexane, 1/1): 0.185; M.p. 134.5-134.9°C;

Anal.calc. for $C_{14}H_{12}O_2S$ (M_r = 244.31): C, 68.83; H, 4.95; S, 13.13; Found: C, 68.58; H, 5.11; S, 13.09;

^{1}H NMR (CD_2Cl_2): δ (ppm) 2.51 (s, 3H, SCH_3), 7.18 (d, *J* = 1.7 Hz, 1H, Ph^A), 7.25 (dd, *J* = 8.1, 1.7 Hz, 1H, Ph^A), 7.35-7.28 (m, 2H, Ph^B), 7.64-7.54 (m, 3H, Ph^A, Ph^B), 9.89 (s, 1H, CHO), 11.08 (s, 1H, OH);

^{13}C NMR (CD_2Cl_2): δ (ppm) 15.2 (SCH_3), 115.1, 118.5, 119.6, 126.4, 127.7, 134.3, 135.6, 140.41, 149.0, 162.0, 196.2 (CHO);

MALDI-TOF (1,8,9-anthracenetriol), m/z (%): 244.8 (100) $[M+H]^+$;

Selected IR (KBr pellet): $\tilde{\nu}$ (cm^{-1}) 3209, 2860, 1667, 1625, 1594, 1567, 1541, 1483, 1430, 1304, 1232,

1187, 1090, 920, 807, 788, 744;

UV-vis (CH_2Cl_2) λ, nm (ε, $M^{-1}cm^{-1}$): 337 (24100), 226 (17600);

Compound 2. *Synthesis of trensal ligand with thiomethyl end groups,* **L**[a]

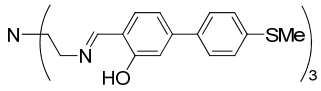

A solution of tris-(2-aminoethyl)-amine (152.4 mg, 1.042 mmol) in EtOH (3 mL) was added to a solution of aldehyde **1** (763.8 mg, 3.126 mmol) in EtOH (70 mL). The solution turned to yellow and a yellow precipitate appeared rapidly. The reaction mixture was stirred at rt overnight. The precipitate was filtered and washed with cold EtOH (2x3mL) and Et_2O (3mL). Recrystallization in EtOH/ CH_2Cl_2 gave the pure ligand 2 (815 mg, 95%).

M.p. 171.5-171.9°C;

Anal.calc. for $C_{48}H_{48}N_4O_3S_3$ (M_r = 825.12): C, 69.87; H, 5.86; N, 6.79; S, 11.66; Found: C, 69.70; H, 5.97; N, 6.88; S, 11.60.

^{1}H NMR (CD_2Cl_2): δ (ppm) 2.51 (s, 9H, SCH_3), 2.85 (t, ^3J = 5.1 Hz, 6H, CH_2), 3.58 (t, ^3J = 5.1 Hz, 6H, CH_2), 6.43 (d, ^3J = 8.0 Hz, 3H, Ph^A, H-6), 6.72 (dd, ^3J = 8.2, ^4J = 1.7 Hz, 3H, Ph^A, H-5), 7.10 (d, ^4J = 1.6 Hz, 3H, Ph^A, H-3), 7.28 (d, ^3J = 8.3 Hz, 6H, Ph^B), 7.47 (d, ^3J = 8.2 Hz, 6H, Ph^B), 7.98 (s, 3H, CH=N), 13.74 (s, 3H, OH);

^{13}C NMR (CD_2Cl_2): δ (ppm) 15.4 (SCH_3), 55.6 (CH_2), 57.9 (CH_2), 114.6, 116.9, 117.8, 126.6, 127.4, 132.1, 136.8, 138.9, 143.9, 161.6 (C-OH), 165.8 (CH=N);

MALDI-TOF (1,8,9-anthracenetriol), m/z (%): 825.1 (100) $[M+H]^+$, 568.0 (77) $[M-A]^+$ (figure 84);

Selected IR (KBr pellet): $\tilde{\nu}$ (cm^{-1}) 3433, 2906, 2815, 1626, 1487, 1377, 1094, 921, 800;

UV-vis (CH_2Cl_2) λ, nm (ε, $M^{-1}cm^{-1}$): 416 (625), 310 (78000), 226 (74100);

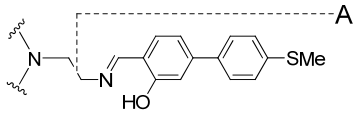

Figure 84. Mass spectrometric fragmentation of the *trensal* ligand **2**

Compound 3. *Synthesis of trensal Ga(III)-complex with thiomethyl end groups*

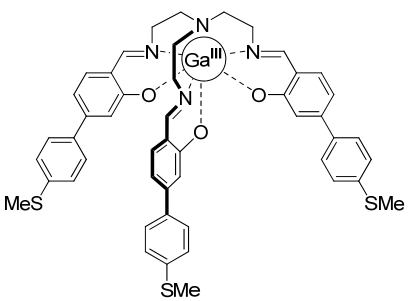

To a suspension of ligand **2** (155.5 mg, 0.182 mmol) in MeOH (35 mL) was added a solution of NaOH (22.6 mg, 0.565 mmol) in MeOH (4 mL). After stirring for 5 min a solution of $Ga(NO_3)_3$ (76 mg, 0.182 mmol) in MeOH (10 mL) was added. The reaction mixture was stirred for 3 h to reflux. The resulted yellow powder was filtered and washed with MeOH (2x2 mL). Recrystallization from CH_2Cl_2/hexane gave the Ga(III)-complex **3** (132 mg, 82%).

Crystals suitable for single crystal X-ray diffraction were obtained by slow evaporation of CH_2Cl_2/hexane.

M.p.>300 °C;

Anal.calc. for $C_{48}H_{45}GaN_4O_3S_3 \bullet H_2O$: C, 63.36; H, 5.21; N, 6.16; S, 10.57; Found: C, 63.61; H, 5.39; N, 6.09; S, 10.62; ^{1}H NMR support the elemental analysis with 1 H_2O molecule;

Anal.calc. for $C_{48}H_{45}GaN_4O_3S_3$ (M_r = 891.81): (dried 100°C, 1 week, 10^{-3} mbar) C, 64.65; H, 5.09; N, 6.28; S, 10.79; Found: C, 64.58; H, 5.24; N, 6.37; S, 10.71;

^{1}H NMR (CD_2Cl_2): δ (ppm) 2.47 (s, 9H, SCH_3), 2.85 (td, *J* = 12.1, 3.3 Hz, 3H, CH_2), 3.07 (dd, *J* = 12.2, 2.8 Hz, 3H, CH_2), 3.32 (dd, *J* = 14.3, 2.7 Hz, 3H, CH_2), 3.80 (td, *J* = 12.0, 2.7 Hz, 3H, CH_2), 6.83 (dd, ^3J = 8.1, ^4J = 1.7 Hz, 3H, Ph^A, H-5), 6.89 (d, ^4J = 1.7 Hz, 3H, Ph^A, H-3), 7.16 (d, ^3J = 8.2 Hz, 3H, Ph^A, H-6), 7.26-7.22 (m, 6H, Ph^B), 7.58-7.53 (m, 6H, Ph^B), 8.14 (s, 3H, CH=N);

^{13}C NMR (CD_2Cl_2): δ (ppm) 15.4 (SCH_3), 57.0 (CH_2), 61.8 (CH_2), 113.1, 116.6, 119.78, 126.4, 127.4, 135.3, 137.0, 138.7, 146.5, 169.0, (CH=N);

MALDI-TOF (1,8,9-anthracenetriol), m/z (%): 890.4 (100) $[M+H]^+$;

Selected IR (KBr pellet): $\tilde{\nu}$ (cm^{-1}) 3424, 2919, 2863, 2832, 1613, 1557, 1520, 1501, 1475, 1432, 1392, 1218, 1096, 942, 794;

UV-vis (CH_2Cl_2) λ, nm (ε, $M^{-1}cm^{-1}$): 386 (35300), 323 (78300), 240 (73700);

Compound 4. *Synthesis of trensal Fe(III)-complex with thiomethyl end groups*

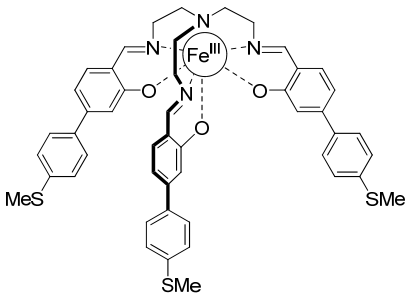

1st method:

To a solution of the ligand **2** (82 mg, 99 μmol) in MeOH/CH_2Cl_2, (40 mL, 1:1) was added a solution of $FeSO_4 \cdot 7H_2O$ (28 mg, 99 μmol) in MeOH (7 mL). The dark brown solution was stirred for 2.5

h at rt under air. During this time a precipitate was formed which was filtered and washed with MeOH (2x2 mL). Recrystallization from DMF/Et_2O gave the Fe(III)-complex (53 mg, 61%).

X-ray crystal structure was determined on single crystal obtained by slow evaporation of DMF/ Et_2O.

Observation: soluble only in warm DMF

Anal.calc. for $C_{48}H_{45}FeN_4O_3S_3$ (M_r = 877.94): C, 65.67; H, 5.17; N, 6.38; S, 10.96;

Anal.calc. for $C_{48}H_{45}FeN_4O_3S_3 \bullet H_2O$: C, 64.35; H, 5.29; N, 6.25; S, 10.74; Found: C, 64.66; H, 5.21; N, 6.48; S, 10.54 (from single crystals recrystallized in DMF/Et_2O and dried vacuum, 10^{-3} mbar);

MALDI-TOF (1,8,9-anthracenetriol), m/z (%): 877.7 (100) $[FeL+H]^+$;

Selected IR (KBr pellet): $\tilde{\nu}$ (cm^{-1}) 3428, 1609, 1598sh, 1502, 1426, 1389, 1111, 1097;

2nd method:

To a solution of the ligand **2** (158.5 mg, 192 µmol) in MeOH/CH_2Cl_2, (80 mL, 1:1) were added a solution of NaOH (23 mg, 565 µmol) in MeOH (2 mL) and $FeCl_3 \cdot 6H_2O$ (52 mg, 192 µmol, 10 mL MeOH). The dark brown solution was stirred for 3 h at rt under air. During this time a precipitate was formed which was filtered and washed with MeOH (2x20 mL). Recrystallization from CH_2Cl_2/MeOH gave the Fe(III)-complex (130 mg, 77%).

X-ray crystal structure was determined on single crystals obtained by slow evaporation of CH_2Cl_2/MeOH.

Observation: soluble in CH_2Cl_2

Anal.calc. for $C_{48}H_{45}FeN_4O_3S_3$ (M_r = 877.94): C, 65.67; H, 5.17; N, 6.38; S, 10.96;

Anal.calc. for $C_{48}H_{45}FeN_4O_3S_3 \bullet H_2O$: C, 64.35; H, 5.29; N, 6.25; S, 10.74; Found: C, 64.65; H, 5.50; N, 6.29; S, 10.44 (powder, recrystallized in CH_2Cl_2/MeOH and dried in vacuum 110°C, 10^{-3}, 1 week)

MALDI-TOF (1,8,9-anthracenetriol), m/z (%): 878.1 (50) $[FeL+H]^+$, 900.1 (100) $[FeL+Na]^+$;

ESI mass spectrum ($CHCl_3$/MeOH), m/z (%) positive: 878.2 (100) $[FeL+H]^{1+}$, 900.2 (2) $[FeL+Na]^{1+}$, 916.2 (2) $[FeL+K]^{1+}$;

Selected IR (KBr pellet): $\tilde{\nu}$ (cm^{-1}) 3428, 1610, 1598sh, 1502, 1424, 1386, 1096;

UV-vis (CH_2Cl_2) λ, nm (ε, $M^{-1}cm^{-1}$): 235 (76050), 315 (85600), 370 sh (38900), 521 (7600);

Compound 5. *Synthesis of trensal Mn(III)-complex with thiomethyl end groups*

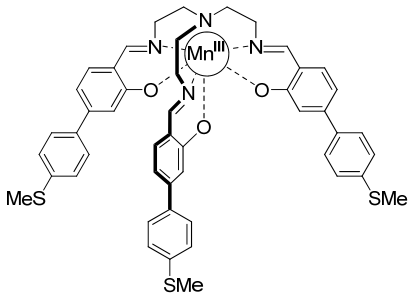

To a solution of the ligand **2** (126.5 mg, 153 μmol) in MeOH/CH_2Cl_2, (80 mL, 1:1) were added a solution of NaOH (18.4 mg, 460 μmol) in MeOH (2 mL) and $Mn(COOCH_3)_3$ (41.1 mg, 153 μmol) in MeOH (5 mL). The dark brown solution was stirred for 3 h at rt under air. During this time a precipitate was formed which was filtered and washed with MeOH (2x10 mL). Recrystallization from CH_2Cl_2/MeOH gave the Fe(III)-complex (95 mg, 71%).

Crystals suitable for single crystal X-ray diffraction were obtained by slow evaporation of CH_2Cl_2/hexane.

Anal.calc. for $C_{48}H_{45}MnN_4O_3S_3$ (M_r = 877.03): C, 65.73; H, 5.17; Mn, 6.26; N, 6.39; O, 5.47; S, 10.97

Anal.calc. for $C_{48}H_{45}MnN_4O_3S_3 \bullet H_2O$: C, 64.41; H, 5.29; N, 6.26; S, 10.75; Found: C, 64.44, H, 5.14; N, 6.27; S, 10.63 (single crystals, recrystallized in CH_2Cl_2/MeOH and dried in vacuum 110°C, 10^{-3}, 2 days);

MALDI-TOF (1,8,9-anthracenetriol), *m*/*z* (%): 878.2 (100) $[MnL+H]^+$, 931.2 (40) $[MnL+CH_3OH+Na]^+$;

ESI mass spectrum (CH_2Cl_2/MeCN), *m*/*z* (%) positive: 877.3 (100) $[MnL]^{1+}$, 651.2 (11) $[MnL-A]^{1+}$, 899.2 (27) $[MnL+Na]^{1+}$, 915.2 (6) $[MnL+K]^{1+}$, 1753.5 (7) $[(MnL)_2+H]^{1+}$, 1775.5 (13) $[(MnL)_2+Na]^{1+}$, 1791.5 (4) $[(MnL)_2+K]^{1+}$, 1807.5 (6) $[(MnL)_2+MeOH+Na]^{1+}$;

Selected IR (KBr pellet): $\tilde{\nu}$ (cm^{-1}) 3422, 1599, 1555, 1516, 1501, 1473, 1445, 1423, 1382, 1308, 1214, 1188, 1096, 940, 796;

UV-vis (CH_2Cl_2) λ, nm (ε, $M^{-1}cm^{-1}$): 236 (64470), 321 (65840), 407 sh (16300), 595 (750);

M(III)-*trensal* complex with pyridine end groups

Compound 6. *Synthesis of 4-(4'-pyridyl)-salicylaldehyde*

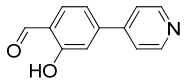

A solution of 4-bromo-salicylaldehyde (472 mg, 2.35 mmol) and 4-pyridine-boronic acid (433 mg, 3.52 mmol) in toluene/MeOH (60 mL, 5/1) was degassed with N2 for 30 min. $Pd(PPh_3)_4$ (136 mg, 0.117 mmol) and degassed Na_2CO_3 aq., 2M (747 mg, 7.04 mmol) were added and the mixture was stirred at 80°C under N_2 overnight. After evaporation of the solvent, the reaction mixture was diluted with CH_2Cl_2 (200 mL), poured into H_2O (200 mL) and extracted with CH_2Cl_2 (3x200 mL). The combined

organic layers were dried over $MgSO_4$ and evaporated under vacuum. The residue was purified by column chromatography (SiO_2, TEA 5%, CH_2Cl_2/ MeOH 1%). Recrystallization in CH_2Cl_2/MeCN gave the pure compound **6** (300 mg, 64%).

R_f (SiO_2, TEA 5%, CH_2Cl_2/MeOH: 95/5): 0.435; M.p. 167.7°C;

Anal.calc. for $C_{12}H_9NO_2$ (M_r = 199.21): C, 72.35; H, 4.55; N, 7.03; Found: C, 72.08; H, 4.56; N, 6.99;

^{1}H NMR (CD_3CN): δ (ppm) 7.32 (d, ^4J = 1.7 Hz, 1H, Ph, H-3), 7.40 (dd, ^3J = 8.0, ^4J = 1.7 Hz, 1H, Ph, H-5), 7.64 (dd, ^3J = 6.2, ^4J = 1.7 Hz, 2H, Py), 7.82 (d, ^3J = 8.0 Hz, 1H, Ph, H-6), 8.68 (d, ^3J = 6.1 Hz, 2H, Py), 10.00 (s, 1H, CHO), 11.03 (s, 1H, OH);

^{13}C NMR (CD_3CN): δ (ppm) 116.6, 119.7, 121.8, 122.7, 135.7, 147.1, 147.1, 151.4, 162.4 (C-2), 198.2 (CHO)

^{1}H NMR (CD_2Cl_2) δ (ppm) 7.25 (d, J = 1.7 Hz, 1H, Ph, H-3), 7.30 (dd, J = 8.0, 1.7 Hz, 1H, Ph, H-5), 7.52 (dd, J = 4.5, 1.7 Hz, 2H, Py), 7.70 (d, J = 8.0 Hz, 1H, Ph, H-6), 8.67 (d, J = 4.6 Hz, 2H, Py), 9.95 (d, J = 0.5 Hz, 1H, CHO), 11.09 (s, 1H, OH);

^{13}C NMR (CD_2Cl_2): δ (ppm) 116.0, 118.7, 120.7, 121.7, 134.5, 146.5, 146.5, 150.5, 161.9 (C-2), 196.4 (CHO);

MALDI-TOF (1,8,9-anthracenetriol), *m/z* (%): 199.7 (100) $[M+H]^+$;

Selected IR (KBr pellet): $\tilde{\nu}$ (cm^{-1}) 2854, 2555, 1678, 1604, 1546, 1422, 1403, 1320, 1277, 1260, 1217, 1008, 820, 797, 721;

UV-vis (CH_2Cl_2) λ, nm (ε, $M^{-1}cm^{-1}$): 340 (6520), 279 (31180), 226 (20130);

Compound 7. *Synthesis of trensal ligand with pyridine end groups,* $\mathbf{L^b}$

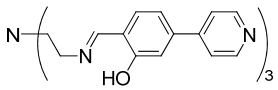

A solution of tris-(2-aminoethyl)-amine (133.3 mg, 0.912 mmol) in EtOH (2 mL) was added to a solution of aldehyde **6** (544.8 mg, 2.735 mmol) in EtOH (30 mL). The reaction mixture was stirred at rt for 12 h. The precipitate formed during the reaction was filtered and washed with cold EtOH (2x3mL). Recrystallization in EtOH/CH_2Cl_2 gave the ligand **2** (530 mg, 84%) as a yellow solid.

M.p. 194.5°C;

Anal.calc. for $C_{42}H_{39}N_7O_3$ (M_r = 689.80): C, 73.13; H, 5.70; N, 14.21;

Anal.calc. for $C_{42}H_{39}N_7O_3$•0,45EtOH: C, 72.52; H, 5.92; N, 13.80; Found: C, 72.38; H, 6.07; N, 13.81; ^{1}H NMR shows 0,45 EtOH molecules;

^{1}H NMR (CD_2Cl_2) δ (ppm) 1.17 (t, J = 7.0 Hz, 0.45EtOH), 2.88 (t, J = 6.0 Hz, 6H, CH_2), 3.73 – 3.52 (m, 6H, CH_2, 0.45EtOH), 6.58 (d, ^3J = 8.0 Hz, 3H, Ph, H-6), 6.78 (dd, ^3J = 8.0, ^4J = 1.8 Hz, 3H, Ph, H-5),

7.17 (d, ^4J = 1.8 Hz, 3H, Ph, H-3), 7.41 (dd, ^3J = 4.5, ^4J = 1.7 Hz, 6H, Py), 8.06 (s, 3H, CH=N), 8.60 (dd, ^3J = 4.5, ^4J = 1.7 Hz, 6H, Py), 13.81 (s, 3H, OH);

^{13}C NMR (CD_2Cl_2): δ (ppm) 55.5 (CH_2), 57.9 (CH_2), 115.2, 116.9, 119.1 (q), 121.5, 132.2, 141.5 (q), 147.2 (q), 150.5, 161.7 (q, Ph, C-2), 165.6 (CH=N);

^{13}C-DEPT 135 NMR (CD_2Cl_2): δ (ppm) 55.4 (CH_2), 57.8 (CH_2), 115.1, 116.8, 121.4, 132.1, 150.4, 165.5 (CH=N);

MALDI-TOF (1,8,9-anthracenetriol), *m/z* (%): 690.2 (100) $[M+H]^+$, 478.1 (40) $[M-A]^+$;

Selected IR (KBr pellet): $\tilde{\nu}$ (cm^{-1}) 2892, 2936, 2838, 1640, 1622, 1596, 1574, 1542, 1488, 1435, 1416, 1391, 1364, 1333, 1293, 1222, 1069, 1032, 931, 920, 885, 870, 834, 804, 734, 541;

UV-vis (CH_2Cl_2) λ, nm (ε, $M^{-1}cm^{-1}$): 331 (18470), 276 (59500), 227 (49160);

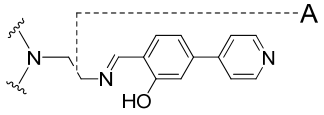

Figure 3. Mass spectrometric fragmentation of the *trensal* ligand **7**

Compound 8. *Synthesis of trensal Ga(III)-complex with pyridine end groups*

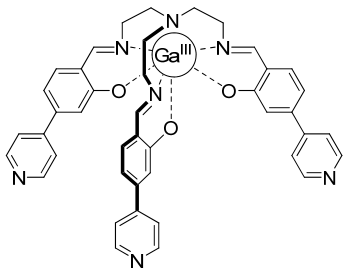

To a suspension of ligand **7** (125 mg, 0.181 mmol) in MeOH (25 mL) was added a solution of NaOH (21.8 mg, 0.544 mmol) in MeOH (4 mL). After stirring for 5 min a solution of $Ga(NO_3)_3$ (73 mg, 0.181 mmol) in MeOH (10 mL) was added. The resulted yellow solution started to precipitate after 30 min stirring to reflux. The reaction mixture was stirred for 3 h to complete the reaction. The resulted yellow powder was filtered and washed with MeOH (2x3 mL). Recrystallization from CH_2Cl_2/MeOH gave the Ga(III)-complex **8** (117 mg, 85%).

Crystals for single crystal X-ray diffraction were obtained by slow evaporation of hexane/CH_2Cl_2.

M.p. 270 °C dec.;

Anal.calc. for $C_{42}H_{36}GaN_7O_3$ (M_r = 756.50): C, 66.68; H, 4.80; N, 12.96;

Anal.calc. for $C_{42}H_{36}GaN_7O_3$•3.5H_2O: C, 61.55; H, 5.29; N, 11.96; Found: C, 61.32; H, 5.22; N, 11.92; ^{1}H NMR shows 3.3 H_2O molecules;

TGA 6% weight loss, 2.68 H_2O molecules;

Anal.calc. for $C_{42}H_{36}GaN_7O_3$•0.5H_2O: C, 65.90; H, 4.87; N, 12.81; Found (dried under vacuum at 100°C,

2 weeks, 10^{-3} mbar): C, 65.82; H, 4.87; N, 12.87; ^{1}H NMR shows 0.4 H_2O molecules;

^{1}H NMR (CD_2Cl_2): δ (ppm) 2.87 (td, *J* = 14.6, 3.5 Hz, 3H, 1B), 3.11 (dd, *J* = 12.1, 3.1 Hz, 3H, 2A), 3.34 (dd, *J* = 14.6, 3.3 Hz, 3H, 1A), 3.81 (td, *J* = 12.5, 3.3 Hz, 3H, 2B), 6.88 (dd, ^3J = 8.1, ^4J = 1.8 Hz, 3H, Ph, H-5), 6.96 (d, ^4J = 1.8 Hz, 3H, Ph, H-3), 7.24 (d, ^3J = 8.1 Hz, 3H, Ph, H-6), 7.50 (dd, ^3J = 4.5, ^4J = 1.7 Hz, 6H, Py), 8.19 (s, 3H, CH=N), 8.56 (dd, ^3J = 4.5, ^4J = 1.7 Hz, 6H, Py);

^{13}C NMR (CD_2Cl_2): δ (ppm) 57.02 (CH_2), 61.9 (CH_2), 113.1, 117.8, 120.6, 121.6, 135.7, 144.3, 147.6, 150.3, 168.9, 170.2 (CH=N);

MALDI-TOF (1,8,9-anthracenetriol), m/z (%): 756.2 (100) $[GaL+H]^+$, 531.0 (20) $[GaL-B]^+$;

ESI mass spectrum ($C_2H_2Cl_4$), *m/z* (%) positive: 756.2 (100) $[GaL+H]^+$, 532.1 (4) $[GaL-B]^+$, 778.2 (2) $[GaL+Na]^+$, 1513.5 (5) $[(GaL)_2+H]^+$, 2271.0 (2) $[(GaL)_3+H]^+$;

Selected IR (KBr pellet): $\tilde{\nu}$ (cm^{-1}) 3410 m br, 1618, 1593, 1554, 1523, 1477, 1434, 1400, 1331, 1204, 798, 729;

UV-vis (CH_2Cl_2) λ, nm (ε, $M^{-1}cm^{-1}$): 390 (21150), 290 (65670), 250 (64270);

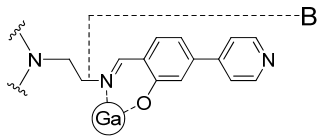

Figure 4. Mass spectrometric fragmentation of the Ga(III)- *trensal* complex **8**

6.2.2.2. M(II)-*trenpy* complexes

M(II) *trenpy* complex with thiomethyl end groups

Compound 9. *Synthesis of 5-(4'-methylthio-phenyl)-pyridine-2-carboxaldehyde*

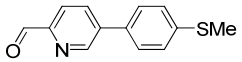

To a solution of 5-bromo-pyridine-2-carboxaldehyde (1.045 g, 6.076 mmol) and 4-(methylthio)-phenyl-boronic acid (1.225 g, 7.290 mmol) in toluene/MeOH (120 mL, 3/1) was added under N_2 atmosphere, $Pd(PPh_3)_4$ (351 mg, 0.304 mmol) and a degassed aqueous solution of Na_2CO_3, 2M (2.576 g, 24.300 mmol). The mixture was stirred under N_2 atmosphere at 80°C for 24 h. The reaction mixture was diluted with toluene (200 mL) and washed with H_2O (100 mL). The aqueous layer was extracted with toluene (3x150 mL). The combined organic layers were dried over $MgSO_4$ and evaporated. The residue was purified twice by column chromatography (SiO_2, CH_2Cl_2/MeOH 1% followed by SiO_2/Et_3N, hexane/CH_2Cl_2, 1/1 to 0/1) to yield the pure compound **9**, as a yellow solid (860 mg, 62%).

R_f (SiO_2, CH_2Cl_2): 0.21; M.p. 98°C;

Anal.calc. for $C_{13}H_{11}NOS$ (M_r = 229.30): C, 68.09; H, 4.84; N, 6.11; S, 13.98; found: C, 67.96; H, 4.93;

N, 6.15; S, 13.78.

^{1}H NMR ($CDCl_3$): δ (ppm) 2.54 (s, 3H, SCH_3), 7.35-7.39 (m, 2H, Ph), 7.55-7.60 (m, 2H, Ph), 8.02 (d, ^{4}J = 1.5 Hz, 2H, Py), 8.99 (t, ^{4}J = 1.5 Hz, 1H, Py), 10.11 (s, 1H, CHO);

^{13}C NMR ($CDCl_3$): δ (ppm) 15.7 (SCH_3), 122.2, 127.1, 128.0, 133.2, 135.0, 140.4, 141.0, 148.6, 151.7, 193.4 (CHO);

MALDI-TOF (no matrix), *m*/*z* (%): 229.8 (100) $[M+H]^+$;

Selected IR (KBr pellet): $\widetilde{\nu}$ (cm^{-1}) 2828 and 2814 comb.(C-H) aldehyde, 1700 *v*(C=O), 1593, 1578 comb. Py, 1503, 1469, 1432, 1411, 1365, 1322, 1292, 1277, 1263, 1213, 1195, 1099, 998, 850, 816, 755, 682, 623, 553;

UV-vis (CH_2Cl_2) λ, nm (ε, $M^{-1}cm^{-1}$): 332 (22050), 246 (13050);

Compound 10. *Synthesis of trenpy ligand with thiomethyl end groups,* **L^{c}**

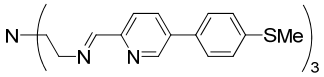

A solution of tris-(2-aminoethyl)-amine (156 mg, 1.07 mmol) in EtOH (5 mL) was added to a solution of aldehyde **9** (734 mg, 3.20 mmol) in EtOH (35 mL). A yellowish precipitate appeared rapidly. The reaction mixture was stirred at rt for 5 h. The precipitate was filtered and washed with cold EtOH (2x3mL). Recrystallization in EtOH/CH_2Cl_2 gave the pure ligand **L^{c}** (717 mg, 86%), as a yellowish solid.

M.p. 146°C dec.;

Anal.calc. for $C_{45}H_{45}N_7S_3$ (M_r = 780.08): C, 69.29; H, 5.81; N, 12.57; S, 12.33; Found: C, 69.10; H, 5.62; N, 12.52; S, 12.47;

^{1}H NMR (CD_2Cl_2): δ (ppm) 2.51 (s, 9H, SCH_3), 2.99 (t, ^{3}J = 6.4 Hz, 6H, CH_2), 3.78 (t, ^{3}J = 6.3 Hz, 6H, CH_2), 7.27-7.31 (m, 6H, Ph), 7.45-7.48 (m, 6H, Ph), 7.80 (dd, ^{3}J = 8.2 Hz, ^{4}J = 2.3 Hz, 3H, Py), 7.93 (dd, ^{3}J = 8.2 Hz, ^{5}J = 0.8 Hz, 3H, Py), 8.32 (s, 3H, CH=N), 8.73 (dd, ^{3}J = 2.3, ^{4}J = 0.8 Hz, 3H, Py);

^{13}C NMR (CD_2Cl_2): δ (ppm) 15.3 (SCH_3), 55.2 (CH_2), 59.9 (CH_2), 120.8, 126.7, 127.3, 133.8, 134.1, 136.4, 139.5, 147.3, 153.6, 162.4 (CH=N);

^{13}C-DEPT 135 NMR (CD_2Cl_2): δ (ppm) 15.2 (SCH_3), 55.2 (CH_2), 59.8 (CH_2), 120.7, 126.6, 127.2, 134.0, 147.2, 162.4 (CH=N);

MALDI-TOF (1,8,9-anthracenetriol), *m*/*z* (%): 802.0 (100) $[M+Na]^+$;

Selected IR (KBr pellet): $\widetilde{\nu}$ (cm^{-1}) 2966, 2845, 2805, 1645, 1588, 1567, 1473, 1539, 1371, 1321, 1296, 1097, 1076, 1040, 1016, 999, 909, 814, 501;

UV-vis (CH_2Cl_2) λ, nm (ε, $M^{-1}cm^{-1}$): 323 (62230), 247 (32420);

Compound 11. *Synthesis of trenpy Fe(II)-complex with thiomethyl end groups*

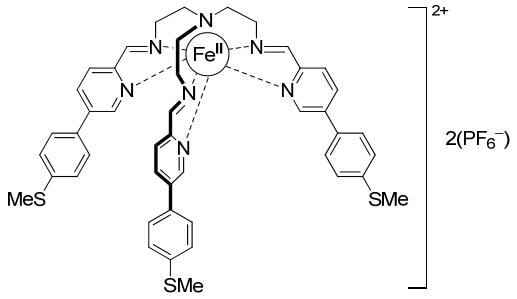

To a suspension of the ligand, **10** (108.5 mg, 0.139 mmol) in MeOH (10 mL) was added a solution of $FeCl_2 \cdot 4H_2O$ (27.7 mg, 0.139 mmol) in MeOH (5 mL). After stirring at rt for 1,5 h, under air, the resulting solution was filtered. Addition of KPF_6 (128 mg, 0.695 mmol) in MeOH (10 mL) gave a dark violet precipitate. After stirring at rt for 1 h, the solid was collected and washed with MeOH (4 mL). Recrystallization in acetone/MeOH gave the *trenpy* Fe(II) complex, **11** (109 mg, 70%) as a violet powder.

Crystals suitable for single crystal X-ray diffraction were obtained by slow evaporation of acetone/MeOH;

M.p. 265 °C dec.;

Anal.calc. for $C_{45}H_{45}F_{12}FeN_7P_2S_3$ (M_r=1125.85): C, 48.01; H, 4.03; N, 8.71; S, 8.54; Found: C, 47.82; H, 4.20; N, 8.73; S, 8.80;

^{1}H NMR (CD_3COCD_3): δ (ppm) 2.46 (s, 9H, SCH_3), 3.34 (t, J = 11.7 Hz, 3H, CH_2), 3.51 (t, J = 11.7 Hz, 3H, CH_2), 3.63 (d, J = 14.1 Hz, 3H, CH_2), 3.89 (d, J = 9.8 Hz, 3H, CH_2), 7.24 (d, ^3J = 8.5 Hz, 6H, Ph), 7.37 (d, ^3J = 8.5 Hz, 6H, Ph), 7.61 (s, 3H, Py), 8.58 (s, 6H, Py), 9.58 (s, 3H, CH=N);

ESI mass spectrum (CH_3CN), *m*/*z* (%), positive: 417.6 (100) $[LFe]^{2+}$, 854.3 (2) $[LFe(F)]^{1+}$, 980.2 (1) $[LFe(PF_6)]^{1+}$; high positive: 980.2 (100) $[LFe(PF_6)]^{1+}$, 1543.4 (4) $[(LFe)_3(PF_6)_4]^{2+}$, 2107.1 (5) $[(LFe)_4(PF_6)_6]^{2+}$; negative: 144.7 (100) $[PF_6]^{1-}$;

Selected IR (KBr pellet): $\tilde{\nu}$ (cm^{-1}) 1591m, 1561 w, 1542 w, 1473 m, 1099 m, 840s, 557 s; Raman (cm^{-1}): 1605 medium, 1592 strong, 1558 m; 1543 weak, 1472 weak.

UV-vis (CH_3CN) λ, nm (ε, $M^{-1}cm^{-1}$): 576 (13400), 528sh (8750), 364 (55650), 269 (58050);

Compound 12. *Synthesis of trenpy Mn(II)-complex with thiomethyl end groups*

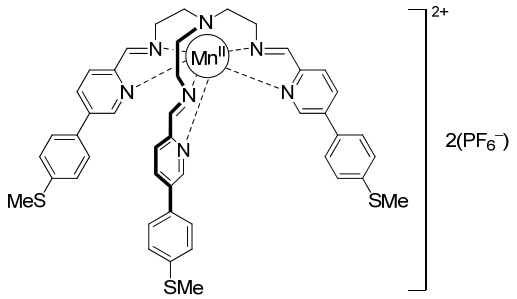

To a suspension of the ligand, **10** (103 mg, 0.132 mmol) in MeOH (10 mL) was added a solution of $MnCl_2 \cdot 4H_2O$ (26.0 mg, 0.132 mmol) in MeOH (10 mL). After stirring at rt for 2 h, under air, the resulting yellow solution was filtered. Addition of KPF_6 (123 mg, 0.662 mmol) in MeOH (10 mL) gave a yellow precipitate. After stirring at rt for 1 h, the solid was collected and washed with MeOH (5 mL). Recrystallization in acetone/MeOH gave the pure Mn(II) complex, **12** (106 mg, 77%) as a yellow powder.

Crystals suitable for single crystal X-ray diffraction were obtained by slow evaporation of acetone/MeOH;

M.p. 240 °C dec.;

Anal.calc. for $C_{45}H_{45}F_{12}MnN_7P_2S_3$ (M_r=1124.95): C, 48.05; H, 4.03; N, 8.72; S, 8.55; Found: C, 48.00; H, 3.82; N, 8.76; S, 8.22;

ESI mass spectrum (CH_3CN), *m*/*z* (%), positive: 417.1 (100) $[LMn]^{2+}$, 979.3 (18) $[LMn(PF_6)]^{1+}$; high positive: 979.2 (100) $[LMn(PF_6)]^{1+}$; 1542.4 (3) $[(LMn)_3(PF_6)_4]^{2+}$, 2105.0 (6) $[(LMn)_4(PF_6)_6]^{2+}$; negative: 144.7 (100) $[PF_6]^{1-}$;

Selected IR (KBr pellet): $\tilde{\nu}$ (cm^{-1}) 1654, 1591, 1440, 1370, 1099, 842, 557;

UV-vis (CH_3CN) λ, nm (ε, $M^{-1}cm^{-1}$): 349 (61900), 265 (63200);

Compound 13. *Synthesis of trenpy Zn(II)-complex with thiomethyl end groups*

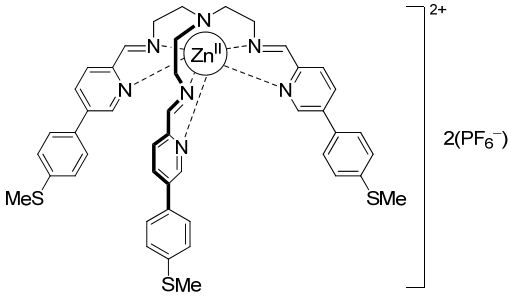

To a suspension of the ligand, **10** (102 mg, 0.131 mmol) in MeOH (10 mL) was added a solution of $Zn(NO_3)_2 \cdot 6H_2O$ (39.0 mg, 0.131 mmol) in MeOH (10 mL). After stirring at rt for 2 h, the resulting yellow solution was filtered. Addition of KPF_6 (120 mg, 0.654 mmol) in MeOH (10 mL) gave a yellow precipitate. After stirring at rt for 1 h, the solid was collected and washed with MeOH (5 mL). Recrystallization in acetone/MeOH gave the pure Zn(II) complex, **13** (112 mg, 75%) as a yellow powder.

Crystals for single crystal X-ray diffraction were obtained by slow evaporation of acetone/MeOH.

M.p. 210 °C dec.;

Anal.calc. for $C_{45}H_{45}F_{12}ZnN_7P_2S_3$ (M_r=1135.42): C, 47.60; H, 3.99; N, 8.64; S, 8.47; Found: C, 47.65; H, 4.02; N, 8.67; S, 8.79;

^{1}H NMR (CD_3COCD_3): δ (ppm) 2.47 (s, 9H, SCH_3), 3.17 (t, J = 13.4 Hz, 3H, CH_2), 3.38 (d, J = 13.8 Hz, 3H, CH_2), 3.78 (d, J = 11.7 Hz, 3H, CH_2), 4.08 (t, J = 11.5 Hz, 3H, CH_2), 7.24 (d, ^3J = 8.7 Hz, 6H, Ph),

7.36 (d, ^{3}J = 8.7 Hz, 6H, Ph), 7.76 (d, 3H, ^{4}J = 2.1 Hz, Py), 8.29 (d, 3H, ^{3}J = 8.1 Hz, Py), 8.64, dd (d, 3H, ^{3}J = 8.1, ^{4}J = 2.4 Hz, Py), 9.04 (d, 3H, J = 1.2 Hz, CH=N);

^{13}C NMR (CD_3COCD_3): δ (ppm) 14.8 (SCH_3), 55.7 (CH_2), 57.2 (CH_2), 127.1, 128.2, 129.6, 132.1, 138.9, 141.6, 142.5, 146.8, 147.5, 164.2 (CH=N);

ESI mass spectrum (CH_3CN), *m*/*z* (%), positive: 421.6 (100) $[LZn]^{2+}$, 988.2 (3) $[LZn(PF_6)]^{1+}$; negative: 144.7 (100) $[PF_6]^{1-}$;

Selected IR (KBr pellet): $\widetilde{\nu}$ (cm^{-1}) 1657, 1590, 1572, 1372, 1099, 838, 557;

UV-vis (CH_3CN) λ, nm (ε, $M^{-1}cm^{-1}$): 351 (50050), 263 (49450);

M(II) *trenpy* complex with pyridine end groups

Compound 14. *Synthesis of 3,4'-bipyridine-6-carbaldehyde*

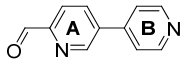

To a solution of 5-bromo-pyridine-2-carboxaldehyde (1.218 g, 6.548 mmol) and pyridine-boronic acid (885 mg, 7.20 mmol) in DME/H_2O (68 mL, 3/1) was added under N_2 atmosphere, $Pd(PPh_3)_4$ (377 mg, 0.327 mmol) and Na_2CO_3 (4.165 g, 39.29 mmol). The mixture was stirred under N_2 atmosphere at 70°C for 24 h. The reaction mixture was diluted with CH_2Cl_2 (300 mL) and washed with H_2O (100 mL). The aqueous layer was extracted with CH_2Cl_2 (3x150 mL). The combined organic layers were dried over $MgSO_4$ and evaporated. The residue was purified twice by column chromatography (SiO_2, CH_2Cl_2/MeOH 1%). The compound **14** (870 mg, 72%), yellow solid was used in the next step without further purification.

R_f (SiO_2, CH_2Cl_2/MeOH= 95:5): 0.52

Anal.calc. for $C_{11}H_8N_2O$ (M_r = 184.19): C, 71.73; H, 4.38; N, 15.21;

Anal.calc. for $C_{11}H_8N_2O$•0,05H_2O: C, 71.38; H, 4.41; N, 15.13; Found: C, 71.20; H, 4.24; N, 15.03; Commercial bipyridine compounds are also known as hydrates with different quantities of H_2O.

^{1}H NMR (CD_2Cl_2): δ (ppm) 7.56 (dd, ^{3}J = 4.4, ^{4}J = 1.7 Hz, 2H, Py^B), 8.04 (dd, J = 8.1, 0.9 Hz, 1H, Py^A), 8.12 (ddd, J = 8.1, 2.1, 0.7 Hz, 1H, Py^A), 8.72 (dd, ^{3}J = 4.5, ^{3}J = 1.7 Hz, 2H, Py^B), 9.04 (dd, J = 2.2, 0.7 Hz, 1H, Py^A, H-2), 10.09 (d, ^{5}J = 0.7 Hz, 1H, CHO reference [289]).

^{1}H NMR ($CDCl_3$): δ (ppm) 7.62 (dd, ^{3}J = 4.5, ^{4}J = 1.7 Hz, 2H, Py^B), 8.22 – 8.01 (m, 2H, Py^A), 8.80 (dd, ^{3}J = 4.6, ^{4}J = 1.7 Hz, 2H, Py^B), 9.06 (dd, J = 2.0, 1.1 Hz, 1H, Py^A), 10.15 (d, ^{5}J = 0.6 Hz, 1H, CHO);

^{13}C NMR (CD_2Cl_2): δ (ppm) 121.7, 121.7, 135.5, 137.8, 144.0, 148.7, 150.8, 152.9, 192.9 (CHO);

Compound 15. *Synthesis of trenpy ligand with pyridine end groups,* $\mathbf{L^d}$

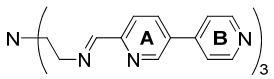

A solution of tris-(2-aminoethyl)-amine (138 mg, 0.945 mmol) in EtOH (5 mL) was added to a suspension of aldehyde **14** (522 mg, 2.834 mmol) in EtOH (45 mL). The resulted intense yellow solution was stirred at rt for 3.5 h. After removing half of the solvent under vacuum, the reaction mixture started to precipitate. After overnight stirring at rt the precipitate was filtered and washed with cold EtOH (2x3mL). Recrystallization in EtOH/CH_2Cl_2 gave the pure ligand **15** (340 mg, 56%), as a slightly yellowish solid.

M.p. 138°C dec.;

Anal.calc. for $C_{39}H_{36}N_{10}$ (M_r = 644.77): C, 72.65; H, 5.63; N, 21.72; Found: C, 72.33; H, 5.68; N, 21.71;

^{1}H NMR (CD_2Cl_2): δ (ppm) 2.99 (t, ^3J = 6.4 Hz, 6H, CH_2), 3.79 (t, ^3J = 6.1 Hz, 6H, CH_2), 7.47 (dd, ^3J = 4.5, ^4J = 1.7 Hz, 6H, Py^B), 7.92 (dd, ^3J = 8.2, ^4J = 2.3 Hz, 3H, Py^A, H-4), 8.04 (d, ^3J = 8.2 Hz, 3H, Py^A, H-5), 8.35 (s, 3H, CH=N), 8.64 (dd, ^3J = 4.5, ^4J = 1.7 Hz, 6H, Py^B), 8.80 (dd, ^4J = 2.2, J = 0.7 Hz, 3H, Py^A, H-2);

^{13}C NMR (CD_2Cl_2) δ (ppm) 55.2 (CH_2), 60.0 (CH_2), 120.9, 121.4, 134.3, 134.8, 144.6, 147.6, 150.6, 155.2, 162.2 (CH=N);

^{13}C-DEPT135 NMR (CD_2Cl_2): δ (ppm) 55.2 (CH_2), 59.9 (CH_2), 120.9, 121.3, 134.7, 147.5, 150.6, 162.1 (CH=N);

MALDI-TOF (1,8,9-anthracenetriol), *m*/*z* (%): 645.0 (100) $[M+H]^+$, 667.0 (18) $[M+Na]^+$, 479.0 (95) $[M-A+H]^+$, 447.9 (95) $[M-B]^+$; 871.1 (8) $[M+matrix]^+$, additionally various not interpreted fragments; decomposition with matrix;

Selected IR (KBr pellet): $\tilde{\nu}$ (cm^{-1}) 2967, 2851, 2795, 1648, 1598, 1569, 1478, 1458, 1440, 1417, 1378, 1228, 1046, 1012, 816, 746, 737, 512;

UV-vis (CH_2Cl_2) λ, nm (ε, $M^{-1}cm^{-1}$): 265 (60960), 283 sh (55340);

Compound 16. *Synthesis of trenpy Fe(II)-complex with pyridine end groups*

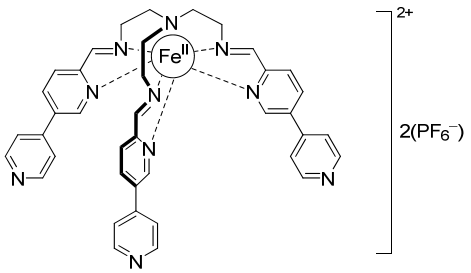

To a solution of the ligand **15** (145 mg, 0.225 mmol) in MeOH (10 mL) was added a solution of $FeCl_2 \cdot 4H_2O$ (45.0 mg, 0.225 mmol) in MeOH (12 mL). After stirring at rt for 1 h, under air, the resulting violet solution was filtered. Addition of a filtered solution of KPF_6 (207 mg, 1.124 mmol) in MeOH (10

mL) gave a dark violet precipitate. After stirring at rt for 1 h, the solid was collected and washed with MeOH (2x3 mL). Recrystallization in acetone/MeOH gave the Fe(II) complex, **16** (158 mg, 71%) as a violet powder.

Crystals suitable for single crystal X-ray diffraction were obtained by slow evaporation of acetone/MeOH solution of complex.

M.p. 230 °C dec.;

Anal.calc. for $C_{39}H_{36}F_{12}FeN_{10}P_2$ (M_r=990.54): C, 47.29; H, 3.66; F, 23.02; Fe, 5.64; N, 14.14;

Anal.calc. for $C_{39}H_{36}F_{12}FeN_{10}P_2 \bullet 2H_2O$: C, 45.63; H, 3.93; N, 13.64; Found: C, 45.85; H, 3.85; N, 13.65;

Observation: the repeated elemental analysis of Fe(II)-complex fits with two water of crystallization molecules evidenced also by ^{1}H NMR; however TGA up to 200°C did not present a significant weight loss, the Fe(II)-complex is hygroscopic; a test of a sample let in air on a balance over night showed increasing of the mass with more than 1% (calculated 0.57 H_2O);

^{1}H NMR (CD_3CN): δ (ppm) 3.30 – 3.16 (m, 6H, CH_2), 3.66 (d, J = 13.2 Hz, 3H, CH_2), 3.81 (d, J = 9.6 Hz, 3H, CH_2), 7.55 – 7.22 (m, 9H, Py^B , Py^A H-2), 8.49 (m, 6H, Py^A), 8.62 (dd, J = 4.5, 1.7 Hz, 6H, Py^B), 9.35 (s, 3H, CH=N).

^{1}H NMR (CD_3COCD_3): δ (ppm) 3.37 (td, J = 14.9, 3.4 Hz, 3H, CH_2), 3.57 (td, J = 11.7, 3.0 Hz, 3H, CH_2), 3.72 (d, J = 13.5 Hz, 3H, CH_2), 3.99 (d, J = 10.0 Hz, 3H, CH_2), 7.40 (dd, J = 4.5, 1.6 Hz, 6H, Py^B), 7.78 (s, 3H, Py^A H-2), 8.56 (dd, J = 4.6, 1.5 Hz, 6H, Py^B), 8.78 – 8.64 (m, 6H, Py^A), 9.72 (s, 3H, CH=N);

^{13}C NMR (CD_3CN): δ (ppm) 54.6 (CH_2), 60.3 (CH_2), 122.4, 129.6, 138.1, 139.3, 143.3, 151. 7, 154.1, 157.8, 172.3 (CH=N);

^{13}C DEPT135 NMR (CD_3CN): δ (ppm) 54.5 (CH_2), 60.1 (CH_2), 122.2, 129.5, 138.0, 151.5, 154.0, 172.2 (CH=N);

ESI mass spectrum (CH_3CN), m/z (%), positive: 350.1 (100) $[LFe]^{2+}$, 845.2 (10) $[LFe(F)]^{1+}$, 1835.9 (1) $[L_4Fe_4(PF_6)_6]^{2+}$; negative: 144.9 (100) $[PF_6]^{1-}$;

Selected IR (KBr pellet): $\tilde{\nu}$ (cm^{-1}) 1603, 1564 w, 1544 w, 1475, 838 s, 816 sh, 557 s;

Raman (cm^{-1}): 1602 s, 1562 m, 1544 w; 1475 m;

UV-vis (CH_3CN) λ, nm (ε, $M^{-1}cm^{-1}$): 579 (10850), 530 sh (8750), 386 (6540), 293 (53920);

Compound 17. *Synthesis of trenpy Mn(II)-complex with pyridine end groups*

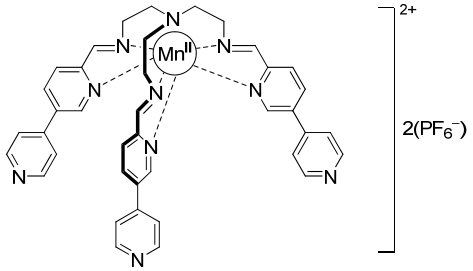

To a suspension of the ligand **15** (118.5 mg, 0.184 mmol) in MeOH (10 mL) was added a solution of $MnCl_2 \cdot 4H_2O$ (36.5 mg, 0.184 mmol) in MeOH (10 mL). After stirring at rt for 1,5 h, under air, the resulting yellow solution was filtered. Addition of KPF_6 (169 mg, 0.919 mmol) in MeOH (10 mL) gave a yellow precipitate. After stirring at rt for 2 h, the solid was collected and washed with MeOH (5 mL). Recrystallization in acetone/MeOH gave the Mn(II)-complex, **17** (110 mg, 60%) as a yellow powder.

Single crystal X-ray structure was determined on single crystal obtained by slow evaporation of acetone/MeOH solution of complex.

M.p. 290 °C dec.;

Anal.calc. for $C_{39}H_{36}F_{12}MnN_{10}P_2$ (M_r=989.64): C, 47.33; H, 3.67; N, 14.15; Found: C, 47.17; H, 3.57; N, 14.11;

ESI mass spectrum (CH_3CN), *m*/*z* (%), positive: 349.6 (100) $[LMn]^{2+}$, 844.2 (7) $[LMn(PF_6)]^{1+}$; wide positive: 349.6 (100) $[LMn]^{2+}$, 718.3 (16) $[LMn(F)]^{1+}$, 844.2 (40) $[LMn(PF_6)]^{1+}$; negative: 144.9 (100) $[PF_6]^{1-}$;

Selected IR (KBr pellet): $\widetilde{\nu}$ (cm^{-1}) 1662, 1599, 1576, 1546 w, 840, 762, 558;

UV-vis (CH_3CN) λ, nm (ε, $M^{-1}cm^{-1}$): 298 (47450), 260 (38000);

Compound 18. *Synthesis of trenpy Zn(II)-complex with pyridine end groups*

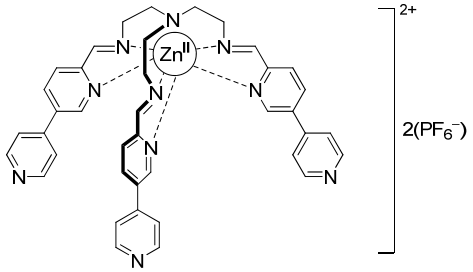

To a suspension of the ligand **15** (81.0 mg, 0.126 mmol) in MeOH (10 mL) was added a solution of $Zn(NO_3)_2 \cdot 6H_2O$ (37.0 mg, 0.126 mmol) in MeOH (10 mL). After stirring at rt for 1 h under air, the resulting yellow solution was filtered. Addition of KPF_6 (117 mg, 0.628 mmol) in MeOH (10 mL) gave a yellow precipitate. After stirring at rt for 1 h, the solid was collected and washed with MeOH (5 mL). Recrystallization in acetone/MeOH gave the Zn(II) complex, **18** (91 mg, 72%) as a yellow powder.

M.p. 285 °C dec.;

Anal.calc. for $C_{39}H_{36}F_{12}ZnN_{10}P_2$ (Mr=1000.11): C, 46.84; H, 3.63; N, 14.01; Found: C, 46.81; H, 3.72; N, 14.01;

^{1}H NMR (CD_3COCD_3): δ (ppm) 3.18 (td, *J* = 13.4, 3.7 Hz, 3H, CH_2), 3.39 (dd, *J* = 13.8, 3.8 Hz, 3H, CH_2), 3.79 (dd, *J* = 11.7, 3.4 Hz, 3H, CH_2), 4.09 (br. t, *J* = 11.2 Hz, 3H, CH_2), 7.40 (dd, *J* = 4.4, 1.7 Hz, 6H, Py^B), 7.95 (d, ^4J = 2.2 Hz, 3H, Py^A, H-2), 8.39 (d, ^3J = 8.0 Hz, 3H, Py^A, H-5), 8.56 (dd, *J* = 4.5, 1.7 Hz, 6H, Py^B), 8.78 (dd, ^3J = 8.0, ^4J = 2.2 Hz, 3H, Py^A, H-4), 9.08 (d, *J* = 1.4 Hz, 3H, CH=N);

^{13}C NMR (CD_3COCD_3): δ (ppm) 55.8 (CH_2), 57.3 (CH_2), 122.1, 129.8, 139.5, 140.4 (q), 143.3 (q), 148.1, 148.4 (q), 151.6, 164.4 (CH=N);

^{13}C-DEPT135 NMR (CD_3COCD_3): δ (ppm) 54.9 (CH_2), 56.4 (CH_2), 121.3, 128.9, 139.5, 147.2, 150.7, 163.5 (CH=N);

ESI mass spectrum (CH_3CN), *m*/*z* (%), positive: 354.1 (100) $[LZn]^{2+}$, 853.2 (5) $[LZn(PF_6)]^{1+}$; negative: 144.9 (100) $[PF_6]^{1-}$;

Selected IR (KBr pellet): $\tilde{\nu}$ (cm^{-1}) 1662, 1600, 1576, 1546 w, 1373, 840, 558;

UV-vis (CH_3CN) λ, nm (ε, $M^{-1}cm^{-1}$): 344 (1920), 298 (51500), 260 (42050);

6.2.2. Facial and meridional Ru(II)-trisbpy complex

Compounds 19^{i}, 19^{ii}. *Synthesis of the 5-ethynyl-2,2'-bipyridine* [160]

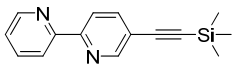

i) A solution of 5-bromo-2,2'-bipyridine (1.093 g, 4.65 mmol) in THF/DIEA anh. (40 mL, 1/1) was degassed 1h under N_2. $[PdCl_2(PPh_3)_2]$ (163 mg, 0.233 mmol), CuI (44.0 mg, 0.233 mmol) and (trimethylsilyl)-acetylene (1.827 g, 18.6 mmol) were added. After stirring overnight at rt, the reaction mixture was diluted with CH_2Cl_2 (400 mL) then washed with H_2O (200 mL). The aqueous layer was extracted with CH_2Cl_2 (3x200 mL). The combined organic layers were dried over $MgSO_4$ and the solvent was removed in vacuum. Purification by column chromatography (SiO_2, hexane/EtOAc, 10/0 to 9/1) afforded the 5-((trimethylsilyl)-ethynyl)-2,2'-bipyridine (1.09 mg, 93%) as a yellowish oil. The spectra agree well with the literature.[160]

R_f (SiO_2, hexane/EtOAc, 8/2): 0.37;

Observation: the 5-((trimethylsilyl)-ethynyl)-2,2'-bipyridine has the same R_f like the starting material 5-bromo-2,2'-bipyridine, but different colour exposed in UV light.

^{1}H NMR ($CDCl_3$): δ (ppm) 0.28 (s, 9H, TMS), 7.32 (ddd, ^3J = 7.5 Hz, ^3J = 4.8, ^4J = 1.2 Hz, 1H, H-5'),

7.85 (ddd, ^3J = 9.4, ^3J = 8.0, ^4J = 2.0 Hz, 2H, H-4,4'), 8.45 – 8.33 (m, 2H, H-3,3'), 8.70 – 8.61 (m, 1H, H-6'), 8.73 (d, ^4J = 2.1 Hz, 1H, H-6)

^{13}C NMR ($CDCl_3$): δ (ppm) 0.0 (TMS), 99.4 (C≡), 101.9 (C≡), 120.37 (q), 120.4, 121.7, 124.1, 137.3, 140.0, 149.2, 152.2, 154.8 (q), 155.8 (q);

^{13}C DEPT 135 NMR ($CDCl_3$): δ (ppm) 0.2 (TMS), 120.3, 121.6, 124.0, 137.2, 139.9, 149.0, 152.0;

MALDI-TOF (1,8,9-anthracenetriol), *m*/*z* (%): 252.9 (100) $[M+H]^+$;

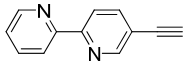

ii) To a N_2 degassed solution of trimethylsilyl-protected compound **19^{i}** (1.093 g, 4.33 mmol) in CH_3OH/CH_2Cl_2 (80 mL, 1/1), K_2CO_3 (2.992 g, 21.65 mmol) was added as a solid. After stirring for 1h at rt, the solution was concentrated by rotary evaporation. Purification by flash chromatography (SiO_2, hexane/EtOAc, 10/0 to 8/2) afforded the 5-ethynyl-2,2'-bipyridine **19^{ii}** (708 mg, 91%) as a white solid. The spectra agree well with the literature. [160]

R_f (SiO_2, hexane/EtOAc, 8/2): 0.30;

^{1}H NMR ($CDCl_3$): δ (ppm) 3.29 (s, 1H, ≡CH), 7.29 (ddd, ^3J = 7.5, ^3J = 4.8, ^4J = 1.1 Hz, 1H, H-5'), 7.80 (td, ^3J = 7.7, ^4J = 1.8 Hz, 1H, H-4'), 7.88 (dd, ^3J = 8.2, ^4J = 2.1 Hz, 1H, H-4), 8.38 (dd, ^3J = 8.1, ^4J = 3.5 Hz, 2H, H-3/3'), 8.66 (d, ^3J = 4.7 Hz, 1H, H-6'), 8.75 (d, ^4J = 1.8 Hz, 1H, H-6);

^{13}C NMR ($CDCl_3$): δ (ppm) 80.8 (C≡), 81.5 (C≡), 119.2, 120.4, 121.5, 124.2, 137.1, 140.1, 149.3, 152.3, 155.35, 155.4;

Compound 20. *Synthesis of the ligand* **L^{e}**

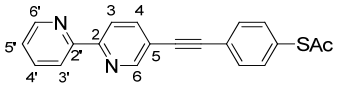

5-ethynyl-2,2'-bipyridine **19^{ii}** , [160] (708 mg, 3.93 mmol), and 4-(thioacetyl)-iodobenzene [161] (1.201 g, 4.322 mmol) were dissolved in THF/DIEA anh. (35 mL, 2.5/1) and degassed 1h under N_2. $Pd(PPh_3)_2Cl_2$ (138 mg, 0.196 mmol) and CuI (37 mg, 0.196 mmol) were added. After stirring overnight at rt, the reaction mixture was diluted with CH_2Cl_2 (300 mL) then washed with H_2O (200 mL). The aqueous layer was extracted with CH_2Cl_2 (3x200 mL). The combined organic layers were dried over $MgSO_4$ and the solvent was removed in vacuum. Twofold purification by column chromatography (SiO_2, hexane/EtOAc, 1/0 to 1/1) afforded the pure ligand (650 mg, 50%) as a white-yellowish solid.

R_f (SiO_2, hexane/EtOAc, 8/2): 0.23; M.p. 136°C.

Anal.calc. for $C_{20}H_{14}N_2OS$ (M_r = 330.40): C, 72.70; H, 4.27; N, 8.48; S, 9.70; Found: C, 72.66; H, 4.33; N, 8.42; S, 9.64;

^{1}H NMR ($CDCl_3$): δ (ppm) 2.44 (s, 3H, CH_3), 7.35 (ddd, ^3J = 7.5, ^3J = 4.9, ^4J = 1.0 Hz, 1H, H-5'), 7.43

(d, ^3J = 8.5 Hz, 2H, Ph), 7.59 (d, ^3J = 8.5 Hz, 2H, Ph,), 7.86 (td, ^3J = 7.9, ^4J = 1.8 Hz, 1H, H-4'), 7.95 (dd, ^3J = 8.3, ^4J = 2.1 Hz, 1H, H-4), 8.45 (dd, ^3J = 8.5, ^4J = 3.3 Hz, 2H, H-3/3'), 8.71 (d, ^3J = 4.3 Hz, 1H, H-6'), 8.82 (d, ^4J = 1.6 Hz, 1H, H-6);

^{13}C NMR ($CDCl_3$): δ (ppm) 30.5 (CH_3), 88.0 (C≡), 93.0 (C≡), 120.3 (q), 120.7 (C-3/3'), 121.7 (C-3/3'), 123.9 (C-5'), 124.2 (q), 128.9 (q), 132.4 (Ph), 134.4 (Ph), 137.5 (C-4'), 139.7 (C-4), 149.1 (C-6'), 151.8 (C-6), 154.7 (q C-2/2'), 155.3 (q C-2/2'), 193.4 (C=O);

^{13}C DEPT135 NMR ($CDCl_3$): δ (ppm) 30.3 (CH_3), 120.5 (C-3/3'), 121.5 (C-3/3'), 124.1 (C-5'), 132.3 (Ph), 134.3 (Ph), 137.3 (C-4'), 139.5 (C-4), 149.1 (C-6'), 151.7 (C-6);

Selected IR (KBr pellet): $\tilde{\nu}$ (cm^{-1}) 2217w, 1696, 1584, 1570, 1539, 1497, 1457, 1432, 1398, 1368, 1352, 1120, 1092, 1017, 955, 828, 796, 747, 629, 621, 613, 545;

MALDI-TOF (no matrix), *m/z* (%): 330.8 (100) $[M+H]^+$;

UV-vis (CH_3CN), λ, nm (ε, $M^{-1}cm^{-1}$): 336 sh (35640), 320 (45870);

Compound 21. *Synthesis of the facial and meridional Ruthenium complex*

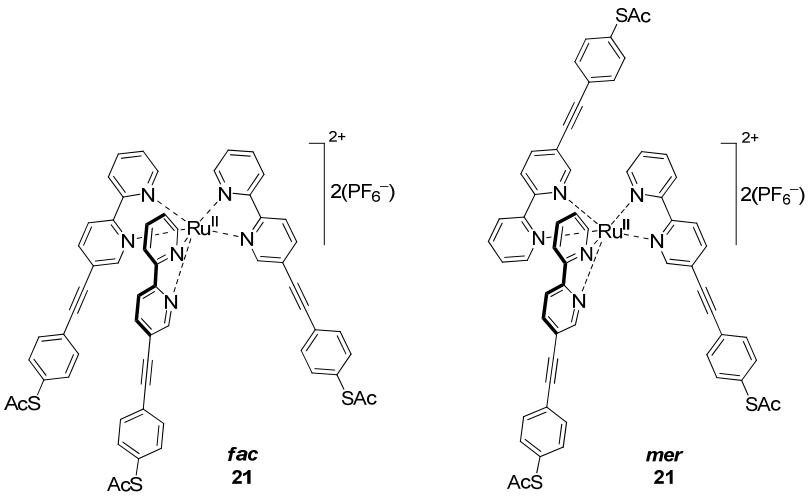

$Ru(DMSO)_4Cl_2$ [162] (195 mg, 0.40 mmol) was added to a solution of the ligand **20** (412 mg, 1.25 mmol) in EtOH (60 mL). After stirring for 48 h at reflux under Ar, the solvent was removed under vacuum. The crude brown solid was separated by column chromatography under Ar (SiO_2, 50 cm, $MeCN/H_2O/KNO_3$ (0.4M), 1/0/0 to 95/5/2). The first red-orange fraction contains the meridional isomer followed by a second fraction containing the facial isomer. The solvent was evaporated to dryness, the solid dissolved in MeCN and filtered to remove the insoluble KNO_3. The fractions were dissolved in $MeCN/H_2O$ (50 mL, 4/1) and were treated separately with KPF_6 aq. (500 mg, 2.717 mmol, 10 mL). They were allowed to stir for 2 h at rt under Ar. The MeCN was evaporated under vacuum. The precipitates were centrifuged, filtered off and washed with H_2O (4x150 mL). Anion exchange metathesis was carried out twice to assure the complete removing of nitrate salts. Recrystallization in CH_2Cl_2/hexane gave the *fac* (141 mg, 26%) and *mer* (52 mg, 10%) Ru(II)-complex as orange-red powder.

Compound 21^{f}. *Facial Ruthenium complex*

Crystals suitable for single crystal X-ray diffraction were grown from a MeCN solution of complex by slow diffusion of Et_2O.

R_f (SiO_2, MeCN/H_2O/KNO_3, 98/2/2%) = 0.05 as PF_6 complex salt;

Anal.calc.for $[C_{60}H_{42}N_6O_3S_3Ru](PF_6)_2$ (M_r = 1382,21): C, 52.14; H, 3.06; N, 6.08; S, 6.96;

Anal.calc.for $[C_{60}H_{42}N_6O_3S_3Ru](PF_6)_2 \bullet 0.5H_2O$: C, 51.80; H, 3.12; N, 6.04; S, 6.91. Found: C, 51.73; H, 3.30; N, 6.10; S, 6.66;

^{1}H NMR (CD_2Cl_2) δ (ppm) 2.39 (s, 2H, CH_3), 7.38 (d, ^3J = 8.4 Hz, 6H, Ph), 7.53 – 7.46 (m, 9H, Ph, H-5'), 7.62 (d, ^3J = 4.8 Hz, 3H, H-6'), 7.86 (d, ^4J = 1.6 Hz, 3H, H-6), 8.10 (td, ^3J = 8.0, ^4J = 1.4 Hz, 3H, H-4'), 8.16 (d, ^3J = 8.3 Hz, 3H, H-4), 8.49 (d, ^3J = 8.5 Hz, 6H, H-3,3');

^{13}C NMR (CD_2Cl_2): δ (ppm) 30.3 (CH_3), 84.9 (C≡), 97.2 (C≡), 122.0 (q = quaternary), 124.2 (C-3/3'), 124.7 (q), 125.2 (C-3/3'), 128.7 (C-5'), 130.8 (q), 132.4 (Ph), 134.5 (Ph), 138.7 (C-4), 140.7 (C-4'), 151.5 (C-6'), 152.7 (C-6), 155.7 (q C-2/2'), 156.0 (q C-2/2'), 192.9 (C=O);

^{13}C DEPT135 NMR (CD_2Cl_2): δ (ppm) 30.2 (CH_3), 124.1 (C-3/3'), 125.1 (C-3/3'), 128.6 (C-5'), 132.3 (Ph), 134.4 (Ph), 138.6 (C-4), 140.6 (C-4'), 151.4 (C-6'), 152.6 (C-6);

^{1}H NMR (CD_3CN): δ (ppm) 2.43 (s, 9H, CH_3), 7.48 – 7.34 (m, 9H, Ph, H-5'), 7.53 (d, ^3J = 8.4 Hz, 6H, Ph), 7.63 (d, ^3J = 4.9 Hz, 3H, H-6'), 8.13 – 7.96 (m, 6H), 8.23 (dd, ^3J = 8.5, ^4J = 1.7 Hz, 3H, H-4), 8.44 (d, ^3J = 8.1 Hz, 3H), 8.54 (d, ^3J = 8.5 Hz, 3H);

ESI mass spectrum (CH_3CN), *m*/*z* (%), positive: 546.1 (100) $[RuL_3]^{2+}$, 1237.2 (2) $[(RuL_3)_2(PF_6)_2]^{2+}$; negative: 144.9 $[PF_6]^{1-}$ (100);

Selected IR (KBr pellet): $\tilde{\nu}$ (cm^{-1}) 3446, 2223m, 2185w, 1702, 1598, 1495, 1465, 1437, 1121, 842, 786, 558;

UV-vis (CH_3CN, aerated), λ, nm (ε, $M^{-1}cm^{-1}$): 471 (11650, ^{1}MLCT), 325 (102 000), 274 sh (48900);

Compound 21^{m}. *Meridional Ruthenium complex*

R_f (SiO_2, MeCN/H_2O/KNO_3, 98/2/2%) = 0.11 as PF_6 complex salt;

Anal.calc.for $[C_{60}H_{42}N_6O_3S_3Ru](PF_6)_2$ (M_r = 1382,21): C, 52.14; H, 3.06; N, 6.08; S, 6.96;

Anal.calc.for $[C_{60}H_{42}N_6O_3S_3Ru](PF_6)_2 \bullet H_2O$: C, 51.47; H, 3.17; N, 6.00; S, 6.87. Found: C, 51.22; H, 3.40; N, 6.12; S, 6.49;

^{1}H NMR (CD_2Cl_2) δ (ppm) 2.39 and 2.40 (2s partially overlapped, 9H, 2CH_3, CH_3), 7.40 (dd, *J* = 8.3, 1.9

Hz, 6H, Ph), 7.47-7.52 (m, 9H, Ph, H-5'), 7.68–7.79 (m, 6H, H-6,6'), 8.06 – 8.19 (m, 6H, H-4,4'), 8.46 – 8.54 (m, 6H, H-3,3');

^{13}C NMR (CD_2Cl_2): δ (ppm) 30.3 (CH_3), 84.8 (C≡), (97.1, 97.2, 97.3) (C≡), (121.9, 122.0) (q), (124.3, 124.4) (C-3/3'), (124.7, 124.8, 124.9) (C-3/3'), 125.2 (q), (128.5, 128.7) (C-5'), (130.8, 130.9) (q), 132.4 (Ph), 134.5 (Ph), 138.7 (C-4), (140.7, 140.7, 140.8) (C-4'),, (151.3, 151.5, 151.7) (C-6), (152.5, 152.6, 152.8) (C-6'), (155.6, 155.6, 155.7), (q), (156.1, 156.25) (q), 192.9 (C=O);

^{1}H NMR (CD_3CN): δ (ppm) 2.43 (3s partially overlapped, 9H, $3CH_3$), 7.41 – 7.49 (m, 9H, Ph, H-5'), 7.54-7.58 (m, 6H, Ph), 7.74 (d, J = 4.9 Hz, 1H), 7.90 – 7.77 (m, 4H), 7.97 (d, J = 1.6 Hz, 1H), 8.11- (m, 3H), 8.25 – 8.16 (m, 3H), 8.62 – 8.48 (m, 6H);

^{13}C NMR (CD_3CN) δ (ppm) 30.7 (CH_3), (86.4, 86.5, 86.6) (C≡), (96.4, 96.4, 96.5) (C≡), (123.3, 123.4, 123.4) (q), 124.7 (q), (125.0, 125.2, 125.3) (C-3/3'), (125.9, 126.0, 126.1) (C-3/3'), (128.9, 129.0) (C-5'), 131.5 (q), 133.2 (Ph), 135.72 (Ph), 139.2 (C-4), 141.1 (C-4'), (153.1, 153.2, 153.4) (C-6'), (154.4, 154.6, 154.7) (C-6), (157.1, 157.2, 157.2) (q), (157.4, 157.5) (q), 194.1 (C=O);

^{13}C DEPT135 NMR (CD_3CN) δ (ppm) 30.5 (CH_3), (124.8, 124.9, 125.0) (C-3/3'), (125.6, 125.8, 125.9) (C-3/3'), (128.7, 128.8) (C-5'), 133.0 (Ph), 135.5 (Ph), 139.0, 140.9, (152.8, 152.9, 153.1) (C-6'), (154.2, 154.4, 154.5) (C-6);

ESI mass spectrum (CH_3CN aerated), *m*/*z* (%), positive: 546.1 (100) $[RuL_3]^{2+}$, 1237.2 (4) $[(RuL_3)_2(PF_6)_2]^{2+}$; negative: 144.9 $[PF_6]^{1-}$ (100);

Selected IR (KBr pellet): $\tilde{\nu}$ (cm^{-1}) 3433, 2223m, 2185w, 1705, 1598, 1494, 1465, 1437, 1122, 842, 787, 558;

UV-vis (CH_3CN), λ, nm (ε, $M^{-1}cm^{-1}$): 471 (11000, ^{1}MLCT), 336 (97 050), 274 sh (44320);

6.3. Homobinuclear helicate complexes

Compound 22. *Synthesis of ligand* $\mathbf{L^f}$

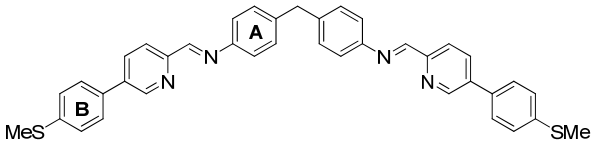

4,4'-Diaminodiphenylmethane (244.4 mg, 1.233 mmol) and pyridine-2-carbaldehyde derivate **9** (570.6 mg, 2.467 mmol) were mixed in EtOH (40 mL) and stirred at rt for 3 h. The obtained yellow precipitate was filtered, washed with EtOH (2x2 mL) and recrystallized from EtOH/CH_2Cl_2 to give the ligand as a yellowish solid (694 mg, 91%).

M.p. 265°C dec.;

Anal.calc. for $C_{39}H_{32}N_4S_2$ (M_r = 620.83): C, 75.45; H, 5.20; N, 9.02; S, 10.33; Found: C, 75.25; H, 5.17; N, 9.07; S, 10.34;

^{1}H NMR ($C_2D_2Cl_2$, over Al_2O_3 basic): δ (ppm) 2.46 (s, 6H, SCH_3), 3.98 (s, 2H, CH_2), 7.21 (s, 8H, Ph^A), 7.29 (d, ^3J = 8.3 Hz, 4H, Ph^B), 7.51 (d, ^3J = 8.3 Hz, 4H, Ph^B), 7.92 (dd, J = 8.3, 2.2 Hz, 2H, Py, H-4), 8.19 (d, J = 8.2 Hz, 2H, Py, H-5), 8.59 (s, 2H, CH=N), 8.83 (d, J = 2.2 Hz, 2H, Py, H-2);

Observation: during the NMR measurement the ligand is hydrolyzed to 10% starting materials in presence of traces of acid present in the deuterated solvent; the ligand is less soluble in $C_2D_2Cl_2$ and CD_2Cl_2 for measuring ^{13}C NMR.

MALDI-TOF (no matrix), *m*/*z* (%): 621.0 (100) $[M+H]^+$;

IR selected (KBr pellet): $\tilde{\nu}$ (cm^{-1}), 1625 *ν*(C=N), 1594 and 1582 comb. Py, 1500, 1472, 1097, 998, 817, 529;

UV-vis (MeCN) λ, nm (ε, $M^{-1}cm^{-1}$): 346 (100800), 232 (54400);

Compound 23. *Synthesis of* $[(L^f)_3Fe_2](PF_6)_4$

To a solution of ligand **22** (226.3 μmol) in CH_2Cl_2/MeOH, 5/1 (90 mL) $FeCl_2{\cdot}4H_2O$ (150.9 μmol) in MeOH (20 mL) was added. After stirring at rt for 3 h, the resulting solution was filtered. Addition of NH_4PF_6 (1.503 mmol) in MeOH (30 mL) gave a dark violet precipitate. After overnight stirring, the solid was collected and washed with MeOH. Recrystallization from MeCN gave the Fe_2-helical complex in 67% yield.

Crystals suitable for single crystal X-ray diffraction were grown from a MeCN solution of complex by slow diffusion of Et_2O.

M.p. 270°C dec.;

Anal.calc. for $[C_{117}H_{96}N_{12}S_6Fe_2](PF_6)_4 \bullet 2H_2O$ C, 54.26, H, 3.89, N, 6.49, S, 7.43; Found: C, 54.23, H, 3.97, N, 6.47. Repeated the synthesis, found: C, 54.61, H, 4.12, N, 6.39, S, 7.06;

Anal.calc. for $[C_{117}H_{96}N_{12}S_6Fe_2](PF_6)_4$ (M_r = 2554.03): C, 55.02, H, 3.79, N, 6.58; S, 7.53; Found (dried at 110°C, 10^{-3} mbar for 2 weeks): C, 54.85, H, 3.96, N, 6.60, S, 7.68.

^{1}H NMR (CD_3CN, 25°C): δ (ppm) 2.52 (s, 18H, SCH_3), 4.08 (s, 6H, CH_2), 5.68 (s, br, 12H, Ph^A), 7.00 (s, br, 12H, Ph^A), 7.33 (d, ^3J = 8.7 Hz, 12H, Ph^B), 7.44 (d, ^3J = 8.7 Hz, 12H, Ph^B), 7.61 (s, 6H, Py), 8.6-8.67 (dd, 12H, Py), 9.07 (s, 6H, CH=N).

ESI (MeCN): *m/z* (%) positive ion 493.4 (100) $[Fe_2L_3]^{4+}$, 664.2 (20) $[Fe_2L_3(F)]^{3+}$, high 1005.7 (5) $[Fe_2L_3(F_2)]^{2+}$, 1068.7 (1) $[Fe_2L_3(PF_7)]^{2+}$, 1132.0 (2) $[Fe_2L_3(P_2F_{12})]^{2+}$, 1557.7 (3) $[Fe_4L_6(P_5F_{30})]^{3+}$, 2409 (0.5) $[Fe_2L_3(PF_6)_3]^{1+}$; negative ion: *m/z* = 144.7 (100) $[PF_6]^{1-}$; at high dilution is not observed a significant aggregation.

IR selected (KBr pellet): $\widetilde{\nu}$ (cm^{-1}) 3439, 1589, 1558, 1541, 1499, 1473, 1199, 1097, 842, 556;

Raman (cm^{-1}): 1586 s, 1557 m, 1537 m; 1503 w, 1471 w.

UV-vis (MeCN) λ, nm (ε, $M^{-1}cm^{-1}$): 589 (16800), 372 (119800), 272 (119900);

Compound 24. *Synthesis of* $[(L^f)_3Ni_2](PF_6)_4$

To a solution of ligand **22** (78.9 μmol) in CH_2Cl_2/MeOH, 5/1 (60 mL) a solution of $NiCl_2$ anh. (52.6 μmol) in MeOH (10 mL) was added. After stirring at rt for 3 h, the resulting solution was filtered. Addition of NH_4PF_6 (0.53 mmol) in MeOH (10 mL) gave an orange precipitate. After overnight stirring, the solid was collected and washed with MeOH. Recrystallization from MeCN/Et_2O gave the Ni_2-helical complex in 77% yield.

Crystals suitable for single crystal X-ray diffraction were grown by slow diffusion of Et_2O in a MeCN solution of complex.

M.p. 285°C, dec..

Anal.calc. for $[C_{117}H_{96}N_{12}S_6Ni_2](PF_6)_4$ (M_r = 2559.73): C, 54.90; H, 3.78; N, 6.57; S, 7.52;

Anal.calc. for $[C_{117}H_{96}N_{12}S_6Ni_2](PF_6)_4 \bullet 2H_2O$: C, 54.14; H, 3.88; N, 6.48; S, 7.41; Found C, 54,31; H, 3.99; N, 6.58; S, 7.44. Anal.calc. for $[C_{117}H_{96}N_{12}S_6Ni_2](PF_6)_4 \bullet 1H_2O$: C, 54.51; H, 3.83; N, 6.52; S, 7.46; Found (recrystallized and dried 100°C, 10^{-2} mbar): C, 54.44; H, 3.92; N, 6.58; S, 7.50.

Observation: repeated recrystallization and drying in special condition (100°C, 10^{-2} mbar) did not remove all the water of crystallization.

^{1}H NMR (CD_3CN): paramagnetic;

ESI (MeCN): *m/z* (%) positive ion 494.6 (100) $[Ni_2L_3]^{4+}$, 707.8 (19) $[Ni_2L_3(PF_6)]^{3+}$, high 1071.28 (80) $[Ni_2L_3(PF_7)]^{2+}$, 1134.2 (40) $[Ni_2L_3(PF_6)_2]^{2+}$, 1561.3 (20) $[(Ni_2L_3)_2(PF_6)_5]^{3+}$; negative 144.7 (100) $[PF_6]^{1-}$;

IR selected (KBr pellet): $\tilde{\nu}$ (cm^{-1}) 1629, 1593, 1567, 1547, 1499, 1476, 1199, 1097, 1007, 843, 557;

UV-vis (MeCN) λ, nm (ε, $M^{-1}cm^{-1}$): 383 (122600), 270 (102000);

Compound 25. *Synthesis of* $[(L^f)_3Zn_2](ClO_4)_4$

$Zn(ClO_4)_2 \cdot 6H_2O$ (59.8 μmol) in MeOH (5 mL) to a solution of the ligand **22** (89.8 μmol) in CH_2Cl_2/MeOH 5/1 (30 mL) was added. After stirring overnight, the precipitate was filtered and washed with MeOH. Recrystallization in MeCN/Et_2O gave the Zn_2-helical complex in 70% yield.

Anal.calc.for $[C_{117}H_{96}N_{12}S_6Zn_2](ClO_4)_4$ (M_r = 2391.11): C, 58.77; H, 4.05; N, 7.03; S, 8.05;

Anal.calc.for $[C_{117}H_{96}N_{12}S_6Zn_2](ClO_4)_4 \bullet 2H_2O$: C:57.90, H:4.15, N:6.93; Found C:57.96, H:4.30, N:6.95.

^{1}H NMR (CD_3CN): δ (ppm) 2.52 (s, 18H, SCH_3), 4.07 (s, 6H, CH_2), 6.32 (d, ^3J = 8.4 Hz, 12H, Ph^A), 7.02 (d, ^3J = 8.3 Hz, 12H, Ph^A), 7.36 (d, ^3J = 8.6 Hz, 12H, Ph^B), 7.54 (d, ^3J = 8.6 Hz, 12H, Ph^B), 8.11 (d, J = 2.1 Hz, 6H, Py), 8.30 (d, J = 8.1 Hz, 6H, Py), 8.61 (s, 6H, CH=N), 8.68 (dd, ^3J = 8.2, ^4J = 2.2 Hz, 6H, Py, H-2).

Caution: perchlorate salts are potentially explosive and should be handled carefully, in low quantities, used as hydrated salts, and never dehydrated under vacuum before used.

Observation: the poor solubility of the Zn complex does not allow ^{13}C NMR characterization.

ESI (MeCN): *m/z* (%) positive ion 498.1 (100) $[Zn_2L_3]^{4+}$; negative ion: 98.8 (100) $[ClO_4]^{1-}$;

IR selected (KBr pellet,): $\tilde{\nu}$ (cm^{-1}) 1629, 1593, 1567, 1501, 1479, 1197, 1098, 1003, 818, 623;

UV-vis (MeCN) λ, nm (ε, $M^{-1}cm^{-1}$): 379 (138500), 272 (104300).

6.4. Chiral (R)- and (S)-binaphthyl Zn(II)-complexes

6.4.1. (S)- and (R)-bromo binaphthyl complexes

Compound 26$^{(S)}$. *Synthesis of (S)-binaphthyl ligand* **L^{g}**

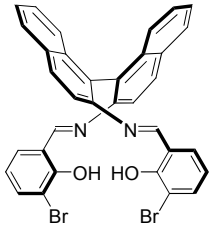

A mixture of (*S*)-(-)-l,l'-binaphthyl-2,2'-diamine, (207.7 mg, 0.73 mmol) and 3-bromo salicylaldehyde (293.7 mg, 1.46 mmol) in EtOH (10 mL) was stirred at reflux for 4.5 h under Ar. During this time an orange precipitate was formed. The resulted precipitate was collected by filtration and washed with EtOH (2x2 mL) to give the pure (S)-**L^{g}** (370 mg, 78%).

M.p. 249°C;

Anal.calc. for $C_{34}H_{22}Br_2N_2O_2$ (M_r = 650.36): C, 62.79; H, 3.41; N, 4.31; Found: C, 62.99; H, 3.58; N, 4.40.

^{1}H NMR (CD_2Cl_2): δ (ppm) 6.70 (t, ^{3}J = 8.5 Hz, 2H, H-5), 7.16-7.23 (m, 4H), 7.27-7.32 (m, 2H), 7.43-7.52 (m, 4H), 7.69 (d, J = 9.0 Hz, 2H), 8.02 (d, J = 9.0 Hz, 2H), 8.16 (d, J = 9.0 Hz, 2H), 8.66 (s, 2H, CH=N), 12.94 (s, 2H, OH);

^{13}C NMR (CD_2Cl_2): δ (ppm) 110.5, 117.2, 119.7, 120.3, 126.3, 126.4, 127.3, 128.4, 129.5, 130.3, 131.7, 132.9, 133.3, 136.2, 143.5, 157.6 (C-OH), 161.9 (CH=N);

MALDI-TOF (1,8,9-anthracenetriol), *m*/*z* (%): 650.8 (100) ^{79}Br, 652.8 (60) ^{81}Br $[M+H]^+$;

Selected IR (KBr pellet): $\tilde{\nu}$ (cm^{-1}), 3424, 3054, 3019, 2927, 2861, 1606, 1587, 1556, 1495, 1441, 1403, 1133, 825, 735.

UV-vis (CH_2Cl_2) λ, nm (ε, M^{-1}cm^{-1}): 231 (86300), 279 (48800), 288 sh (46100), 324 (30400) to 369 (25500) br, 388 sh (17300);

Compound 26$^{(R)}$. *Synthesis of (R)-binaphthyl ligand* **L^{g}**

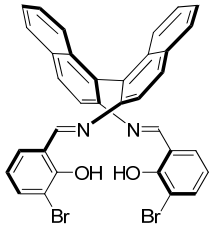

The (R)-**L^{g}** isomer (303, 94%) was obtained by the same method as for its (S)-analogue from (*R*)-(+)-l,l'-binaphthyl-2,2'-diamine (142.2 mg, 0.50 mmol) and 3-bromo salicylaldehyde (201.0 mg, 1.00 mmol).

M.p. 248.2°C;

Anal.calc. for $C_{34}H_{22}Br_2N_2O_2$ (M_r = 650.36): C, 62.79; H, 3.41; N, 4.31; Found: C, 62.91; H, 3.41; N, 4.23.

^{1}H NMR (CD_2Cl_2): δ (ppm) 6.70 (t, *J* = 8.5 Hz, 2H, H-5), 7.16-7.23 (m, 4H), 7.27-7.32 (m, 2H), 7.43-7.52 (m, 4H), 7.69 (d, *J* = 9.0 Hz, 2H), 8.01 (d, *J* = 9.0 Hz, 2H), 8.16 (d, *J* = 9.0 Hz, 2H), 8.66 (s, 2H, CH=N), 12.95 (s, 2H, OH);

^{13}C NMR (CD_2Cl_2): δ (ppm) 110.4, 117.1, 119.6, 120.2, 126.3, 126.4, 127.2, 128.4, 129.5, 130.3, 131.7, 132.8, 133.2, 136.1, 143.4, 157.5 (C-OH), 161.9 (CH=N);

MALDI-TOF (1,8,9-anthracenetriol), *m/z* (%): 650.8 (100) ^{79}Br, 652.8 (70) ^{81}Br $[M+H]^+$;

Selected IR (KBr pellet): $\tilde{\nu}$ (cm^{-1}) 3418, 3058, 2924, 2858, 1602, 1588, 1556, 1490, 1437, 1131, 825, 745, 734.

UV-vis (CH_2Cl_2) λ, nm (ε, $M^{-1}cm^{-1}$): 231 (85900), 279 (48900), 287 sh (46300), 324 (30500) to 369 br (25700), 391 sh (16600);

Compound 27$^{(S)}$. *Synthesis of (S)-Zn(II)-bromo-binaphthyl complex*

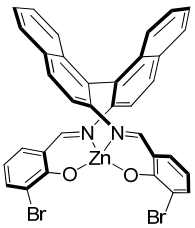

To solution of (S)-binaphthyl ligand **L^{g}** (92.0 mg, 0.142 mmol) in THF anh./EtOH p.a. (20mL, 1:1) under Ar, MeONa (38.0 mg, 0.707 mmol) was added. After stirring for 5 min, $Zn(OAc)_2$ anh. (54.0 mg, 0.294 mmol) was added sequential during 6 h. The solution colour changed from orange to yellow. The resulting solution was stirred at 65°C for 18 h. The reaction mixture was concentrated to a solid that was dissolved into CH_2Cl_2 and removed the CH_3COONa salt. Recrystallization in CH_2Cl_2/MeOH gave a yellow precipitate of (S)-**ZnL^{g}** (72 mg, 71%).

Crystals suitable for single crystal X-ray diffraction were grown by slow diffusion of hexane/CH_2Cl_2 solution of complex.

Anal.calcd. for $C_{34}H_{20}Br_2N_2O_2Zn$ (M_r = 713.75): C, 57.21; H, 2.82; N, 3.92;

Anal.calcd. for $C_{34}H_{20}Br_2N_2O_2Zn$•1.25 CH_2Cl_2/0.25 MeOH: C, 51.50; H, 2.86; N, 3.38. Found: C, 51.11; H, 3.16; N, 3.36; ^{1}H NMR shows 1.23 CH_2Cl_2/0.25 MeOH;

^{1}H NMR (CD_2Cl_2) δ (ppm) 6.44 (t, *J* = 7.7 Hz, 2H), 6.87 (d, *J* = 8.5 Hz, 2H), 7.07 (dd, *J* = 7.9 Hz, 2H), 7.20 (t, *J* = 7.7 Hz, 2H), 7.40 - 7.44 (m, 4H), 7.63 (dd, *J* = 7.6 Hz, 1.7 Hz, 2H), 7.91 (d, *J* = 8.1, 2H), 8.06 (d, *J* = 8.7 Hz, 2H), 8.37 (s, 2H, CH=N);

^{13}C NMR (CD_2Cl_2): δ (ppm) 115.7, 117.8, 119.1, 121.0, 125.8, 126.0, 126.5, 127.3, 128.5, 131.3, 132.4, 133.8, 136.0, 138.8, 144.4, 166.0 (C-2), 171.0 (CH=N);

^{1}H NMR ($C_2D_2Cl_4$) δ (ppm) 6.42 (t, *J* = 7.7 Hz, 2H), 6.80 (d, *J* = 8.7 Hz, 2H), 7.01 (d, *J* = 8.0 Hz, 2H), 7.15 (t, *J* = 7.8 Hz, 2H), 7.26 (d, *J* = 8.4 Hz, 2H), 7.37 (t, *J* = 7.5 Hz, 2H), 7.60 (dd, *J* = 7.6, 1.7 Hz, 2H), 7.85 (d, *J* = 8.4 Hz, 2H), 7.99 (d, *J* = 8.7 Hz, 2H), 8.24 (s, 2H, CH=N);

MALDI-TOF (1,8,9-anthracenetriol), *m*/*z* (%): 712.7 (100) ^{79}Br, 714.7 (90) ^{81}Br $[ZnL+H]^+$, 734.6 (19) $[ZnL+Na]^+$, 650.8 (18) $[L^g+H]^+$;

Selected IR (KBr pellet): $\tilde{\nu}$ (cm^{-1}) 3432, 3051, 1603, 1588, 1521, 1425, 1391, 1176, 1132, 745.

UV-vis (CH2Cl2) λ, nm (ε, $M^{-1}cm^{-1}$): 229 (91300), 290 (54000), 328 sh (12800), 390 (18600);

Compound 27$^{(R)}$. *Synthesis of (R)- Zn(II)-bromo-binaphthyl complex*

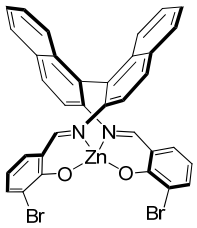

The (R)-**ZnL^g** complex (93 mg, 69%) was similarly prepared as its (S)-**ZnL^g** analogue, from (R)-***L*^{g}** ligand (124.5 mg, 0.191 mmol), MeONa (52.0 mg, 0.957 mmol) and sequential addition of $Zn(OAc)_2$ anh. (68.5 mg, 0.373 mmol).

Crystals suitable for single crystal X-ray diffraction were grown by slow diffusion of MeOH/CH_2Cl_2 solution of complex.

Anal.calcd. for $C_{34}H_{20}Br_2N_2O_2Zn$•1.30 CH_2Cl_2/0.15 MeOH: C, 51.36; H, 2.82; N, 3.38. Found: C, 51.15; H, 2.96; N, 3.38; ^{1}H NMR shows 1.30 CH_2Cl_2/0.15 MeOH.

^{1}H NMR (CD_2Cl_2) δ (ppm) 6.44 (t, *J* = 7.7 Hz, 2H), 6.87 (d, *J* = 8.5 Hz, 2H), 7.07 (dd, *J* = 7.9 Hz, 2H), 7.20 (t, *J* = 7.7 Hz, 2H), 7.39 - 7.45 (m, 4H), 7.63 (dd, *J* = 7.6 Hz, 1.7 Hz, 2H), 7.91 (d, *J* = 8.1, 2H), 8.06 (d, *J* = 8.7 Hz, 2H), 8.37 (s, 2H, CH=N);

^{13}C NMR (CD_2Cl_2): δ (ppm) 115.7, 117.9, 119.2, 121.1, 125.8, 126.0, 126.5, 127.3, 128.5, 131.3, 132.4, 133.8, 136.0, 139.0, 144.4, 166.0 (C-2), 171.0 (CH=N);

^{1}H NMR ($C_2D_2Cl_4$) δ (ppm) 3.36 (0.15 MeOH), 5.24 (1.30 CH_2Cl_2), 6.42 (t, *J* = 7.7 Hz, 2H), 6.80 (d, *J* = 8.5 Hz, 2H), 7.01 (dd, *J* = 8.0, 1.7 Hz, 2H), 7.14 (t, *J* = 7.2 Hz, 2H), 7.26 (d, *J* = 8.6 Hz, 2H), 7.37 (t, *J* = 7.1 Hz, 2H), 7.60 (dd, *J* = 7.6, 1.7 Hz, 2H), 7.84 (d, *J* = 8.1 Hz, 2H), 7.98 (d, *J* = 8.6 Hz, 2H), 8.24 (s, 2H);

MALDI-TOF (1,8,9-anthracenetriol), *m*/*z* (%): 712.7 (90) ^{79}Br, 714.7 (100) ^{81}Br $[ZnL+H]^+$, 734.6 (20) $[ZnL+Na]^+$, 650.8 (18) $[L^g+H]^+$;

Selected IR (KBr pellet): $\tilde{\nu}$ (cm^{-1}) 3423, 3051, 1603, 1588, 1521, 1426, 1391, 1176, 1132, 745.

UV-vis (CH_2Cl_2) λ, nm (ε, $M^{-1}cm^{-1}$): 228 (89500), 290 (53700), 329 sh (12800), 390 (18600);

6.4.2. (S)- and (R)-binaphthyl complexes thiophene functionalized

6.4.2.1. Zn(II)-(5)-thiophene binaphthyl complexes

Compound 28. *Synthesis of 5-(thiophen-2-yl)-salicylaldehyde*

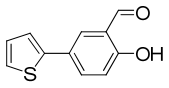

A solution of 5-bromo-salicylaldehyde (1.041 g, 5.179 mmol) and 2-thiophene-boronic acid (876 mg, 6.85 mmol) in toluene/MeOH (150 mL, 1/1) was degassed with N_2 for 30 min. $Pd(PPh_3)_4$ (304 mg, 0.288 mmol) and degassed Na_2CO_3 aq., 2M (2.745 g, 25.89 mmol) were added and the mixture was stirred at 75°C overnight. After evaporation of the solvent, the reaction mixture was diluted with CH_2Cl_2 (200 mL), poured into H_2O (100 mL) and extracted with CH_2Cl_2 (3x150 mL). The combined organic layers were dried over $MgSO_4$ and evaporated under vacuum. The residue was purified by column chromatography (SiO_2, hexane/EtOAc, 10/0 to 9/1) to give the pure aldehyde **28** (651 mg, 62%).

R_f (SiO_2, hexane /EtOAc, 9/1): 0.34; M.p. 108 °C;

Anal.calc. for $C_{11}H_8O_2S$ (M_r = 204.25): C, 64.69; H, 3.95; S, 15.70; Found: C, 64.86; H, 4.03; S, 15.72;

^{1}H NMR (CD_2Cl_2): δ (ppm) 6.98 – 7.01 (m, 1H), 7.06 – 7.09 (m, 1H), 7.25 – 7.29 (m, 2H), 7.77 (dd, *J* = 8.2, 1.9 Hz, 2H), 9.93 (s 1H, CHO), 10.98 (s, 1H, OH),

^{13}C NMR (CD_2Cl_2): δ (ppm) 118.2, 120.8, 123.0, 124.7, 126.9, 128.3, 130.7, 134.5, 142.6, 161.0 (C-2), 196.8 (CHO);

Selected IR (KBr pellet): $\tilde{\nu}$ (cm^{-1}) 1667, 1649, 1619, 1589, 1526, 1479, 1425, 1377, 1284, 1255, 1223, 1204, 1172, 887, 849, 825, 769, 738, 718, 699

UV-vis (CH_2Cl_2) λ, nm (ε, $M^{-1}cm^{-1}$): 366 (2620), 292 (12945), 254 (22500);

Compound 29$^{(S)}$. *Synthesis of (S)-(5) thiophene binaphthyl ligand* **L^h**

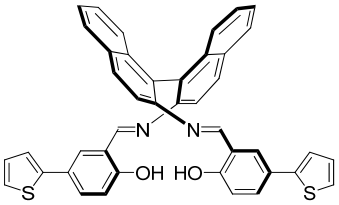

A mixture of (*S*)-(-)-l,l'-binaphthyl-2,2'-diamine, (316.5 mg, 1.113 mmol) and aldehyde **28** (455.0 mg, 2.226 mmol) in EtOH (20 mL) was stirred at 50°C for 3.5 h under Ar. During this time an orange precipitate was formed. The resulted precipitate was collected by filtration and washed with EtOH (2x2 mL). Recrystallization in CH_2Cl_2/EtOH gave the pure (S)-**L^h** (670 mg, 92%).

M.p. 156°C dec.;

Anal.calc. for $C_{42}H_{28}N_2O_2S_2$ (M_r = 656.81): C, 76.80; H, 4.30; N, 4.27; S, 9.76; Found: C, 76.88; H, 4.51; N, 4.43; S, 9.55;

^{1}H NMR (CD_2Cl_2): δ (ppm) 6.66 (d, *J* = 8.6 Hz, 2H), 6.99 (dd, *J* = 5.1, 3.6 Hz, 2H), 7.11 (dd, *J* = 3.6, 1.2 Hz, 2H), 7.17 (dd, *J* = 5.1, 1.2 Hz, 2H), 7.22 – 7.33 (m, 4H), 7.41 – 7.51 (m, 6H), 7.72 (d, *J* = 8.9 Hz, 2H), 8.01 (d, *J* = 8.2 Hz, 2H), 8.16 (d, *J* = 8.8 Hz, 2H), 8.75 (s, 2H, CH=N), 12.23 (s, 2H, OH);

^{13}C NMR (CD_2Cl_2): δ (ppm) 116.7, 117.5, 119.4 (q), 122.2, 124.0, 125.7 (q), 126.2, 126.4, 127.2, 128.1, 128.4, 129.4, 130.0 (q), 130.1, 130.6, 132.8 (q), 133.3 (q), 143.5 (q), 143.5 (q), 160.4 (q, C-2), 161.6 (CH=N);

^{13}C DEPT135 NMR (CD_2Cl_2): δ (ppm) 116.7, 117.4, 122.2, 123.9, 126.2, 126.3, 127.1, 128.0, 128.3, 129.3, 130.1, 130.5, 161.5 (CH=N);

MALDI-TOF (1,8,9-anthracenetriol), *m/z* (%): 657.0 (100) $[M+H]^+$;

Selected IR (KBr pellet): $\tilde{\nu}$ (cm^{-1}) 1626, 1612, 1579, 1506, 1484, 1288, 1260, 1169, 818, 801, 749, 697;

UV-vis (CH_2Cl_2) *λ*, nm (*ε*, $M^{-1}cm^{-1}$): 227 (5870), 280 (63790), 315 sh (43520), 371 (20250);

Compound 29$^{(R)}$. *Synthesis of (R)-(5) thiophene binaphthyl ligand* **L^h**

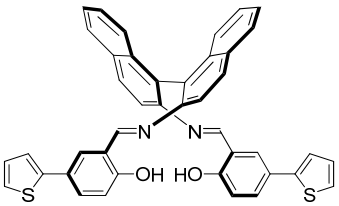

The (R)-**L^h** isomer (303, 94%) was obtained by the same method as for its (S)-analogue, from (*R*)-(+)-l,l'-binaphthyl-2,2'-diamine (121.5 mg, 0.427 mmol) and aldehyde **28** (174.5 mg, 0.855 mmol).

M.p. 156°C dec.;

Anal.calc. for $C_{42}H_{28}N_2O_2S_2$ (M_r = 656.81): C, 76.80; H, 4.30; N, 4.27; S, 9.76; Found: C, 76.67; H, 4.31; N, 4.34; S, 10.04;

^{1}H NMR (CD_2Cl_2): δ (ppm) 6.66 (d, *J* = 8.6 Hz, 2H), 6.99 (dd, *J* = 5.1, 3.6 Hz, 2H), 7.11 (dd, *J* = 3.6, 1.2 Hz, 2H), 7.17 (dd, *J* = 5.1, 1.1 Hz, 2H), 7.22 – 7.33 (m, 4H), 7.41 – 7.51 (m, 6H), 7.72 (d, *J* = 8.9 Hz, 2H), 8.01 (d, *J* = 8.1 Hz, 2H), 8.16 (d, *J* = 8.8 Hz, 2H), 8.75 (s, 2H, CH=N), 12.23 (s, 2H, OH);

^{13}C NMR (CD_2Cl_2): δ (ppm) 116.7, 117.5, 119.4 (q), 122.2, 124.0, 125.7 (q), 126.2, 126.4, 127.2, 128.0, 128.3, 129.3, 130.0 (q), 130.1, 130.6, 132.8 (q), 133.2 (q), 143.4 (q), 143.5 (q), 160.4 (q, C-2), 161.6 (CH=N);

^{13}C DEPT135 NMR (CD_2Cl_2): δ (ppm) 116.6, 117.4, 122.1, 123.9, 126.2, 126.3, 127.1, 128.0, 128.3, 129.3, 130.1, 130.5, 161.5 (CH=N);

MALDI-TOF (1,8,9-anthracenetriol), *m*/*z* (%): 657.0 (100) $[M+H]^+$;

Selected IR (KBr pellet): $\widetilde{\nu}$ (cm^{-1}) 1623, 1603, 1587, 1548, 1503, 1428, 1378, 1356, 1341, 1199, 1136, 809, 748, 698;

Compound 30$^{(S)}$. *Synthesis of (S)-Zn binaphthyl complex,* **ZnL^h**

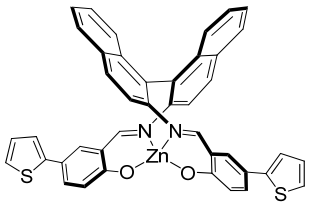

To a THF/MeOH anh. (20mL, 1:1) solution of (S)-binaphthyl ligand ***L*^{h}** (297 mg, 0.452 mmol) under Ar MeONa (122 mg, 2.26 mmol) was added. $Zn(OAc)_2$ anh. (166 mg, 0.904 mmol) was added sequential in two portions. The resulting solution was stirred at 50°C under Ar. The solution colour changed from orange to yellow. The second portion of $Zn(OAc)_2$ anh. was added after 3 h and stirred additionally for 3 h. The reaction mixture was concentrated to a solid that was dissolved into CH_2Cl_2 anh. and removed the CH_3COONa salt. Recrystallization in CH_2Cl_2/MeOH anh. gave a yellow precipitate of (S)-**ZnL^h** (265 mg, 81%).

Crystals suitable for single crystal X-ray diffraction were grown by slow diffusion of MeOH/CH_2Cl_2 solution of complex.

Anal.calcd. for $C_{42}H_{26}N_2O_2S_2Zn$ (M_r = 720.21): C, 70.04; H, 3.64; N, 3.89; S, 8.90;

Anal.calcd. for $C_{42}H_{26}N_2O_2S_2Zn$•0.25 CH_2Cl_2/0.71 MeOH/1.65 H_2O: C, 64.99; H, 4.14; N, 3.53; S, 8.08; Found: C, 65.26; H, 4.16; N, 3.65; S, 7.90; ^{1}H NMR shows 0.25 CH_2Cl_2/0.71 MeOH/1.65 H_2O;

^{1}H NMR (CD_2Cl_2 anh.) δ (ppm) 6.78 (d, *J* = 8.9 Hz, 2H), 6.88 (dd, *J* = 8.5, 0.7 Hz, 2H), 6.97 (dd, *J* = 5.1, 3.6 Hz, 2H), 7.06 (dd, *J* = 3.6, 1.2 Hz, 2H), 7.12 (dd, *J* = 5.1, 1.2 Hz, 2H), 7.17 – 7.23 (m, 2H), 7.31 (d, *J*

= 2.5 Hz, 2H), 7.37 – 7.46 (m, 4H), 7.52 (dd, *J* = 8.9, 2.6 Hz, 2H), 7.91 (d, *J* = 8.1 Hz, 2H), 8.07 (d, *J* = 8.5 Hz, 2H), 8.44 (s, 2H, CH=N);

^{1}H NMR (CD_3CN anh.) δ (ppm) 2.15 (H_2O), 3.30 (MeOH), 5.47 (CH_2Cl_2), 6.75 (d, *J* = 8.9 Hz, 2H), 6.90 (d, *J* = 8.5 Hz, 2H), 7.01 (dd, *J* = 5.1, 3.6 Hz, 2H), 7.13 (dd, *J* = 3.6, 1.1 Hz, 2H), 7.22 (dd, *J* = 5.1, 1.1 Hz, 2H), 7.32 – 7.24 (m, 2H), 7.60 – 7.41 (m, 8H), 7.99 (d, *J* = 8.2 Hz, 2H), 8.13 (d, *J* = 8.6 Hz, 2H), 8.53 (s, 2H, CH=N);

^{13}C NMR (CD_2Cl_2 anh.): 118.1, 121.1, 121.4, 121.8, 123.2, 124.1, 125.9, 125.9, 126.5, 127.2, 128.0, 128.5, 131.1, 132.4, 132.8, 133.8, 133.9, 143.9, 144.6, 170. 8, 171.0;

Observation: the complex is fast decomposed to ligand in presence of traces of water;

MALDI-TOF (1,8,9-anthracenetriol), *m/z* (%): 718.8 (100) $[ZnL+H]^+$, 657.0 (90) $[L^i+H]^+$;

MALDI-TOF (no matrix), *m/z* (%): 718.8 (100) $[ZnL+H]^+$, 740.9 (70) $[ZnL+Na]^+$, 657.0 (15) $[L^i+H]^+$;

UV-vis (CH_2Cl_2 anh.) λ, nm (ε, $M^{-1}cm^{-1}$): 230 (75230), 282 (78570), 312 sh (50230), 419 (13220);

Compound 30$^{(R)}$. *Synthesis of (R)-Zn binaphthyl complex,* **ZnL^h**

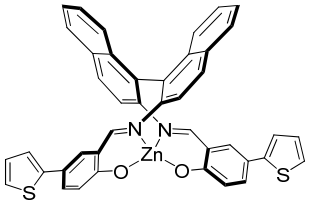

The (R)-**ZnL^h** complex (140 mg, 80%) was similarly prepared as its (S)-**ZnL^h** analogue, from (R)-**L^h** ligand (160 mg, 0.244 mmol), MeONa (66.0 mg, 1.218 mmol) and sequential addition of $Zn(OAc)_2$ anh. (77 mg, 0.42 mmol).

Anal.calcd. for $C_{42}H_{26}N_2O_2S_2Zn$ (M_r = 720.21): C, 70.04; H, 3.64; N, 3.89; S, 8.90; Anal.calcd. for $C_{42}H_{26}N_2O_2S_2Zn$•0.25 MeOH/1.63 H_2O: C, 66.98; H, 4.03; N, 3.70; S, 8.47; Found: C, 66.66; H, 3.97; N, 3.78; S, 8.70; ^{1}H NMR shows 0.25 MeOH/1.63 H_2O;

^{1}H NMR (CD_2Cl_2 anh.) δ (ppm) 1.52 (1.63 H_2O), (0.25 MeOH), 6.78 (d, *J* = 8.9 Hz, 2H), 6.88 (d, *J* = 8.5 Hz, 2H), 6.97 (dd, *J* = 5.1, 3.6 Hz, 2H), 7.07 (dd, *J* = 3.6, 1.1 Hz, 2H), 7.12 (dd, *J* = 5.1, 1.1 Hz, 2H), 7.17 – 7.23 (m, 2H), 7.32 (d, *J* = 2.5 Hz, 2H), 7.39 – 7.46 (m, 4H), 7.53 (dd, *J* = 8.9, 2.6 Hz, 2H), 7.92 (d, *J* = 8.1 Hz, 2H), 8.07 (d, *J* = 8.6 Hz, 2H), 8.45 (s, 2H, CH=N);

^{1}H NMR (CD_3CN anh.) δ (ppm) 6.75 (d, *J* = 8.9 Hz, 2H), 6.90 (d, *J* = 8.5 Hz, 2H), 7.00 (dd, *J* = 5.1, 3.6 Hz, 2H), 7.12 (dd, *J* = 3.5, 1.1 Hz, 2H), 7.21 (dd, *J* = 5.1, 0.9 Hz, 2H), 7.27 (t, *J* = 7.7 Hz, 2H), 7.43 - 7.49 (m, 6H), 7.55 (dd, *J* = 8.9, 2.6 Hz, 2H), 7.98 (d, *J* = 8.2 Hz, 2H), 8.12 (d, *J* = 8.7 Hz, 2H), 8.52 (s, 2H, CH=N);

^{13}C NMR (CD_2Cl_2 anh.): 118.2 (q), 121.2, 121.3, 121.8 (q), 123.1, 124.0, 125.8, 125.9 (q), 126.5, 127.2, 127.9, 128.5, 131.0, 132.3 (q), 132.8, 133.7, 133.8 (q), 143.9 (q), 144.7 (q), 170.7 (q), 170.8;

^{13}C DEPT135 NMR (CD_2Cl_2 anh.): δ (ppm) 121.1, 121.2, 123.0, 123.9, 125.8, 126.4, 127.1, 127.9, 128.4, 131.0, 132.7, 133.6, 170.7;

MALDI-TOF (1,8,9-anthracenetriol), *m/z* (%): 718.9 (100) $[ZnL+H]^+$, 657.0 (55) $[L^i+H]^+$;

UV-vis (CH_2Cl_2 anh.) λ, nm (ε, $M^{-1}cm^{-1}$): 228 (84350), 282 (82250), 312 sh (52080), 419 (14060);

6.4.2.2. Zn(II)-(4)-thiophene binaphthyl complexes

Compound 31. *Synthesis of 4-(thiophen-2-yl)-salicylaldehyde*

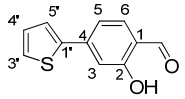

A solution of 4-bromo-salicylaldehyde (666 mg, 3.313 mmol) and 2-thiophene-boronic acid (509 mg, 3.97 mmol) in DME/H20 (40 mL, 3/1) was degassed with N_2 for 30 min. $Pd(PPh_3)_4$ (191 mg, 0.166 mmol) and Na_2CO_3 (1.756 g, 16.56 mmol) were added and the mixture was stirred at 80°C overnight. The reaction mixture was diluted with CH_2Cl_2 (200 mL), poured into H_2O (100 mL) and extracted with CH_2Cl_2 (3x150 mL). The combined organic layers were dried over $MgSO_4$ and evaporated under vacuum. The residue was purified by column chromatography (SiO_2, hexane/EtOAc, 10/0 to 9/1) to give the pure aldehyde ***31*** (517 mg, 76%).

R_f (SiO_2, hexane /EtOAc, 98/2): 0.56; M.p. 96.5°C;

Anal.calc. for $C_{11}H_8O_2S$ (M_r = 204.25): C, 64.69; H, 3.95; Found: C, 64.49; H, 3.91;

^{1}H NMR (CD_2Cl_2): 7.13 (dd, ^3J = 5.1, ^3J = 3.7 Hz, 1H, H-4'), 7.21 (d, ^4J = 1.6 Hz, 1H, H-3), 7.29 (dd, ^3J = 8.1, ^4J = 1.7 Hz, 1H, H-5), 7.43 (dd, ^3J = 5.1, ^4J = 1.1 Hz, 1H, H-3'/5'), 7.49 (dd, ^3J = 3.7, ^4J = 1.1 Hz, 1H, H-3'/5'), 7.57 (d, ^3J = 8.1 Hz, 1H, H-6), 9.84 (d, J = 0.4 Hz, 1H, CHO), 11.12 (s, 1H, OH);

^{13}C NMR (CD_2Cl_2): δ (ppm) 113.6, 117.4, 119.7 (q), 125.8, 127.6, 128.6, 134.5, 142.3 (q), 142.4 (q), 162.1(q, C-2), 195.8 (CHO);

^{13}C DEPT135 NMR (CD_2Cl_2): δ (ppm) 113. 6, 117.3, 125.8, 127.5, 128.5, 134.4, 195.8;

Selected IR (KBr pellet): $\tilde{\nu}$ (cm^{-1}) 1649, 1627, 1559, 1531, 1495, 1434, 1376, 1311, 1235, 1206, 1187, 998, 801, 695;

UV-vis (CH_2Cl_2) λ, nm (ε, $M^{-1}cm^{-1}$): 225 (12040), 256 br (4600), 254 (23050);

***Compound 32$^{(S)}$.** *Synthesis of (S)-(4)-thiophene binaphthyl ligand* **L^{i}** (*compound not isolated pure)

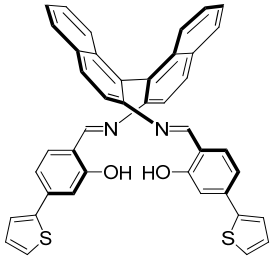

The (S)-**L^{i}** ligand (220 mg, 91%) was similarly prepared as its (S)-**L^{h}** analogue, from (*S*)-(-)-l,l'-binaphthyl-2,2'-diamine (105 mg, 0.37 mmol) and aldehyde **31** (151 mg, 0.74 mmol).

*Anal.calc. for $C_{42}H_{28}N_2O_2S_2$ (M_r = 656.81): C, 76.80; H, 4.30; N, 4.27; S, 9.76; Found: C, 76.22; H, 4.32; N, 4.24; S, 9.56;

^{1}H NMR (CD_2Cl_2): δ (ppm) 6.91 (d, *J* = 1.8 Hz, 2H), 7.02 – 7.08 (m, 4H), 7.21 – 7.32 (m, 10H), 7.45 – 7.51 (m, 2H), 7.73 (d, *J* = 8.9 Hz, 2H), 8.01 (d, *J* = 8.2 Hz, 2H), 8.15 (d, *J* = 8.7 Hz, 2H), 8.72 (s, 2H, CH=N), 12.31 (s, 2H, OH);

^{13}C NMR (CD_2Cl_2): δ (ppm) 113.4, 116.4, 116.6, 118.6 (q), 124.5, 126.1, 126.3, 126.4, 127.1, 128.2, 128.3, 130.0, 130.1 (q), 132.7 (q), 132.8, 133.3 (q), 138.5 (q), 143.2 (q), 143.6 (q), 161.0 (CH=N), 161.2 (q);

^{13}C DEPT135 NMR (CD_2Cl_2): δ (ppm) 113.3, 116.3, 116.6, 124.5, 126.0, 126.2, 126.3, 127.0, 128.2, 128.22, 129.9, 132.8, 160.9 (CH=N);

MALDI-TOF (1,8,9-anthracenetriol), *m/z* (%): 657.0 (100) $[M+H]^+$;

Compound 32$^{(R)}$. *Synthesis of (R)-(4)- thiophene binaphthyl ligand* **L^{i}**

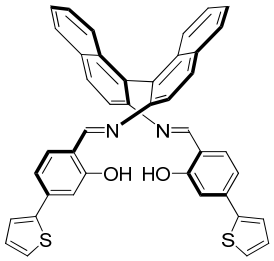

The (R)-***L*^{i}** ligand (134 mg, 81%) was similarly prepared as its (S)-**L^{h}** analogue, from (R)-(+)-l,l'-binaphthyl-2,2'-diamine (71.7 mg, 0.252 mmol) and aldehyde **31** (103 mg, 0.504 mmol).

Anal.calc. for $C_{42}H_{28}N_2O_2S_2$ (M_r = 656.81): C, 76.80; H, 4.30; N, 4.27; Found: C, 76.46; H, 4.39; N, 4.24;

^{1}H NMR (CD_2Cl_2): δ (ppm) 6.91 (d, *J* = 1.8 Hz, 2H), 7.02 – 7.08 (m, 4H), 7.21 – 7.32 (m, 10H), 7.45 – 7.51 (m, 2H), 7.73 (d, *J* = 8.9 Hz, 2H), 8.01 (d, *J* = 8.2 Hz, 2H), 8.15 (d, *J* = 8.7 Hz, 2H), 8.72 (s, 2H, CH=N), 12.31 (s, 2H, OH);

^{13}C NMR (CD_2Cl_2): δ 113.4, 116.4, 116.6, 118.6 (q), 124.5, 126.1, 126.3, 126.4, 127.1, 128.2, 128.3, 130.0, 130.1 (q), 132.7 (q), 132.8, 133.3 (q), 138.5 (q), 143.2 (q), 143.6 (q), 160.9 (CH=N), 161.2 (q)

^{13}C DEPT135 NMR (CD_2Cl_2): δ (ppm) 113.3, 116.3, 116.5, 124.5, 126.0, 126.2, 126.3, 127.0, 128.2, 128.22, 129.9, 132.8, 160.9 (CH=N);

MALDI-TOF (1,8,9-anthracenetriol), *m*/*z* (%): 657.0 (100) $[M+H]^+$.

***Compound 33$^{(S)}$.** *Synthesis of (S)-Zn binaphthyl complex,* **ZnL^i** (*compound not isolated pure)

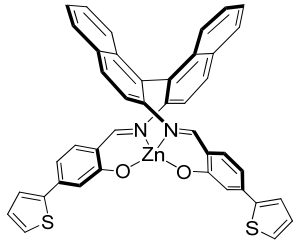

The (S)-**ZnL^i** complex was similarly prepared as its (S)-**ZnL^h** analogue, from (R)-**L^i** ligand (139 mg, 0.212 mmol), MeONa (57.0 mg, 1.06 mmol) and sequential addition of $Zn(OAc)_2$ anh. (78 mg, 0.42 mmol).

*****Observation: in the NMR spectrum is observed 8% decomposition to ligand for one molecule of complex; the decomposition takes place in presence of traces of water even in deuterated solvent, as proved for the other isomers;

^{1}H NMR (CD_2Cl_2 dried) δ (ppm) 6.81 (dd, *J* = 8.2, 1.8 Hz, 2H). 6.72 (d, *J* = 8.5 Hz, 2H), 7.02 – 7.08 (m, 6H), 7.16 -7.21 (m, 2H), 7.30 – 7.43 (m, 8H), 7.89 (d, *J* = 8.1 Hz, 2H), 8.02 (d, *J* = 8.6 Hz, 2H), 8.34 (s, 2H);

^{13}C NMR (CD_2Cl_2 dried) δ (ppm) 113.0, 118.0 (q), 119.4, 121.4, 124.8, 125.7, 126.0 (q), 126.3, 126.5, 127.0, 128.2, 128.5, 130.8, 132.2 (q), 133.8 (q), 136.7, 140.9 (q), 143.5 (q), 145.0 (q), 169.8 (CH=N), 171.0 (q);

^{13}C DEPT135 NMR (CD_2Cl_2 dried): δ (ppm) 113.0, 119.3, 121.3, 124.7, 125.6, 126.2, 126.5, 126.9, 128.1, 128.4, 130.7, 136.6, 169.7;

Compound 33$^{(R)}$. *Synthesis of (R)-Zn binaphthyl complex,* **ZnL^i**

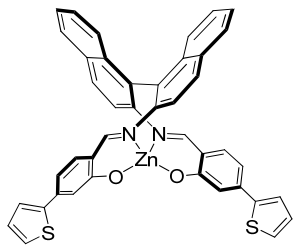

The (R)-**ZnL^{i}** complex (56 mg, 67%) was similarly prepared as its (S)-**ZnL^{h}** analogue, from (R)-***L*^{i}** ligand (76.0 mg, 0.116 mmol), MeONa (31.3 mg, 0.579 mmol) and sequential addition of $Zn(OAc)_2$ anh. (42.4 mg, 0.231 mmol).

Anal.calcd. for $C_{42}H_{26}N_2O_2S_2Zn$ (M_r = 720.21): C, 70.04; H, 3.64; N, 3.89; S, 8.90; Anal.calcd. for $C_{42}H_{26}N_2O_2S_2Zn$•1 H_2O: C, 68.33; H, 3.82; N, 3.79; S, 8.69; Found: C, 68.41; H, 3.99; N, 3.83; S, 8.31;

^{1}H NMR (CD_2Cl_2 anh.) δ (ppm) 6.78 (dd, *J* = 8.2, 1.8 Hz, 2H). 6.89 (d, *J* = 8.4 Hz, 2H), 7.00 – 7.03 (m, 6H), 7.16 -7.22 (m, 2H), 7.29 (d, *J* = 4.4 Hz, 4H), 7.36 – 7.43 (m, 4H), 7.87 (d, *J* = 8.1 Hz, 2H), 7.97 (d, *J* = 8.6 Hz, 2H), 8.30 (s, 2H),

^{1}H NMR (CD_3CN anh.) δ (ppm) 6.96 – 6.81 (m, 4H), 7.01 (d, *J* = 1.7 Hz, 2H), 7.18 – 7.08 (m, 4H), 7.25 - 7.31 (m, 2H), 7.58 – 7.39 (m, 8H), 7.98 (d, *J* = 7.9 Hz, 2H), 8.11 (d, *J* = 8.6 Hz, 2H), 8.45 (s, 2H, CH=N);

^{13}C NMR (CD_2Cl_2 anh.): 113.0, 118.0 (q), 119.4, 121.4, 124.8, 125.7, 126.0 (q), 126.3, 126.5, 127.0, 128.2, 128.5, 130.8, 132.2 (q), 133.8 (q), 136.7, 141.0 (q), 143.5 (q), 145.0 (q), 169.8, 171.0 (q);

^{13}C DEPT135 NMR (CD_2Cl_2): δ (ppm) 112.9, 119.3, 121.3, 124.7, 125.6, 126.3, 126.4, 127.0, 128.1, 128.4, 130.7, 136.6, 169.7;

MALDI-TOF (1,8,9-anthracenetriol), *m*/*z* (%): 718.8 (80) $[ZnL+H]^+$, 657.0 (100) $[L^i+H]^+$;

6.5. Functionalized thioketal compounds for SAM study

Compound 34a. *Introduction of thioketal group*

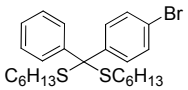

To a solution of 4-bromo-benzophenone (1.200 g, 4.595 mmol) in $CHCl_3$ anh. (40 mL), with activated molecular sieves, (4Å) 1-hexanthiol (4.348 g, 36.78 mmol) and trimethylchlorosilane anh. (0.990 g, 9.19 mmol) were added. The reaction mixture was stirred at 60°C under Ar for 48 h. The molecular sieves were removed by filtration, the reaction mixture was diluted with $CHCl_3$ (300 mL) and washed with $NaHCO_3$ aq. 5% (100 mL). The aqueous layer was extracted with $CHCl_3$ (2x200 mL). The combined organic layers were dried over $MgSO_4$ and evaporated under vacuum. Purification by column chromatography (SiO_2, hexane) afforded the compound **34a** as colourless oil (1.60 g, 73%).

R_f (SiO_2, CH_2Cl_2/hexane 1/1): 0.89

Anal.calcd. for $C_{25}H_{35}BrS_2$, (M_r = 479.58): C, 62.61; H, 7.36; S, 13.37; Found: C, 62.93; H, 7.14; S, 13.38.

^{1}H NMR (CD_2Cl_2): δ (ppm) 0.83 (t, ^3J = 6.9 Hz, 6H, CH_3), 1.11-1.29 (m, 12H, CH_2), 1.32-1.42 (m, 4H, CH_2), 2.30 (t, ^3J = 8.5 Hz, 4H, CH_2), 7.18-7.30 (m, 3H), 7.37-7.44 (m, 4H), 7.48-7.51 (m, 2H);

^{13}C NMR (CD_2Cl_2): δ (ppm) 13.9 (CH_3), 22.6 (CH_2), 28.3 (CH_2), 28.9 (CH_2), 31.0 (CH_2), 31.5 (CH_2), 68.9 (C-thioketal), 120.9, 127.2, 127.9, 128.4, 130.4, 130.8, 144.0, 144.1.

MALDI-TOF (1,8,9-anthracenetriol), *m/z* (%):360.77 (95) Br^{79}, 362.77 (100) Br^{81} $[M\text{-}SC_6H_{13}]^+$;

Selected IR (KBr pellet): $\tilde{\nu}$ (cm^{-1}) 3435, 2956, 2927, 2871, 2856, 1664w, 1587w, 1486, 1466, 1445, 1393, 1076, 1009, 790, 746, 696;

UV-vis (CH_2Cl_2) λ, nm (ε, $M^{-1}cm^{-1}$): 226 (17500), 258 (6650), 318 (960);

Compound 34b.

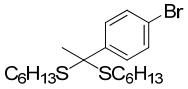

The compound **34b** was synthesized as described for its analogue **34a** using 4-bromo-acetophenone (2.809 g, 14.12 mmol), 1-hexanthiol (6.676 mg, 56.46 mmol) and trimethylchlorosilane anh. (3.067 g, 28.23 mmol) in $CHCl_3$ anh. (80 mL). Purification by column chromatography (SiO_2, hexane) afforded the compound **34b** as colourless oil (2.661 g, 45%).

R_f (SiO_2, CH_2Cl_2/hexane 1/1): 0.83

Anal.calcd. for $C_{20}H_{33}BrS_2$, (M_r = 417.51): C, 57.53; H, 7.97; S, 15.36; Found: C, 57.85; H, 7.73; S, 15.43.

^{1}H NMR (CD_2Cl_2): δ (ppm) 0.87 (t, ^3J = 6.9 Hz, 6H, CH_3), 1.19-1.37 (m, 12H, CH_2), 1.44-1.56 (m, 4H, CH_2), 1.96 (s, 3H, CH_3), 2.48 (t, J = 7.4 Hz, 4H, CH_2), 7.43 (td, ^3J = 9.0, ^4J = 2.4 Hz, 2H, Ph), 7.58 (td, ^3J = 8.7, ^4J = 2.4 Hz, 2H, Ph);

^{13}C NMR (CD_2Cl_2): δ (ppm) 14.0 (CH_3), 22.7 (CH_2), 29.0 ($2CH_2$), 30.1 (CH_3), 30.9 (CH_2), 31.6 (CH_2), 59.9 (C-thioketal), 121.1 (q, Ph), 129.1, 131.2, 143.7 (q, Ph);

^{13}C-DEPT135 NMR (CD_2Cl_2): δ (ppm) 13.9 (CH_3), 22.6 (CH_2), 28.9 ($2CH_2$), 30.0 (CH_3), 30.8 (CH_2), 31.5 (CH_2), 129.0 (Ph), 131.1 (Ph);

MALDI-TOF (1,8,9-anthracenetriol), *m/z* (%): 298.82 (75) Br^{79}, 300.83 (100) Br^{81}, $[M\text{-}SC_6H_{13}]^+$;

Selected IR (KBr pellet): $\tilde{\nu}$ (cm^{-1}) 3434, 2957, 2927, 2856, 1682, 1636, 1587, 1486, 1463, 1394, 1375, 1262, 1078, 1008, 827, 804, 730;

UV-vis (CH_2Cl_2) λ, nm (ε, $M^{-1}cm^{-1}$): 227 (5260), 256 (12500);

Compound 35a.

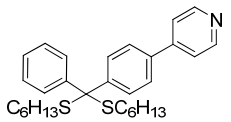

A solution of compound **34a** (460 mg, 0.959 mmol) and 4-pyridine-boronic acid (177 mg, 1.44 mmol) in DME/ H_2O (40 mL, 3:1) was degassed with Ar for 30 min. $Pd(PPh_3)_4$ (55.0 mg, 0.048 mmol) and Na_2CO_3 (610 mg, 5.76 mmol) were added and the mixture was stirred at 80°C for 6 h. The reaction mixture was diluted with CH_2Cl_2 (200 mL), poured into H_2O (100 mL) and separated. The aqueous layer was extracted with CH_2Cl_2 (3x100 mL). The combined organic layers were dried over $MgSO_4$ and the solvent was evaporated under vacuum. The product was purified by column chromatography (SiO_2, TEA, hexane/CH_2Cl_2, 4/1 to 1/1) to yield the pure compound **35a** as yellow oil (275 mg, 60%).

R_f (SiO_2, TEA, CH_2Cl_2/hexane 1/1): 0.39;

Anal.calcd. for $C_{30}H_{39}NS_2$ (M_r = 477.77): C, 75.42; H, 8.23; N, 2.93; S, 13.42; Found: C, 75.49; H, 8.00; N, 3.00; S, 13.37.

^{1}H NMR (CD_2Cl_2): δ (ppm) 0.85 (t, ^3J = 6.9 Hz, 6H, CH_3), 1.16-1.33 (m, 12H, CH_2), 1.37-1.48 (m, 4H, CH_2), 2.39 (t, ^3J = 7.2 Hz, 4H, CH_2), 7.28-7.34 (m, 3H, Ph), 7.51 (dd, ^3J = 4.5; ^4J = 1.5 Hz, 2H, Py), 7.57-7.61 (m, 4H, Ph), 7.67-7.70 (m, 2H, Ph), 8.62 (dd, ^3J = 4.5; ^4J = 1.5 Hz, 2H, Py);

^{13}C NMR (CD_2Cl_2): δ (ppm) 13.9 (CH_3), 22.6 (CH_2), 28.3 (CH_2), 28.9 (CH_2), 31.0 (CH_2), 31.5 (CH_2), 69.2 (C-thioketal), 121.4, 126.4, 127.2, 127.9, 128.5, 129.2, 136.6, 144.3, 145.8, 147.4, 150.4;

MALDI-TOF (1,8,9-anthracenetriol), *m/z* (%): 478.0 (100) $[M+H]^+$, 359.9 (97) $[M\text{-}SC_6H_{13}]^+$;

Selected IR (KBr pellet): $\tilde{\nu}$ = 2955, 2927, 2856, 1594, 1488, 1466, 1444, 794, 734, 696;

UV-vis (CH_2Cl_2) λ, nm (ε, $M^{-1}cm^{-1}$): 225 (18520), 261 (23160);

Compound 35b.

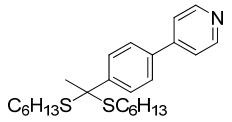

The compound **35b** was synthesized as described previously for **35a** from 4-pyridine-boronic acid (249 mg, 2.023 mmol), compound **34b** (563 mg, 1.348 mmol), $Pd(PPh_3)_4$ (124 mg, 0.107 mmol), Na_2CO_3 (715 mg, 6.742 mmol) in DME/ H_2O (3/1, 40 mL). Purification by column chromatography (SiO_2, TEA, hexane/CH_2Cl_2, 4/1 to 1/1) yielded the pure compound **35b** as yellow oil (413 mg, 74%).

R_f (SiO_2, CH_2Cl_2/hexane 1/1): 0.38;

Anal.calcd. for $C_{25}H_{37}NS_2$ (M_r = 417.70): C, 72.23; H, 8.97; N, 3.37; S, 15.43; Found: C, 72.15; H, 8.68; N, 3.35; S, 15.23;

^{1}H NMR (CD_2Cl_2): δ (ppm) 0.84 (t, ^3J = 6.8 Hz, 6H, CH_3), 1.16-1.37 (m, 12H, CH_2), 1.44-1.54 (m, 4H, CH_2), 2.02 (s, 3H, CH_3), 2.51 (t, J = 7.4 Hz, 4H, CH_2), 7.51 (dd, ^3J = 4.5; ^4J = 1.8 Hz, 2H, Py), 7.60-7.65 (m, 2H, Ph), 7.79-7.84 (m, 2H, Ph), 8.61 (dd, ^3J = 4.5; ^4J = 1.8 Hz, 2H, Py);

^{13}C NMR (CD_2Cl_2): δ (ppm) 13.9 (CH_3), 22.6 (CH_2), 28.9 (CH_2), 28.94 (CH_2), 30.0 (CH_3), 30.9 (CH_2), 31.5 (CH_2), 60.0 (C-thioketal), 121.4, 126.7, 127.9, 136.7 (q), 145.5 (q), 147.5 (q), 150.3.

^{13}C-DEPT135 NMR (CD_2Cl_2): δ (ppm) 13.8 (CH_3), 22.5 (CH_2), 28.8 (CH_2), 28.9 (CH_2), 29.9 (CH_3), 30.8 (CH_2), 31.4 (CH_2), 121.4, 126.6, 127.8, 150.2;

MALDI-TOF (1,8,9-anthracenetriol), *m*/*z* (%): 416.1 (100) $[M+H]^+$, 299.0 (48) $[M-SC_6H_{13}]^+$;

Selected IR (KBr pellet): $\tilde{\nu}$ (cm^{-1}) 3429, 2956, 2927, 2856, 1596, 1461, 1439, 1067, 814;

UV-vis (CH_2Cl_2) λ, nm (ε, $M^{-1}cm^{-1}$): 226 (7330), 257 (9840);

Compound 36a.

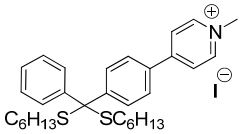

The compound **35a** (230 mg, 0.4814 mmol) was dissolved in MeCN (40 mL). An excess of MeI (342 mg, 2.207 mmol) was added and the reaction was stirred for 24 hours at rt. The solvent was removed by evaporation and the pyridinium salt was precipitated in hexane at low temperature. The yellow precipitate was filtered, washed with cold hexane and dried to give the pure methyl-pyridinium iodide salt **36a** (229 mg, 77%).

Anal.calcd. for $C_{31}H_{42}INS_2$ (M_r = 619.71): C, 60.08; H, 6.83; N, 2.26; S, 10.35; Found: C, 59.86; H, 6.46; N, 2.39; S, 10.16;

^{1}H NMR (CD_2Cl_2): δ (ppm) 0.82 (t, ^3J = 6.9 Hz, 6H, CH_3), 1.13-1.31 (m, 12H, CH_2), 1.35-1.43 (m, 4H, CH_2), 2.32 (t, ^3J = 6.9 Hz, 4H, CH_2), 4.58 (s, 3H, N^+-CH_3), 7.24-7.33 (m, 3H), 7.52-7.55 (m, 2H), 7.73-7.80 (m, 4H), 8.20 (d, ^3J = 6.9 Hz, 2H, Py^+), 9.09 (d, ^3J = 6.9 Hz, 2H, Py^+);

^{13}C NMR (CD_2Cl_2): δ (ppm) 13.8 (CH_3), 22.5 (CH_2), 28.2 (CH_2), 28.8 (CH_2), 30.9 (CH_2), 31.4 (CH_2), 48.6 (N^+-CH_3), 68.9 (C-thioketal), 124.7, 127.3, 127.4, 128.0, 128.4, 129.9, 131.9, 143.5, 145.4, 149.8, 155.8.

MALDI-TOF (1,8,9-anthracenetriol), *m/z* (%): 492.0 (60) $[M\text{-}I]^+$, 374.9 (100) $[M\text{-}I\text{-}SC_6H_{13}]^+$;

ESI mass spectrum , *m/z* (%): 492.3 (100) $[C_{31}H_{42}NS_2]^{1+}$, 376.3 (20) $[C_{25}H_{29}NS]^{1+}$; negative: 126.9 (100) $[I]^{1-}$;

Selected IR (KBr pellet): $\tilde{\nu}$ (cm^{-1}) 3460, 3013, 2956, 2925, 2872, 2852, 1637, 1601, 1491, 1482, 1467, 1440, 1187, 809, 760, 719, 519;

UV-vis (CH_2Cl_2) λ, nm (ε, $M^{-1}cm^{-1}$): 225 (26200), 240 sh (21500), 313 (19800);

Compound 37a.

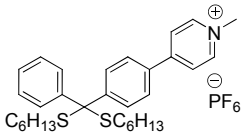

To a solution of methyl-pyridinium iodide salt **36a** (130 mg, 0.21 mmol) in acetone (40 mL) was added a solution of KPF_6 aq. (200 mg, 1.09 mmol, 10 mL H_2O) and stirred 1 h at rt. The acetone was evaporated under vacuum and the reaction mixture was extracted with CH_2Cl_2 (300 mL). The organic layer was washed with H_2O (2x100 mL) and evaporated the solvent. The colourless oil obtained was purified by chromatography (neutral Al_2O_3, CH_2Cl_2/acetone, 4:1). The methyl-pyridinium hexafluorophosphate salt **37a** was obtained as a white solid after drying under vacuum (10^{-2} mbar) for several days (49.5 mg, 37%).

Anal.calcd. for $C_{31}H_{42}F_6NPS_2$ (M_r = 637.77): C, 58.38; H, 6.64; N, 2.20; S, 10.06; Found: C, 58.34; H, 6.62; N, 2.39; S, 9.86

^{1}H NMR (CD_2Cl_2): δ (ppm) 0.82 (t, ^3J = 6.9 Hz, 6H, CH_3), 1.13-1.31 (m, 12H, CH_2), 1.36-1.45 (m, 4H, CH_2), 2.35 (t, ^3J = 6.9 Hz, 4H, CH_3), 4.37 (s, 3H, N^+-CH_3), 7.26-7.33 (m, 3H), 7.51-7.56 (m, 2H), 7.72-7.79 (m, 4H), 8.15 (d, ^3J = 6.9 Hz, 2H, Py^+), 8.58 (d, ^3J = 6.9 Hz, 2H, Py^+);

^{13}C NMR (CD_2Cl_2): δ (ppm) 13.8 (CH_3), 22.5 (CH_2), 28.2 (CH_2), 28.8 (CH_2), 31.0 (CH_2), 31.4 (CH_2), 48.0 (N^+-CH_3), 68.9 (C-thioketal), 125.0, 127.4, 127.5, 128.1, 128.4, 130.0, 131.8, 143.5, 144.8, 150.1, 156.3.

^{31}P-NMR ($CDCl_3$): δ (ppm) -144.43 (J_{P-F} = 712 Hz), binomial septet with six equivalent ^{19}F (1/2) attached to the central ^{31}P.

MALDI-TOF (1,8,9-anthracenetriol), *m*/*z* (%): 492.0 (50) $[M\text{-}PF_6]^+$, 374.9 (100%) $[M\text{-}PF_6\text{-}SC_6H_{13}]^+$;

ESI mass spectrum, *m*/*z* (%): 492.3 (100) $[C_{31}H_{42}NS_2]^{1+}$, 376.3 (10) $[C_{25}H_{29}NS]^{1+}$, 144.9 (100) $[PF_6]^{1-}$;

Selected IR (KBr pellet): $\tilde{\nu}$ (cm^{-1}) 2957, 2926, 2872, 2854, 1643, 1604, 1494, 1190, 865, 830, 759, 720, 556

UV-vis (CH_2Cl_2) λ, nm (ε, $M^{-1}cm^{-1}$): 225 (15300), 317 (16550);

Compound 38a.

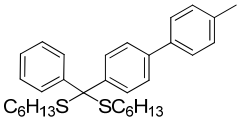

The compound **38a** was synthesized as described previously for its analogue **35a**, from compound **34a** (350 mg, 0.730 mmol), p-tolyl-boronic acid (149 mg, 1.1 mmol), DME/ H_2O (28 mL, 3:1), $Pd(PPh_3)_4$ (42.0 mg, 0.037 mmol) and Na_2CO_3 (464 mg, 4.38 mmol). The product was purified by column chromatography (SiO_2 hexane/ CH_2Cl_2, 1/0 to 3/1) to yield the pure compound **38a** as colourless oil (227 mg, 63%).

R_f (SiO_2, CH_2Cl_2/hexane 2/1): 0.7;

Anal.calcd. for $C_{32}H_{42}S_2$ (M_r = 490.81): C, 78.31; H, 8.63; S, 13.07; Found: C, 78.46; H, 8.48; S, 12.68.

^{1}H NMR (CD_2Cl_2): δ (ppm) 0.91 (t, ^3J = 7.0 Hz, 6H, CH_3), 1.18-1.54 (m, 16H, CH_2), 2.42-2.49 (m, 7H, CH_2, CH_3), 7.25-7.38 (m, 5H), 7.55-7.60 (m, 4H), 7.67-7.70 (m, 4H)

^{13}C NMR (CD_2Cl_2): δ (ppm) 14.0 (CH_3), 21.1 (CH_2), 22.7 (CH_2), 28.5 (CH_2), 29.0 (CH_2), 31.1 (CH_2), 31.6 (CH_3), 69.5 (C-thioketal), 126.2, 126.7, 127.1, 127.9, 128.6, 129.0, 129.7, 137.4, 137.6, 139.7, 143.5, 144.7

MALDI-TOF (1,8,9-anthracenetriol), *m*/*z* (%): 372.9 (100) $[M\text{-}SC_6H_{13}]^+$;

Selected IR (KBr pellet): $\tilde{\nu}$ (cm^{-1}) 3430, 2956, 2927, 2856, 1618, 1494, 1444, 795, 750, 704;

UV-vis (CH_2Cl_2) λ, nm ($M^{-1}cm^{-1}$): 225 (17800), 264 (24350);

Compound 38b.

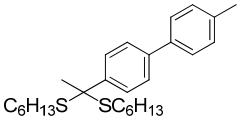

The compound **38b** was synthesized as described previously for its analogue **35a**, from compound **34b** (350 mg, 0.838 mmol), p-tolyl-boronic acid (137 mg, 1.01 mmol), $Pd(PPh_3)_4$ (48.0 mg, 0.042 mmol) and Na_2CO_3 (533 mg, 5.03 mmol) in DME/ H_2O (28 mL, 3:1). Purification by column chromatography (SiO_2, hexane/CH_2Cl_2, 1/0 to 8/2) afforded compound **38b** as colourless oil (313 mg, 89%).

R_f (SiO_2, CH_2Cl_2/hexane 2/1): 0.6;

Anal.calcd. for $C_{27}H_{40}S_2$ (M_r = 428.74): C, 75.64; H, 9.40; S, 14.96; Found: C, 75.91; H, 9.03; S, 14.74;

^{1}H NMR (CD_2Cl_2): δ (ppm) = 0.86 (t, ^3J = 6.8 Hz, 6H, CH_3), 1.19-1.38 (m, 12H, CH_2), 1.45-1.33 (m, 4H, CH_2), 2.02 (s, 3H, CH_3), 2.37 (s, 3H, CH_3), 2.52 (t, ^3J = 7.4 Hz, 4H, CH_2) 7.24 (d, ^3J = 8.1 Hz, 2H), 7.48-7.57 (m, 4H), 7.73-7.77 (m, 2H);

^{13}C NMR (CD_2Cl_2): δ (ppm) = 14.0 (CH_3), 21.0 (CH_3), 22.7 (CH_2), 29.0 (CH_2), 29.1 (CH_2), 30.1 (CH_3), 31.0 (CH_2), 31.6 (CH_2), 60.2 (C-thioketal), 126.5, 126.8, 127.6, 129.6, 137.4 (q), 137.6 (q), 139.8 (q), 143.1 (q).

^{13}C-DEPT135-NMR (CD_2Cl_2): 13.9 (CH_3), 20.9 (CH_3), 22.6 (CH_2), 28.9 (CH_2), 29.0 (CH_2), 30.0 (CH_3), 30.9 (CH_2), 31.5 (CH_2), 126.4, 126.7, 127.5, 129.5;

MALDI-TOF (1,8,9-anthracenetriol), *m*/*z* (%): 310.9 (100) $[M\text{-}SC_6H_{13}]^+$;

Selected IR (KBr pellet): $\tilde{\nu}$ (cm^{-1}) 3436, 2956, 2927, 2856, 1494, 1458, 1067, 812;

UV-vis (CH_2Cl_2) λ, nm ($M^{-1}cm^{-1}$): 225 (12530), 265 (26160);

Bibliography

1. G.E. Moore, *Electronics*, **1965**, *38*, 114
2. C. Joachim and M. A. Ratner, *Proc. Nat. Acad. Soc*, **2005**, *102*, 8801
3. B. Xu, N. Tao, *Science*, **2003**, *301*, 1221
4. N. J. Tao, *Nature Nanot*echnology, **2006**, *1*, 1973
5. N. Weibel, S. Grunder and M. Mayor, *Org. Biomol. Chem.*, **2007**, *5*, 2343
6. V.I. Minkin, *Russ.Chem.Bull., Int.Ed.,* **2008**, *57*, 687
7. J.R. Heath and M.A. Ratner, *Physics Today*, **2003**, 43
8. A. Bagrets, A. Arnold, F. Evers, *J. Am. Chem. Soc*, **2008**, 9013
9. C. Li, A. Mishchenko, Z. Li, I. Pobelov, Th. Wandlowski, X.Q. Li, F. Würthner, A. Bagrets and F. Evers, *J. Phys.: Condens. Matter*, **2008**, *20*, 374122
10. H. Kuhn and D. Möbius, *Angew. Chem. Int. Ed.*, **1971**, *10*, 620
11. A. Aviram and M. A. Ratner, *Chem. Phys. Lett.* **1974**, *29,* 277
12. R. M. Metzger, *Acc. Chem. Res.,* **1999**, *32*, 950
13. M. Elbing, R. Ochs, M. Koentopp, M. Fischer, C. von Hänisch, F.Weigend, F. Evers, H.B. Weber and M. Mayor, *Proc. Natl. Acad. Sci. U.S.A.,* **2005**, *102*, 8815
14. N.S. Hush, *Ann. NY Acad. Sci*., **2003**, *1*, 1006
15. F. Chen, J. Hihath, Z. Huang, X. Li, and N.J. Tao, *Annu. Rev. Phys. Chem.*, **2007**, *58*, 535
16. X. Xiao, B. Xu, N. Tao, *Angew. Chem. Int. Ed. Engl.,* **2004**, *43,* 6148
17. C. Vericat, M.E. Vela, G.A. Benitez, J.A. Martin Gago, X. Torrelles and R.C. Salvarezza, *J. Phys.: Condens. Matter*, **2006**, *18*, R867
18. C.K. Chiang, C.R. Fincher, Y.W. Park, A.J. Heeger, H. Shirakawa, E.J. Louis, S.C. Gau, A.J. MacDiarmid, *Phys. Rev. Lett.*, **1977**, *39*, 1098
19. J.G. Kushmerick, D.B. Holt, J.C. Yang, J. Naciri, M.H. Moore and R. Shashidhar, *Physical Review Letters*, **2002**, *89*, 086802
20. J.G. Kushmerick, D.B. Holt, S.K. Pollack, M.A. Ratner, J.C. Yang, T.L. Schull, J. Naciri, M.H. Moore, and R. Shashihar, *J. Am. Chem. Soc.,* **2002**, *124*, 10654
21. C.J. Muller, J.M. van Ruitenbeek, L.J. de Jongh, *Physica C: Superconductivity*, **1992**, *191*, 485
22. C. Kergueris, J.P.Bourgoin, S.Palacin, D.Esteve, C.Urbina, M.Magoga, C.Joachim, *Phys. Rev. B*, **1999**, *59*, 12505
23. M.A. Reed, C. Zhou, C.J.Muller, T.P. Burgin, J.M. Tour, *Science*, **1997**, *278*, 292
24. G. Binnig, H. Rohrer, *Rev. Mod. Phys.*, **1987**, *59*, 615
25. T.W. Kelley, E.L. Granstrom, C.D. Frisbie, *Adv. Mater.*, **1999**, *11*, 261
26. C. Joachim, J.K. Gimzewski, *Chem. Phys. Lett.*, **1997**, *265*, 353
27. J.G. Kushmerick, J. Naciri, J.C. Yang and R. Shashidhar, *Nano Letters*, **2003**, *3*, 897
28. M.A. Reed, C. Zhou, C.J. Mullen, T.P. Burgin and J.M. Tour, *Science*, **1997**, *278*, 252
29. M.A. Rampi and G.M. Whitesides, *Chemical Physics*, **2002**, *281,* 373
30. M.L. Chabinyc, X.X. Chen, R.E. Holmlin, H. Jacobs, H. Skulason, C.D. Frisbie, V. Mujica, M.A. Ratner, M.A. Rampi, and G.M. Whitesides, *J. Am. Chem. Soc*., **2002**, *124*, 11730

31. A. Bezryadin, C. Dekker, G. Schmid, *Appl. Phys. Lett*., **1997**. *71*, 1273
32. M. Schöck, C. Sürgers, and H. v. Löhneysen, *Europhys. Lett.*, **2006**, *74*, 473
33. M. Lukas, R.E.A. Kelly, L.N. Kantorovich, R. Otero, W. Xu, E. Laegsgaard, I. Stensgaard and F. Besenbacher, *J. Chem. Phys*., **2009**, *130*, 024705 and the references therein
34. A.M. Moore and P.S. Weiss, *Annu. Rev. Anal. Chem*., **2008**, 857
35. W. Ho, *J. Chem. Phys*, **2002**, *117*, 11033
36. J. Repp and G. Meyer, *Applied Physics A: Materials Science and Processing*, **2006**, *85*, 399
37. F. Schreiber, *Progress in Surface Science*, **2000**, *65*, 151
38. J.-M. Lehn, *Supramolecular Chemistry: Concepts and Perspectives*, VCH, Weinheim, **1995**
39. J.-M. Lehn, *Science*, **2002**, *295*, 2400
40. A. Ulman, *Chem. Rev.*, **1996**, *96*, 1533
41. M.-a. Haga, K. Kobayashi, K.Terada, *Coord. Chem. Rev.*, **2007**, *251*, 2688 and the references therein
42. W.J. Miller and N.L. Abbott, *Langmuir*, **1997**, *13*, 7106
43. G.E. Poirier, E.D. Pylant, *Scince*, **1996**, *272*, 1145
44. X.D. Cui, A. Primak, X. Zarate, J. Tomfohr, O.F. Sankey, A.L. Moore, T.A. Moore, D. Gust., L.A. Nagahara, S.M. Lindsay, *J.Phys.Chem.B*, **2002**, *106*, 8609
45. C. Li, I. Pobelov, T. Wandlowski, A. Bagrets, A. Arnold and F. Evers, *J. Am. Chem. Soc*., **2008**, *130*, 318
46. D.K. James and J.M. Tour, *Chem. Mater*., **2004**, *16*, 4423
47. J. Kröger, N. Néel, L. Limot, *J. Phys*.: *Condens*. Matter., **2008**, *20*, 223001
48. L. Lafferentz, F. Ample, H. Yu, S. Hecht, C. Joachim, L. Grill, *Science*, **2009**, *323*, 1193
49. D. Hirayama, K. Takimiya, Y. Aso, T. Otsubo, T. Hasobe, H. Yamada, H. Imahori, S. Fukuzumi, Y. Sakata, *J. Am. Chem. Soc.*, **2002**, *124*, 532
50. E. Galoppini, W. Guo, W. Zhang, P.G. Hoertz, P. Qu, G.J. Meyer, *J. Am. Chem. Soc.*, **2002**, *124*, 7801
51. B. Long, K. Nikitin, D. Fitzmaurice, *J. Am. Chem. Soc.*, **2003**, *125*, 5152.
52. K. Nikitin, D. Fitzmaurice, *J. Am. Chem. Soc.*, **2005**, *127*, 8067
53. L. Wei, K. Padmaja, W.J. Youngblood, A.B. Lysenko, J.S. Lindsey, D.F. Bocian, *J. Org. Chem*., **2004**, *69*, 1461
54. K. Padmaja, W. J. Youngblood, L. Wei, D. F. Bocian, and J.S. Lindsey, *Inorganic Chemistry*, **2006**, *45*, 5479
55. B.J. Hong, S.J. Oh, T.O. Youn, S.H. Kwon, J.W. Park, *Langmuir*, **2005**, *21*, 4257
56. J. Rochford, D. Chu, A. Hagfeldt, and E. Galoppini, *J. Am. Chem. Soc*., **2007**, *129*, 4655
57. H. Imahori, H. Norieda, H. Yamada, Y. Nishimura, I. Yamazaki, Y. Sakata, and S. Fukuzumi, *J. Am. Chem. Soc*., **2001**, *123*, 100
58. H. Imahori, H. Yamada, Y. Nishimura, I. Yamazaki, Y. Sakata, *J. Phys. Chem. B*, **2000**, *104*, 2099
59. K. Terada, K. Kobayashi and M.-a. Haga, *Dalton Trans*., **2008**, 4846
60. H. Jian, and J.M. Tour, *J. Org. Chem*., **2003**, *68*, 5091
61. X. Xiao, D. Brune, J. He, S. Lindsay, C. B. Gorman, N. Tao, *Chemical Physics*, **2006**, *326*, 138
62. C.B. Gorman, R.L. Carroll, R.R. Fuierer, *Langmuir*, **2001**, *17* , 6923
63. A.V. Tivanski and G.C. Walker, *J. Am. Chem. Soc*., **2005**, *127*, 7647
64. J.A.M. Dinglasan, M. Bailey, J.B. Park and A. Dhirani, *J. Am. Chem. Soc*., **2004**, *126*, 6491
65. R.A. Wassel, G.M. Credo, R.R. Fuierer, D.L. Feldheim and C.B. Gorman, *J. Am. Chem. Soc*., **2004**, *126*, 295

66. V. Arima, E. Fabiano, R.I.R. Blyth, F. Della Sala, F. Matino, J. Thompson, R. Cingolani and R. Rinaldi, *J. Am. Chem. Soc*., **2004**, *126*, 16951
67. F. Matino, V. Arima, G. Maruccio, R.J. Phaneuf, R. Del Sole, G. Mele, G. Vasapollo, R. Cingolani, and R. Rinaldi, *J. Physics: Conference Series*, **2007**, *61*, 795
68. T. Ohshiro, T. Ito, P. Bhlmann, and Y. Umezawa, *Anal. Chem*., **2001**, *73*, 878
69. K. M. Roth, N. Dontha, R. B. Dabke, D. T. Gryko, C. Clausen, J. S.. Lindsey, D. F. Bocian, and W. G. Kuhr, *J. Vac. Sci.Technol. B*., **2000**, *18*, 2359
70. K. M. Roth, J. S. Lindsey, D. F. Bocian, and W. G. Kuhr, *Langmuir*, **2002**, *18*, 4030
71. L. Wei, K. Padmaja, W. J. Youngblood, A.B. Lysenko, J.S. Lindsey, and D.F. Bocian, *J. Org. Chem.*, **2004**, *69*, 1461
72. X. Lu, M. Li, C. Yang, L. Zhang, Y. Li, L.Jiang, H. Li, L. Jiang, C. Liu, and W. Hu, *Langmuir*, **2006**, *22*, 3035
73. C. Li, J. Ly, B. Lei, W. Fan, D. Zhang, J. Han, M. Meyyappan, M. Thompson, and C. Zhou , *J. Phys. Chem. B*, **2004**, *108*, 9646
74. P. Zell, F. Mögele, U. Ziener, and B. Rieger, *Chem. Eur. J.*, **2006**, *12*, 3847 and the references therein
75. P. Zell, F. Mögele, U. Ziener, and B. Rieger , *Chem. Commun*, **2005**, 1294
76. I. Sakata and K. Miyamura, *Chem. Commun*., **2003**, 156 and the references therein
77. M. Nielsen, N.B. Larsen, and K.V. Gothelf, *Langmuir*, **2002**, *18*, 2795
78. T. Albrecht, A. Guckian, J. Ulstrup, and J.G. Vos, *Nano Lett*., **2005**, *5*, 1451
79. T. Albrecht, A. Guckian, A.M. Kuznetsov, J. G. Vos, and J. Ulstrup, *J. Am. Chem. Soc.*, **2006**, *128*, 17132
80. E. Figgemeier, L. Merz, B. A. Hermann, Y. C. Zimmermann, C. E. Housecroft, H.-J. Güntherodt, and E. C. Constable, *J. Phys. Chem. B*, **2003**, *107*, 1157
81. M. Ruben, A. Landa, E. Lörtscher, H. Riel, M Mayor, H. Görls, H.B. Weber, A. Arnold, and F. Evers, *Small*, **2008**, *4*, 2229
82. J. Park, A. N. Pasupathy, J. I. Goldsmith, C. Chang, Y. Yaish, J.R. Petta, M. Rinkoski, J.P. Sethna, H.D. Abruna, P.L. McEuen, D.C. Ralph, *Nature*, **2002**, *417*, 722
83. O. Waldmann, *Phys. Rev. B 71*, **2005**, 094412
84. J.-M. Lehn, M. Ruben, H.S.J. van der Zant, *J. Phys.: Condens. Matter*, **2008**, *20*, 374121
85. M. Ruben, J. Rojo, F.J. Romero-Salguero, L.H. Uppadine, and J.-M. Lehn, *Angew. Chem. Int. Ed.*, **2004**, *43*, 3644
86. A. Semenov, J. P. Spatz, J.-M. Lehn, C. H. Weidl, U. S. Schubert, M. Möller, *Appl. Surf. Sci*., **1999**, *144–145*, 456
87. A. Semenov, J. P. Spatz, M. Möller, J.-M. Lehn, B. Sell, D. Schubert, C. H. Weidl, U. S. Schubert, *Angew. Chem.*, **1999**, *111*, 2701; *Angew. Chem. Int. Ed*., **1999**, *38*, 2547
88. U. Ziener, J.-M. Lehn, A. Mourran, M. Möller, *Chem. Eur. J*., **2002**, *8*, 951
89. M.S. Alam, S. Strömsdörfer, V. Dremov, P. Müller, M. Ruben, and J.-M. Lehn, *Angew. Chem. Int. Ed.*, **2005**, *44*, 7896
90. E.A. Osorio, T. Bjornholm, J-M. Lehn, M. Ruben and H.S.J. van der Zant, *J. Phys.: Condens. Matter*, **2008**, *20*, 374121
91. M. Ruben, J-M Lehn, and P. Müller, *Chem.Soc.Rev*., **2006**, 1056
92. V. Balzani, *Photochem. Photobiol. Sci.*, **2003**, *2*, 459
93. B.A. Hermann, L.J. Scherer, C.E. Housecroft, and E.C. Constable, *Adv. Funct. Mater*., **2006**, *16*, 221

94. D.J. Diaz, G.D. Storrier, S. Bernhard, K. Takada, and H.D. Abruňa, *Langmuir*, **1999**, *15*, 7351
95. L. Merz, J. Hitz, U. Hubler, P. Weyermann, F. Diederich, P. Murer, D. Seebach, I. Widmer, M. Stöhr, H.-J. Güntherodt, B. A. Hermann, *Single Mol.,* **2002**, *3*, 295
96. L.J. Scherer, L. Merz, E.C. Constable, C.E. Housecroft, M. Neuburger, and B. A. Hermann, *J. Am. Chem. Soc.*, **2005**, *127*, 4033;
97. C.J. Fleming, Y.X. Liu, Z.Deng, and G.-y Liu, *J. Phys. Chem. A*, **2009**, *113*, 4168 and the references therein
98. M. Mayor, C. von Hänisch, H.B. Weber, J. Reichert, and D. Beckmann, *Angew. Chem. Int. Ed.,* **2002**, *41*, 1183
99. A.M. Ako, H. Maid, S. Sperner, S.H.H. Zaidi, R.W. Saalfrank, M.S. Alam, P. Müller, F.W. Heinemann, *Supramolecular Chemistry*, **2005**, *17*, 315
100. P. Wahl, L. Diekhöner, G. Wittich, L. Vitali, M. A. Schneider, and K. Kern, *Physical Review Letters*, **2005**, *95*, 166601
101. J. Hu and D. L. Mattern, *J. Org. Chem*., **2000**, *65*, 2277
102. D.F. Cook, D. Cummins, and E.D. McKenzie, *J.C.S. Dalton*, **1976**, 1369
103. M. Figuet, M.T. Averbuch-Pouchout, A. du Moulinet d'Hardemare and O. Jarjayes, *Eur. J. Inorg. Chem.*, **2001**, 2089
104. P. Kremminger, and W. Weissensteiner, *Monatshefte für Chemie*, **1991**, *122*, 571
105. D.J. Berg, S.J. Rettig, and C. Onig, *J. Am. Chem. Soc.*, **1991**, *113*, 2528
106. A. Smith, S.J. Rettig, and C. Orvig, *Inorg. Chem*., **1988**, *27*, 3929
107. S. Liu, S.J. Rettig, and C.Onig, *Inorganic Chemistry*, *31*, **1992**, 5400
108. S. Mizukami, H. Houjou, M. Kanesato and K. Hiratani, *Chem. Eur. J*., **2003**, *9*, 1521
109. R.M. Kirchner, C. Mealli, M. Bailey, N. Howe, L.P. Torre, L.J. Wilson, L.C. Andrews, N.J. Rose, and E.C. Lingafelter, *Coordin.Chem. Rev*., **1987**, *77*, 89
110. L.J. Wilson and N.J. Rose, *J. Am. Chem. Soc*., **1968**, *90*, 6041
111. E.C. Lingafelter, L.C. Andrews, R.M. Kirchner, N.J. Rose and L.J. Wilson, *Coord. Chem. Rev*., **1972**, *8*, 55
112. C. Mealli and E.C. Lingafelter, *J. Chem. Soc. Chem. Commun*., **1970**, 885
113. M.A. Hoselton, L.J. Wilson and R.S. Drago, *J. Am. Chem. Soc*., **1975**, *97*, 1722
114. L.J. Wilson, D. Georges and M.A. Hoselton, *Inorg. Chem*., **1975**, *14*, 2968
115. M.G.B. Drew, C.J. Harding, G.G. Morgan, V. McKee and J. Nelson, *J. Chem. Soc., Chem. Commun.*, **1995**, 1035
116. P. Gutlich and A. Hauser, *Coord. Chem. Rev*., **1990**, *97*, 1
117. S.K. Chandra, P. Chakraborty and A. Chakravorty, *J. Chem. Soc. Dalton Trans*., **1993**, 863
118. N. Gündüz, T. Gündüz, M.B. Hursthouse, H.G. Parkes, L.S. Shaw, R.A. Shaw, M. Tüzün, *J. Chem. Soc. Perkin Trans. 2*, **1985**, 899
119. S. Liu, L. Gelmini, S.T. Rettig, R.C. Thompson, C. Orvig , *J. Am. Chem. Soc*., **1992**, *114* , 6081
120. K. Ramesh, D. Bhuniya and R. Mukherjee, *J. Chem. Soc. Dalton Trans.*, **1991**, 2917
121. Y. Elerman, M. Kabak, I. Svoboda, H. Fuess and O. Atakal, *J. Chem. Crystallogr*., **1995**, *25*, 227
122. N.W. Alcock, D.F. Cook, E.D. McKenzie and J.M. Worthinton, *Inorganica Chimica Acta*, **1980**, *38*, 107
123. N.A. Bailey, D.F. Cook, D. Cummins and E.D. McKenzie, *Inorg. Nucl. Chem. Letters*, **1975**, *11*, 51
124. N.S. Hosmane, L. Jia, H. Zhang, J. W. Baush, G. K. Suryaprakash. R. E.. Williams, T. P. Onak, *Inorg. Chem*., **1991**, *30*, 3795

125. K. Boubekeur, A. Deroche, F. Lambert, I. Morgenstern-Badarau, *Acta Cryst*., **1995**, 2244
126. M. Qian, S.H. Gou, L. He, Y.M. Zhou, C.M. Duan, *Acta cryst*, **1999**, 742
127. A.J. Conti, C. Liang Xie, D.N. Hendrickson, *J. Am. Chem. Soc*., **1989**, *111*, 1171
128. W. H. Batschelet, and N. J. Rose, *Inorg. Chem*., **1983**, *22*, 2078
129. E.A. Boudreaux, L. N. Mulay, "*Theory and Applications of Molecular Paramagnetism*", John Wiley & Sons, New York, **1976**
130. V.V. Pavlishchuk, A.W. Addison, *Inorg. Chim Acta*, **2000**, *298*, 97
131. R.R. Gagné, C.A. Koval, G.C. Lisensky, *Inorg. Chem*., **1980**, 2855
132. M.A. Hoselton, L.J. Wilson, and R.S. Drago, *J. Am. Chem. Soc*., **1975**, *97*, 1722
133. V. Balzani, A. Juris, M. Venturi, S. Campagna, and S. Serroni, *Chem. Rev*., **1996**, *96*, 759
134. A. Juris, V. Balzani, F. Barigelletti, S. Campagna, P. Belser, A. von Zelewsky, *Coordin.Chem. Rev.*, **1988**, *84*, 85
135. K. Ohkubo, T. Hamada and H. Ishida, *J. Chem. Soc. Chem. Commun*., **1993**, 1423
136. T. J. Meyer, *Nature*, **2008**, *451*, 778
137. A. Hagfeldt, and M. Grätzel, *Acc. Chem. Res*., **2000**, *33*, 269
138. M. Chen, K. P. Ghiggino, S. H. Thang and G. J. Wilson, *Angew. Chem. Int. Ed*., **2005**, *44*, 4368 and the references therein
139. M.K. Nazeeruddin, S.M. Zakeeruddin, J.J. Lagref, P. Liska, P. Comte, C. Barolo, G. Viscardi, K. Schenk, and M. Graetzel, *Coord. Chem. Rev.*, **2004**, *248*, 1317
140. M. K. Nazeeruddin, C. Klein, P. Liska and M. Graetzel, *Coord. Chem. Rev*., **2005**, *249*, 1460
141. S. Serroni, S. Campagna, F. Puntoriero, C. Di Pietro, N. D. McClenaghan and F. Loiseau, *Chem. Soc. Rev.*, **2001**, *30*, 367
142. C. A. Bignozzi, R. Argazzi, F. Scandola, J. R. Schoonover and G. J. Meyer, *Sol. Energy Mater. Sol. Cells*, **1995**, *38*, 187
143. T. Bessho, E. C. Constable, M. Graetzel, A. Hernandez Redondo, C. E. Housecroft, W. Kylberg, Md. K. Nazeeruddin, M. Neuburger and S. Schaffner, *Chem. Commun*, **2008**, 3717
144. N. Alonse-Vante, J.-F. Nierengarten, and J.-P. Sauvage, *J. Chem. Soc. Dalton Trans*., **1996**, 1649 and the references therein
145. A. Petitjean, F., Puntoriero, S., Campagna, A.Juris, and J.-M. Lehn, *Eur. J. Inorg. Chem*., **2006**, *19*, 3878
146. V. Balzani, G. Bergamini, F. Marchioni, and P. Ceroni, *Coord. Chem. Rev*., **2006**, *250*, 1254
147. J.D. Badjic, C.M. Ronconi, J.F. Stoddart, V. Balzani, S. Silvi, and A. Credi, *J. Am. Chem. Soc*., **2006**, *128*, 1489
148. V. Balzani, A. Credi, S. Silvi, and M. Venturi, *Chem. Soc. Rev*., **2006**, *35*, 1135;
149. V. Balzani, M. Clemente-León, A. Credi, B. Ferrer, M.Venturi, A.H. Flood, and J.F. Stoddart, *Proc. Natl. Acad. Sci. U.S.A.*, **2006**, *103*, 1178
150. E.A.P. Armstrong, R.T. Brown, M.S. Sekwale, N.C. Fletcher, X.-Q. Gong, P. Hu, *Inorg. Chem*., **2004**, *43*, 1714
151. N.C. Fletcher, M. Nieuwenhuyzen, S. Rainey, *J. Chem. Soc. Dalton Trans*., **2001**, 2641
152. G. Predieri, C. Vignali, G. Denti, S. Seroni, *Inorg. Chim Acta*, **1993**, *205*, 145
153. G. Orellana, C.A. Ibarra, and J. Santorot, *Inorganic Chemistry*, **1988**, *27*, 1025
154. R.T. Brown, N.C. Fletcher, M. Nieuwenhuyzen, T.E. Keyes, *Inorg. Chim. Acta*, **2005**, *358*, 1079
155. N.C. Fletcher, R.T. Brown and A.P. Doherty, *Inorg. Chem*., **2006**, *45*, 6132

156. N.C. Fletcher, M. Niewenhuyzen, R. Prabarahan and A. Wilson, *Chem. Commun*., **2002**, 1188
157. N.C. Fletcher, C.Martin and H.J. Abraham, *New J. Chem*., **2007**, *31*, 1407
158. A. Grabulosa, M. Beley and P.C. Gros, *Eur. J. Inorg. Chem*., **2008**, 1747
159. N.C.A. Baker, N. McGaughey, N.C. Fletcher, A.V. Chernikov, P.N. Horton, M.B. Hursthouse, *Dalton Transactions*, **2009**, 965
160. V. Grosshenny, F.M. Romero, and R. Ziessel, *J. Org. Chem*., **1997**, *62*, 1491
161. D.T. Gryko, C. Clausen, K.M. Roth, N. Dontha, D.F. Bocian, W.G. Kuhr, and J.S. Lindsey, *J. Org. Chem.,* **2000**, *65*, 7345
162. E. Dulière, M. Devillers, J. Marchand-Brynaert, *Organometallics*, **2003**, *22*, 805
163. I.P. Evans, A. Spencer, G. Wilkinson , *J. Chem. Soc. Dalton Trans*, **1973**, 204
164. A.K. Flatt, S.M. Dirk, J.C. Henderson, D.E. Shen, J. Su, M.A. Reed, and J.M. Tour, *Tetrahedron*, **2003**, *59*, 8555
165. A.A. Schilt and R.C. Taylor, *J. Inorg. Nucl. Chem*., **1959**, *9*, 211
166. F.E. Lytle and D.M. Hercules, *J. Am. Chem. Soc*, **1969**, 253
167. P.A. Anderson, G.B. Deacon, K.H. Haarmann, F.R. Keene, T.J. Meyer, D.A. Reitsma, B.W. Skelton, G.F. Strouse, N.C. Thomas, J.A. Treadway, and A.H. White, *Inorg. Chem*., **1995**, *24*, 6145
168. N.C. Fletcher, F.R. Keene, H. Viebrock, and A. von Zelewsky, *Inorg. Chem*., **1997**, *36*, 1113
169. J. Otsuki, H. Kameda, S. Tomihira, H. Sakaguchi and T. Takido, *Chemistry Letters*, **2002**, *31*, 610
170. J.-M. Lehn et al., *Proc. Natl. Acad. Sci. USA*, **1987**, *84*, 2565
171. M. Hannon, L.J. Childs, *Supramolecular Chemistry*, **2004**, *16*, 7
172. E.C. Constable, *Tetrahedron*, **1992**, *48*, 10013
173. R. Ziessel, *Coord. Chem. Rev*., **2001**, *216-217*, 195
174. M. Albrecht, *Chem. Rev*., **2001**, *101*, 3457
175. C. Piguet, M. Borkovec, J. Hamacek, K. Zeckert, *Coord. Chem. Rev*., **2005**, *249*, 705
176. C. Piguet, G. Bernardinelli, G. Hopfgartner, *Chem. Rev*., **1997**, *97*, 2005
177. E.C. Constable, *Angew. Chem. Int. Ed. Engl*., **1991**, *30*, 1450
178. A. von Zelewky, *Stereochemistry of Coordination Compounds*, John Wiley & Sons, **1996**
179. A. F. Williams, C. Piguet, G. Bernardinelli, *Angew. Chem. Int. Ed. Engl.*, **1991**, *30*, 1490
180. A. F. Williams, C. Piguet, G. Bernardinelli, *Angew. Chem*., **1991**, *103*, 1530
181. D.L. Caulder and K.N. Raymond, *Dalton Trans*, **1999**, 1185
182. M.-T. Youinou, R. Ziessel, J.-M. Lehn, *Inorg. Chem*., **1991**, *30*, 2144
183. R. Kramer, J.-M. Lehn, A. De Cian, J. Fischer, *Angew. Chem. Int. Ed. Engl*., **1993**, *32*, 704
184. M.J. Hannon, C.L. Painting, N.W. Alcock, *Chem. Commun*., **1999**, 2023
185. W.-H. Sun, T. Zhang, L. Wang, Y. Chen, R. Froehlich, *J. Organomet. Chem*., **2004**, *689*, 43
186. L.J. Childs, M. Pascu, A.J. Clarke, N.W. Alcock, M.J. Hannon, *Chem.-Eur. J*., **2004**, *10*, 4291
187. A. Lavalette, F. Tuna, G. Clarkson, N.W. Alcock, M.J. Hannon, *Chem. Commun*. **2003**, 2666
188. M. Pascu, G.J. Clarkson, B.M. Kariuki and M.J. Hannon, *Dalton Trans,* **2006**, 2635
189. J. Keegan, P.E. Kruger, M. Nieuwenhuyzen, N. Martin, *Cryst.Growth Des*., **2002**, *2*, 329
190. H. Cheng, D. Chun-ying, F. Chen-jie, M. Qing-jin, *Dalton Trans*. **2000**, 2419
191. M.J. Hannon,C.L. Painting, A. Jackson, J. Hamblin, W. Errington, *Chem. Commun*., **1997**, 1807
192. M.J. Hannon, M. Moreno, M.J. Prieto, E. Moldrheim, E. Sletten, I. Meistermann, C.J. Isaac, K.J. Sanders, A. Rodger, *Angew. Chem*., **2001**, *113*, 903; *Angew. Chem. Int. Ed*., **2001**, *40*, 879

193. N. Yoshida, K. Ichikawa, M. Shiro, *J. Chem. Soc. Perkin Trans. 2*, **2000**, 17
194. N. Yoshida, K. Ichikawa*, Chem. Commun*., **1997**, 1091
195. I. Meistermann, V. Moreno, M.J. Prieto, E. Moldrheim, E. Sletten, S. Khalid, P.M. Rodger, J.C. Peberdy, C.J. Isaac, A. Rodger, M.J. Hannon, *Proc. Natl. Acad. Sci. U.S.A*., **2002**, *99*, 5069
196. G. Dong, P. Ke-liang, D. Chun-ying, H. Cheng, M. Qing-jin, *Inorg. Chem*., **2002**, *41*, 5978
197. G.I. Pascu, A.C.G. Hotze, C. Sanchez-Cano, B.M. Kariuki, and M.J. Hannon, *Angew. Chem. Int. Ed*., **2007**, *46*, 4374
198. F. Tuna, M.R. Lees, Clarkson, G.; and M.J. Hannon, *Chem. Eur.J*., **2004**, 5737
199. A. Oleksi, A.G. Blanco, R. Boer, I. Usón, J. Aymamí, A. Rodger, M.J. Hannon, M. Coll, *Angew. Chem. Int.Ed.*, **2006**, *40*, 1227
200. A. Oleksi, A.G. Blanco, R. Boer, I. Usón, J. Aymamí, A. Rodger, M.J. Hannon, M. Coll, *Angew. Chem*., **2006**, *118*, 1249
201. C. Uerpmann, J. Malina, M. Pascu, G. J. Clarkson, V. Moreno, A. Rodger, A. Grandas, M. J. Hannon, *Chem. Eur. J.*, **2005**, *11*, 1750
202. J. Malina, M.J. Hannon, V. Brabec, *Chem. Eur. J*, **2007**, *13*, 3871 and the references therein.
203. M.J. Hannon, A. Rodger, N.H. Mann, PCT/GP **2004**/004227
204. M.J. Hannon, *Pure and Applied Chemistry*, **2007**, *79*, 2243
205. J. Müller and B. Lippert, *Angew. Chem. Int. Ed*., **2006**, *45*, 2503
206. N. Fatin-Rouge, S. Blanc, A. Pfeil, A. Rigault, A. M. Albrecht-Gary, J.-M. Lehn, *Helv. Chim. Acta* **2001**, *84*, 1694
207. M. Albrecht, *Chem. Rev*. **2001**, *101*, 3457
208. S.-Y. Lin, I-W.P. Chen, C. Chen, M.-H. Hsieh, C.-Y. Yeh, T.-W. Lin, Y.-H. Chen, S.-M. Peng, *J. Phys. Chem. B,* **2004**, *108*, 959 and the references therein
209. P. Cai, M.-x. Li, C.-Y. Duan, F. Lu, D. Guo and Q.-J. Meng, *New J. Chem*., **2005**, *29*, 1011
210. J.M.C.A. Kerckhoffs, J.C. Peberdy, I.Meistermann, L.J. Childs, C.J. Isaac, C.R. Pearmund, V. Reudegger, S. Khalid, N.W. Alcock, M.J. Hannon, A. Rodger, *Dalton Trans*., **2007**, 734
211. D. Gust and K. Mislow, *J. Am Chem. Soc*, **1973**, *95*, 1535
212. W. Weissensteiner, J. Scharf, and K. Schlögl, *J. Org. Chem*., **1987**, *52*, 1210
213. W.S. Trahanovsky, D.J. Kowalski, and M.J. Avery, *J. Am. Chem. Soc*., **1974**, *96*, 1502
214. W. Weissensteiner, J. Scharf, and K. Schlögl, *J. Org. Chem*., **1987**, *52*, 1210
215. L.M. Jackman and F.A. Cotton, *Dynamic Nuclear Magnetic Resonance* Spectroscopy, Academic Press, **1975**
216. F.P. Gasparro, N.H. Kolodny, *J. Chem. Education*, 258
217. H. Friebolin, *Basic One- and Two – Dimensional NMR Spectroscopy*, Wiley-VCH, 4th Ed., **2005**
218. H.S. Gutowsky and C.H. Holm, *J. Chem. Phys*., **1956**, *25*, 1228
219. R. Noyori, H. Takaya, *Acc. Chem. Res*., **1990**, *23*, 345
220. V. Humblot, R. Raval, *Applied Surface Science* , **2005**, *241*, 150
221. J. Crassous, *Chem. Soc. Rev*., **2009**, *38*, 830
222. Sai-Long Xu, Shi-Zhao Kang, Jun Lu, Chen Wang, Li-Jun Wan, and Chun-Li Bai, *Surface Science*, **2003**, *527*, 171
223. H. Junxiang, H. Sato, Y. Umemura, and A.Yamagishi, *J. Phys. Chem. B*, **2005**, *109*, 4679

224. M. Lingenfelder, G. Tomba, G. Costantini, L. Colombi Ciacchi, A. De Vita, K. Kern, *Angew. Chem. Int. Ed.*, **2007**, *46*, 4492
225. Y. Zhu, N. Gergel, N. Majumdar, L.R. Harriott, J.C. Bean, and L. Pu, *Org. Lett*., **2006**, *8*, 355
226. W.S. Knowles et al, *Acc. Chem. Res*., **1993**, *16*, 106
227. T. Katsuki and K.B. Sharpless, *J. Am. Chem. Soc.*, **1980**, *102*, 5974
228. A. Miyashita, A. Yasuda, H. Takaya, K. Toriumi, T. Ito, T. Souchi, R. Noyori, *J. Am. Chem. Soc*., **1980**, *102*, 7932
229. K. Toriumi, T. Ito, H. Takaya, T. Souchi, R. Noyori, *Acta Crystallogr. B*, **1982**, *38*, 807
230. C.M. Che, J.S. Huang, *Coordination Chemistry Reviews*, **2003**, *242*, 97
231. K. Bernando, S. Leppard, A. Robert, G. Commenges, F. Dahan and B. Meunier, *Inorg. Chem*., **1996**, *35*, 387
232. A.V. Wiznycia, J. Desper and C.J. Levy, *Chem. Commun*., **2005**, 4693
233. A.V. Wiznycia, J. Desper and C.J. Levy, *Dalton Trans*., **2007**, 1520
234. S. Di Bella, N. Leonardi, G. Consiglio, S. Sortino, I. Fragalà, *Eur. J. Inorg. Chem*., **2004**, 4561
235. A. Voiturez, M. Mellah, E. Schulz, *Synthetic Metals*, **2006**, *156*, 166
236. K. Mullen, G.Wegner, *Electronic Materials: The Oligomer Approach*, Wiley-VCH, New York, **1998**
237. H. E. Katz, A. Dodabalapur, L. Torsi, D. Elder, *Chem. Mater*., **1995**, *7*, 2238
238. G. Horowitz, *Adv. Mater*., **1998**, *10*, 365
239. F. Garnier, G. Horowitz, X. Z. Peng, D. Fichou, *Adv. Mater*., **1990**, *2*, 592
240. S.V. Elshocht, T. Verbiest, M. Kauranen, L.Ma, H. Cheng, K.Y. Musick, L.Pu, A. Persoons, *Chem. Phys. Lett*., **1999**, *309*, 315.
241. A. Ulmann, *An introduction to Ultrathin Organic Thin Films: from Langmuir-Blodgett to Self-Assembly*, Academic Press, Inc., Boston, **1991**.
242. C.L. Bird and A.T. Kuhn., *Chemistry Society Review*, **1981**, 1049
243. Z. Li, I. Pobelov, B. Han, T. Wandlowski, A. Błaszczyk, M. Mayor, *Nanotechnology*, **2007**, *18*, 044018
244. B. Han, Z. Li, T. Wandlowski, A. Błaszczyk, M. Mayor, *J. Phys. Chem. C*, **2007**, *111*, 13855
245. W. Haiss, H. van Zalinge, S. J. Higgins, D. Bethell, H. Hörbenreich,. D. J. Schiffrin, R. J. Nichlos, *J. Am. Chem. Soc*., **2003**, *125*, 15294
246. N.-S. Lee, H.-K. Shin and Y.-S. Kwon, *International J. of Nanoscience*, **2006**, *5*, 907
247. J. March, *Advanced organic chemistry: reactions, mechanism, and structure*, John Wiley & Sons, 4th Ed., **1992**
248. J. Pernak and J. Feder-Kubis, *Tetrahedron: Asymmetrs*, **2006**, *17*, 1728
249. T.W. Green, P.G.M. Wuts, *Protective Groups* in Organic Synthesis, Wiley, New York, 3th Ed., **1999** and the references therein
250. J.W. Ralls, R.M. Dobson, B. Reigel, *J. Am. Chem. Soc*., **1949**, *71*, 3320
251. P.D. Sattsangi, *J. Org. Chem*., **1968**, *33*, 1337
252. R.P. Hatch, J. Shringarpure and S.M. Weinreb, *J. Org. Chem*., **1978**, *43*, 4172
253. L.F. Fieser, *J. Am. Chem. Soc*., **1954**, *76*, 1945
254. D. A. Evans, K. G. Grimm, L. K. Truesdale, *J. Am. Chem. Soc*., **1975**, 97, 3229
255. B.S. Ong, T.H. Chan, *Synthetic Commun*., **1977**, *7*, 283
256. W.C. Chrisophel, and L.L., Miller, *J. Org. Chem*., **1984**, *49*, 5198
257. N. Rehnberg, and G. Magnusson, *J. Org. Chem*., **1990**, *55*, 434

258. C. Djerassi, M. Gorman, *J. Am. Chem. Soc*., **1953**, *75*, 3704
259. M.H. Ali, M. Goretti Gomes, *Synthesis*, **2005**, 1326
260. H. Miyake, Y. Nakao, and M. Sasaki, *Chemistry Letters*, **2007**, *36*, 104
261. J.P. Chupp, and J.M. Molyneaux, *J. Heterocyclic Chem*., **1989**, 645
262. V. Kumar, S. Dev, *Tetrahedron Lett*., **1983**, *24*, 1289
263. B.S. Ong, M. Ontario, *Tetrahedron Letters*, **1980**, *21*, 4225
264. R. Varala, S. Nuvula, and S.R. Adapa, *Bull. Korean Chem. Soc*. **2006**, *27*, 1081
265. B. Das, R. Ramu, M. R. Reddy, G. Mahender, *Synthesis*, **2005**, 250
266. S. Goswami, A.C. Maity, *Tetrahedron Letters*, **2008**, *49*, 3092
267. Y. Kamitori, M. Hojo, R. Masuda, T. Kimura, T. Yoshida, *J. Org. Chem*,. **1986**, *51*, 1427
268. G.R. Newkome and H.W. Lee, *J. Am. Chem. Soc*., **1983**, *105*, 5956
269. T.J. Brown, R.F. Chapman, D.C. Cook, T.W. Hart, I.M. McLay, R. Jordan, J.S. Mason, M.N. Palfreyman, R.J. Walsh, M.T. Withnall, *J. Med. Chemistry*, **1992**, *35*, 3613
270. J.C. Aloup, J. Bouchaudon, D. Farge, C. James, J. Deregnaucourt and M. Hardy-Houis, *J. Med. Chemistry*, **1987**, *30*, 24
271. Y. Haramoto, Y. Akiyama, R. Segawa, M. Nanasawa, A.B. Holmes, S. Ujiie, *Liquid Crystals*, **1999**, *26*, 1425
272. A. Barco, S. Benetti, G.P. Pollini, and R. Taddia, *Synthesis*, **1974**, 877
273. P. A. van der Meulen, and H.A. Heller, *J.Am.Chem.Soc*, **1932**, *54*, 4404
274. I.H. Hillier, M.A. Vincent, J.A. Connor, M.F. Guest, A.A. MacDowell and W. von Niessen, *J. Chem. Soc., Faraday Trans. 2*, **1988**, *84*, 409
275. T. Taguchi, M.Nishi, K. Watanabe and T. Mukaiyama, *Chemistry Letters*, **1973**, 1307
276. V. Mamane, E. Aubert, Y. Fort, *J. Org. Chem.*, **2007**, *72*, 7294
277. S. Bernhardt, M. Baumgarten, M. Wagner and K. Mülen, *J. Am. Chem. Soc*., **2005**, *127*, 12392
278. J. Pernak, J. Feder-Kubis, *Tetrahedron: Asymmetry* **2006**, *17*, 1728
279. C.E. Housecroft and A.G. Sharpe, *Inorganic Chemistry*, Prentice-Hall, 3rd Ed., **2008**
280. E. Pretsch, P. Bühlmann, C. Affolter, M. Badertscher, *Spectroskopische Daten zur Strukturaufklärung organischer Verbindungen*, Springer, Germany, **2001**
281. D.W.A. Sharp et al, *J. Inorg. Nucl. Chem*., **1961**, *18*, 79
282. H. Fuhrer and Hs.H. Günthard, *Helvetica Chimica Acta*, **1962**, *242*, 2036
283. H.G.O. Becker, W. Berger, G. Domschke, E. Fanghänel, J. Faust, M. Fischer, F. Gentz, K. Gewald, R. Gluch, W. D. Habicher, R. Mayer P. Metz, K. Müller, D. Pavel, H. Schmidt, K. Schollberg, K. Schwetlick, E. Seiler, G. Zeppenfeld, *Organikum*, Wiley-VCH, Weinheim, **2001**
284. W.L.F. Armarego, C.L.L. Chai, *Purification of laboratory chemicals*, Elsevier Butterworth Heinemainn, 5th Ed., **2003**
285. F.M. Romero and R. Ziessel, *Tetrahedron Letters*, **1995**, *36*, 6471
286. J.J. Song, N.K.Yee, Z. Tan, J. Xu, S.R. Kapadia, C.H. Senanayake, *Org. Letters*, **2004**, *6*, 4905
287. G.H. Clever, K. Polborn, and T. Carell, *Angew. Chem. Int. Ed*., **2005**, *44*, 7204
288. H.E. Gottlieb, V. Kotlyar, and A. Nudelman, *J. Org. Chem*. **1997**, *62*, 7512
289. W. Danchura, T. Schaefer, J.B. Rowbotham and D.J Wood, *Can. J. Chem*., **1974**, 52

Annex 1.

Spectral data

2. Tripodal metal complexes

2.1 Tripodal *trensal* and *trenpy* Schiff base complexes

2.1.2.1. M(III)-*trensal* complexes

M(III)-*trensal* complexes with thiomethyl end units

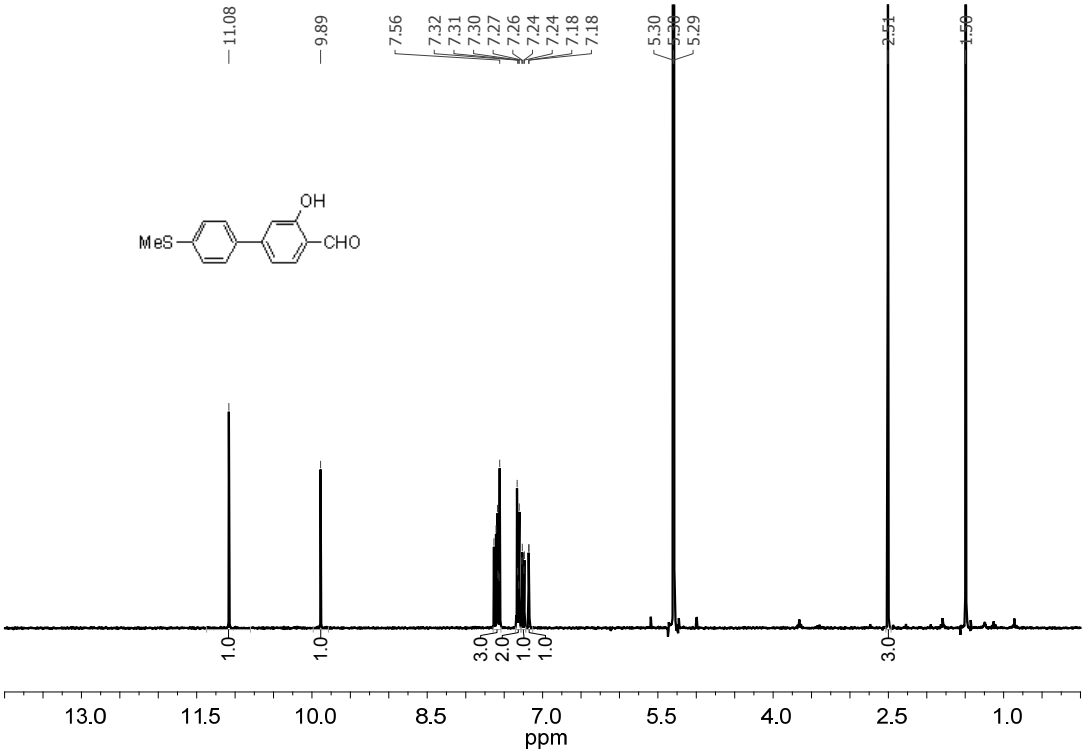

Figure A. 1. ^{1}H-NMR spectrum in CD_2Cl_2 of the compound **1**

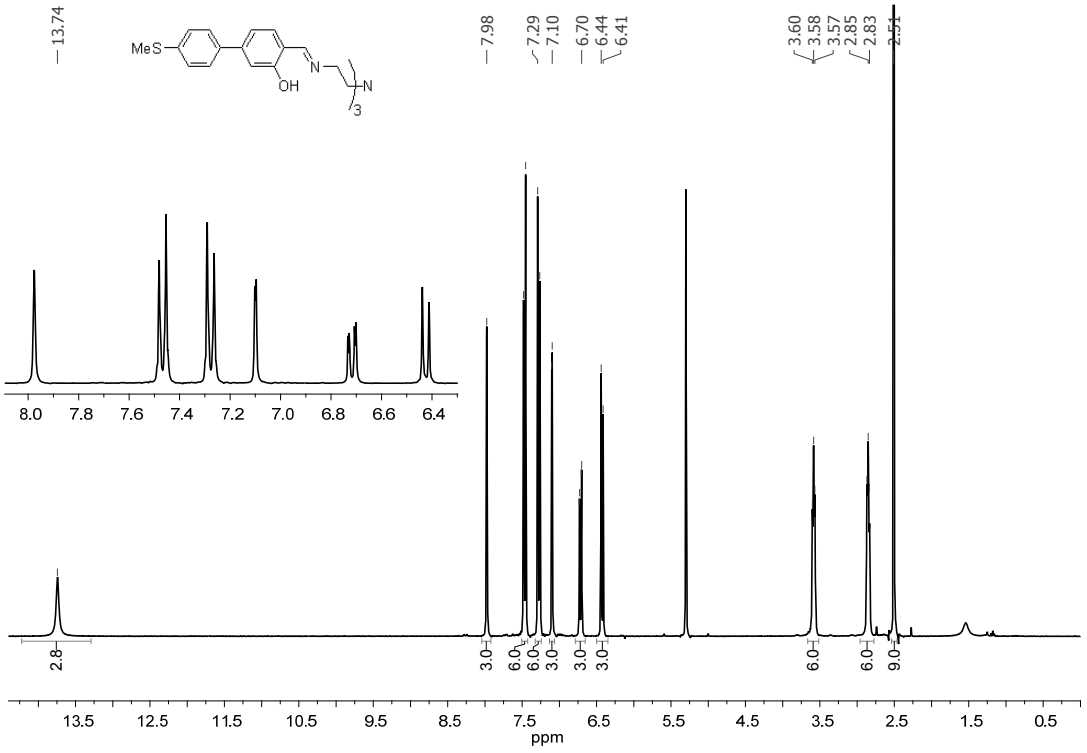

Figure A. 2. ^{1}H-NMR spectrum in CD_2Cl_2 of the compound **2**

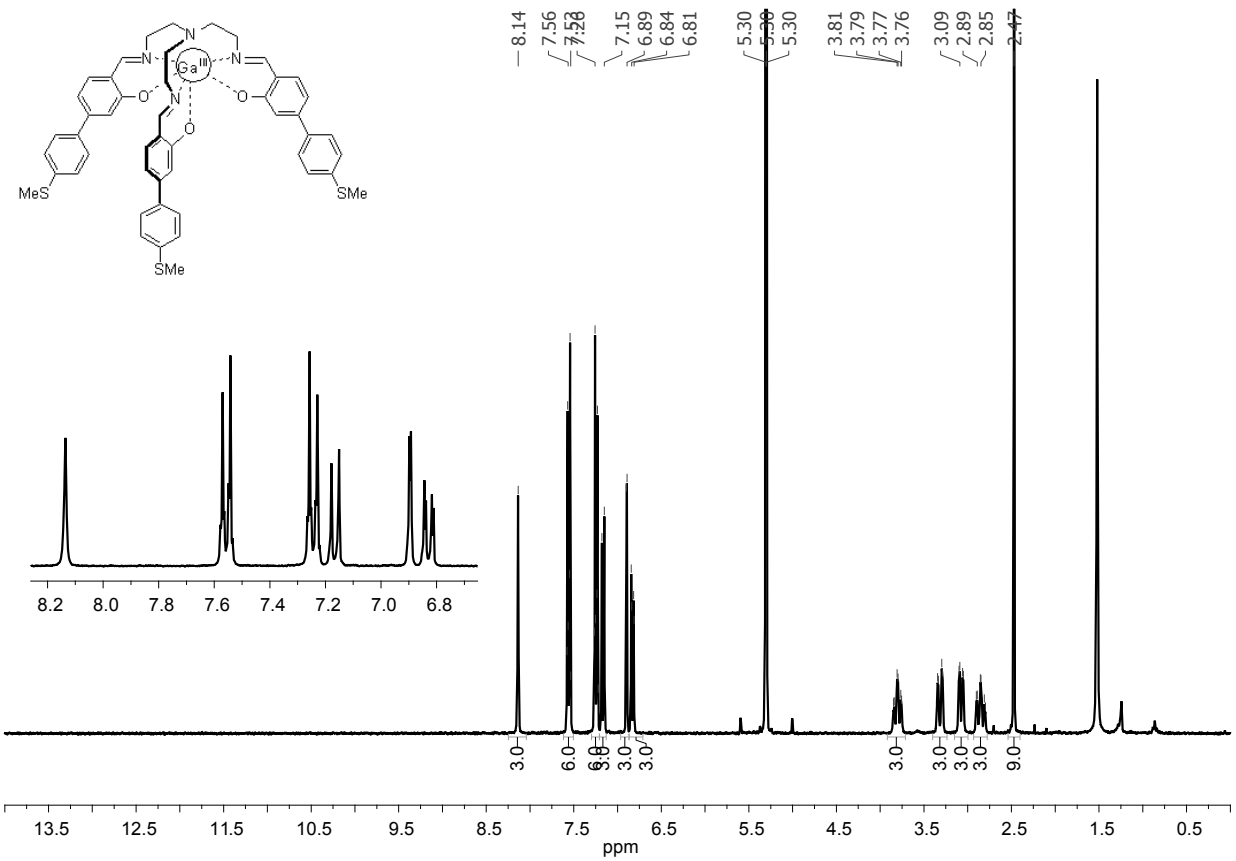

Figure A. 3. ^{1}H-NMR spectrum in CD_2Cl_2 of the Ga(III)-*trensal* complex **3**

M(III)-*trensal* complexes with pyridine end units

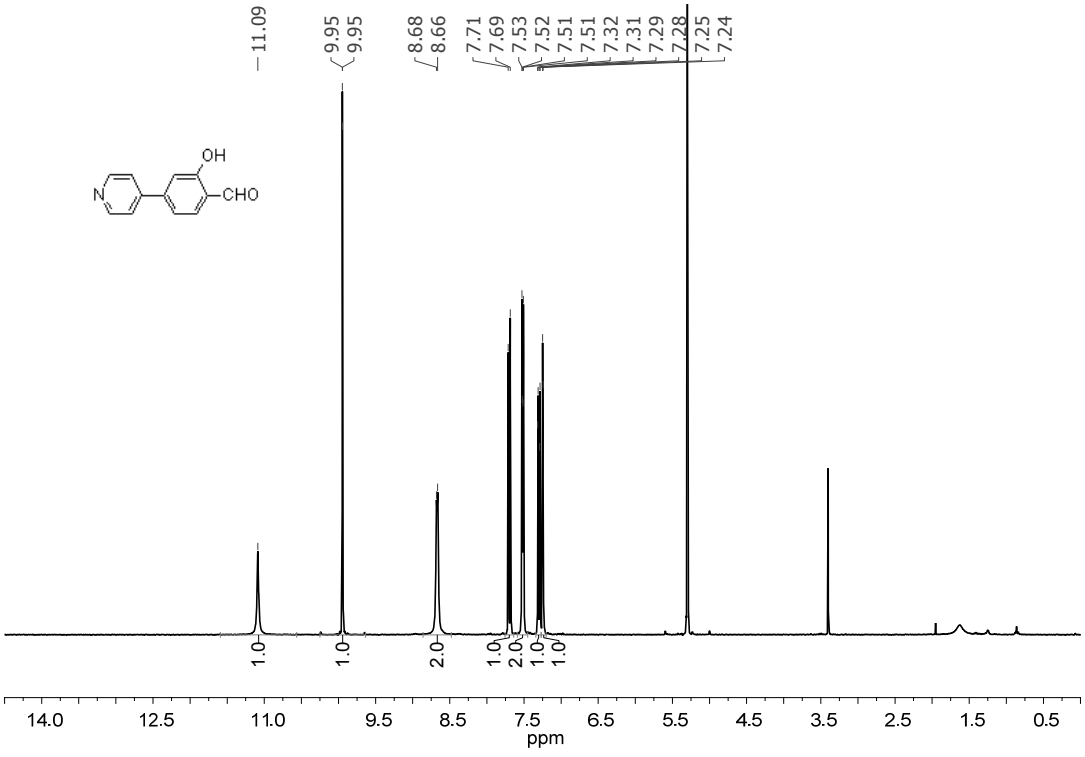

Figure A. 4. ^{1}H-NMR spectrum in CD_2Cl_2 of the compound **6**

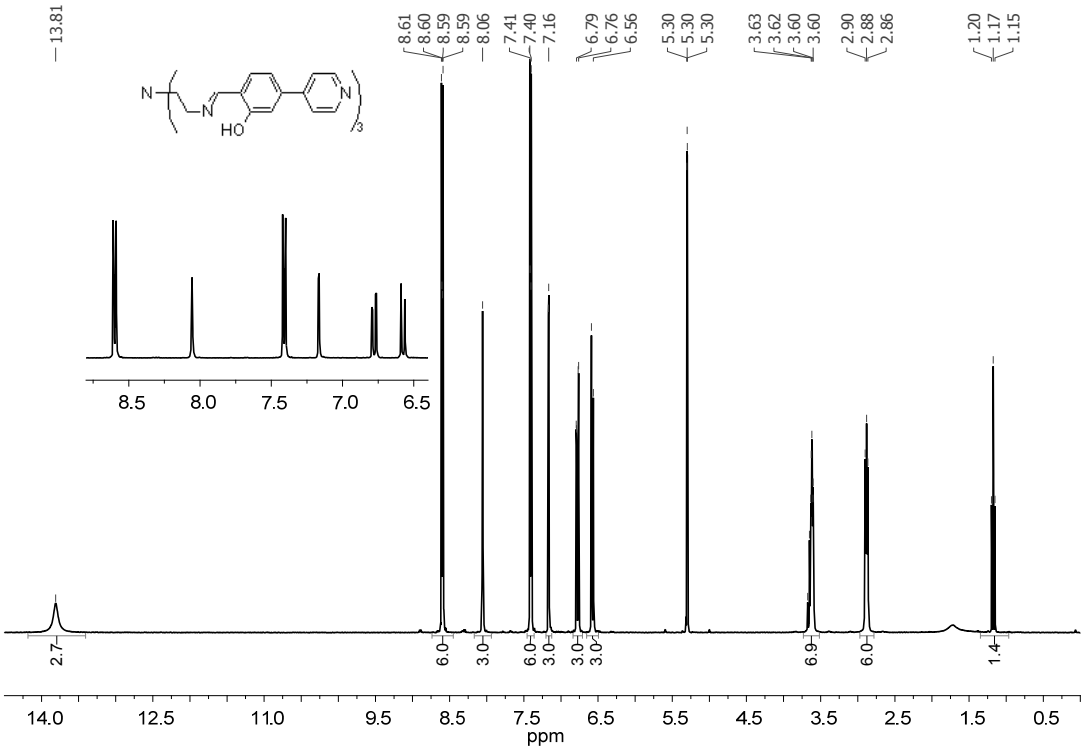

Figure A. 5. ^{1}H-NMR spectrum in CD_2Cl_2 of the compound **7**

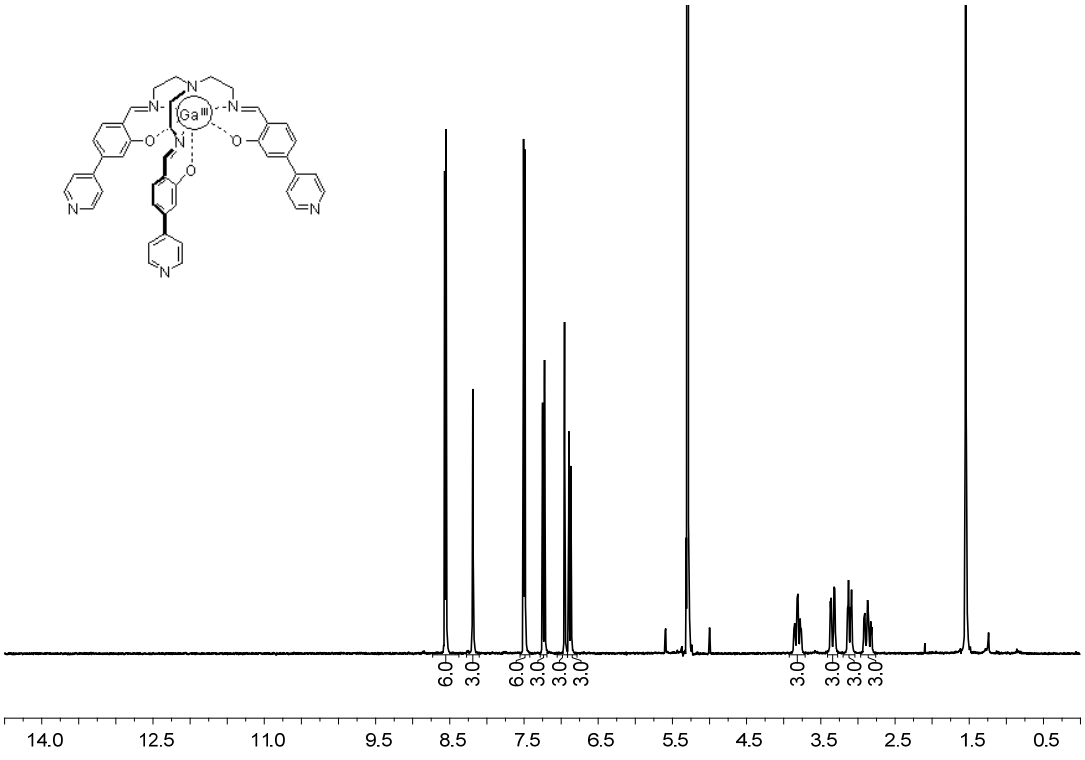

Figure A. 6. ^{1}H-NMR spectrum in CD_2Cl_2 of the Ga(III)-*trensal* complex **8**

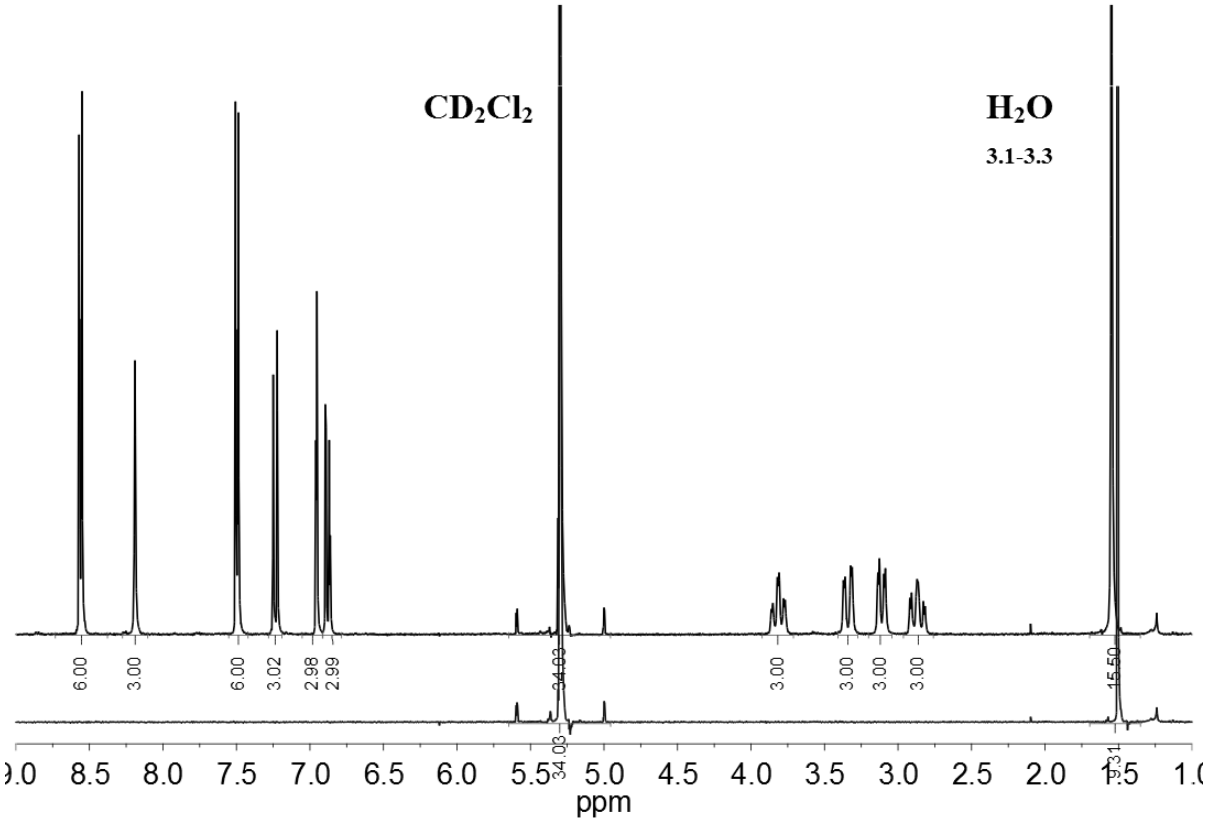

Figure A. 7. ^{1}H-NMR spectrum in CD_2Cl_2 of the Ga(III)-*trensal* complex **8** compared to the ^{1}H-NMR spectrum of pure CD_2Cl_2 before measuring the Ga(III)-*trensal* complex shows almost 3.3 water molecules per complex molecule

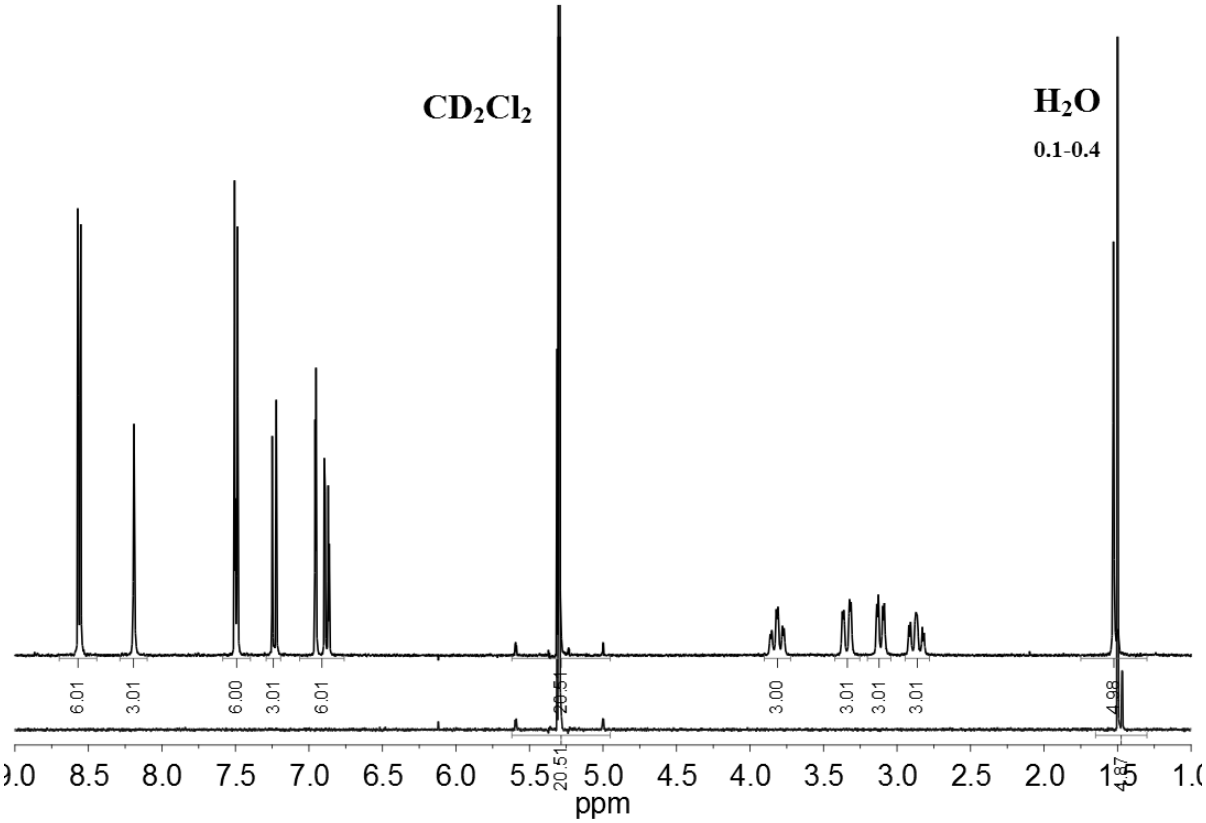

Figure A. 8. ^{1}H-NMR spectrum in CD_2Cl_2 of the Ga(III)-*trensal* complex **8** after high vacuum drying (100°C) compared to the ^{1}H-NMR spectrum of pure CD_2Cl_2 before measuring the Ga(III)-*trensal* complex shows almost 0.4 water molecules per complex molecule

2.1.2.2. M(II)-*trenpy* complexes

M(II)-*trenpy* complexes with thiomethyl end units

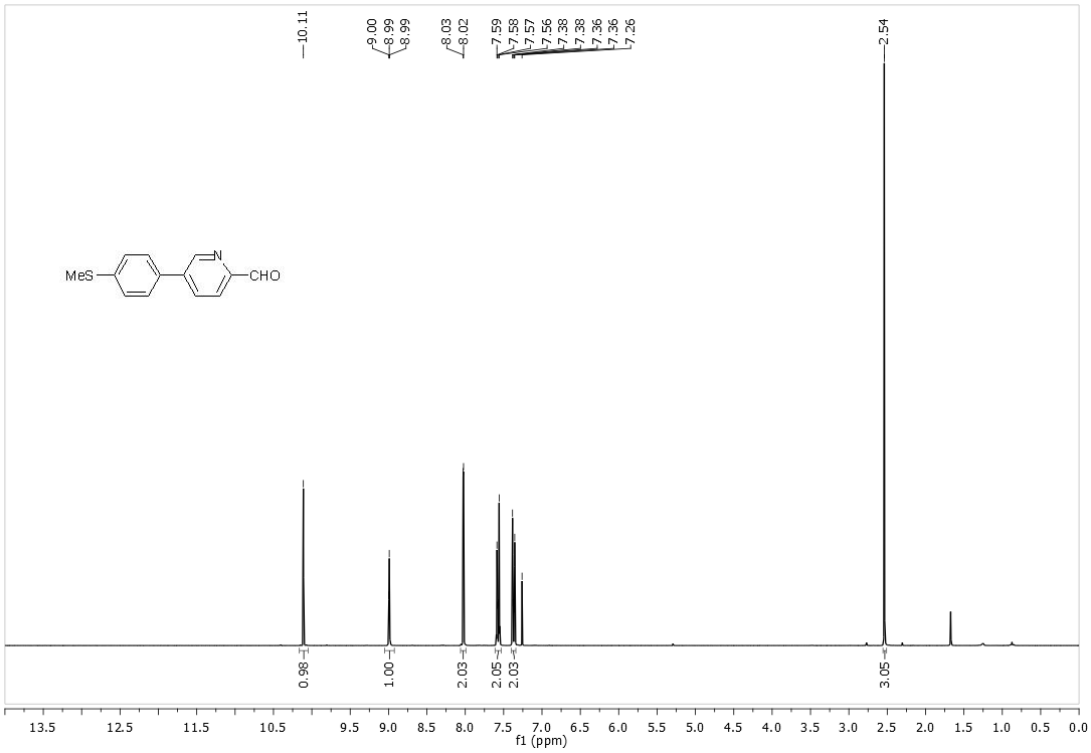

Figure A. 9. ^{1}H-NMR spectrum in $CDCl_3$ of the compound **9**

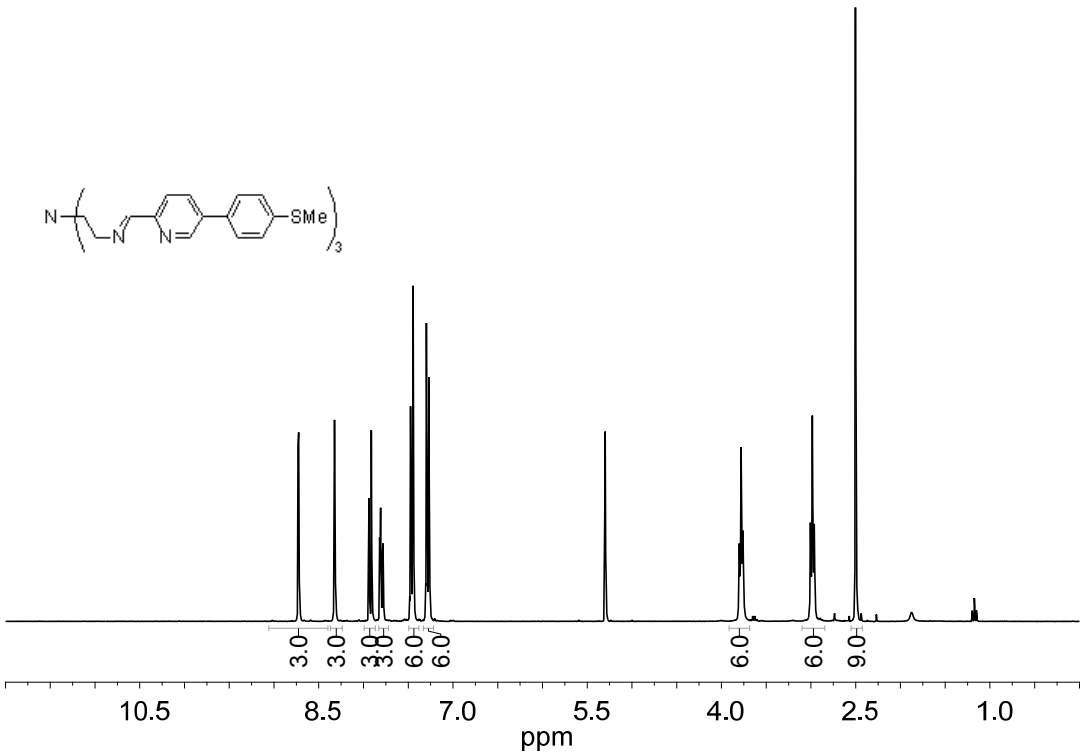

Figure A. 10. ^{1}H-NMR spectrum in CD_2Cl_2 of the compound **10**

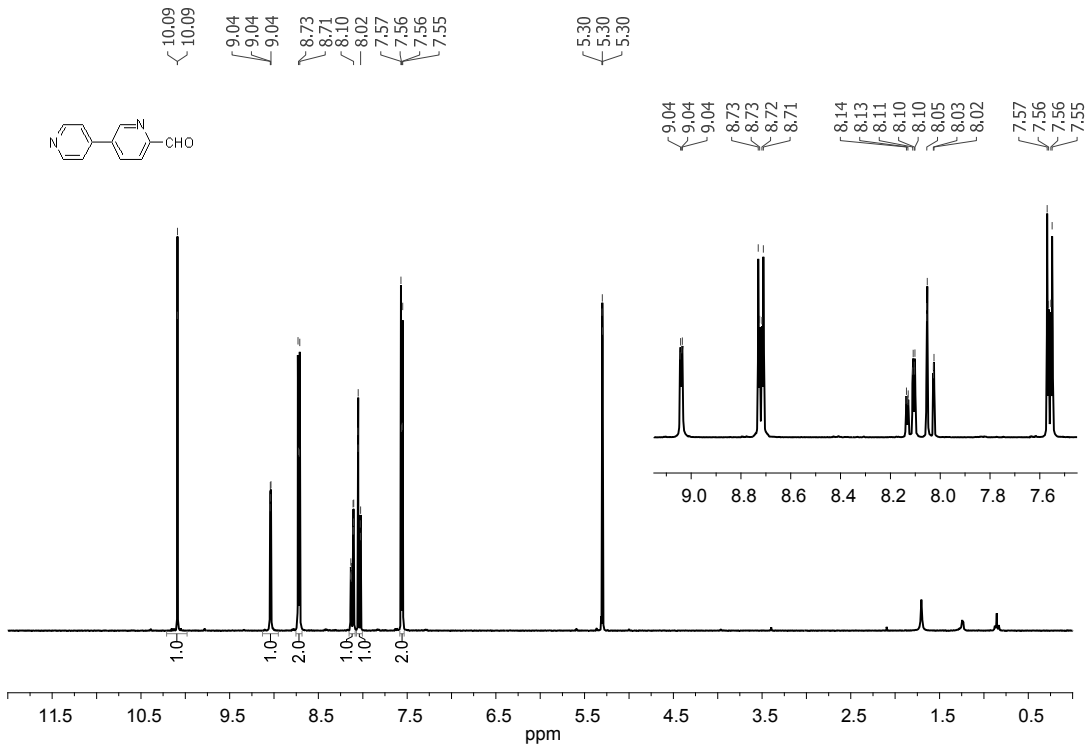

Figure A. 11. ^{1}H-NMR spectrum in CD_2Cl_2 of the compound **14**

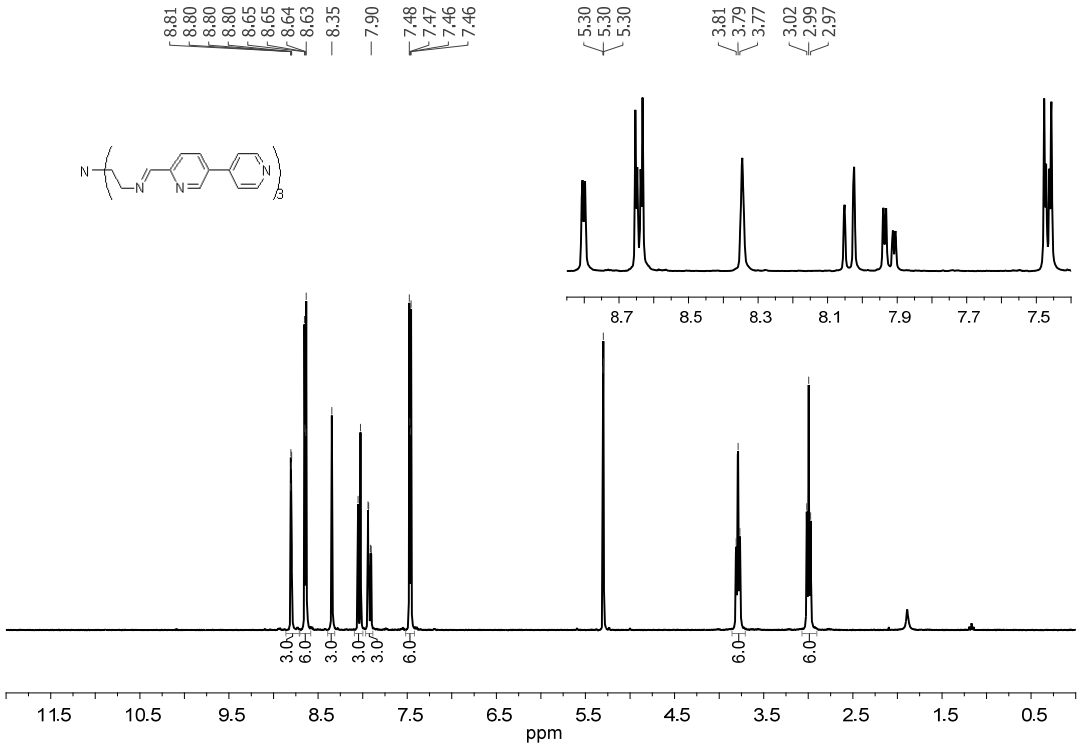

Figure A. 12. ^{1}H-NMR spectrum in CD_2Cl_2 of the compound **15**

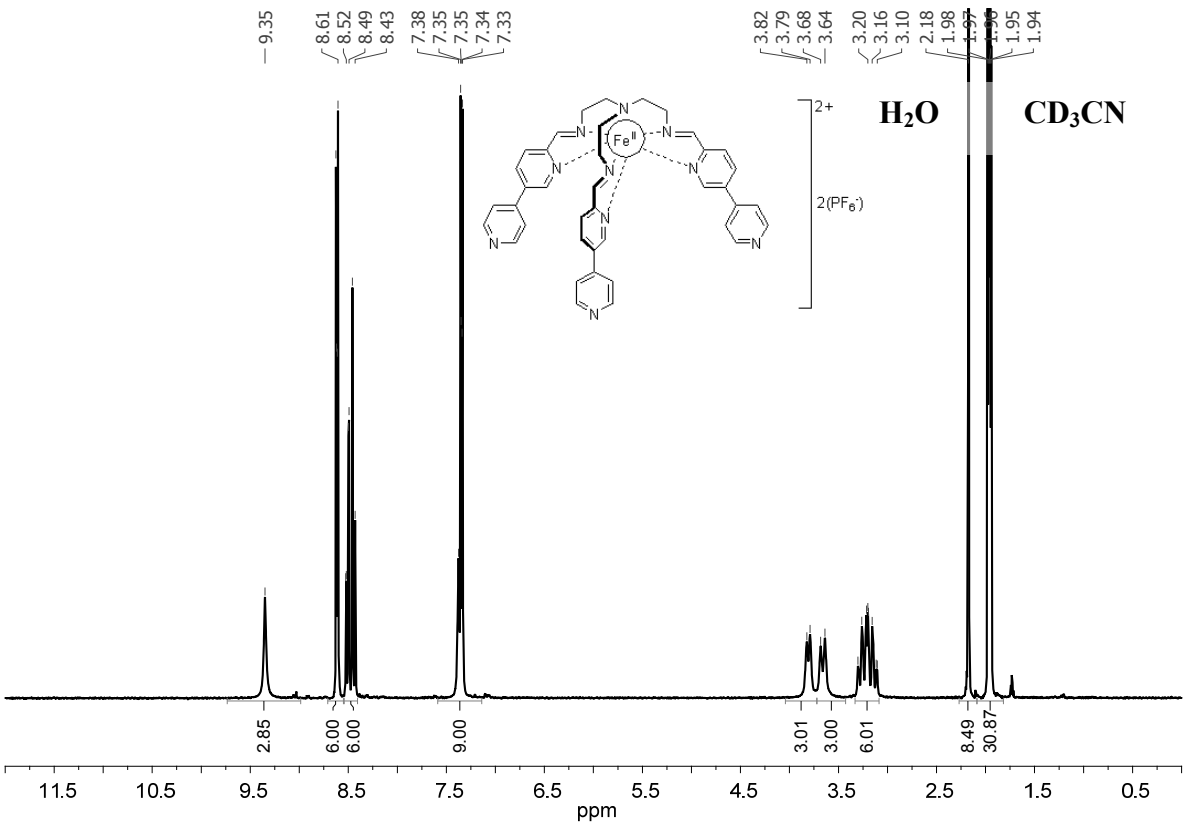

Figure A. 13. ^{1}H-NMR spectrum in CD_3CD of the Fe(II)-complex **16**

A comparative ^{1}H-NMR study shows almost two water molecules per complex molecule

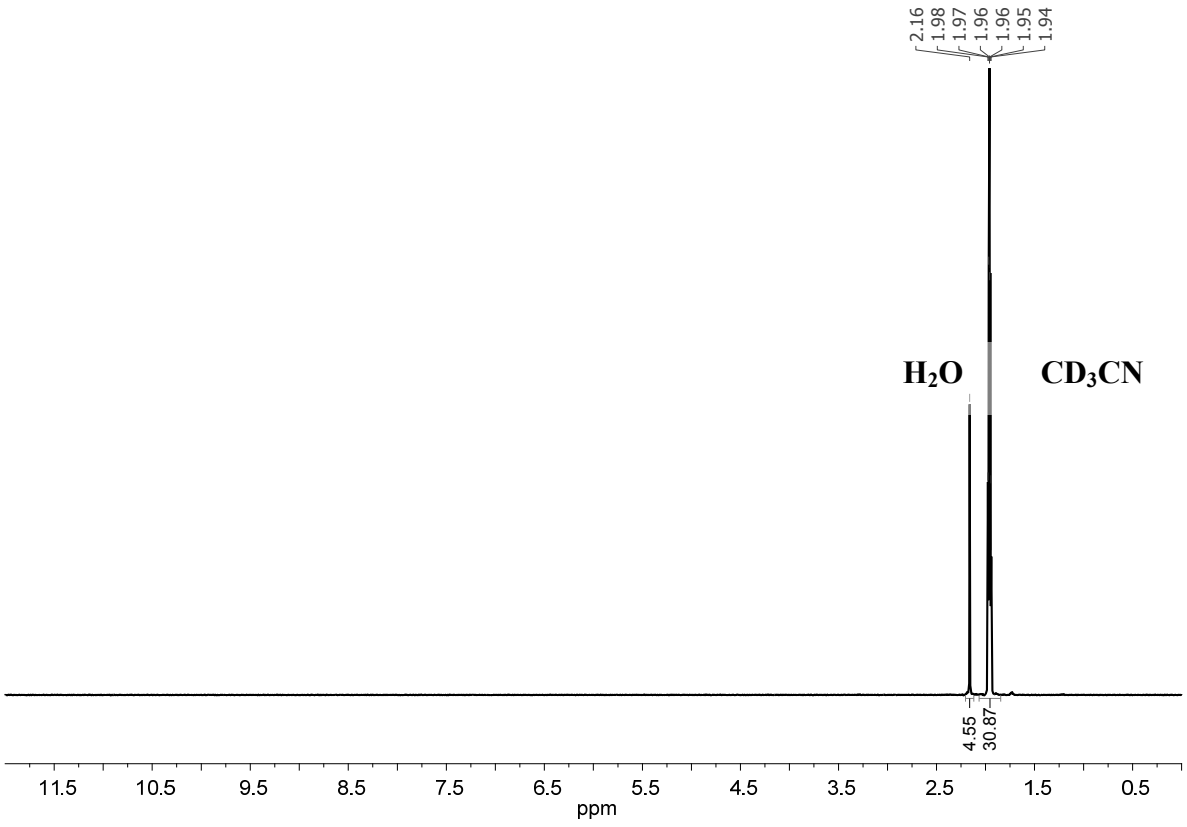

Figure A. 14. ^{1}H-NMR spectrum of CD_3CD before measuring the Fe(II)-complex **16**

2.2. *Fac* and *mer* Ru(II)-bipyridine complex

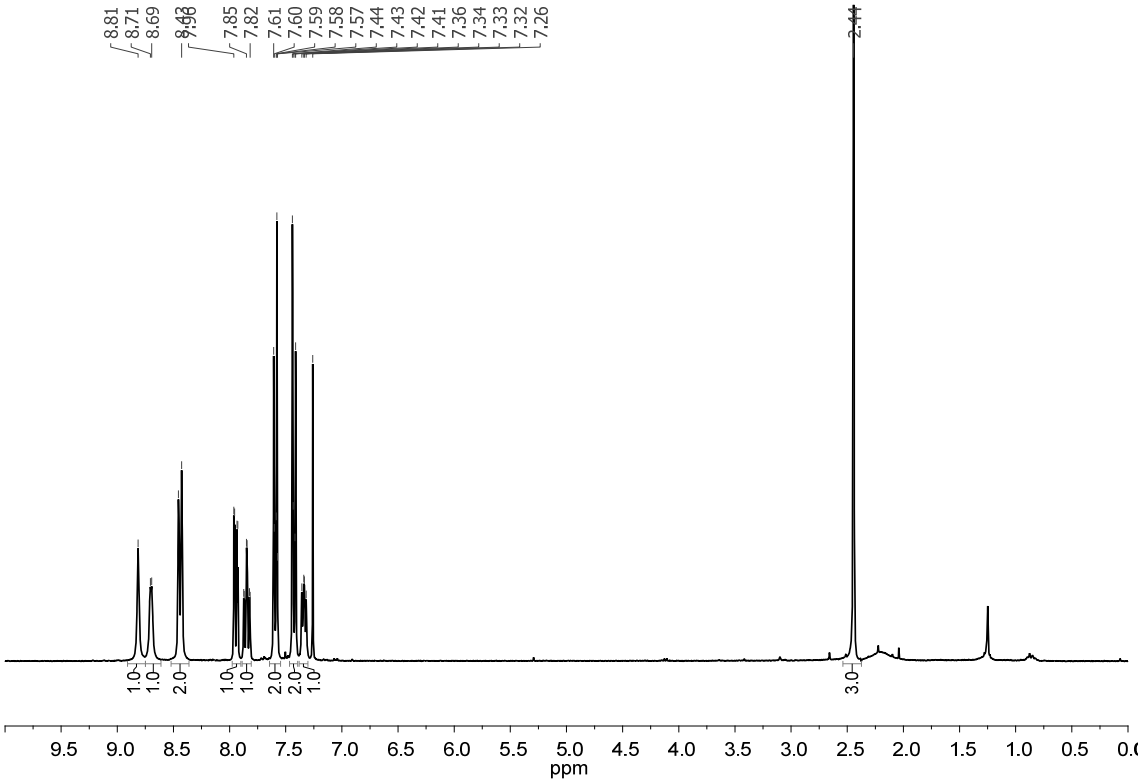

Figure A. 15. ^{1}H-NMR spectrum in $CDCl_3$ of the ligand **L^{e}**, **20**

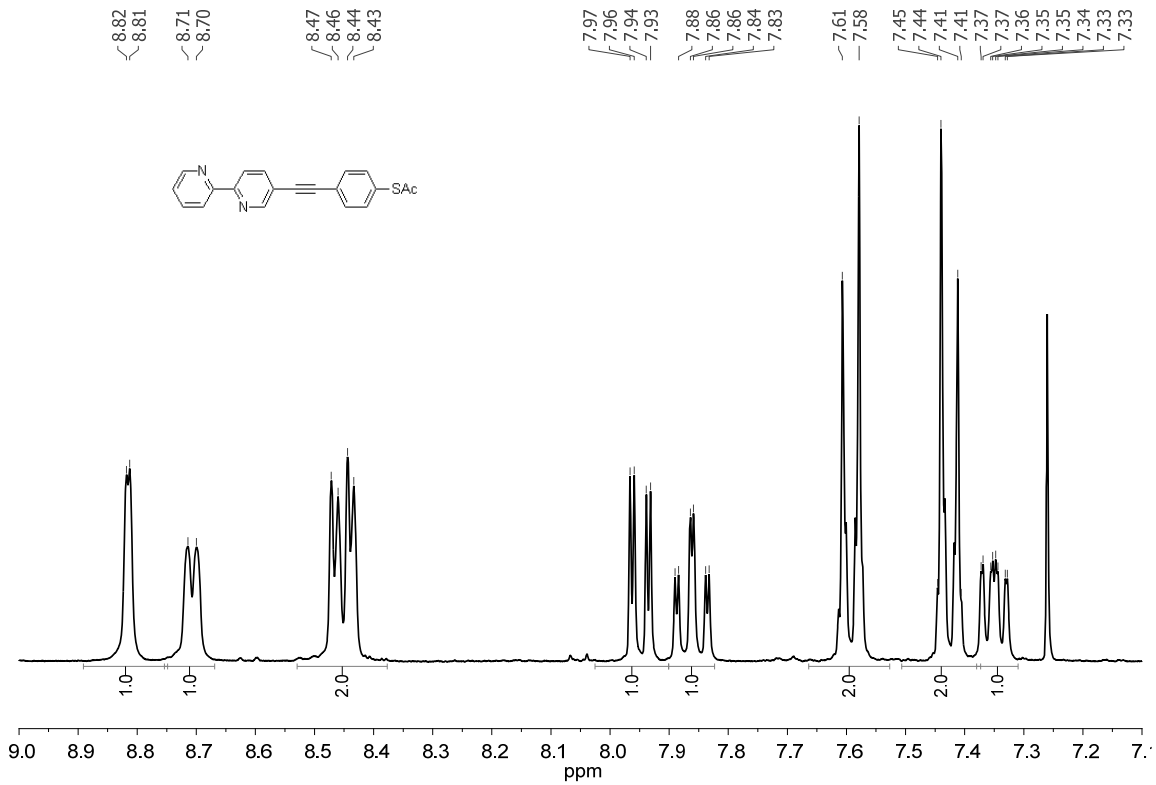

Figure A. 16. Zoom of the ^{1}H-NMR spectrum in $CDCl_3$ of the ligand **L^{e}**, **20**

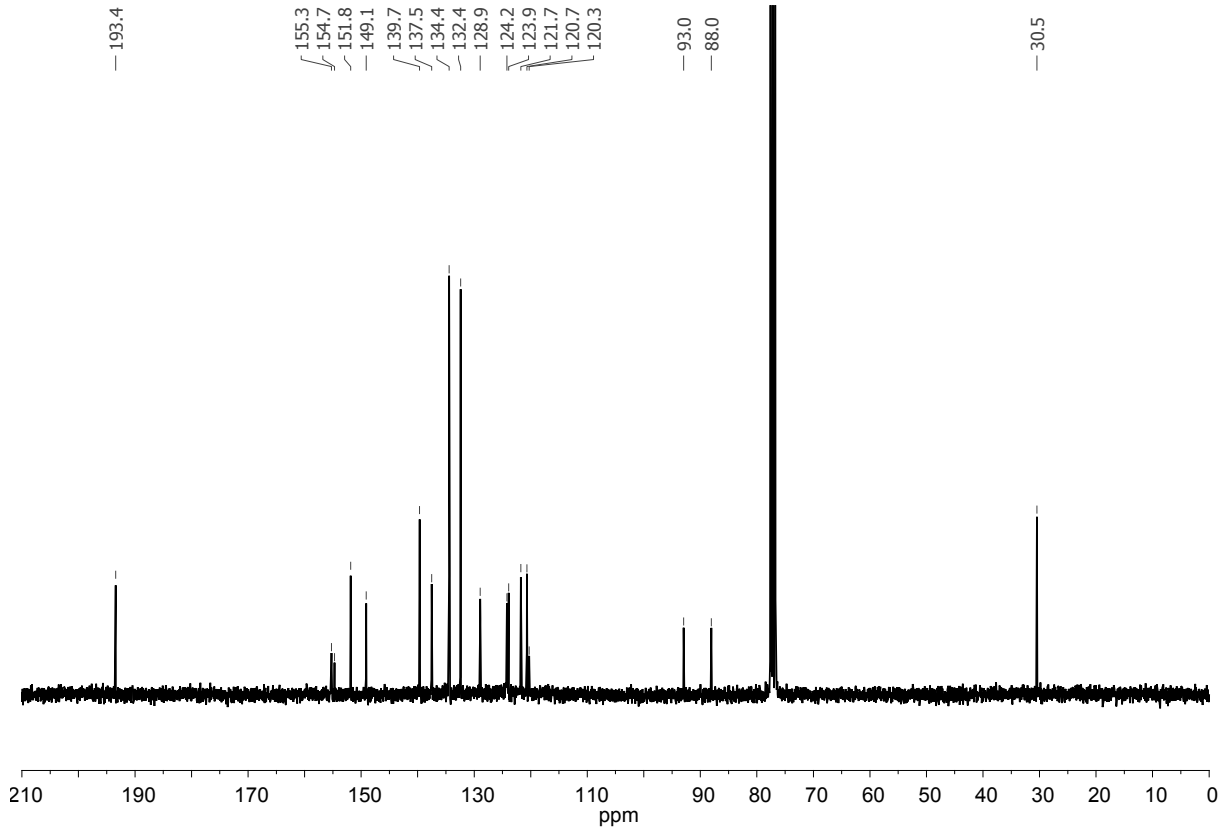

Figure A. 17. ^{13}C NMR spectrum in $CDCl_3$ of the ligand **L**^{e}, **20**

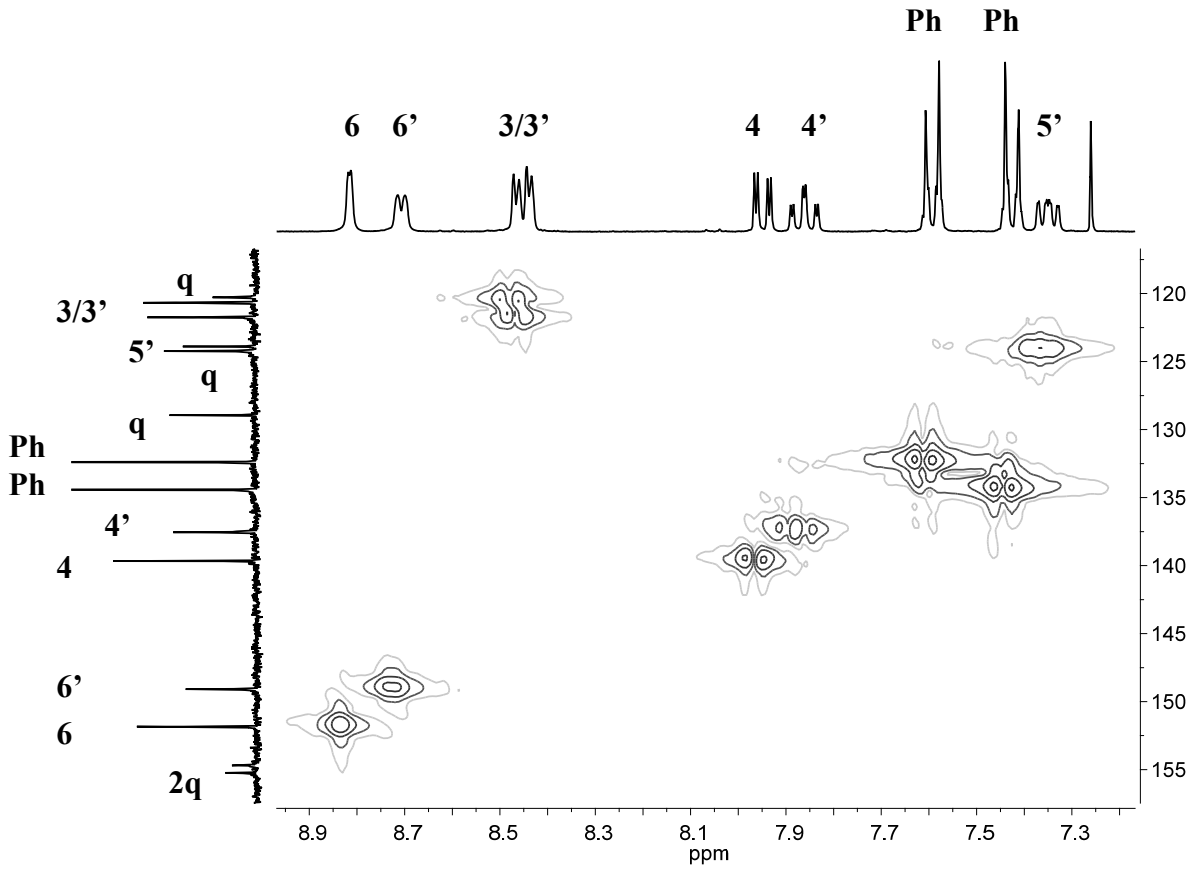

Figure A. 18. ^{1}H ^{13}C NMR spectrum in $CDCl_3$ of the ligand **L**^{e}, **20**

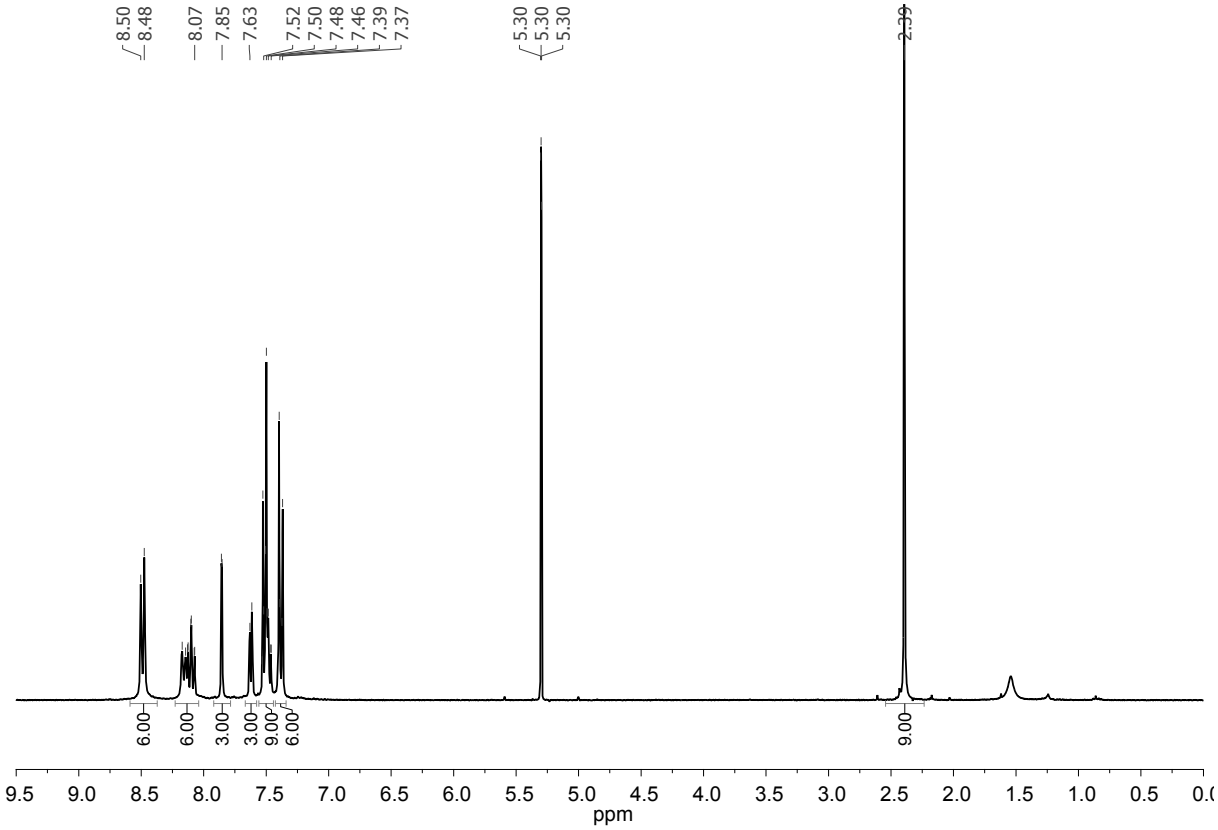

Figure A. 19. ^{1}H-NMR spectrum in CD_2Cl_2 of the *fac* Ru(II)-complex **21^{f}**

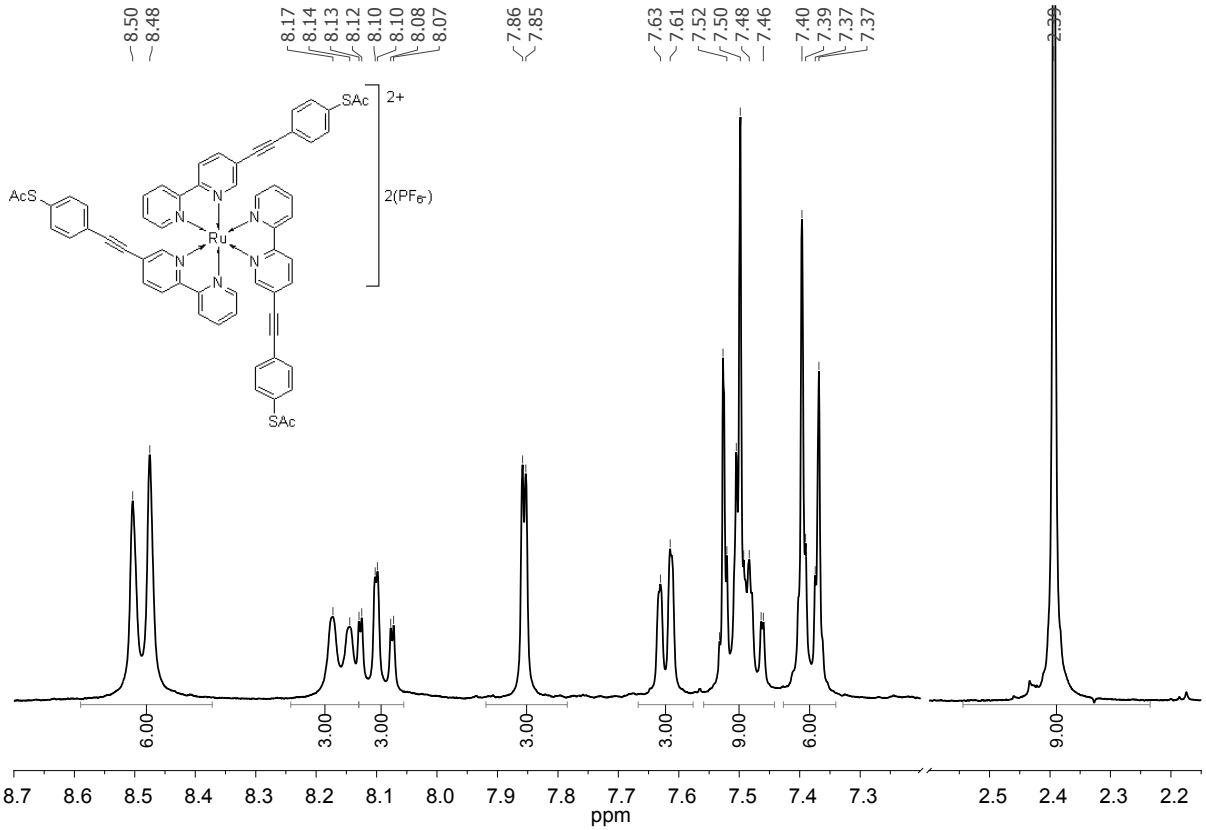

Figure A. 20. Zoom of the ^{1}H-NMR spectrum in CD_2Cl_2 of the *fac* Ru(II)-complex **21^{f}**

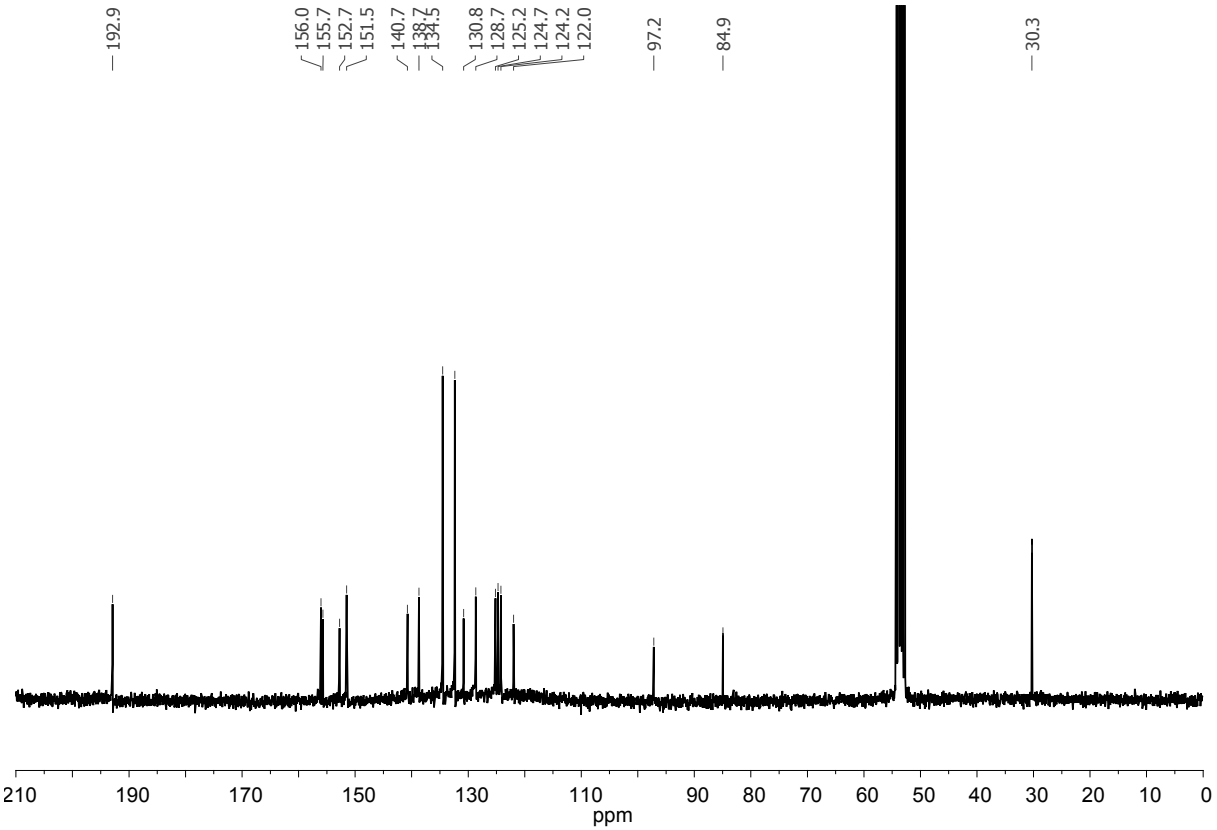

Figure A. 21. ^{13}C NMR spectrum in CD_2Cl_2 of the *fac* Ru(II)-complex **21**^{f}

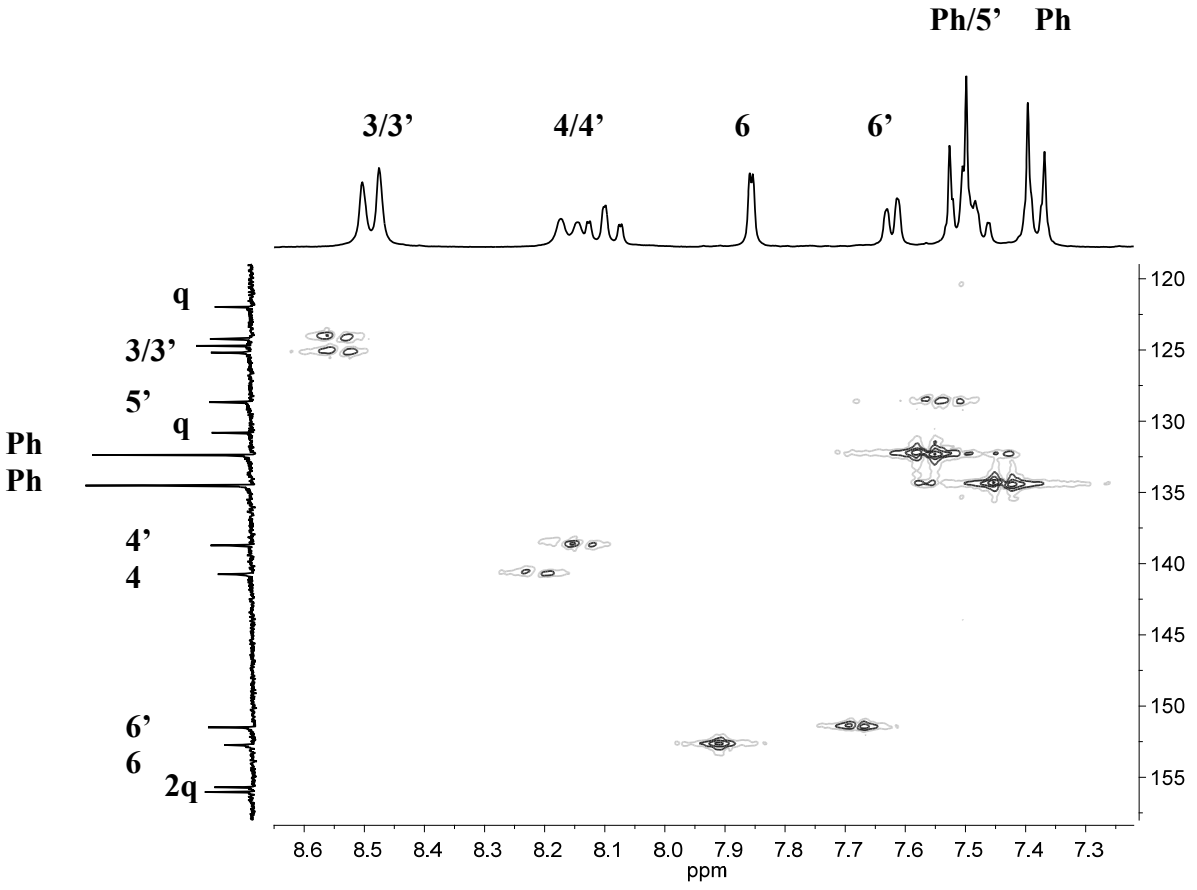

Figure A. 22. ^{1}H ^{13}C NMR spectrum in CD_2Cl_2 of the *fac* Ru(II)-complex, **21**^{f}

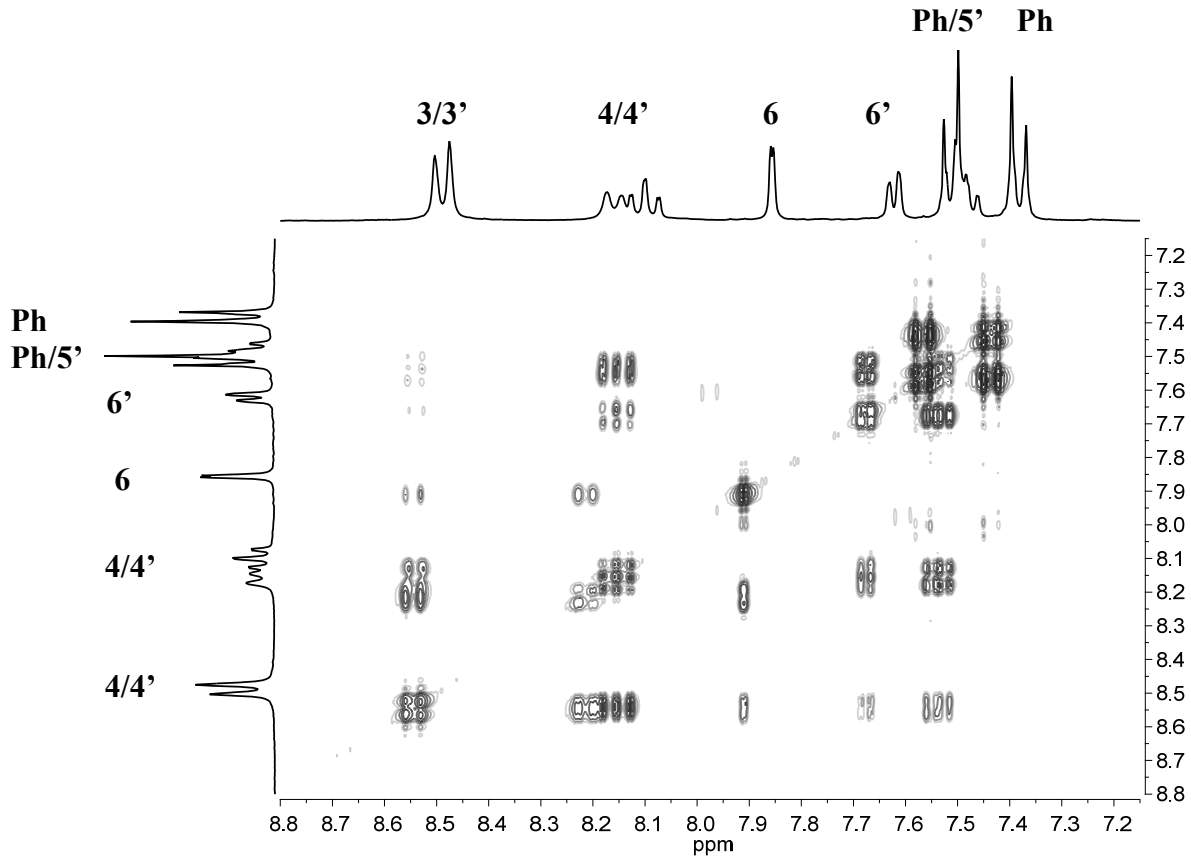

Figure A. 23. ^{1}H ^{1}H COSY90 NMR spectrum in CD_2Cl_2 of the *fac* Ru(II)-complex, **21^{f}**

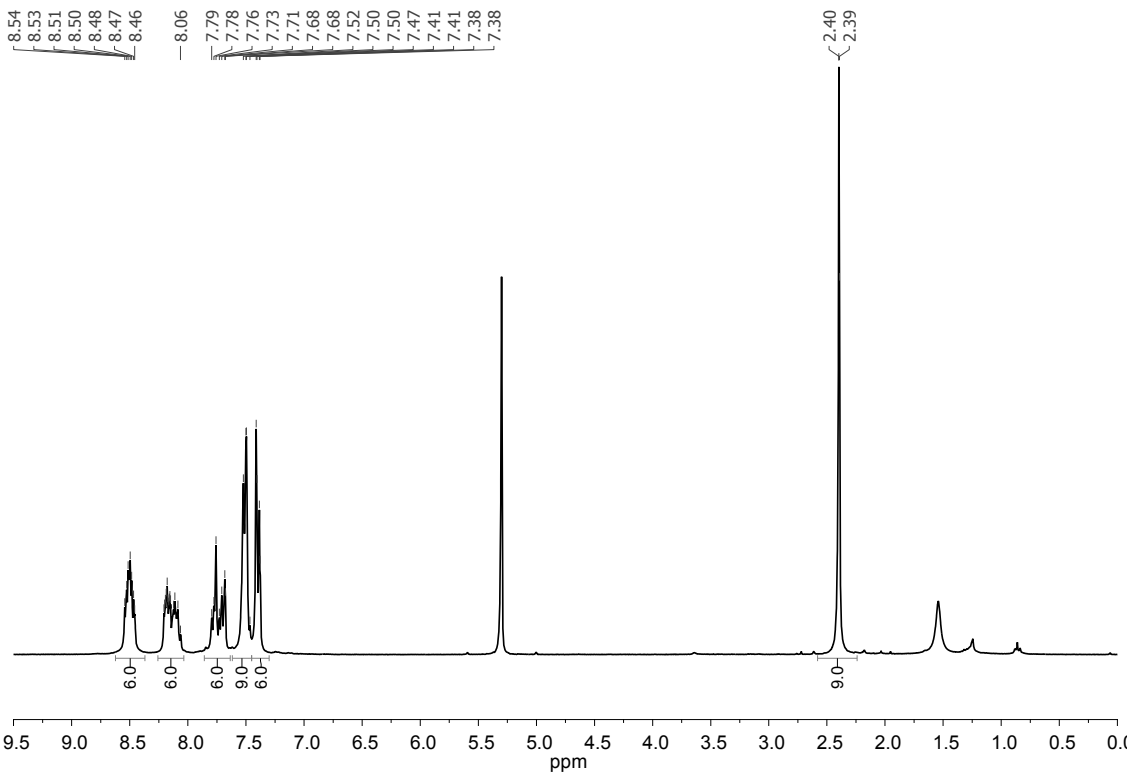

Figure A. 24. ^{1}H-NMR spectrum in CD_2Cl_2 of the *mer* Ru(II)-complex, **21^{m}**

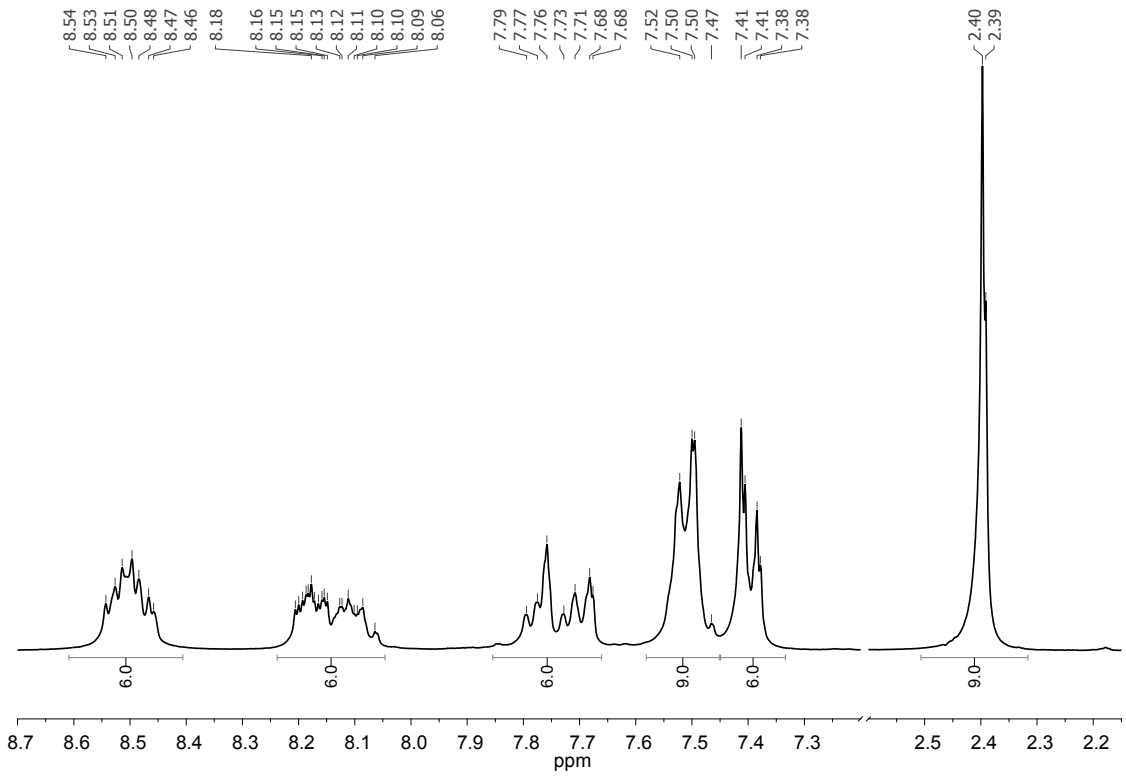

Figure A. 25. Zoom of the ^{1}H-NMR spectrum in CD_2Cl_2 of the *mer* Ru(II)-complex **21^{m}**

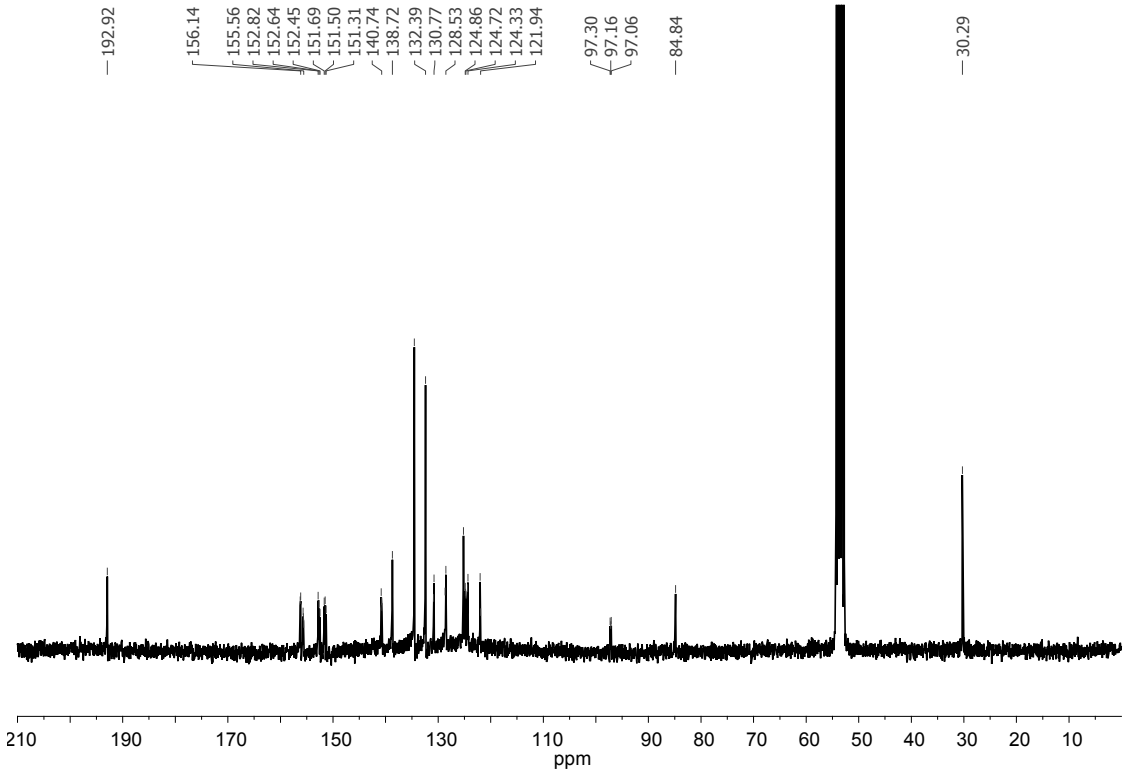

Figure A. 26. ^{13}C NMR spectrum in CD_2Cl_2 of the *mer* Ru(II)-complex, **21^{m}**

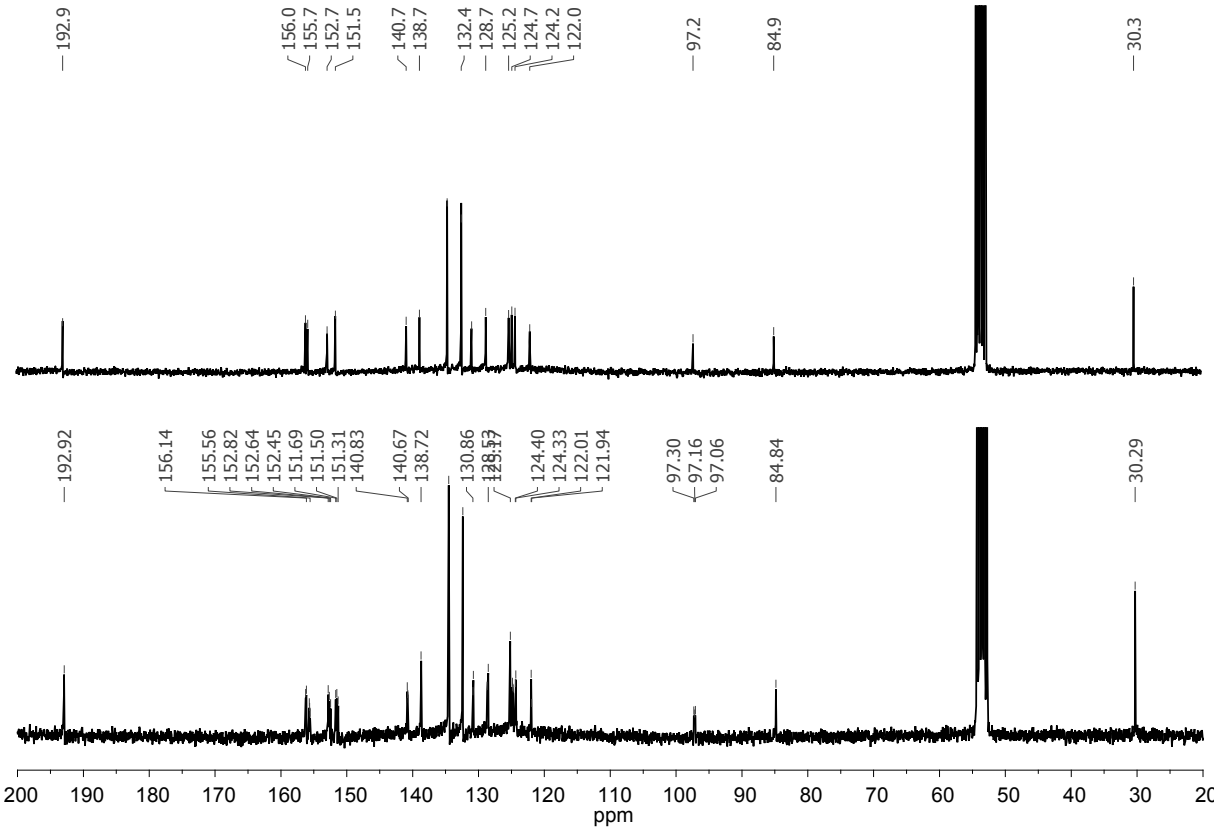

Figure A. 27. ^{13}C NMR spectra comparison in CD_2Cl_2 of the *fac* (up) and *mer* (down) Ru(II)-complex, **21**$^{f, m}$

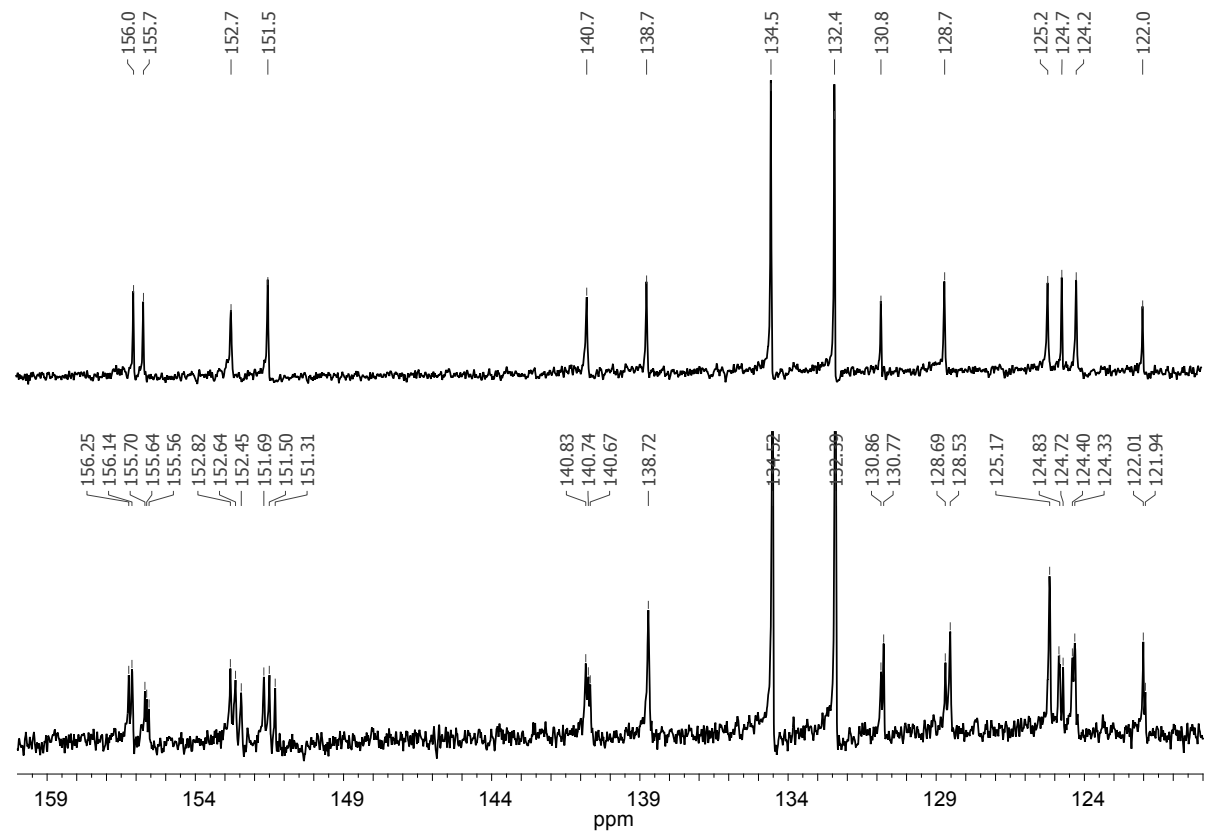

Figure A. 28. Zoom of the ^{13}C NMR spectra in CD_2Cl_2 of the *fac* (up) and *mer* (down) Ru(II)-complex, **21**$^{f, m}$

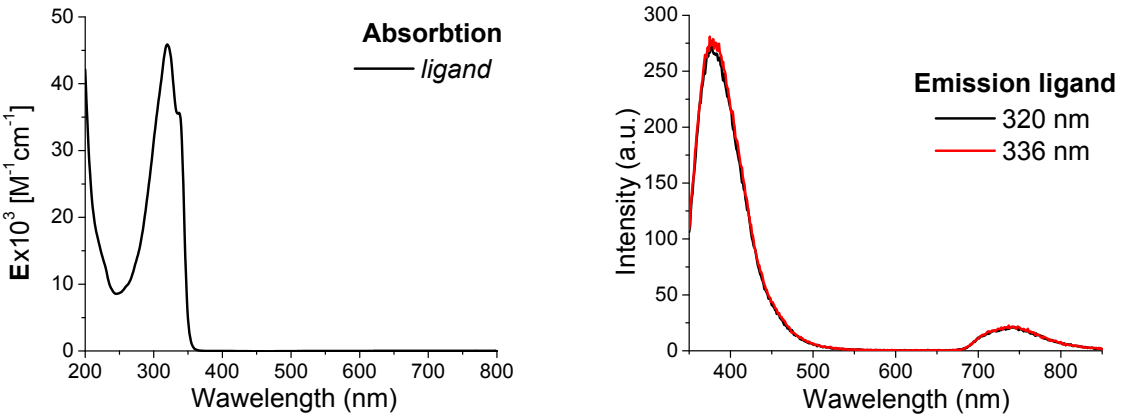

Figure A. 29. Electronic spectra of the ligand ***20*** recorded in aerated CH_3CN at rt under normal atmosphere; (a) absorbtion spectrum (b) emission spectra by excitation at 320 and 336 nm;

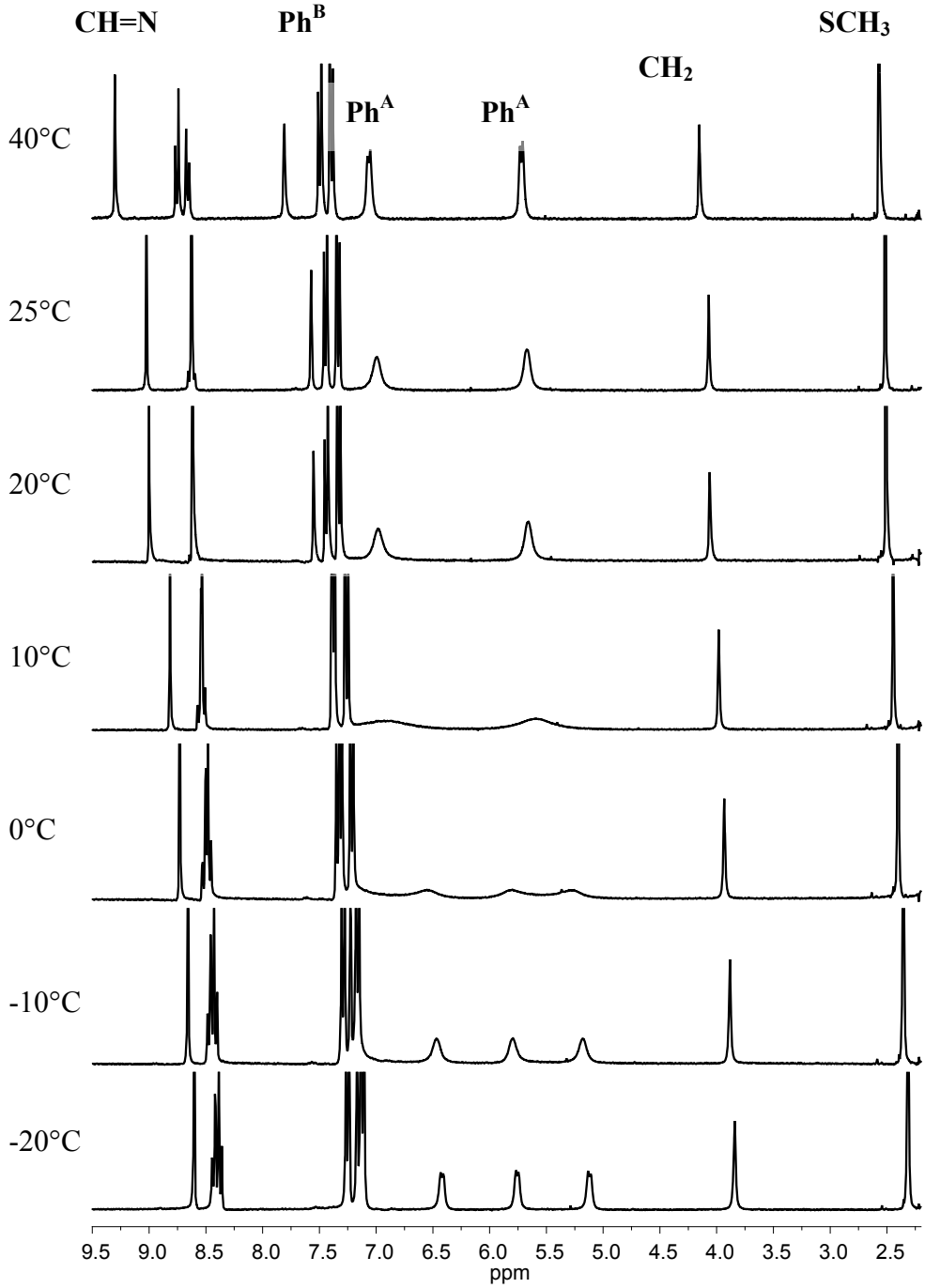

Figure A. 30. Zoom of the dynamic ^{1}H-NMR spectra of dinuclear Fe(II)-helix, **23**

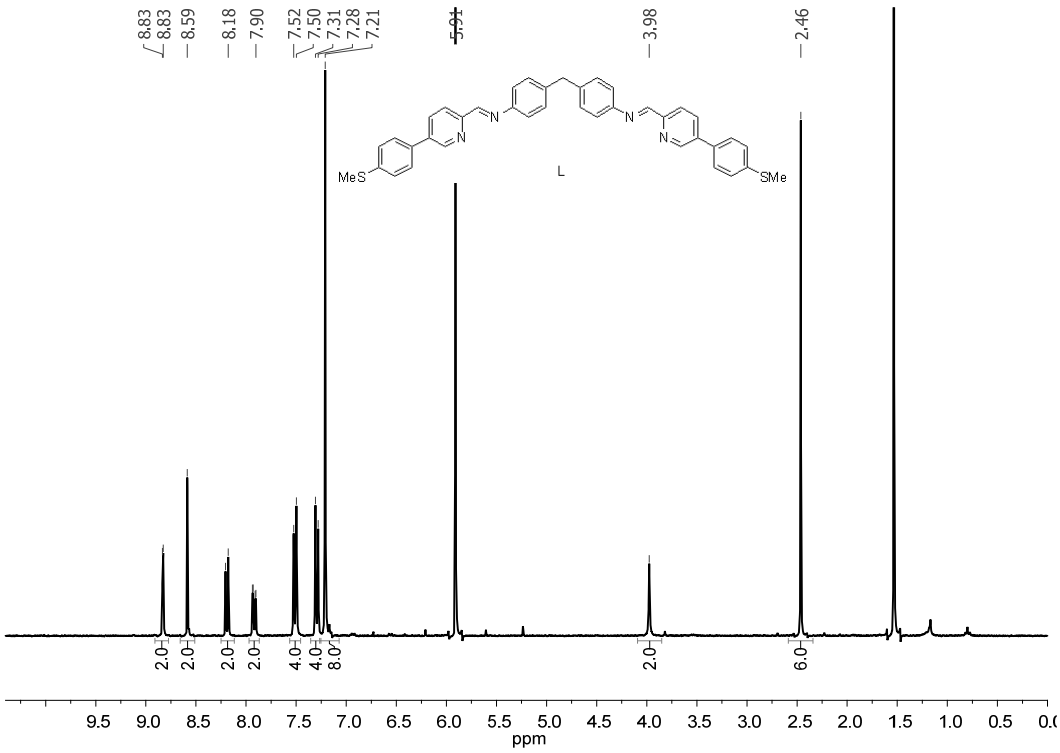

Figure A. 31. ^{1}H-NMR spectrum in $C_2D_2Cl_4$ of the ligand L^f, **9**

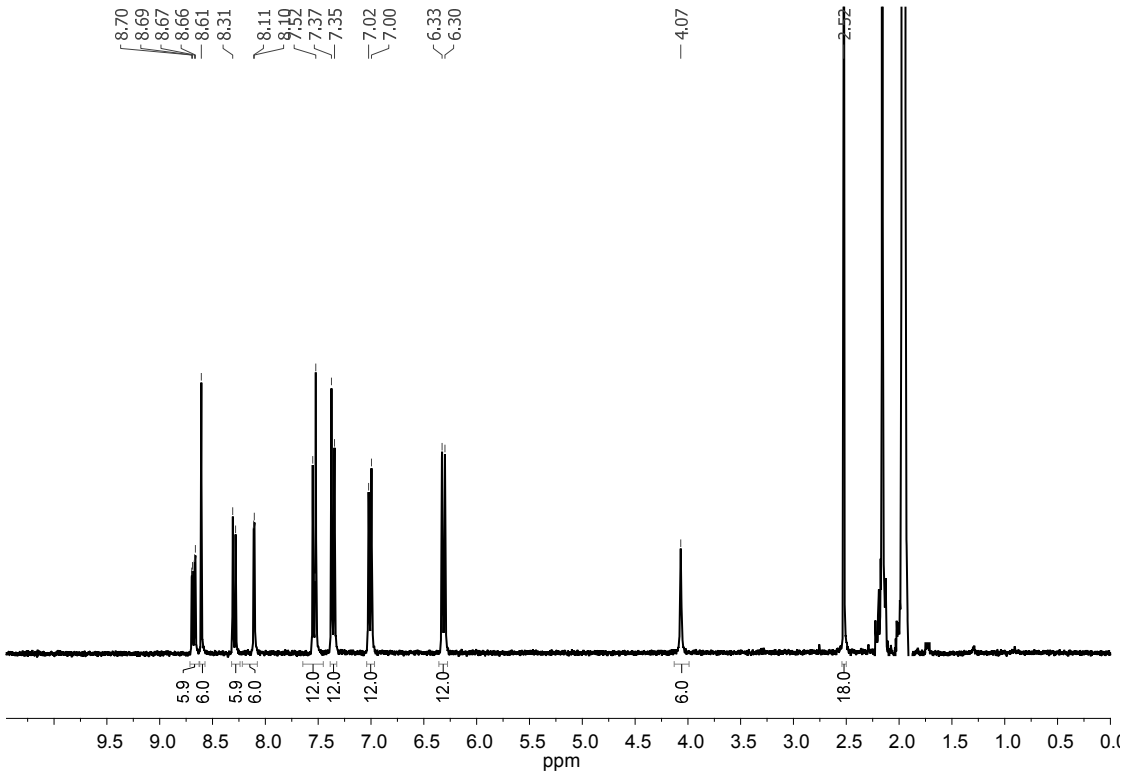

Figure A. 32. ^{1}H-NMR spectrum in CD_3CN at 25°C of the dinuclear Zn(II)-helix **25**

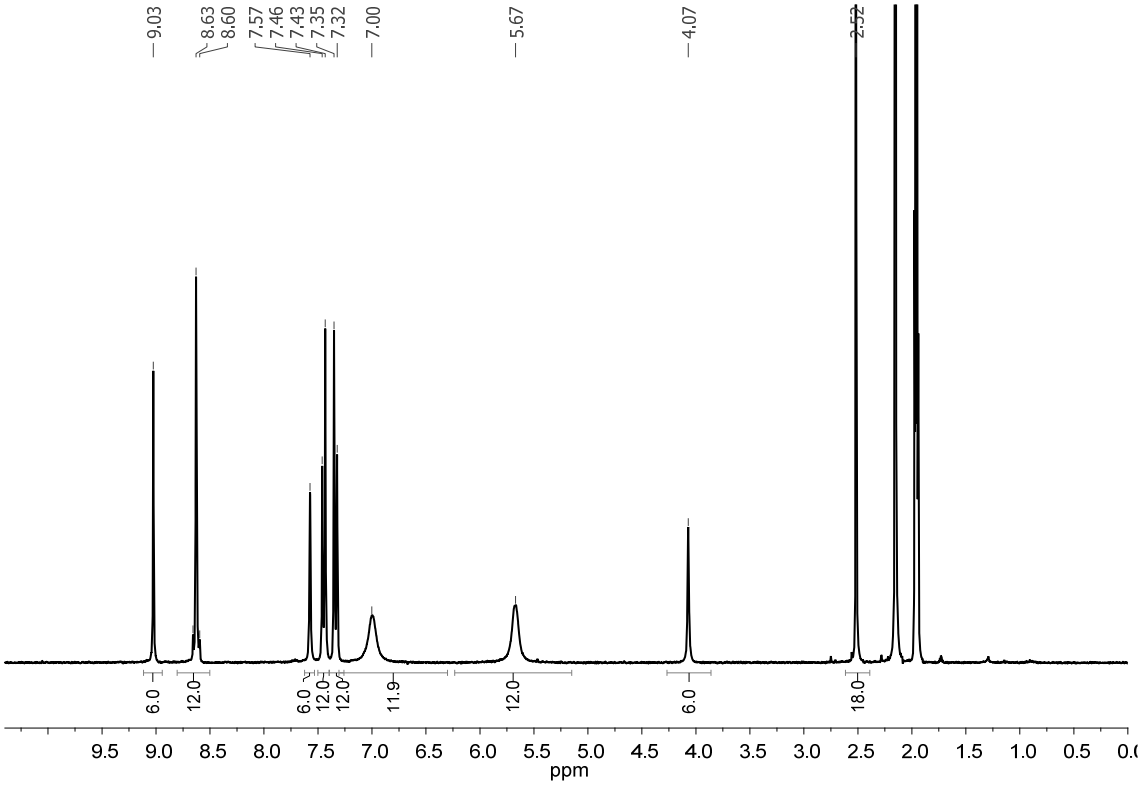

Figure A. 33. ^{1}H-NMR spectrum in CD_3CN at 25°C of the dinuclear Fe(II)-helix, **23**

4. Chiral (S)- and (R)-binaphthyl ligands and their Zn(II)-complexes

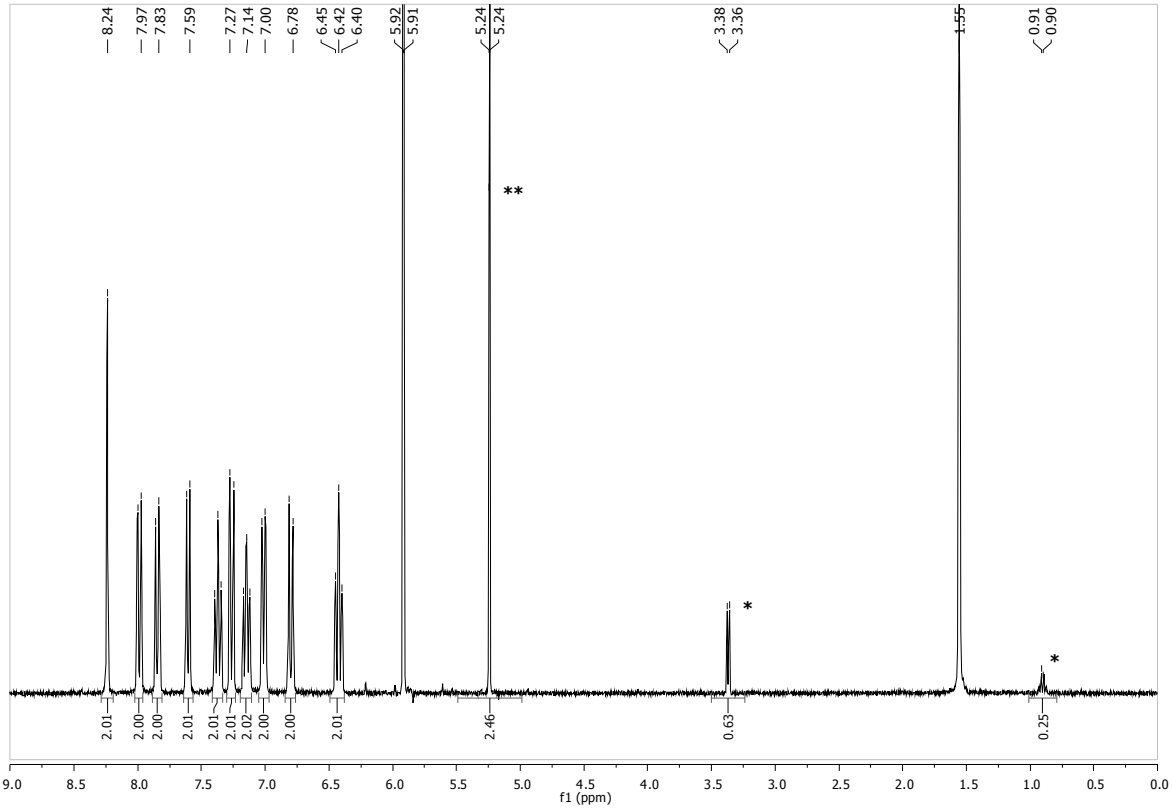

Figure A. 34. ^{1}H-NMR spectrum of the (S)-ZnL^{g} complex, **27$^{(S)}$**, in $C_2D_2Cl_4$ showing the quantity of solvents per molecule of complex: * 0.25 MeOH, ** 1.23 CH_2Cl_2.

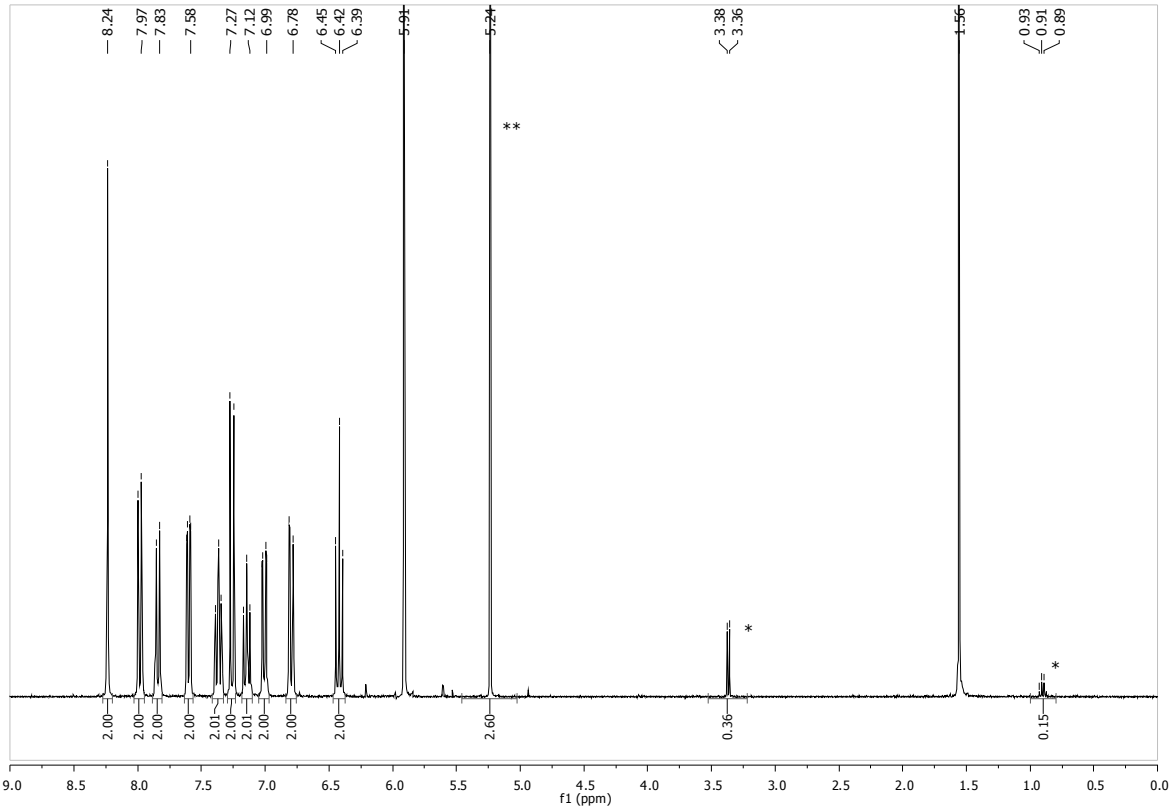

Figure A. 35. ^{1}H-NMR spectrum of the (R)-ZnL^{g} complex, **27$^{(R)}$**, in $C_2D_2Cl_4$ showing the quantity of solvents per molecule of complex: * 0.15 MeOH, ** 1.30 CH_2Cl_2

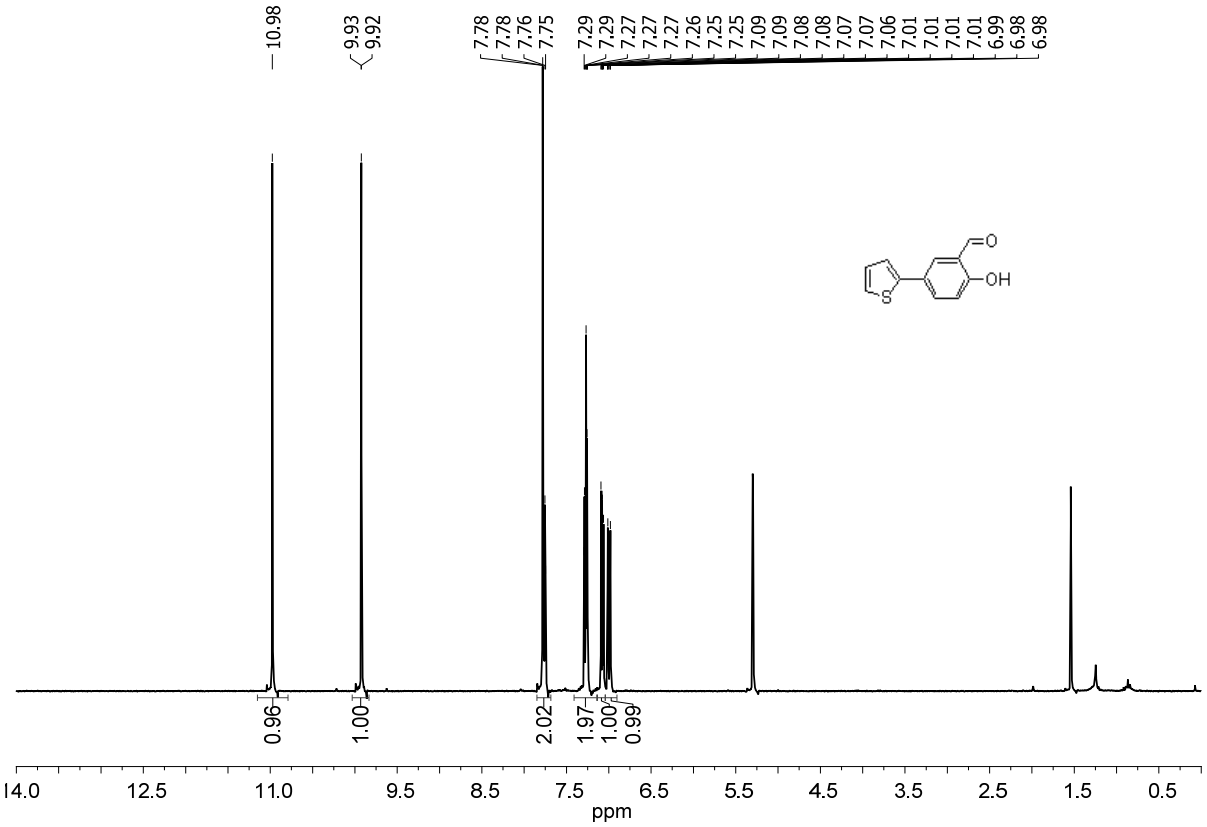

Figure A. 36. ^{1}H-NMR spectrum in CD_2Cl_2 of the compound **28**

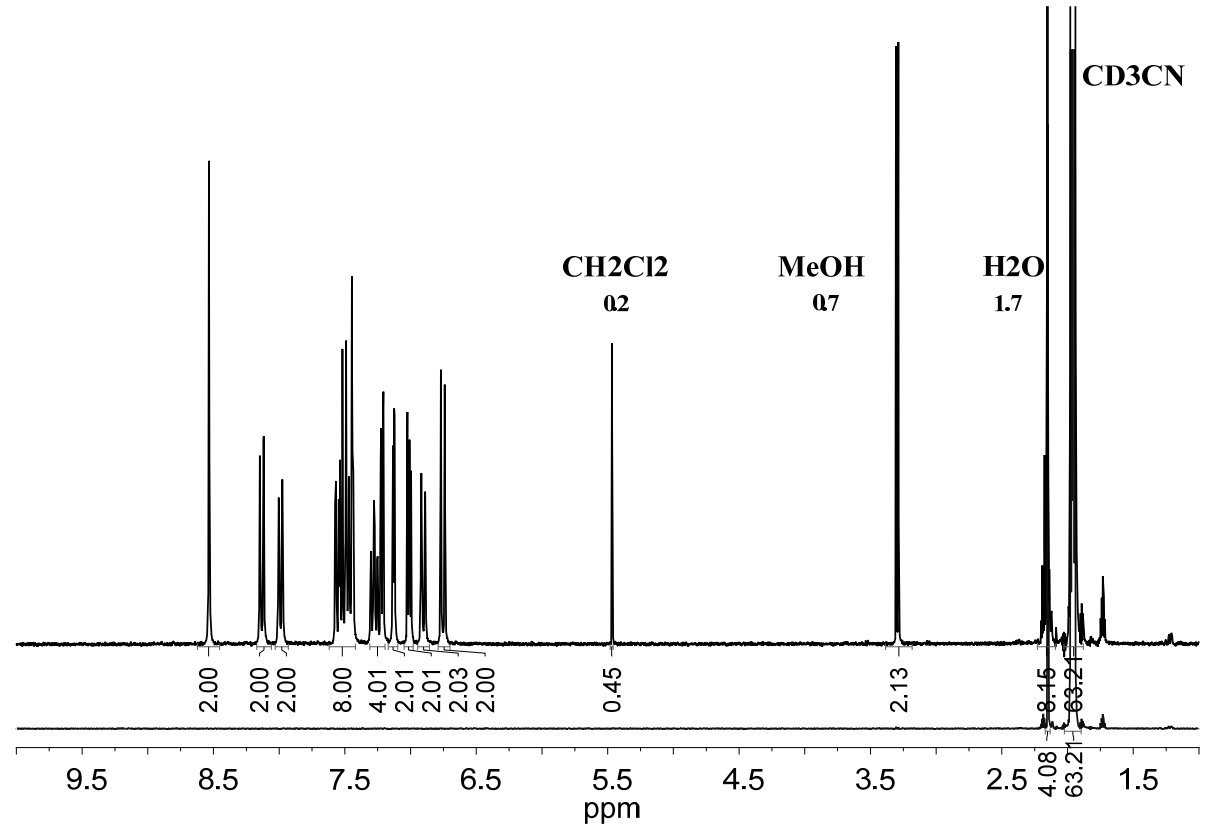

Figure A. 37. ^{1}H-NMR spectrum in CD_3CN of the (S)-ZnL^{h} complex **30**$^{(S)}$ compared to the ^{1}H-NMR spectrum of pure CD_3CN before measuring the complex showing the quantity of solvents per molecule of complex.

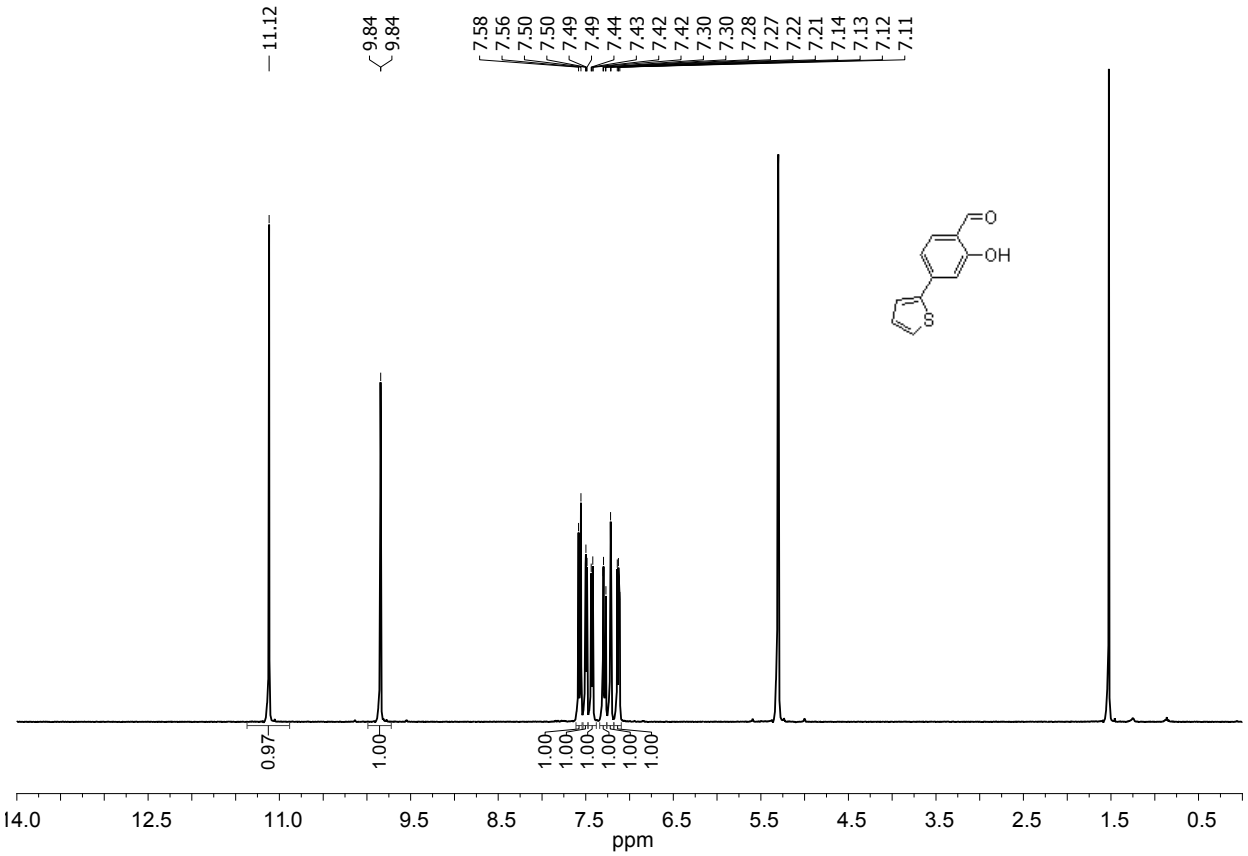

Figure A. 38. ^{1}H-NMR spectrum in CD_2Cl_2 of the compound **31**

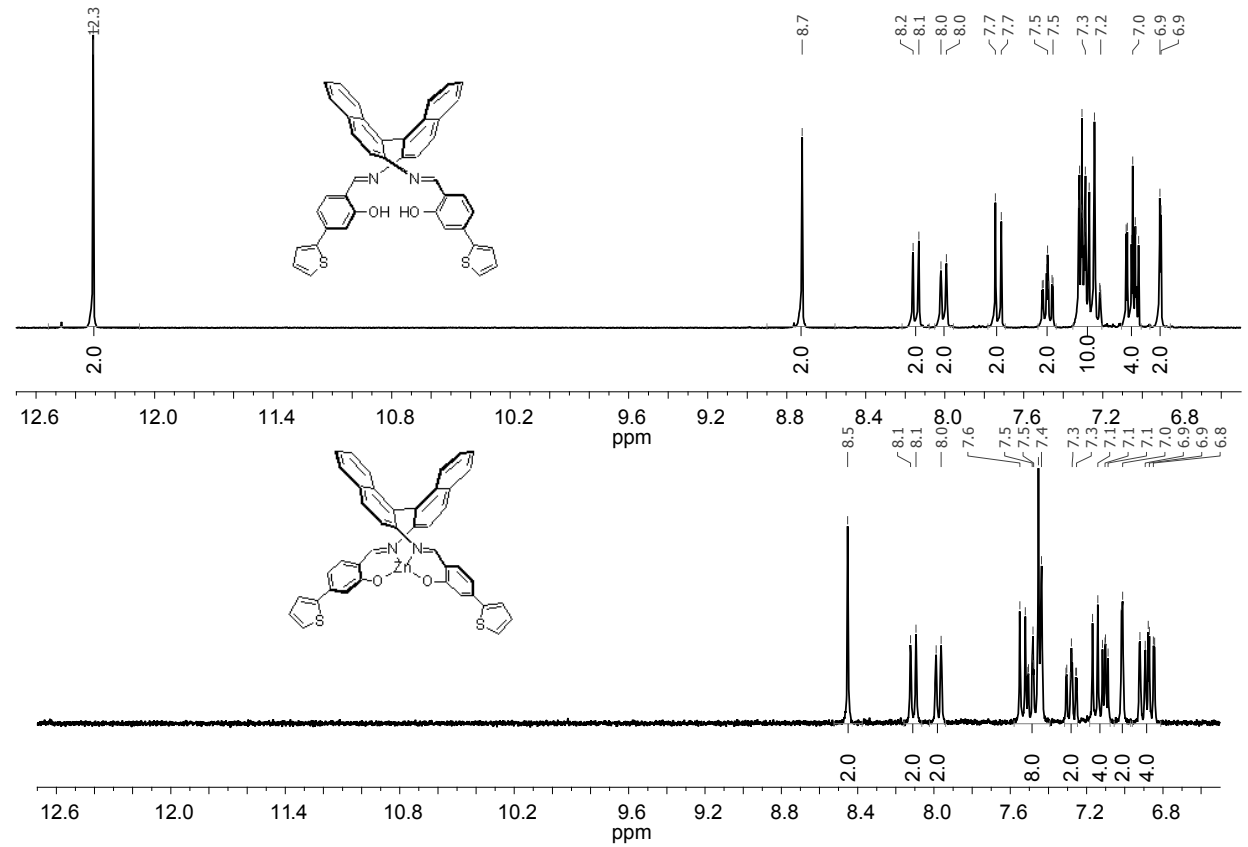

Figure A. 39. ^{1}H-NMR spectra in CD_2Cl_2 of the (R)-L^{i} ligand **32$^{(R)}$**, and (R)-ZnL^{i} complex **33$^{(R)}$**

5. Functionalized thioketal compounds for SAM study

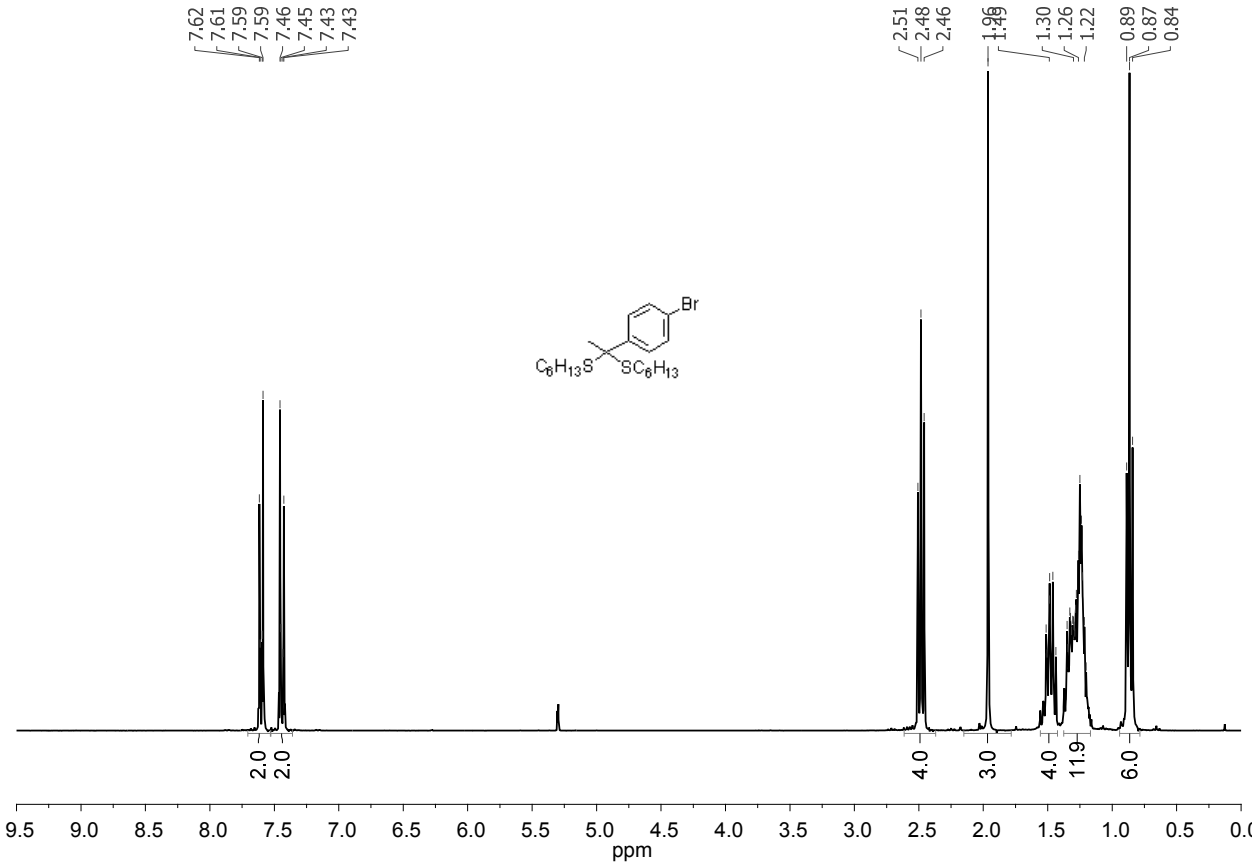

Figure A. 40. ^{1}H-NMR spectrum in CD_2Cl_2 of the compound **34b**

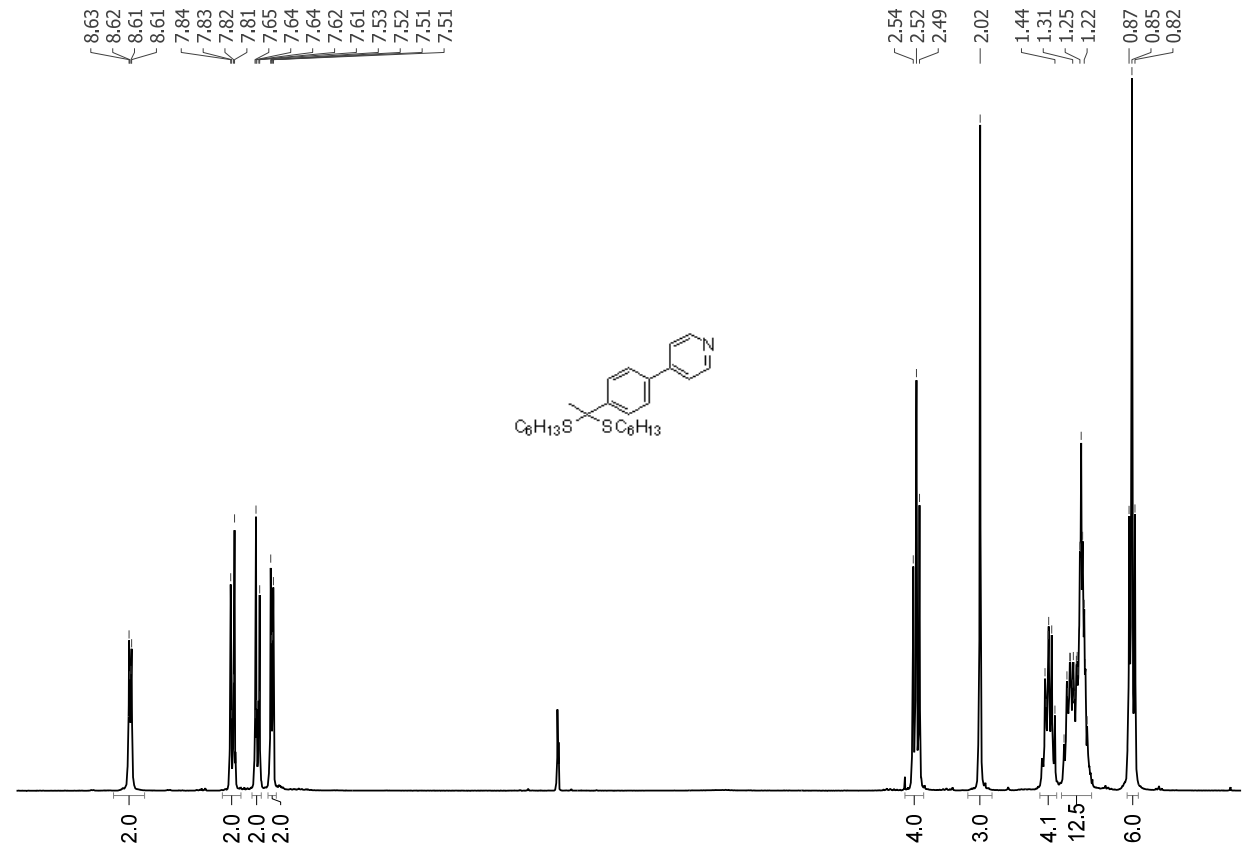

Figure A. 41. ^{1}H-NMR spectrum in CD_2Cl_2 of the compound **35b**

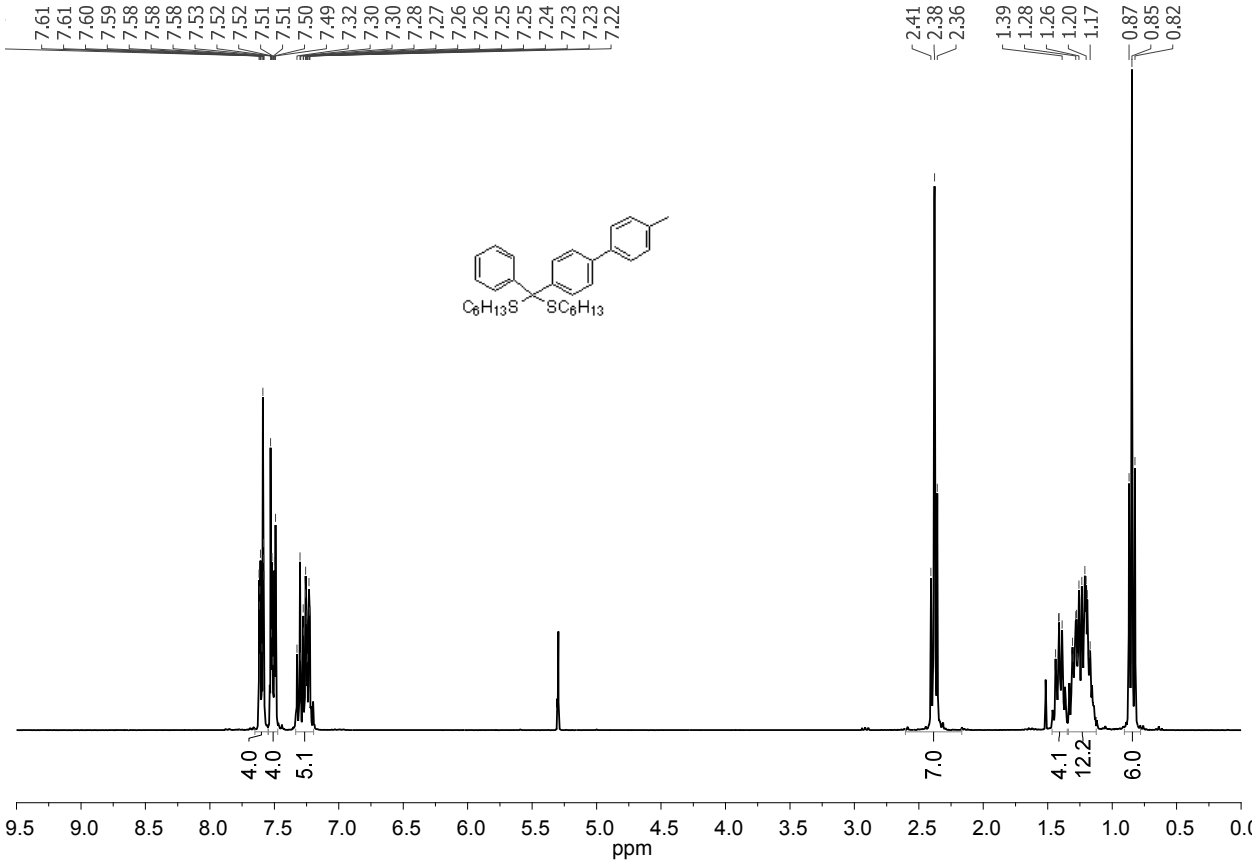

Figure A. 42. ^{1}H-NMR spectrum in CD_2Cl_2 of the compound **38a**

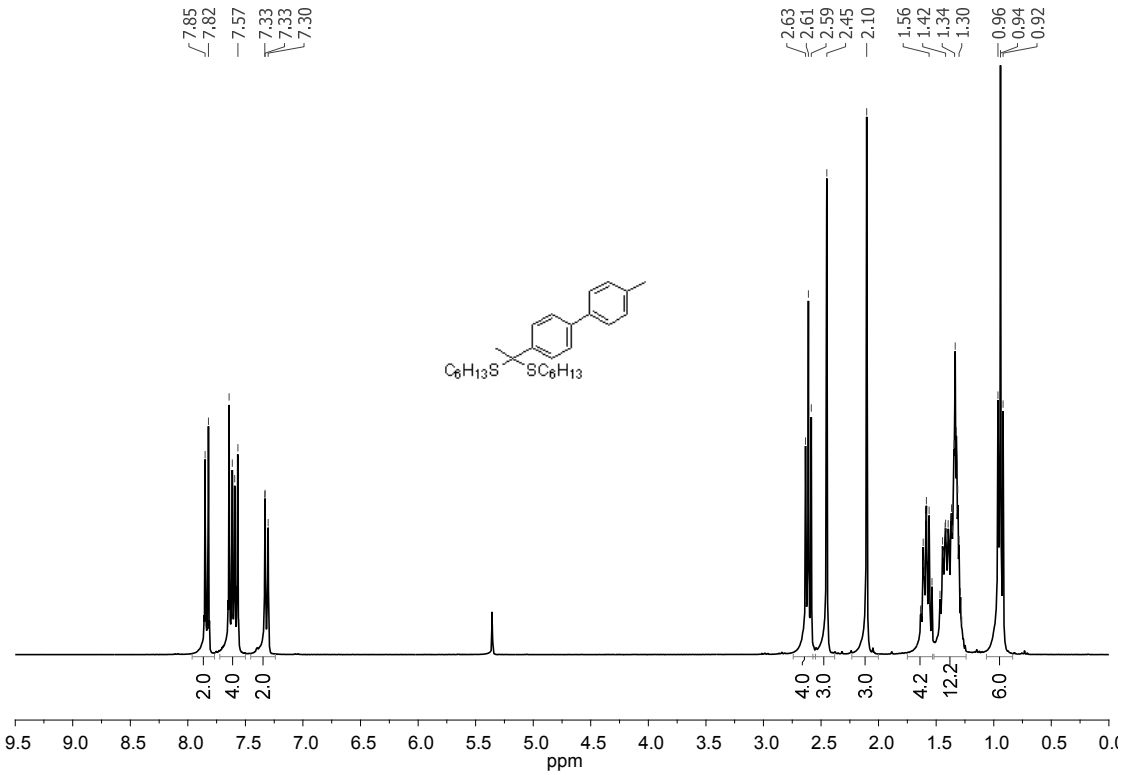

Figure A. 43. ^{1}H-NMR spectrum in CD_2Cl_2 of the compound **38b**

Annex 2.

Crystallographic data

Table A1. Summary of crystallographic data for *trensal* M(III)-complexes **3**, **4**, **5** and **8**; standard deviations are given in parentheses.

Identification code		Ga(III)-complex, **3**	Fe(III)-complex, **4** *1st method*	Fe(III)-complex, **4** *2nd method*	Mn(III)-complex, **5**	Ga(III)-complex, **8**
Formula		C49 H47 Cl2 Ga N4 O3 S3	C48 H45 Fe N4 O3 S3	C48 H45 Fe N4 O3 S3	C49.5 H48 Cl3 Mn N4 O3 S3	C43 H38 Cl2 Ga N7 O3
Solvates		1 (CH2Cl2)	-	-	1.5 (CH_2Cl_2)	1 (CH_2Cl_2)
Formula weight (g/Mol)		976.71	877.91	877.91	1004.39	841.42
Temperature (K)		180 (2)	180 (2)	180 (2)	180 (2)	180 (2)
Crystal system, space group		Trigonal, $R\overline{3}$	Monoclinic, C2/c	Monoclinic, $P2_1/n$	Monoclinic, $P2_1$	Monoclinic, $P2_1/n$
Unit cell dimensions	a (Å)	13.3377 (19)	18.352(4)	18.244(4)	11.036(2)	11.152(2)
	b (Å)	13.3377 (19)	21.329(4)	21.227(4)	21.306(4)	18.552(4)
	c (Å)	43.063 (9)	22.576(5)	22.611(5)	20.494(4)	18.319(4)
	α (°)	90	90	90	90	90
	β (°)	90	104.43(3)	104.51(3)	98.81(3)	95.91(3)
	γ (°)	120	90	90	90	90
Crystal size (mm)		0.45 x 0.30 x 0.09	0.35 x 0.09 x 0.04	0.32 x 0.31 x 0.13	0.34 x 0.33 x 0.28	0.34 x 0.32 x 0.29
Volume ($Å^3$)		6634.3 (19)	8558(3)	8477(3)	4761.8(17)	3769.8(13)
Z; Calculated density (g/cm^3)		6; 1.467	8; 1.363	8; 1.376	4; 1.401	4; 1.483
Absolute structure parameter		-	-	-	0.129(12)	-

Table A2. Main bond distances [Å] and angles [°] for *trensal* M(III)-complexes **3**, **4**, **5** and **8**; standard deviations are given in parentheses.

trensal Ga(III)-complex **3** [a]		Fe(III)-*trensal* **4** (**1st method**)		Fe(III)-*trensal* **4** (**2st method**)		*trensal* Mn(III)-complex **5**		*trensal* Ga(III)-complex **8**	
Bond atoms	**Distance [Å]**	**Bond atoms**	**Distance [Å]**	**Bond atoms**	**Distance [Å]**	**Bond atoms**	**Distance [Å]**	**Bond atoms**	**Distance [Å]**
Ga(1)-O(1)	1.9356 (19)	Fe(1)-O(1)	1.927(4)	Fe(1)-O(1)	1.940(3)	Mn(1)-O(1)	2.85(3)	Ga(1)-O(3)	1.9243(13)
Ga(1)-O(1)#1	1.9360 (2)	Fe(1)-O(2)	1.936(4)	Fe(1)-O(2)	1.934(3)	Mn(1)-O(2)	1.12(2)	Ga(1)-O(2)	1.9368(12)
Ga(1)-O(1)#2	1.9356 (19)	Fe(1)-O(3)	1.937(4)	Fe(1)-O(3)	1.941(3)	Mn(1)-O(3)	1.86(2)	Ga(1)-O(1)	1.9402(12)
Ga(1)-N(2)	2.1070 (2)	Fe(1)-N(2)	2.178(5)	Fe(1)-N(2)	2.174(4)	Mn(1)-N(2)	2.71(3)	Ga(1)-N(6)	2.0964(15)
Ga(1)-N(2)#1	2.1070 (2)	Fe(1)-N(3)	2.186(5)	Fe(1)-N(3)	2.189(4)	Mn(1)-N(3)	2.33(3)	Ga(1)-N(2)	2.1070(14)
Ga(1)-N(2)#2	2.1070 (2)	Fe(1)-N(4)	2.189(4)	Fe(1)-N(4)	2.173(4)	Mn(1)-N(4)	2.71(3)	Ga(1)-N(4)	2.1254(15)
				Fe(2)-O(4)	1.932(3)	Mn(2)-O(4)	1.12(2)		
				Fe(2)-O(5)	1.937(3)	Mn(2)-O(5)	2.68(3)		
				Fe(2)-O(6)	1.941(3)	Mn(2)-O(6)	1.91(2)		
				Fe(2)-N(8)	2.182(3)	Mn(2)-N(6)	2.41(3)		
				Fe(2)-N(6)	2.186(4)	Mn(2)-N(7)	2.57(3)		
				Fe(2)-N(7)	2.190(3)	Mn(2)-N(8)	2.89(3)		
Angle atoms	**Bond Angles (°)**	**Angle atoms**	**Bond Angles (°)**	**Angle atoms**	**Bond Angles (°)**	**Angle atoms**	**Bond Angles (°)**	**Angle atoms**	**Bond Angles (°)**
O(1)-Ga(1)-N(2)	90.16 (9)	O(1)-Fe(1)-O(2)	89.96(15)	O(1)-Fe(1)-O(2)	91.26(13)	O(3)-Mn(1)-O(2)	87.48(10)	O(3)-Ga(1)-O(2)	92.02(5)
O(1)#1-Ga(1)-N(2)#1	90.16 (9)	O(1)-Fe(1)-O(3)	95.78(18)	O(1)-Fe(1)-O(3)	94.27(13)	O(3)-Mn(1)-N(2)	171.93(11)	O(3)-Ga(1)-O(1)	85.77(5)
O(1)#1-Ga(1)-N(2)#2	90.16 (9)	O(2)-Fe(1)-O(3)	93.57(17)	O(2)-Fe(1)-O(3)	95.23(12)	O(2)-Mn(1)-N(2)	85.82(11)	O(2)-Ga(1)-O(1)	90.93(5)
N(2)-Ga(1)-N(2)#1	93.85 (9)	O(1)-Fe(1)-N(2)	86.25(15)	O(1)-Fe(1)-N(2)	87.49(13)	O(3)-Mn(1)-N(4)	90.09(11)	O(3)-Ga(1)-N(6)	89.62(5)
N(2)#2-Ga(1)-N(2)#1	93.85 (9)	O(2)-Fe(1)-N(2)	175.46(18)	O(2)-Fe(1)-N(2)	85.78(13)	O(2)-Mn(1)-N(4)	175.74(11)	O(2)-Ga(1)-N(6)	84.69(5)
N(2)-Ga(1)-N(2)#2	93.85 (9)	O(3)-Fe(1)-N(2)	84.34(18)	O(3)-Fe(1)-N(2)	177.95(14)	N(2)-Mn(1)-N(4)	96.87(12)	O(1)-Ga(1)-N(6)	173.53(5)
O(1)-Ga(1)-N(2)#1	175.98 (9)	O(1)-Fe(1)-N(3)	86.80(19)	O(1)-Fe(1)-N(3)	176.05(13)	O(3)-Mn(1)-O(1)	89.43(10)	O(3)-Ga(1)-N(2)	86.80(6)
O(1)#1-Ga(1)-N(2)#2	175.98 (9)	O(2)-Fe(1)-N(3)	86.86(17)	O(2)-Fe(1)-N(3)	86.06(13)	O(2)-Mn(1)-O(1)	95.08(11)	O(2)-Ga(1)-N(2)	177.43(5)
O(1)#2-Ga(1)-N(2)	175.98 (9)	O(3)-Fe(1)-N(3)	177.38(15)	O(3)-Fe(1)-N(3)	83.10(14)	N(2)-Mn(1)-O(1)	86.69(11)	O(1)-Ga(1)-N(2)	91.26(5)
O(1)#1-Ga(1)-N(2)	85.54 (9)	N(2)-Fe(1)-N(3)	95.41(19)	N(2)-Fe(1)-N(3)	95.19(14)	N(4)-Mn(1)-O(1)	88.40(11)	N(6)-Ga(1)-N(2)	93.01(6)
O(1)-Ga(1)-N(2)#2	85.54 (9)	O(1)-Fe(1)-N(4)	176.20(18)	O(1)-Fe(1)-N(4)	85.82(13)	O(3)-Mn(1)-N(3)	84.17(11)	O(3)-Ga(1)-N(4)	173.37(5)
O(1)#2-Ga(1)-N(2)#1	85.54 (9)	O(2)-Fe(1)-N(4)	87.16(16)	O(2)-Fe(1)-N(4)	176.51(13)	O(2)-Mn(1)-N(3)	85.08(11)	O(2)-Ga(1)-N(4)	89.40(5)
O(1)-Ga(1)-O(1)#1	90.48 (8)	O(3)-Fe(1)-N(4)	86.88(16)	O(3)-Fe(1)-N(4)	86.90(13)	N(2)-Mn(1)-N(3)	99.72(11)	O(1)-Ga(1)-N(4)	87.73(5)
O(1)-Ga(1)-O(1)#2	90.48 (8)	N(2)-Fe(1)-N(4)	96.74(16)	N(2)-Fe(1)-N(4)	92.18(14)	N(4)-Mn(1)-N(3)	91.19(11)	N(6)-Ga(1)-N(4)	96.96(5)
O(1)#1-Ga(1)-O(1)#2	90.48 (8)	N(3)-Fe(1)-N(4)	90.56(18)	N(3)-Fe(1)-N(4)	96.96(13)	O(1)-Mn(1)-N(3)	173.59(10)	N(2)-Ga(1)-N(4)	92.04(6)
				O(4)-Fe(2)-O(5)	96.21(12)	O(6)-Mn(2)-O(4)	89.56(10)		
				O(4)-Fe(2)-O(6)	90.18(12)	O(6)-Mn(2)-N(7)	169.04(10)		
				O(5)-Fe(2)-O(6)	94.24(12)	O(4)-Mn(2)-N(7)	83.37(10)		
				O(4)-Fe(2)-N(8)	87.10(13)	O(6)-Mn(2)-O(5)	86.72(10)		
				O(5)-Fe(2)-N(8)	176.68(12)	O(4)-Mn(2)-O(5)	100.68(11)		
				O(6)-Fe(2)-N(8)	85.87(13)	N(7)-Mn(2)-O(5)	86.37(10)		
				O(4)-Fe(2)-N(6)	85.82(12)	O(6)-Mn(2)-N(8)	89.72(11)		
				O(5)-Fe(2)-N(6)	85.43(13)	O(4)-Mn(2)-N(8)	172.57(11)		
				O(6)-Fe(2)-N(6)	175.93(13)	N(7)-Mn(2)-N(8)	98.36(11)		
				N(8)-Fe(2)-N(6)	94.70(13)	O(5)-Mn(2)-N(8)	86.66(11)		
				O(4)-Fe(2)-N(7)	176.95(13)	O(6)-Mn(2)-N(6)	82.23(10)		
				O(5)-Fe(2)-N(7)	86.16(12)	O(4)-Mn(2)-N(6)	83.40(10)		
				O(6)-Fe(2)-N(7)	87.73(13)	N(7)-Mn(2)-N(6)	105.16(11)		
				N(8)-Fe(2)-N(7)	90.53(13)	O(5)-Mn(2)-N(6)	168.21(10)		
				N(6)-Fe(2)-N(7)	96.29(13)	N(8)-Mn(2)-N(6)	89.17(11)		

a) Symmetry transformations used to generate equivalent atoms: #1 (-y+1,x-y,z) and #2 (-x+y+1,-x+1,z).

Table A3. Summary of crystallographic data for *trenpy* M(II)-complexes **11**, **12**, **13**, **16**, **17**; standard deviations are given in parentheses.

Identification code		*trenpy* Fe(II)-complex, **11**	*trenpy* Mn(II)-complex, **12**	*trenpy* Fe(II)-complex, **16**	*trenpy* Mn(II)-complex, **17**	*trenpy* Zn(II)-complex, **13**
Formula		C45 H45 F12 Fe N7 P2 S3	C45 H44 F12 Mn N7 P2 S3	C43.50 H54 F12 Fe N10 O4.50 P2	C39 H36 F12 Mn N10 P2	C45 H45 F12 N7 P2 S3 Zn
Solvates		-	-	3.5 (CH3OH)	-	-
Formula weight (g/Mol)		1125.85	1123.93	1134.76	989.66	1135.37
Temperature (K)		190(2)	100(2)	200(2)	180(2)	180(2)
Crystal system, space group		Orthorhombic, $P2_12_12_1$	Monoclinic, $P2_1/c$	Monoclinic, $P2_1/n$	Orthorhombic, $P2_12_12_1$	Monoclinic, $P2_1/n$
Unit cell dimensions	a (Å)	11.648(3)	12.975(3)	20.275(4)	11.945(2)	12.417(3)
	b (Å)	13.494(4)	14.586(3)	12.877(3)	17.101(3)	20.849(4)
	c (Å)	31.410(10)	25.430(5)	21.456(4)	21.210(4)	20.486(4)
	α (°)	90	90	90	90	90
	β (°)	90	97.28(3)	104.78(3)	90	104.36(3)
	γ (°)	90	90	90	90	90
Crystal size (mm)		0.37 x 0.19 x 0.08	0.12 x 0.07 x 0.05	0.39 x 0.14 x 0.08	0.35 x 0.09 x 0.04	0.46 x 0.16 x 0.11
Volume ($Å^3$)		4937(3)	4774.2(17)	5416.4(19)	4332.8(15)	5138.0(18)
Z; Calculated density (g/cm^3)		4; 1.515	4; 1.564	4; 1.392	4; 1.517	4; 1.468
Absolute structure parameter		0.48(4)	-	-	0.009(17)	-

Table A4. Main bond distances [Å] and angles [°] for *trenpy* M(II)-complexes **11**, **12**, **13**, **16**, **17**; standard deviations are given in parentheses.

trenpy Fe(II)-complex, **11**		*trenpy* Fe(II)-complex, **16**		*trenpy* Mn(II)-complex, **12**		*trenpy* Mn(II)-complex, **17**		*trenpy* Zn(II)-complex, **13**	
Bond atoms	Distance [Å]	Bond atoms	Distance [Å]	Bond atoms	Distance [Å]	Bond atoms	Distance [Å]	Bond atoms	Distance [Å]
Fe(1)-N(4)	1.938(8)	Fe(1)-N(5)	1.933(4)	Mn(1)-N(6)	2.207(2)	Mn(1)-N(5)	2.211(3)	Zn(1)-N(2)	2.105(3)
Fe(1)-N(6)	1.947(7)	Fe(1)-N(2)	1.946(4)	Mn(1)-N(4)	2.221(2)	Mn(1)-N(8)	2.216(3)	Zn(1)-N(6)	2.108(3)
Fe(1)-N(2)	1.961(8)	Fe(1)-N(8)	1.955(4)	Mn(1)-N(2)	2.222(2)	Mn(1)-N(2)	2.219(3)	Zn(1)-N(4)	2.117(3)
Fe(1)-N(7)	1.964(8)	Fe(1)-N(3)	1.957(4)	Mn(1)-N(3)	2.401(2)	Mn(1)-N(6)	2.361(3)	Zn(1)-N(7)	2.230(3)
Fe(1)-N(5)	1.967(7)	Fe(1)-N(9)	1.989(4)	Mn(1)-N(5)	2.409(2)	Mn(1)-N(9)	2.374(3)	Zn(1)-N(5)	2.305(3)
Fe(1)-N(3)	1.989(8)	Fe(1)-N(6)	1.992(4)	Mn(1)-N(7)	2.414(2)	Mn(1)-N(3)	2.395(3)	Zn(1)-N(3)	2.315(3)
				Mn(1)-N(1)	2.539(2)				
Angle atoms	Bond Angles (°)	Angle atoms	Bond Angles (°)	Angle atoms	Bond Angles (°)	Angle atoms	Bond Angles (°)	Angle atoms	Bond Angles (°)
N(4)-Fe(1)-N(6)	97.4(3)	N(5)-Fe(1)-N(2)	95.89(19)	N(6)-Mn(1)-N(4)	110.22(9)	N(5)-Mn(1)-N(8)	109.26(10)	N(2)-Zn(1)-N(6)	104.06(12)
N(4)-Fe(1)-N(2)	97.2(4)	N(5)-Fe(1)-N(8)	96.58(19)	N(6)-Mn(1)-N(2)	108.93(9)	N(5)-Mn(1)-N(2)	109.75(10)	N(2)-Zn(1)-N(4)	105.22(12)
N(6)-Fe(1)-N(2)	95.1(3)	N(2)-Fe(1)-N(8)	94.61(19)	N(4)-Mn(1)-N(2)	111.79(9)	N(8)-Mn(1)-N(2)	104.18(11)	N(6)-Zn(1)-N(4)	106.51(11)
N(4)-Fe(1)-N(7)	90.2(4)	N(5)-Fe(1)-N(3)	174.43(18)	N(6)-Mn(1)-N(3)	151.63(8)	N(5)-Mn(1)-N(6)	72.18(9)	N(2)-Zn(1)-N(7)	159.97(10)
N(6)-Fe(1)-N(7)	81.3(3)	N(2)-Fe(1)-N(3)	81.54(19)	N(4)-Mn(1)-N(3)	95.35(9)	N(8)-Mn(1)-N(6)	98.91(10)	N(6)-Zn(1)-N(7)	76.12(11)
N(2)-Fe(1)-N(7)	172.2(4)	N(8)-Fe(1)-N(3)	88.58(18)	N(2)-Mn(1)-N(3)	70.57(9)	N(2)-Mn(1)-N(6)	154.31(10)	N(4)-Zn(1)-N(7)	93.68(11)
N(4)-Fe(1)-N(5)	80.3(4)	N(5)-Fe(1)-N(9)	87.55(18)	N(6)-Mn(1)-N(5)	94.56(8)	N(5)-Mn(1)-N(9)	157.57(10)	N(2)-Zn(1)-N(5)	92.02(11)
N(6)-Fe(1)-N(5)	174.7(4)	N(2)-Fe(1)-N(9)	174.79(18)	N(4)-Mn(1)-N(5)	70.78(9)	N(8)-Mn(1)-N(9)	72.09(10)	N(6)-Zn(1)-N(5)	162.64(11)
N(2)-Fe(1)-N(5)	90.0(3)	N(8)-Fe(1)-N(9)	81.08(18)	N(2)-Mn(1)-N(5)	152.69(9)	N(2)-Mn(1)-N(9)	91.02(10)	N(4)-Zn(1)-N(5)	74.80(11)
N(7)-Fe(1)-N(5)	93.8(3)	N(3)-Fe(1)-N(9)	95.35(18)	N(3)-Mn(1)-N(5)	82.13(8)	N(6)-Mn(1)-N(9)	85.43(9)	N(7)-Zn(1)-N(5)	86.53(10)
N(4)-Fe(1)-N(3)	174.2(4)	N(5)-Fe(1)-N(6)	81.02(18)	N(6)-Mn(1)-N(7)	70.92(9)	N(5)-Mn(1)-N(3)	94.47(10)	N(2)-Zn(1)-N(3)	75.45(11)
N(6)-Fe(1)-N(3)	88.3(3)	N(2)-Fe(1)-N(6)	87.98(17)	N(4)-Mn(1)-N(7)	152.74(9)	N(8)-Mn(1)-N(3)	155.72(10)	N(6)-Zn(1)-N(3)	90.90(10)
N(2)-Fe(1)-N(3)	81.4(4)	N(8)-Fe(1)-N(6)	176.65(18)	N(2)-Mn(1)-N(7)	92.48(8)	N(2)-Mn(1)-N(3)	71.16(10)	N(4)-Zn(1)-N(3)	161.58(11)
N(7)-Fe(1)-N(3)	91.6(3)	N(3)-Fe(1)-N(6)	93.91(17)	N(3)-Mn(1)-N(7)	80.73(8)	N(6)-Mn(1)-N(3)	83.16(9)	N(7)-Zn(1)-N(3)	84.53(10)
N(5)-Fe(1)-N(3)	94.1(3)	N(9)-Fe(1)-N(6)	96.43(17)	N(5)-Mn(1)-N(7)	81.96(8)	N(9)-Mn(1)-N(3)	84.04(9)	N(5)-Zn(1)-N(3)	86.79(10)
				N(6)-Mn(1)-N(1)	71.73(8)				
				N(4)-Mn(1)-N(1)	71.41(8)				
				N(2)-Mn(1)-N(1)	71.03(8)				
				N(3)-Mn(1)-N(1)	130.41(8)				
				N(5)-Mn(1)-N(1)	131.66(8)				
				N(7)-Mn(1)-N(1)	130.94(8)				

Table A5. Summary of crystallographic data for *facial* Ru(II)-*trisbpy* complex, **21**^{f}; standard deviations are given in parentheses.

Identification code		Ru(II)-complex, **21**^{f}
Formula		C63 H46.50 F12 N7.50 O3 P2 Ru S3
Solvates and counter ions		1,5 (CH3CN), 2(PF6)
Formula weight		1443.77
Temperature (K)		143 (2)
Crystal system, space group		Triclinic, $P\bar{1}$
Unit cell dimensions	a (Å) b (Å) c (Å) α (°) β (°) γ (°)	13.081 (5) 15.083 (6) 18.470 (8) 95.06 (3) 108.12 (3) 104.55 (3)
Crystal size (mm)		0.52 x 0.05 x 0.04
Volume (Å^3)		3297 (2)
Z, Calculated density (g/cm^3)		2; 1.454
Absolute structure parameter		-

Table A6. Main Bond lengths [Å] and angles [°] for *facial* Ru(II)-*trisbpy*, **21**^{f}; standard deviations are given in parentheses.

Ru(II)-complex, **21**^{f}	
Bond atoms	Distance [Å]
Ru(1)-N(6)	2.058(6)
Ru(1)-N(5)	2.058(6)
Ru(1)-N(2)	2.065(6)
Ru(1)-N(1)	2.065(6)
Ru(1)-N(3)	2.065(6)
Ru(1)-N(4)	2.066(5)
Angle atoms	Bond Angles (°)
N(6)-Ru(1)-N(5)	78.6(2)
N(6)-Ru(1)-N(2)	99.0(2)
N(5)-Ru(1)-N(2)	174.4(2)
N(6)-Ru(1)-N(1)	89.9(2)
N(5)-Ru(1)-N(1)	96.3(2)
N(2)-Ru(1)-N(1)	78.6(2)
N(6)-Ru(1)-N(3)	171.0(2)
N(5)-Ru(1)-N(3)	93.6(2)
N(2)-Ru(1)-N(3)	89.2(2)
N(1)-Ru(1)-N(3)	95.4(2)
N(6)-Ru(1)-N(4)	96.3(2)
N(5)-Ru(1)-N(4)	88.2(2)
N(2)-Ru(1)-N(4)	97.1(2)
N(1)-Ru(1)-N(4)	172.9(2)
N(3)-Ru(1)-N(4)	78.8(2)

Table A7. Summary of crystallographic data for homodinuclear helicate complexes $[(L^f)_3Fe_2]^{4+}(PF_6)_4$, **23** and $[(L^f)_3Ni_2]^{4+}(PF_6)_4$, **24**; standard deviations are given in parentheses.

Identification code		$[(L^f)_3Ni_2]^{4+}(PF_6)_4$	$[(L^f)_3Fe_2]^{4+}(PF_6)_4$
Reported Formula		C129 H122 F24 N14 Ni2 O2 P4 S6	C133 H115 F24 Fe2 N20 P4 S6
Solvates		2(C4H10O), 2(CH3CN)	7.x (CH3CN)
Formula weight (g/Mol)		2790.07	2877.39
Temperature (K)		180(2)	180(2)
Crystal system, space group		Monoclinic, C2/c	Monoclinic, C2
Unit cell dimensions	a (Å)	51.640(10)	30.542(6)
	b (Å)	10.309(2)	20.286(4)
	c (Å)	25.917(5)	11.599(2)
	α (°)	90	90
	β (°)	113.55(3)	94.39(3)
	γ (°)	90	90
Crystal size (mm)		0.44 x 0.13 x 0.05	0.45 x 0.10 x 0.08
Volume ($Å^3$)		12649(4)	7165(2)
Z; Calculated density (g/cm^3)		4; 1.465	2; 1.334
Absolute structure parameter		-	0.44(4)

Table A8. Main Bond lengths [Å] and angles [°] for homodinuclear helicate complexes $[(L^f)_3Fe_2]^{4+}(PF_6)_4$, **23** and $[(L^f)_3Ni_2]^{4+}(PF_6)_4$, **24**; standard deviations are given in parentheses.

$[(L^f)_3Ni_2]^{4+}(PF_6)_4$		$[(L^f)_3Fe_2]^{4+}(PF_6)_4$	
Bond atoms	Distance [Å]	Bond atoms	Distance [Å]
Ni(1)-N(2)	2.091(4)	Fe(1)-N(4)	1.935(11)
Ni(1)-N(6)#1	2.109(4)	Fe(1)-N(5)#1	1.944(9)
Ni(1)-N(4)	2.113(4)	Fe(1)-N(2)	1.961(9)
Ni(1)-N(3)	2.116(4)	Fe(1)-N(3)	1.969(10)
Ni(1)-N(1)	2.125(4)	Fe(1)-N(6)#1	1.976(9)
Ni(1)-N(5)#1	2.134(4)	Fe(1)-N(1)	2.011(11)
Angle atoms	Bond Angles (°)	Angle atoms	Bond Angles (°)
N(2)-Ni(1)-N(6)#1	93.92(15)	N(4)-Fe(1)-N(5)#1	98.2(4)
N(2)-Ni(1)-N(4)	98.49(15)	N(4)-Fe(1)-N(2)	96.7(4)
N(6)#1-Ni(1)-N(4)	163.21(13)	N(5)#1-Fe(1)-N(2)	95.3(4)
N(2)-Ni(1)-N(3)	173.19(13)	N(4)-Fe(1)-N(3)	80.0(4)
N(6)#1-Ni(1)-N(3)	90.09(14)	N(5)#1-Fe(1)-N(3)	174.2(4)
N(4)-Ni(1)-N(3)	78.73(15)	N(2)-Fe(1)-N(3)	90.4(4)
N(2)-Ni(1)-N(1)	79.09(14)	N(4)-Fe(1)-N(6)#1	89.2(4)
N(6)#1-Ni(1)-N(1)	98.68(14)	N(5)#1-Fe(1)-N(6)#1	81.3(4)
N(4)-Ni(1)-N(1)	94.75(14)	N(2)-Fe(1)-N(6)#1	173.6(4)
N(3)-Ni(1)-N(1)	94.87(14)	N(3)-Fe(1)-N(6)#1	93.1(4)
N(2)-Ni(1)-N(5)#1	97.60(14)	N(4)-Fe(1)-N(1)	174.6(4)
N(6)#1-Ni(1)-N(5)#1	78.46(14)	N(5)#1-Fe(1)-N(1)	87.1(4)
N(4)-Ni(1)-N(5)#1	88.69(14)	N(2)-Fe(1)-N(1)	82.0(4)
N(3)-Ni(1)-N(5)#1	88.60(13)	N(3)-Fe(1)-N(1)	94.8(4)
N(1)-Ni(1)-N(5)#1	175.53(14)	N(6)#1-Fe(1)-N(1)	92.3(4)

a) Symmetry transformations used to generate equivalent atoms: #1 -x,y,1/2-z+1
b) Symmetry transformations used to generate equivalent atoms: #1 -x+2,y,-z #2 -x+3,y,-z+1

Table A9. Summary of crystallographic data for (S)- and (R)-Zn(II)-binaphthyl complexes; standard deviations are given in parentheses.

Identification code		(S)-**ZnL**^{g} , **27**$^{(S)}$	(R)-**ZnL**^{g} , **27**$^{(R)}$	(S)-**ZnL**^{h} , **30**$^{(S)}$
Reported Formula		C35 H22 Br2 Cl2 N2 O2 Zn	C36.33333 H29.33333 Br2 N2 O4.33333 Zn	C43.6667 H31.3333 Cl1.3333 N2 O3 S2 Zn
Solvates		1 (CH2Cl2)	2.3333 (CH3OH)	0.6667 (CH2Cl2)
Formula weight (g/Mol)		798.64	788.47	808.80
Temperature (K)		180(2)	190(2)	180(2)
Crystal system, space group		Trigonal, R3	Trigonal, R3	Trigonal, P3(1)
Unit cell dimensions	a (Å)	23.434(3)	23.223(3)	25.710(4)
	b (Å)	23.434(3)	23.223(3)	25.710(4)
	c (Å)	15.672(3)	16.105(3)	14.770(3)
	α (°)	90	90	90
	β (°)	90	90	90
	γ (°)	120	120	120
Crystal size (mm)		0.42 x 0.31 x 0.29	0.41 x 0.38 x 0.19	0.28 x 0.25 x 0.19
Volume (Å^{3})		7453(2)	7522(2)	8455(2)
Z; Calculated density (g/cm^{3})		9; 1.601	9; 1.567	9; 1.430
Absolute structure parameter		0.06(2)	-0.003(11)	0.017(13)

Table A10. Main Bond lengths [Å] and angles [°] for (S)- and (R)-Zn(II)-binaphthyl complexes; standard deviations are given in parentheses.

(S)-**ZnL**^{g} , **27**$^{(S)}$		(R)-**ZnL**^{g} , **27**$^{(R)}$		(S)-**ZnL**^{h} , **30**$^{(S)}$	
Bond atoms	Distance [Å]	Bond atoms	Distance [Å]	Bond atoms	Distance [Å]
Zn(1)-O(1)	1.905(8)		1.905(4)	Zn(1)-O(1)	1.951(5)
Zn(1)-O(2)	1.926(6)		1.930(4)	Zn(1)-O(2)	1.954(6)
Zn(1)-N(1)	2.002(8)		2.025(4)	Zn(1)-N(1)	2.093(6)
Zn(1)-N(2)	2.003(7)		2.029(4)	Zn(1)-N(2)	2.114(6)
				Zn(1)-O(7)	2.183(6)
				Zn(2)-O(3)	1.957(5)
				Zn(2)-O(4)	2.000(5)
				Zn(2)-N(3)	2.089(6)
				Zn(2)-N(4)	2.097(6)
				Zn(2)-O(8)	2.118(5)
				Zn(3)-O(6)	1.926(6)
				Zn(3)-O(5)	2.005(5)
				Zn(3)-N(6)	2.101(6)
				Zn(3)-N(5)	2.114(6)
				Zn(3)-O(9)	2.152(6)
Angle atoms	Bond Angles (°)	Angle atoms	Bond Angles (°)	Angle atoms	Bond Angles (°)
O(1)-Zn(1)-O(2)	107.8(3)		108.93(16)	O(1)-Zn(1)-O(2)	96.5(2)
O(1)-Zn(1)-N(1)	95.5(3)		94.10(16)	O(1)-Zn(1)-N(1)	90.6(2)
O(2)-Zn(1)-N(1)	134.2(4)		134.69(16)	O(2)-Zn(1)-N(1)	170.3(3)
O(1)-Zn(1)-N(2)	134.8(3)		134.52(16)	O(1)-Zn(1)-N(2)	130.8(2)
O(2)-Zn(1)-N(2)	93.9(3)		93.29(15)	O(2)-Zn(1)-N(2)	89.5(2)
N(1)-Zn(1)-N(2)	96.8(3)		97.45(16)	N(1)-Zn(1)-N(2)	90.9(2)
				O(1)-Zn(1)-O(7)	102.9(2)
				O(2)-Zn(1)-O(7)	85.8(3)
				N(1)-Zn(1)-O(7)	86.2(2)
				N(2)-Zn(1)-O(7)	126.2(2)
				O(3)-Zn(2)-O(4)	98.4(2)
				O(3)-Zn(2)-N(3)	90.4(2)
				O(4)-Zn(2)-N(3)	169.4(2)
				O(3)-Zn(2)-N(4)	127.9(2)
				O(4)-Zn(2)-N(4)	89.6(2)
				N(3)-Zn(2)-N(4)	89.7(2)
				O(3)-Zn(2)-O(8)	106.2(2)
				O(4)-Zn(2)-O(8)	85.5(2)
				N(3)-Zn(2)-O(8)	86.3(2)
				N(4)-Zn(2)-O(8)	125.8(2)
				O(6)-Zn(3)-O(5)	106.4(2)
				O(6)-Zn(3)-N(6)	91.5(2)
				O(5)-Zn(3)-N(6)	161.2(3)
				O(6)-Zn(3)-N(5)	123.9(3)
				O(5)-Zn(3)-N(5)	86.8(2)
				N(6)-Zn(3)-N(5)	88.1(2)
				O(6)-Zn(3)-O(9)	98.1(2)
				O(5)-Zn(3)-O(9)	83.3(2)
				N(6)-Zn(3)-O(9)	88.3(2)
				N(5)-Zn(3)-O(9)	137.9(3)

Curriculum Vitae

Alexandrina STUPARU

PERSONAL DATA:

Date of birth	March 15, 1977
Nationality	Romanian
E-mail	stuparu_alexandra@yahoo.com

EDUCATION AND TRAINING:

04.2007 – 05.2010	PhD student, University of Basel, Switzerland PhD work at Institute of Nanotechnology, Karlsruhe Institute of Technology, Germany PhD Thesis: "*Tailor-made molecules for the functionalization of electrodes: from tripodal complexes to thioketal compounds"*
11.2004 – 03.2007	PhD student, Faculty of Chemistry, Departament of Physical Chemistry University of Bucharest, Romania Topic: *„Kinetics of the complex reactions in continuous stirred tank reactors"*
04.2005	Training Module for Environmental Pollution Control, Leonardo da Vinci Programme, Bucharest, Romania Course: "*Environmental Pollution Monitoring*" – Pollution, Analysis, Legislation, Quality and Management.
10.2001 – 08.2003	Master of Science, Faculty of Chemistry, Department of Organic Chemistry, University of Bucharest, Romania Specialization: Natural and Synthesized Multifunctional Organic Compounds". Thesis of degree: *"Antiglaucoma drugs from Prostaglandin class"*.
10.1997 – 08.2001	Bachelor of Science, Faculty of Chemistry, Bucharest University, Romania, Department of Physical Chemistry. Licence Thesis: "*Synthesis of pyrolo-[1, 2-b]-pyridasines"*.

WORK EXPERIENCE:

07.2001 - 09.2004	Chemist National Institute for Chemical and Pharmaceutical Research and Development Bucharest, Romania Section: Synthesis of Drugs, Intermediaries and Auxiliary Compounds *Research and micro-production of Prostaglandins*

List of Scientific Publications:

- *"Estimation of the overall kinetic parameters of enzyme inactivation using an isoconversional method",* D. Oancea, Alexandrina Stuparu, Madalina Nita, Mihaela Puiu, Adina Raducan - *Biophysical Chemistry*, *138*, **2008**, 50

- "*Conductometric study of urease inhibition by heavy metal ions in urea hydrolysis in a self-buffering system*", Alexandrina Stuparu, Dumitru Oancea - *Prog. Catal.*, **2006**, *12*, 73

- *"Contributions to the establishment of the chemical composition of the oil extracted from Squalus Acanthias liver",* Dana Mihele, Valeria Radulescu, Florea Cocu, Irina Predescu, Alexandra Stuparu - *Rev. Chim. (Bucuresti)*, **2005**, *56,* 973

- *"New N-Substituted Pyrazolyl-Benzenesulfonamide Compounds as Analogues of COX-2 Selective Inhibitors"*, Maria Croitoru, Lucia Pintilie, Constantin Tanase, Alexandrina Stuparu, Catalina Cioates, Florea Cocu, Miron Teodor Căproiu, Constantin Drăghici - *Rev. Chim. (Bucuresti)*, **2004***, 55,* 993

Posters and presentations at diverse Conferences in Romania in organic chemistry and kinetic